Indian Ocean Climate Initiative

Second Research Report - Towards Understanding Climate Variability in south western Australia

Research reports on the Second Research Phase of the Indian Ocean Climate Initiative

IOCI October, 2001 **Second Research Report**

Second Research Report -
Towards an Understanding
of
Climate Variability in south western Australia

Research reports on the Second Research Phase
of the Indian Ocean Climate Initiative

Bureau of Meteorology Research Centre

CSIRO Atmospheric Research

CSIRO Land and Water

CSIRO Mathematical and Information Sciences

Indian Ocean Climate Initiative a Contributing Partnership

Department of Premier and Cabinet
Dept of Industry and Technology
Agriculture WA
Dept of Environment Water & Catchment Protection
Water Corporation
Dept of Conservation and Land Management
WA Region of the Bureau of Meteorology
Fire & Emergency Services

IOCI - A WA initiated partnership to foster -

- *research in climate variability; and*
- *developments in seasonal forecasting;*

for regions of western and southern Australia affected by the Indian and Southern Oceans; and particularly for south western Australia

Core Research Team -

Bureau of Meteorology Research Centre
CSIRO Atmospheric Research
CSIRO Land and Water
CSIRO Mathematical and Information Sciences

CONTENTS

ISBN: 0 7307 6679 9

Published by: Indian Ocean Climate Initiative Panel
Address:
Executive Officer IOCIP,
C/- Dept of Environment, Water and Catchment Protection
Hyatt Centre, 3 Plain St.
East Perth, WA 6004, Australia
October, 2001

Abstract:

This report describes the research findings of Phase 3 of the Indian Ocean Climate Initiative (IOCI). IOCI is a five-year program of research into the effects of the Indian and Southern Oceans on interseasonal to interdecadal climate variability in the South West region of Western Australia, and the development of operational seasonal outlooks that have sufficient skill for effective decision making. IOCI was established through a partnership of federal and state government agencies. Key findings include: (1) the underlying causes of the observed winter rainfall decline is not simply due to changes in Indian Ocean sea surface temperatures; (2) there has been an abrupt shift and a clearly defined trend in the frequency characteristics of the synoptic patterns that influence rainfall occurrence; (3) the timing of the shift appears to coincide with the well-documented change in the behaviour of the El-Niño that occurred in the mid 1970s. The trend appears to be due to a different mechanism, and its interaction with El-Niño; (4) a new approach to modelling shifts in, and interactions between, climate processes has been developed to investigate this phenomenon further; (5) long climate model simulations indicate that the recent low precipitation sequence is uncommon but not extreme; (6) natural climate variability is the most likely major cause of the observed reduction in winter rainfall; (7) the enhanced greenhouse effect may have contributed to the winter rainfall decline; and (8) there is some skill in predicting total rainfall and mean temperatures for spring and summer, and extreme temperatures in summer.

Foreword

The Indian Ocean Climate Initiative (IOCI) was established in Western Australia on January 1, 1998. Its role is to pursue the overlapping interests of several economic sectors in respect to research, development and applications relating to climate variability. The program was stimulated by desire to gain regional economic and environmental benefit from contemporary national and international climate research. The Initiative was given added impetus by concerns as to the implications of the 25-30 year long sequence of low winter rainfalls which was being experienced in south-west Western Australia.

The low rainfall sequence continues, and the winter of 2001 has been the driest on record for a large area of the South West. This situation is of major concern to climate-affected industries and to natural resources management in the region. Regional averages and understandings of climate variability and risk are being altered forever by this experience. The changes are large and have major implications economically, environmentally and socially. There is a need to assist decision-making with a greater understanding of the climatic phenomena of southern and western Australia, including the influences of the Indian and Southern Oceans.

Initially, IOCI was formed as a program of strategic research into the effects of the Indian and Southern Oceans on climate variability in south-western Australia. It is a contributing partnership of central government and government agencies in Western Australia with involvement in climate issues. A number of agencies that had worked, semi-independently, on climate research saw the need for a program that could develop regional applications from broader scale national research activities. The initial research contracts provide $300,000 per year for a core program from Jan 1998 to Dec 2002. The core research is conducted by the Bureau of Meteorology Research Centre, and by the CSIRO divisions of Atmospheric Research, Land and Water, and Mathematical and Information Sciences. The research institutions match the partnership inputs through in-kind contributions.

The objectives of IOCI are to gainfully improve management decisions of climate-affected industries, and environmental management, through:

- i*mproved understanding and definition of inter-annual and inter-decadal climate variability; and*
- *enabling seasonal outlooks with sufficient skill for operational decision making.*

The potential beneficiaries include: agriculture; water supply; forest fire control; wetlands management; water resources management; public health; tourism; conservation of bio-diversity and nature reserves; urban and industrial infrastructure; finance and insurance.

The initial 5 year program has three research phases as follows:

First Research Phase: *Jan 1998 to June 1999 (report published)*

Second Research Phase: *June 1999 to Dec 2000 (this report)*

Third Research Phase: *December 2000 to December 2002 (work in progress)*

Since embarking on its strategic program IOCI has become increasingly aware of the significance of longer-term change and variability to its research goals and to the issues confronting decision-makers. IOCI research has reached a view that the observed climate behaviour of the last 25 - 30 years in south-western Australia is best interpreted as a change of climate state. This altered state is associated with changes in atmospheric circulation and is evident as changes in some previously recognised climatic relationships and norms.

As a consequence of these changes IOCI has needed to look at human influences on climate behaviour as well as natural change and long term natural variation. Although there is a strong probability that Greenhouse gas accumulations in the atmosphere will lead to a rainfall decline in south-western Australia, the evidence suggests that the observed rainfall decline began too soon to be solely attributable to enhanced Greenhouse effects and that there are other, possibly natural, causes involved. Modelling also suggests such dry situations may have occurred before under natural conditions. The explanation for the decline is important to adaptive decision-making and is being pursued further in current research.

The climate application issues of south-western Australia, for which IOCI is providing support, might be seen in two distinct priority levels. Support to inter-seasonal forecasting represents opportunity. Support for adaptation to climate change represents necessity. Large changes in south-western climate have made the adaptation issue one of immediate concern. Decision-makers need support in making appropriate judgements about future climate baselines as a basis for sound adaptation strategies and these issues are occupying increasing attention in IOCI's program .

IOCI is already progressing on the third research phase of its core program. A key part of this current phase will be the publication of a report, especially for decision-makers, consolidating the state of knowledge on South West climate variability up to June 2002. This proposed publication will be accompanied by educative seminars or workshops.

The IOCI Panel is now pleased to be distributing the underlying report of its second phase of core research activity. The Panel believes the report represents another important step in consolidating and developing an understanding of the variability of the climate in southern and western Australia.

The report is commended for study by those who have need to make plans or decisions which must consider the effects of climate variability.

Brian Sadler
Chair IOCIP
October 2001

Summary

This report marks the conclusion of IOCI Phase 3. It follows a two-day national seminar and workshop (IOCI2000) held in Perth in November 2000 at which progress reports were presented by the research groups in draft form. Leaders in the science and application of interseasonal climate forecasts were invited to IOCI2000, and a high level of national and international expertise was assembled. The seminar program provided an overview of the growing state of knowledge about climate variability in southwest Western Australia (SWA) while the workshop provided a peer review of the research findings and the direction of the proposed research program for 2001 to 2002. The workshop was productive and led to general agreement about future research directions.

The following report is comprised of four parts. The research outcomes support a number of broad conclusions that may be summarised as follows:

The Drying Trend

- Further investigation supports the viewpoint that the underlying causes of the observed reduction in SWA winter rainfall is not simply due to changes in Indian Ocean sea surface temperatures (SSTs).
- Analysis of the results obtained from a stochastic downscaling model revealed an abrupt shift and a clearly defined trend in the frequency characteristics of the synoptic patterns that influence precipitation occurrence over SWA. The timing and nature of these changes are consistent with the characteristics of the observed low precipitation sequence.
- The changes in the frequency characteristics of the synoptic patterns and the resultant low precipitation sequence since the mid 1970s are due to changes in a combination of atmospheric variables reflecting the location and intensity of low and high pressure systems, and the moisture content of the lower troposphere. The low precipitation sequence cannot be ascribed to change(s) in a single variable such as mean sea level pressure.
- The timing of the shift appears to coincide with the well-documented change in the behaviour of the El-Niño – Southern Oscillation that occurred in the mid 1970s. The trend appears to be due to a different mechanism, and its interaction with El-Niño.

Seasonal Predictions

Linear Statistical Methods

The potential for using near-global patterns of sea surface temperature variation in seasonal climate prediction for SWA was examined. The climate variables examined were proposed by Panel members as being important for agriculture or environmental and water resource management in the southwest. Some skill was possible in predicting total rainfall and mean temperatures for spring and summer, as well as predicting extreme temperatures in summer. These predictions would be available a month or two in advance of the season predicted.

The potential use of some newly proposed modes of climate variation, known as the Antarctic Circumpolar Wave (ACW) and the Indian Ocean Dipole (IOD), was also examined. Some evidence was found that these modes might be related to SWA climate. Subsequent work, since the end of the second IOCI research phase, has found, however, that these modes

do not improve on the predictions available using the near-global patterns of sea surface temperature variability referred to above. This is because both the ACW and the IOD are closely related to the El Niño - Southern Oscillation, which is also represented in the near-global sea surface temperature patterns.

At the request of Panel members, some preliminary work was done to investigate whether observed climate variations could be used to predict crop yields. It was found that early seasonal rainfall and temperature were good predictors of wheat yield. This provided more accurate predictions than did the near-global sea surface temperature patterns. The relationship between early winter climate and yield probably occurs partly because of farmer reactions to the early winter climate – if the climate early in the season is good, then farmers will plant early and this will tend to lead to good yields.

Nonlinear Statistical Methods

An alternative perspective on seasonal prediction could be provided by so-called nonlinear statistical methods. These methods allow for behaviour such as the sudden break that has been observed in the southwest's rainfall, which is not a feature of straightforward linear behaviour. Nonlinear methods therefore provide a broader framework within which to search for climate predictors.

- A physically motivated statistical model for modelling nonlinear climate processes has been developed. The approach can now be applied to practical problems.
- The nonlinear method can identify good predictors and the lags at which they influence climate variables, such as rainfall. Within this modelling framework, changes between climate regimes are triggered by a switching variable, and comparisons between alternative switching variables can be made.
- We would expect broad scale climate features to be good candidates to cause switching behaviour. Examples include, amongst others, large-scale circulation patterns, the El Niño-Southern Oscillation (as measured by SOI), and Indian Ocean SSTs. These may operate individually or in combination.
- There is some evidence that SOI and mid-Indian Ocean SST gradients play a role in switching between rainfall regimes. At this stage, this is cited as evidence that the new nonlinear method is producing sensible results, rather than new insights *per se*.
- Interactions between climate processes are likely to influence rainfall in SWA. Some reasonably straightforward extensions to the nonlinear method will facilitate the search for subtler climate teleconnections arising from such interactions.

Numerical Climate Models and Stochastic Downscaling

The Phase 1 report documented results from the CSIRO climate model referred to as Mark2. Further analysis of these results has continued but, at the same time, a new climate model (Mark3) has been developed and used to address several key questions. When forced by observed sea surface temperatures (SSTs), the Mark3 model provides better simulations of rainfall over SWA. This improvement is seen in both the representation of the seasonal cycle, the amplitude of the seasonal cycle and the amplitude of interannual variations.

The downscaling model described in the Phase 1 report has also been further tested in order to improve the representation of rainfall at both the local and monthly time scale.

Interdecadal Variability

- Stochastic downscaling of the 1000-year long simulation with the Mark2 model indicates that the recent low precipitation sequence over SWA is uncommon but not extreme.
- Results from a much longer 10,000-year simulation with the Mark2 model confirm the earlier analyses, which indicate that annual rainfall totals over SWA can exhibit variability on decadal, multi-decadal, and even millennial time scales due to internal processes. The results did not reveal any links between changes in rainfall at these time scales and changes in other variables such as SSTs.
- The Mark3 model has been forced by observed SSTs for the period 1949 to 1990. The results from an ensemble of three such experiments do not show any evidence of a protracted reduction in rainfall over the period when the observed reduction took place. This type of result has also been noted in other climate model experiments. This tends to suggest that:
    1. Owing to sparse observations in some regions, the SST data used in the model experiments may not accurately reflect changes that may have taken place and which may be responsible for the decline, or
    2. There are other factors involved which are not represented in these "forced" SST experiments, or
    3. Rainfall is not sufficiently well simulated by large scale climate models to capture trends at the relatively small scales.

Interannual variability

- After revision of the set of atmospheric predictor variables used in the stochastic downscaling model, it was found that parameter estimates derived from atmospheric and precipitation data for the period 1978 to 1992, inclusive, could be used to simulate monthly precipitation over SWA for the period 1958-1998. This suggests that the model is robust against secular breaks in atmospheric circulation and precipitation, and that it may be a useful tool for downscaling an interseasonal climate forecast produced by a numerical climate model.
- Results from the Mark2 1000-year simulation indicate that links between Indian Ocean SSTs and rainfall over SWA can be simulated as a consequence of changes in the atmospheric circulation driving pressure, winds, rainfall and SST changes rather than as a consequence of the SSTs driving the other variables. This tends to confirm previous results suggesting that the Indian Ocean offers little in the way of predictability of SWA winter rainfall.
- Similarly, an analysis of the relationship between an Antarctic Circumpolar Wave -type phenomenon in the Mark2 model did not indicate that this provides a source of predictability for SWA winter rainfall. Nor was it possible to identify any link between high latitude Indian Ocean SSTs and SWA winter rainfall.
- The Mark3 model results reveal weak evidence of links between SWA rainfall anomalies and SST anomalies in the Pacific Ocean, but no evidence of any significant links to the Indian Ocean. This is consistent with what is known about the limited predictability for this region during winter.

- A seasonal prediction model based on the Mark2 model has been developed and exhibits skill at predicting an index of El Nino/La Nina events. This suggests that, to the extent that these events have any effect on SWA winter rainfall, there may be some limited value in these predicted indices - particularly as they are predicted with lead times up to 12 months.

Greenhouse Simulations

CSIRO climate model

- The latest CSIRO climate change simulations using the Mark2 model comprise ensembles and also take into account a range of CO_2 loadings and the effects of increased atmospheric sulphate content. The different experiments all yield decreases in annual rainfall of about -10% by the end of the 21st century. Combined with increased temperatures of up to +3.0 ^oC, they also indicate a decrease in soil moisture of about -15%.
- In addition, an equilibrium climate change simulation ($2\times CO_2$ only) has been performed with the Mark3 model. This is a simplified, but relatively inexpensive, greenhouse simulation. The simulated global changes are somewhat less than the Mark2 results. Despite these differences, the results for SWA are similar.
- None of the greenhouse simulations from either of the models show evidence of any significant decrease in rainfall for the SWA region over the period 1970-2000 (as has been observed). The internal (or "natural") variability in the various time series for rainfall tends to dominate any long-term trends over the latter part of the 20th century.
- One interpretation of the CSIRO results is that the enhanced greenhouse effect may have made only a minor contribution to the observed reduction in SWA winter rainfall.

Other climate models

- The results of climate change experiments from several different models have been stratified according the ability of each model to reproduce the seasonal cycle of rainfall for SWA. As a result, only three models (the Hadley Centre model, the Geophysical Fluid Dynamics Laboratory (GFDL) model and the CSIRO Mark2 model) were selected.
- Of these three, the Hadley Centre model yields the largest percentage decrease in SWA winter rainfall by the end of the 21st century while the GFDL model yields the least. As is the case with the Mark2 model, these two models do not simulate a significant reduction for the end of the 20th century.
- However, the Hadley Centre model does simulate a similar magnitude reduction in winter rainfall over the period 2000-2025. If it is assumed that the Hadley Centre model is correct, except for an error in timing of about 25 years, then it is possible that the observed reduction may represent a substantial contribution from the enhanced greenhouse effect.
- Reducing the uncertainties in the interpretation of the observed reduction and estimates for the future climate can be achieved by:

  (i) careful scrutiny of climate change simulations as they become available

  (ii) performing a range of analyses to detect significant signals in the results

  (iii) applying downscaling techniques in order to achieve more realistic estimates of expected changes in rainfall

The first three years of the IOCI has been productive, and has heightened international scientific attention on southwestern Australia. The numerous and substantial findings of the third phase of research inspire confidence that further knowledge gains are possible, and that these gains will provide valuable social and economic benefits for the region.

Bryson Bates
CSIRO Land and Water

Climate variability and predictability for southwest Western Australia

Neville Nicholls, Lynda Chambers, and Wasyl Drosdowsky
Bureau of Meteorology Research Centre, Melbourne

Report of Second Research Phase
for the
Indian Ocean Climate Initiative

"You get a quite different set of meteorological conditions in the Indian Ocean – quite different. Any fool knows that." (quoted in *Down Under*, Bill Bryson, Doubleday, 2000).

TABLE OF CONTENTS

LIST OF TABLES

LIST OF FIGURES

SUMMARY OF BMRC PHASE 1 IOCI WORK (FROM NICHOLLS ET AL., 1999)

"BMRC has, through the first half of the IOCI (1998-99), been investigating the following problems, for the southwest of Western Australia:

- Selection of high-quality climate data for the southwest
- How surprising is the decrease in rainfall?
- Has extreme rainfall declined as well as total rainfall?
- Is the rainfall decrease due to changes in atmospheric circulation?
- Is the rainfall decrease attributable to changes in Indian Ocean SSTs?
- Can we develop better methods for seasonal prediction in the southwest?
- How does the El Niño - Southern Oscillation affect southwest rainfall?
- Can climate models help us in seasonal prediction in the southwest?

Our achievements and preliminary conclusions from this work include:

- We have selected stations with high-quality daily/monthly rainfall, and daily temperature data over a long period, for analysis. These data sets can be made available to others interested in using high-quality climate data for the southwest.

- We have fitted statistical models to station rainfall and estimated the likely frequency of the observed runs of dry years in recent decades. They are unusual, in the historical context. We also have estimated breakpoints in the rainfall data series, where there is a sudden change in mean rainfall. The date of these breakpoints shows considerable spatial consistency, indicating that the breaks are real physical phenomena.

- Changes in the numbers of days of rain, and the amount of rain falling in extreme events, both have contributed to the decline in total rainfall.

- About half of the observed decline in rainfall is related to changes in regional atmospheric circulation, as represented by Perth atmospheric pressure. Part of the observed increase in Perth pressure represents changes in the El Niño - Southern Oscillation, as measured by the SOI. However, little of the observed rainfall decline is attributable to long-term changes in the El Niño - Southern Oscillation.

- Interannual variations in Indian Ocean SSTs are only weakly related to southwest rainfall, and even this weak relationship simply represents the effect of the El Niño - Southern Oscillation on both Indian Ocean SST and southwest rainfall, rather than an independent effect of the SSTs on rainfall. Since the interannual variations are not related, it seems unlikely that the long-term changes in both Indian Ocean SSTs and southwest rainfall are causally related. This conclusion is supported by the inability of climate models, when forced with observed SSTs over the 20th century to reproduce the observed decline in southwest rainfall.

- Secular changes have confounded the interannual relationships between the SOI and southwest rainfall, disguising some of the predictability achievable through the use of the SOI. An approach using year-to-year differences in the SOI has been proposed to overcome this confounding effect."

BMRC PROPOSAL FOR IOCI SECOND RESEARCH PHASE (JULY 1999-DECEMBER 2000) AGREED JUNE 1999

1. Specific seasonal climate forecast system for SWWA

- Develop techniques using changes in the SOI from year-to-year, to predict southwest WA rainfall for selected stations at selected times of the year and at selected lead-times.
- The possibility of developing an operational system for predicting summer climate factors, especially those relating to water demand, also will be investigated using near-global SSTs and the SOI.
- The selected stations, seasons, and lead-times of the forecasts have been chosen after discussions with WA agency representatives.
  The stations will include a station representative of the Perth catchments area (Jarrahdale), Manjimup, and Kalgoorlie. If possible, Mingenew, Merredin, and Lake Grace will also be analysed
  The seasons will be winter (for rainfall May-October), and summer (December-February), for factors affecting water demand, eg,, mean temperature, temperature extremes, and rainfall).
- The possibility of developing an operational system for forecasting winter rainfall at the end of April, using the SOI, will be investigated.
- The possibility of forecasting the summer demand factors using September data (SSTs and SOI) will be investigated.
- The possible value of the Antarctic Circumpolar Wave and southern Indian Ocean SSTs in prediction will be examined.

There is a perception that the Southern Oscillation Index (SOI), until recently the basis for operational *seasonal rainfall forecasting in Australia, is less effective in prediction for the southwest, relative to the eastern states. Nicholls (1989) identified a mode of variability of Indian Ocean SST that appeared to be related to rainfall in the south and southeast of the continent, somewhat distinct from the El Nino-Southern Oscillation mode affecting the eastern states. As a result, Drosdowsky and Chambers (1998) developed a new system for seasonal rainfall forecasting, now operationally implemented in the Bureau of Meteorology's National Climate Centre, using Indian and Pacific Ocean SST patterns as predictors (replacing the earlier system which used just the SOI as a single predictor). The new method provides a longer lead time for the predictions, is more stable, and exhibits somewhat increased skill. However, skill in the new system is still greater in the east and north of the country and the system seems less effective in the southwest. At the start of Phase 1, however, it was considered that further development of an SST- based system for seasonal prediction could lead to potentially useful forecasts for the southwest. This was because other work had identified an apparent link between southwest rainfall and Indian Ocean SSTs (eg, Smith et al 1999). However, work in Phase 1 found that interannual variations in Indian Ocean SSTs are only weakly related to southwest rainfall, and even this weak relationship simply represents the effect of the El Nino - Southern Oscillation on both Indian Ocean SST and southwest rainfall, rather than an independent effect of the SSTs on rainfall. Phase 1 work also revealed that secular changes have confounded the interannual relationships between the SOI and southwest rainfall, disguising some of the predictability achievable through the use of the SOI. An approach using year-to-year differences in the SOI has been proposed to overcome this confounding effect, and may lead to potentially useful seasonal rainfall forecasts based on the SOI, rather than SSTs. Other Phase I work has indicated that seasonal temperature for the southwest, at least in some seasons, may be predictable using SSTs.*

BMRC Proposal for IOCI Second Research Phase (July 1999- December 2000), agreed June 1999

2. Causes of decadal decline in rainfall in SWWA

- Empirical studies and model studies will be used to continue our investigations of the underlying causes of the recent trend in rainfall in the southwest.
- These investigations will include the use of model simulations forced with observed global SSTs, to determine whether the models can simulate the decline in rainfall.
- Path analysis will be used in empirical studies to provide further light on the causes of this decline.
- Variables such as wind direction will be investigated, to determine whether these can explain the apparent decline in rainfall and the secular changes in relationships between, for instance, the SOI and rainfall.

Since the interannual variations of southwest rainfall are not related to interannual variations in Indian *Ocean SSTs (see above), it seems unlikely that the long-term changes in Indian Ocean SSTs and southwest rainfall are causally related. This conclusion is supported by the inability of climate models, when forced with observed SSTs over the 20th century to reproduce the observed decline in southwest rainfall (Phase 1). Further model studies are needed to estimate the predictability of southwest rainfall from SSTs, using long-term simulations of the climate, and experimental model predictions conducted in real-time through 1997-98. As well, empirical studies using a path analysis technique may provide some guidance as to the possible causes of the apparent decline.*

****

Additions to BMRC Second Research Phase studies requested by IOCI7, 15 October 1999:

- Examine predictability of September-November rainfall (for agricultural purposes), from data available at end of May, end of June, end of July, using stations selected for winter and summer.
- Examine predictability of September-November temperature (for curing for fire risk), from data available at end of May, end of June, end of July, using stations selected for winter and summer.
- Examine predictability of wheat yield (David Stephens to provide time series of wheat yield data).

Further additions (March-May 2000):

- Investigate whether equatorial Indian Ocean SST dipole is independent of the El Niño - Southern Oscillation, and consider its possible use in seasonal prediction for SWWA.
- Investigate whether long-term variations in SWWA rainfall are related to distant factors (e.g., rainfall trends in other parts of the globe).
- Investigate whether SST gradients in the Indian Ocean are useful predictors for SWWA

RESULTS OF SECOND RESEARCH PHASE

Specific seasonal climate forecast system for SWWA

Seasonal climate predictability

Target forecasts

The forecasts requested were:

- Winter (May to October) rainfall using the SOI and sea surface temperatures (SSTs) up to the end of April
- Spring (September to November) rainfall using the SOI and SSTs up to the end of May, end of June and end of July
- Spring (September to November) temperature (mean, mean maximum and mean minimum) using the SOI and SSTs up to the end of July
- Summer (December to February) rainfall using the SOI and SSTs up to the end of September
- Summer (December to February) mean maximum temperature
- Summer (December to February) temperature extremes

When considering extreme temperatures, the mean maximum temperature, the number of days over 35°C, and the number of days over 40°C were examined.

Method

A statistical forecast scheme similar to that of Drosdowsky and Chambers (1998) and Jones (1998) was adopted. This is an empirical forecast scheme based upon linear discriminant analysis. Lagged values of the predictor variables time series (eg., SST time scores, SOI) are used to forecast the probability of the predictand (eg., rainfall) being in pre-defined categories (terciles - three equally probable categories). Linear Error in Probability Space (LEPS) was used to assess the potential skill of the prediction systems, using cross-validation to account for artificial skill (Drosdowsky and Chambers, 1998). The LEPS skill score ranges from 100 (for perfect forecasts) to –100 (worst possible forecasts). Positive values over indicate potentially useful forecast system. LEPS is notoriously difficult to interpret, other than in relative terms (i.e., comparing two forecast methods). We provide, therefore, scatter diagrams of predictor versus predictand for selected, representative pairs of predictor-predictand, to allow a more ready interpretation of skill. These also illustrate how typical ranges of LEPS translate into more readily interpretable skill scores such as the number of "hits".

Station Information

Available data for the six sites of interest are listed in Table 1. As the forecast models were based on data from 1950 to the present, some filling of the temperature data sets was needed and is described below. For most of the stations in Table 1 additional temperature data, to fill in the missing data, were available from stations within a 100 km (or even 50 km) radius. Table 2 lists the additional temperature stations selected for further testing for each of the stations of interest (Table 1).

Table 1: Station information. * indicates that temperature data is available from 1957 from a site within a few kilometres (09573).

Station Name	Station Number	Rainfall From	Temperature From/To
Mingenew	08088	1896	1965-1975
Jarrahdale	09023	1882	not available
Lake Grace	10592	1912	1956 -
Merredin	10092	1903	1966 -
Manjimup	09619	1900	not available*
Kalgoorlie	12013	1897	not available

Table 2: Additional stations (used for filling missing data).

Station Name	Additional Station Numbers
Mingenew	08025, 08039, 08051, 08093, 08095
Jarrahdale	09021, 09538, 09534, 10648
Lake Grace	10073, 10035, 10536, 10579
Merredin	10007, 10035, 10073, 10093, 10536
Manjimup	09510, 09534, 09538, 09573
Kalgoorlie	10073, 10092, 10093, 12038

A simple linear correlation test was used to select the station (or stations) with the strongest (linear) relationship to the stations in Table 1. In the case where no temperature was recorded at the station in Table 1 the closest station was used and gaps filled using other nearby stations. For Jarrahdale the closest station was 09538, for Manjimup, 09573 and for Kalgoorlie, 12038. Table 3 lists the order in which stations were used to fill gaps. The first station listed was used unless a gap exists in that record, in which case the second station was used, and so on. On all occasions we were able to fill all gaps using the lists in Table 3 and, in most cases, used only the first 2 or 3 stations.

Table 3: Order of stations used to fill gaps in the record.

Station Name	Station Order
Mingenew	08088, 08095, 08093, 08025, 08039
Jarrahdale	09538, 09021, 09534, 10648
Lake Grace	10592, 10536, 10579, 10073, 10035
Merredin	10092, 10093, 10007, 10035, 10073
Manjimup	09573, 09510, 09534, 09538
Kalgoorlie	12038, 10092, 10093, 10073

Linear regression was used to relate the temperature at the stations in Table 1 (or the first station in the list of Table 3) with subsequent stations in the list (Table 3), for gap filling.

Predictors

Time series of the first two principal components (SST1 & SST2) of a near global empirical orthogonal function (EOF) analysis of sea surface temperatures (SST) were included as possible predictors. The first EOF, SST1, (Figure 1) has highest loadings in the central and eastern equatorial Pacific Ocean and in the Indian Ocean and represents the mature phase of an El Niño / Southern Oscillation (ENSO) event. The second EOF, SST2, has highest loadings just west of the Australian continent,

extending northwest to the central equatorial region. The southern oscillation index (SOI) was also included as a potential predictor.

Winter (May to October)

Forecasts were made for winter (May to October) rainfall terciles at each of the six stations in Table 1. A number of different predictors were considered:

April SST1;
April SST2;
April SST1 and SST2;
February and April SST1;
February and April SST2;
February and April SST1 and SST2;
February to April (FMA) SST1;
FMA SST2;
FMA SST1 and SST2;
Mean of December to February (DJF) and FMA SST1;
DJF and FMA SST2;
DJF and FMA SST1 and SST2;
April SOI;
February and April SOI;
FMA SOI; and
DJF and FMA SOI.

This represents a total of 16 possible forecast systems for each of the six stations, i.e. there are four systems using the SOI (with the SOI in different as predictor), four using just SST1, four using SST2, and four systems using both SST1 and SST2.

Table 4 lists the number of times that a positive LEPS score was obtained from these various systems, categorised according to whether the SOI, SST1 only, SST2 only, or both SST1 and SST2, were used. The LEPS scores were below 10 in all cases, with the highest LEPS score of 7.73 for Manjimup using the DJF and FMA SOI values.

Table 4: Winter Rainfall: Number of positive LEPS scores obtained. A maximum of four is possible in each of the grid cells.

Station Name	SST1	SST2	SST1&2	SOI
Mingenew	2	1	2	1
Jarrahdale	3	0	1	3
Lake Grace	2	0	1	2
Merredin	0	0	0	0
Manjimup	4	1	2	4
Kalgoorlie	1	1	1	1

The skill of the forecast systems was also examined using the first differences of all the data (i.e., the rainfall, SST and SOI data series). The results are summarised in Table 5. The number of skilful rainfall forecasts for Mingenew increased when the data were differenced, while for Manjimup the number tended to decrease. As was the case with the "raw", undifferenced data, there were no LEPS scores over 10. The highest score was 5.47, for Mingenew using DJF and FMA SSTs 1 and 2.

The question of whether these forecasts could be improved by using May, April and May (MAM), or JFM and MAM SSTs or SOI values, was then addressed. The results for the raw data are listed in Table 6, while Table 7 lists the results for the first differenced data. Comparing Tables 4 and 6 indicates that there are some improvements in skill when using the later data in the forecasts (Table 6). This is also

the case for the differenced data (compare Tables 5 and 7). With the later data used in the forecast we get the first LEPS score over 10 (11.48 for Manjimup using May SST1 and 2 values). The LEPS scores for the differenced data were generally lower than for the raw data.

Table 5: Differenced Winter Rainfall: Number of positive LEPS scores obtained for first differenced data. A maximum of four is possible in each of the grid cells.

Station Name	SST1	SST2	SST1&2	SOI
Mingenew	4	1	4	0
Jarrahdale	2	3	2	0
Lake Grace	1	0	0	1
Merredin	0	2	2	2
Manjimup	0	2	0	0
Kalgoorlie	0	2	1	1

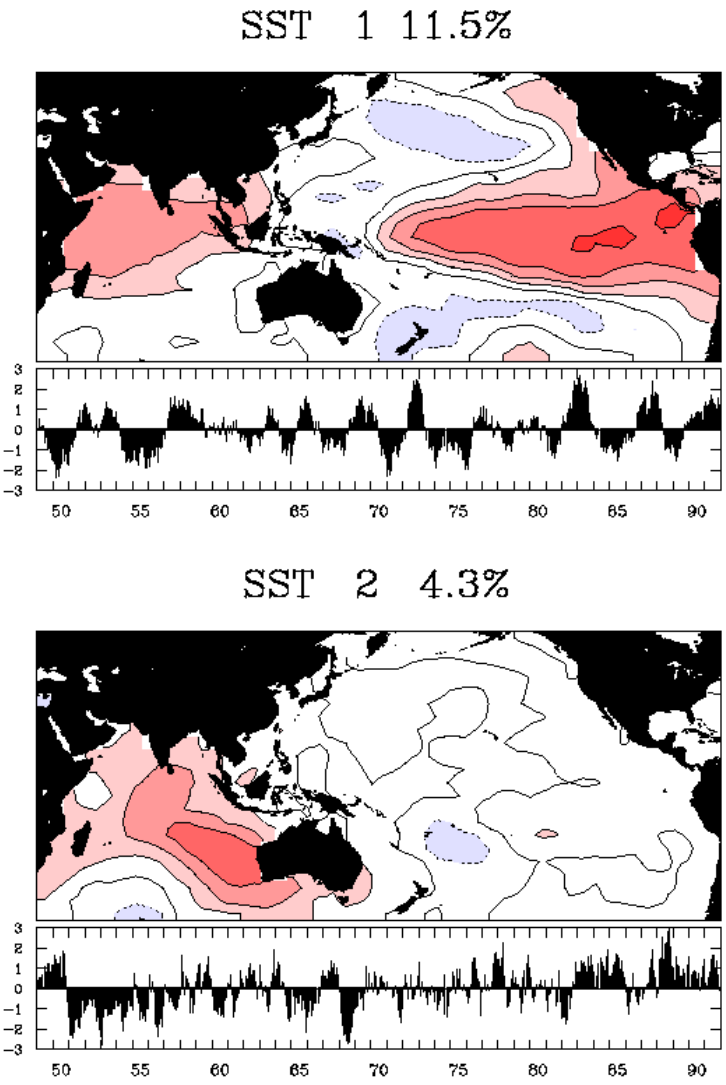

Figure 1. First two VARIMAX rotated empirical orthogonal functions (EOFs) of the standardised monthly anomalies of the sea surface temperature data (Drosdowsky and Chambers, 1998).

Table 6: Winter Rainfall using later predictors: Number of positive LEPS scores obtained. A maximum of four is possible in each of the grid cells.

Station Name	SST1	SST2	SST1&2	SOI
Mingenew	2	0	0	4
Jarrahdale	4	0	3	4
Lake Grace	4	0	2	4
Merredin	2	0	0	0
Manjimup	3	2	2	1
Kalgoorlie	1	1	1	1

Table 7: Differenced Winter Rainfall using later predictors: Number of positive LEPS scores obtained for first differenced data. A maximum of four is possible in each of the grid cells, except for SST1&2 where only three combinations were possible.

Station Name	SST1	SST2	SST1&2	SOI
Mingenew	4	3	1	1
Jarrahdale	0	1	0	0
Lake Grace	0	2	1	3
Merredin	0	1	0	1
Manjimup	0	1	1	1
Kalgoorlie	4	0	2	0

No predictor set gave positive LEPS scores for all six stations. Overall, the performance of the linear forecast techniques on winter rainfall was poor, with little evidence that useful forecasts would be obtainable.

Spring (September to November)

Rainfall

A similar analysis to that outlined above was carried out for spring (September to November) rainfall. Four groups of analyses were considered. These used predictors available at the end of May, June or July, or used differenced data with predictors ending in July. Tables 8 to 10 indicate that the prediction of spring rainfall was generally more skillful when using data from up until the end of July rather than relying only on the earlier (May or June) predictors. However, the skill levels in all cases were fairly low with very few cases of LEPS scores over 10. The 'best' predictor overall, when using data until the end of July, was (marginally) SST1. However, if Mingenew and Kalgoorlie are excluded, then the SOI is also a potentially useful predictor. For most stations, using differenced data tended to either reduce the skill of the predictions, or have little effect (Merredin and Kalgoorlie).

Table 8: Spring rainfall (predictors until end of May): Number of positive LEPS scores obtained. A maximum of four is possible in each of the grid cells (i.e., using either May, March and May, MAM, or JFM and MAM, as predictors). The number of LEPS scores greater than 10 are given in brackets.

Station Name	SST1	SST2	SST1&2	SOI
Mingenew	0 (0)	2 (0)	1 (0)	0 (0)
Jarrahdale	4 (0)	4 (0)	4 (0)	3 (0)
Lake Grace	2 (0)	4 (0)	4 (0)	4 (0)
Merredin	0 (0)	0 (0)	0 (0)	4 (0)
Manjimup	4 (1)	1 (0)	4 (1)	4 (0)
Kalgoorlie	1 (0)	0 (0)	0 (0)	0 (0)

Table 9: Spring rainfall (predictors until end of June): Number of positive LEPS scores obtained. A maximum of four is possible in each of the grid cells (June, April and June, AMJ, FMA and AMJ). There were no LEPS scores greater than 10.

Station Name	SST1	SST2	SST1&2	SOI
Mingenew	0	3	2	0
Jarrahdale	4	4	4	4
Lake Grace	3	3	4	3
Merredin	1	0	0	3
Manjimup	4	1	4	4
Kalgoorlie	0	0	0	1

Table 10: Spring rainfall (predictors until end of July): Number of positive LEPS scores obtained. A maximum of four is possible in each of the grid cells (July, May and July, MJJ, MAM and MJJ). The number of LEPS scores greater than 10 are given in brackets.

Station Name	SST1	SST2	SST1&2	SOI
Mingenew	2 (0)	2 (0)	4 (0)	0 (0)
Jarrahdale	4 (0)	4 (0)	4 (0)	4 (0)
Lake Grace	2 (0)	4 (0)	4 (0)	4 (0)
Merredin	2 (0)	0 (0)	0 (0)	3 (0)
Manjimup	4 (1)	3 (0)	4 (1)	4 (0)
Kalgoorlie	1 (0)	1 (0)	1 (0)	0 (0)

Table 11: Differenced Spring Rainfall (predictors until end of July): Number of positive LEPS scores obtained for first differenced data. A maximum of four is possible in each of the grid cells, except for SST1&2 where there were only three possible combinations. There were no LEPS scores over 10.

Station Name	SST1	SST2	SST1&2	SOI
Mingenew	1	1	1	2
Jarrahdale	2	3	2	1
Lake Grace	4	2	3	2
Merredin	2	0	1	3
Manjimup	3	0	1	2
Kalgoorlie	1	1	0	3

Temperature

Forecast systems for mean temperature, and for mean maximum and mean minimum temperatures for spring (September to November) were tested. As spring rainfall was best predicted using data until the end of July, spring temperature predictions were only tested with systems using data available up to the end of July (rather than only using earlier data). SST1&2 gave the highest LEPS scores for spring mean temperature, though SOI and SST1 also performed fairly well (Table 12).

Table 12: Spring mean temperature: Number of positive LEPS scores obtained. A maximum of four is possible in each of the grid cells. The number of LEPS scores greater than 10 are given in brackets.

Station Name	SST1	SST2	SST1&2	SOI
Mingenew	4 (0)	0 (0)	3 (0)	4 (0)
Jarrahdale	4 (4)	4 (4)	4 (4)	4 (2)
Lake Grace	4 (0)	2 (0)	4 (0)	4 (0)
Merredin	4 (3)	4 (0)	4 (4)	4 (4)
Manjimup	4 (0)	4 (0)	4 (0)	4 (4)
Kalgoorlie	4 (0)	4 (0)	4 (0)	4 (0)

The SOI was the ‘best’ predictor of spring mean maximum temperature (Table 13), though no method worked particularly well for Manjimup. SST2 was the clearly the worst potential predictor of spring mean maximum temperature. No methods worked particularly well for Manjimup.

Table 13: Spring mean maximum temperature: Number of positive LEPS scores obtained. A maximum of four is possible in each of the grid cells. The number of LEPS scores greater than 10 are given in brackets.

Station Name	SST1	SST2	SST1&2	SOI
Mingenew	4 (0)	0 (0)	4 (0)	4 (0)
Jarrahdale	4 (2)	1 (0)	3 (1)	4 (2)
Lake Grace	4 (0)	0 (0)	4 (0)	4 (1)
Merredin	4 (2)	0 (0)	4 (0)	4 (3)
Manjimup	1 (0)	0 (0)	0 (0)	1 (0)
Kalgoorlie	2 (0)	2 (0)	2 (0)	4 (0)

The most consistently skilful system, over all stations, of spring mean minimum temperature (Table 14) used both SST 1&2, however SST1, SST2, and the SOI also performed relatively well for most stations. The LEPS scores associated with prediction of mean minimum temperature were generally higher than those for mean spring temperature, and much greater than those for mean maximum temperature. The results of using differenced spring mean minimum temperatures are in Table 15. When differenced data were used the resulting LEPS scores were considerably lower than for the raw data (except for Mingenew using SST2). This is particularly evident when using SST1 or SST1&2.

Table 14: Spring mean minimum temperature: Number of positive LEPS scores obtained. A maximum of four is possible in each of the grid cells. The number of LEPS scores greater than 10 are given in brackets.

Station Name	SST1	SST2	SST1&2	SOI
Mingenew	4 (0)	0 (0)	4 (0)	4 (0)
Jarrahdale	4 (0)	4 (4)	4 (4)	4 (1)
Lake Grace	4 (0)	4 (4)	4 (4)	4 (1)
Merredin	4 (0)	4 (4)	4 (4)	4 (4)
Manjimup	4 (4)	4 (0)	4 (4)	4 (4)
Kalgoorlie	4 (0)	4 (0)	4 (0)	4 (0)

Table 15: Spring mean minimum temperature: Number of positive LEPS scores obtained for first differenced data. A maximum of four is possible in each of the grid cells.

Station Name	SST1	SST2	SST1&2	SOI
Mingenew	2	4	3	3
Jarrahdale	0	2	0	2
Lake Grace	0	3	1	4
Merredin	0	4	3	4
Manjimup	0	4	3	4
Kalgoorlie	0	4	2	2

Summer (December to February)

Rainfall

A similar analysis was carried out for summer (December to February) rainfall. Here September, July and September, averaged July to September (JAS), and averaged May to July (MJJ) and JAS SST and SOI data were used to forecast the rainfall. The results for the raw data are given in Table 16 and for the first differenced data in Table 17.

From Table 16 it is clear that the SST forecast system tends to perform better than the SOI based system for summer rainfall. Comparing Tables 4, 6, 10 and 16 it is also apparent that forecasts of summer rainfall have generally higher LEPS scores than those for winter and spring, with a number of LEPS scores over 10. There are now four combinations of predictors that give positive LEPS scores for all six stations: September SSTs 1 and 2; JAS SSTs 1 and 2; MJJ and JAS SST1 only; and MJJ and JAS SSTs 1 and 2.

When the differenced data were used the LEPS scores were greatly reduced with no LEPS scores over 8 and many negative scores (Table 17). No set of (differenced) predictors gave positive LEPS scores for all six stations.

Table 16: Summer rainfall: Number of positive LEPS scores obtained. A maximum of four is possible in each of the grid cells. The number of LEPS scores greater than 10 are given in brackets.

Station Name	SST1	SST2	SST1&2	SOI
Mingenew	4 (0)	4 (0)	4 (4)	2 (0)
Jarrahdale	4 (0)	4 (0)	4 (0)	1 (0)
Lake Grace	4 (3)	0 (0)	4 (3)	4 (0)
Merredin	3 (0)	4 (0)	4 (3)	0 (0)
Manjimup	1 (0)	4 (0)	3 (0)	0 (0)
Kalgoorlie	4 (0)	1 (0)	4 (0)	1 (0)

Table 17: Summer rainfall: Number of positive LEPS scores obtained for first differenced data. A maximum of four is possible in each of the grid cells, except for SST1&2 where only three combinations were possible. There were no LEPS scores over 10.

Station Name	SST1	SST2	SST1&2	SOI
Mingenew	0	2	1	0
Jarrahdale	0	1	0	2
Lake Grace	1	0	0	0
Merredin	0	1	0	1
Manjimup	0	2	1	1
Kalgoorlie	0	1	0	1

Mean Maximum Temperature

Using the same set of predictors as for summer rainfall the average maximum summer (DJF) temperature was forecast and the skill assessed using LEPS scores. The results are given in Table 18 (raw data) and Table 19 (differenced data).

Table 18: Summer mean maximum temperature: Number of positive LEPS scores obtained. A maximum of four is possible in each of the grid cells. The number of LEPS scores greater than 10 are given in brackets.

Station Name	SST1	SST2	SST1&2	SOI
Mingenew	1 (0)	2 (0)	3 (0)	2 (0)
Jarrahdale	4 (1)	0 (0)	3 (1)	2 (0)
Lake Grace	4 (0)	2 (0)	4 (0)	3 (0)
Merredin	4 (0)	0 (0)	4 (0)	4 (0)
Manjimup	1 (0)	4 (1)	4 (2)	0 (0)
Kalgoorlie	2 (0)	0 (0)	0 (0)	1 (0)

Only one set of predictors gave positive LEPS scores for all stations: JAS SST 1 only, though all the LEPS scores were less than 5. When differenced the SST forecast

schemes generally gave lower LEPS scores than the SOI based schemes. The only differenced scheme to give positive LEPS scores at all six stations (one over 10) was MJJ and JAS SOI.

Table 19: Summer mean maximum temperature: Number of positive LEPS scores obtained for first differenced data. A maximum of four is possible in each of the grid cells, except for SST1&2 where only three combinations were possible.

Station Name	SST1	SST2	SST1&2	SOI
Mingenew	1	2	0	1
Jarrahdale	0	0	0	2
Lake Grace	0	0	0	1
Merredin	0	2	0	3
Manjimup	0	0	0	4 (2)
Kalgoorlie	0	2	1	2

Number of days over 35°C

Forecasts of the number of days over 35°C were made using the same predictors as for summer rainfall. The results are given in Table 20. Merredin and Manjimup are the 'best' forecast stations with positive LEPS scores regardless of the predictors used. The only predictor to give positive LEPS scores for all six stations was JAS SST1.

Table 20: Number of days over 35°C: Number of positive LEPS scores obtained. A maximum of four is possible in each of the grid cells. The number of LEPS scores greater than 10 are given in brackets.

Station Name	SST1	SST2	SST1&2	SOI
Mingenew	4	0	4	2
Jarrahdale	2	0	2	2
Lake Grace	2	0	0	1
Merredin	4	4	4	4
Manjimup	4	4	4 (2)	4
Kalgoorlie	2	0	0	4

Number of days over 40°C

Forecasts of the number of days over 40°C were made using the same predictors as for summer rainfall (Table 21). No forecasts were possible for Jarrahdale and Lake Grace. Only Kalgoorlie (using SSTs 1 and 2) had LEPS scores over 10. Except for Kalgoorlie, the LEPS scores for forecasts of the number of days over 40°C were generally lower than for forecasts of the number of days over 35°C.

Table 21: Number of days over 40°C: Number of positive LEPS scores obtained. A maximum of four is possible in each of the grid cells. The number of LEPS scores greater than 10 are given in brackets.

Station Name	SST1	SST2	SST1&2	SOI
Mingenew	1	0	0	2
Merredin	0	1	0	0
Manjimup	1	3	1	0
Kalgoorlie	4	2	4 (2)	4

Summary

Overall the results presented above are mixed.

There does appear to be some skill in predicting summer rainfall, summer mean maximum temperature, and extreme temperature events (such as the number of days over 35°C). In general, for the raw data, predictions using SST1 only or SST1 and SST2 together tended to give more consistently positive LEPS scores than those using SST2 only or the SOI. However, when the original data were differenced the SOI and SST2 only tended to give better results.

For winter rainfall, the LEPS scores tended to be lower than for summer rainfall and temperature forecasts. There were mixed results with forecasts for Mingenew showing some skill both in the raw and differenced data. The stations selected in this analysis differ in their yearly rainfall distributions with Mingenew and Kalgoorlie having less peaked winter rainfall maxima. This may mean that different predictors could be needed for Mingenew and Kalgoorlie than for the other stations.

The skill obtainable for spring rainfall predictions lies between that of summer and winter rainfall. In order of increasing overall skill, the spring predictions were rainfall, mean maximum temperature, mean temperature and mean minimum temperature, with the temperature forecasts tending to have considerably greater skill than the rainfall forecasts. There appears to be some skill in predicting spring temperatures, and to some extent rainfall, using data up to the end of July.

A few representative illustrations of the strength of the better relationships are shown in Figures 2-5. The degree to which the symbols for the three terciles are separated in the figures indicates the strength of the predictive relationships.

The first example (Figure 2) shows the prediction of September-November rainfall using May-July values of the SST predictors. This example has a moderate LEPS score and there is considerable separation of the tercile symbols, suggesting a potentially useful level of skill.

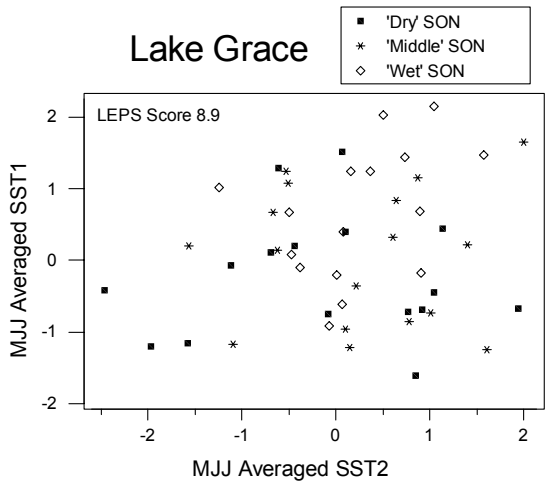

Figure 2: Lake Grace September-November rainfall versus May-July SST patterns

Figure 3 illustrates that summer rainfall exhibits some predictability, with most wet summers at Manjimup being preceded by negative values of SST1 in July-September, i.e., La Niña episodes. One of the higher values of LEPS scores, 21.6, is illustrated in Figure 4, which shows that September-November mean minimum temperature at Jarrahdale appears to be strongly related to values of the SST patterns in May-July. Finally, extreme summer temperatures, as measured by the number of days with maximum temperatures exceeding 35ºC at Lake Grace, seem to be predictable using July-September SST patterns (Figure 5).

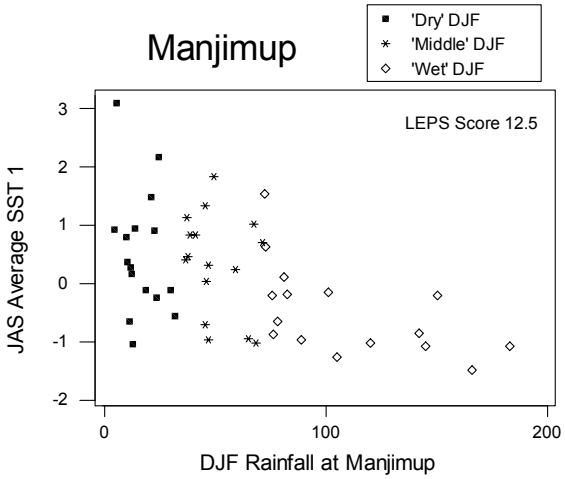

Figure 3: Manjimup summer rainfall versus July-September SST1

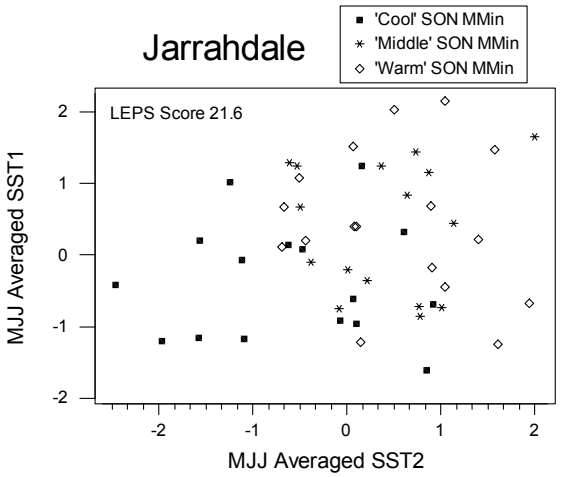

Figure 4: Jarrahdale September-November mean minimum temperature versus SST1 & SST2 in May-July

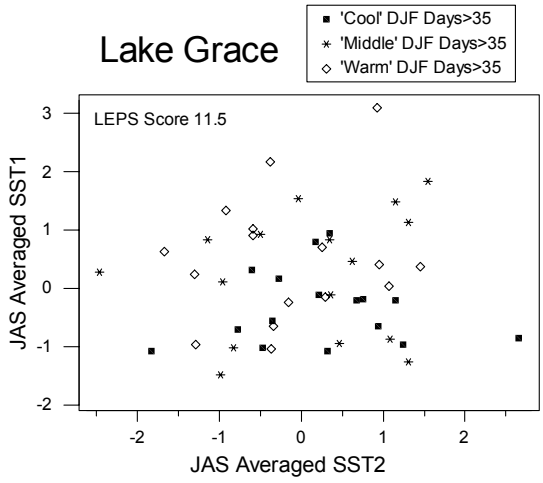

Figure 5: Number of days at Lake Grace in December-February with maximum temperatures exceeding 35C, versus SST patterns in July-September

Sea Surface Temperature Gradients and Prediction

Some preliminary work suggested that SST gradients in the Indian Ocean might be of use in predicting SWWA rainfall, especially during winter (May-October). A comprehensive study of this possibility was undertaken, in an attempt to determine if other SST predictors other than SST1 and SST2 could provide useful predictive information.

Rainfall and Temperature Data

May to October rainfall totals and averaged May to October temperature data were available for Mingenew, Jarrahdale, Manjimup, Merredin, Lake Grace and Kalgoorlie.

SST Data

We used 2-degree reconstructed near-global SST (NCEP) data from the period 1950 to 1998. This data was then averaged to produce a 4° x 4° gridded data set, covering latitudes 44° S to 68° N. Temperature gradients were obtained by calculating the latitudinal change in temperature from one grid box to the next.

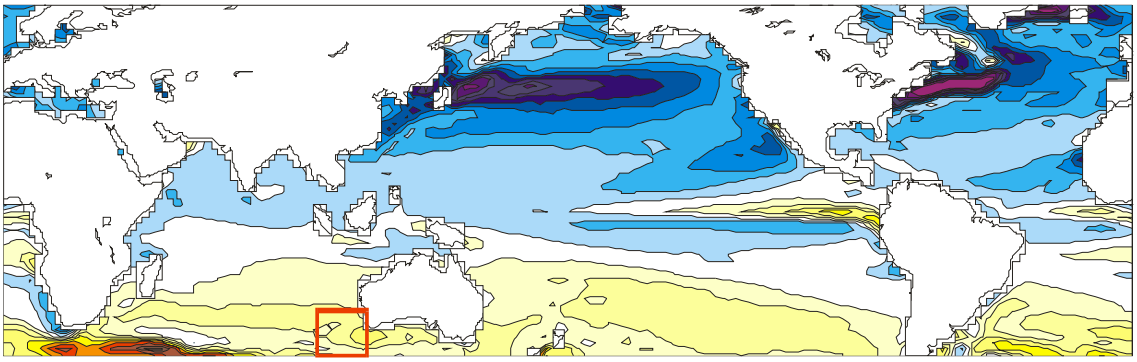

Figure 6. Averaged May to October SST gradients (1950 to 1998). The red box shows the location of the 9 gradient boxes (each 4° latitude x 4° longitude) mentioned in the text.

Correlations of SST Gradients with SW Rainfall

A group of nine SST gradient grid boxes, covering the region 29° to 41° S and 104° to 116° E, were selected as potential SWWA rainfall and temperature predictors (see Figure 6). The selection of these boxes was based on unpublished work by Dr. D. A. Jones who found that an SST gradient box within this region was highly correlated with winter rainfall at Manjimup during the period 1982 to 1994. The relationship was less strong when longer time periods were used, indicating a possible change in the relationship between rainfall and SST gradients in the SWWA area may have occurred sometime prior to 1982.

When a similar analysis was carried out using the SST gradients described above, two of the nine SST gradient boxes indicated possible predictive skill for Manjimup winter rainfall, particularly when only using more recent years. Table 22 lists the correlations (and significance levels) for two of the gradient boxes. Table 22 indicates that a change in the relationship between the SST gradients and Manjimup

rainfall most likely occurred prior to 1965. The relationship is shown graphically in Figure 7.

Table 22.Simultaneous correlation of SST gradient boxes with Manjimup May to October rainfall. Box 3 is centred on 106°E, 31°S and Box 8 on 114°E, 35°S. The p-values for the correlation coefficients are given in brackets.

Period	Box 3	Box 8
1950-1998	0.148 (0.311)	0.050 (0.736)
1965-1998	0.429 (0.011)	0.377 (0.028)
1982-1998	0.812 (0.000)	0.583 (0.018)

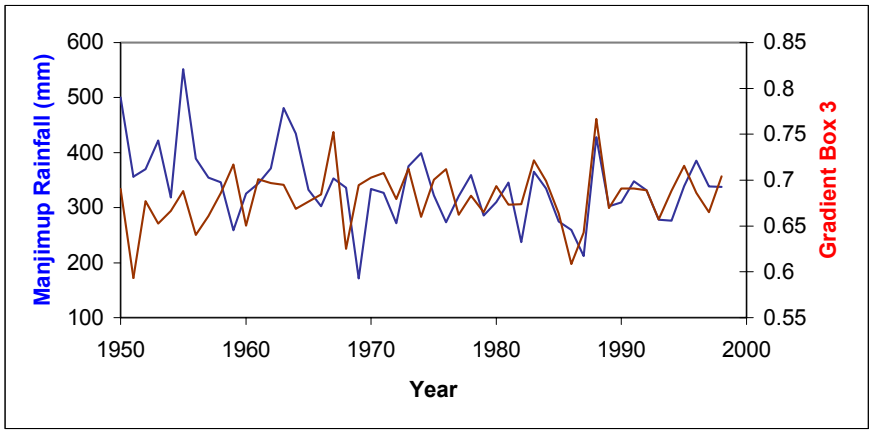

Figure 7. Graphical illustration of the relationship between SST gradient in Box 3 and Manjimup May to October rainfall.

Rainfall Tercile Prediction Using SST Gradients

When the full data set (1950 to 1998) is used to assess the potential to predict May to October rainfall from SST Gradients no significant skill is obtained.

If data from the period 1965 to 1998 only is used, marginally skilful rainfall predictions were possible for Manjimup using a single months SST gradient (Box 3; from February to May) with slight increases in skill achievable if three month averaged SST gradients are used (see Table 23). No significant skill was achieved for the other five rainfall stations.

Although the number of years in the period 1982 to 1998 is relatively small, the skill of rainfall predictions, using SST gradients for Boxes 3 and 8 was assessed with the results given in Tables 24 and 25. For brevity only the results for the single month gradients are given with generally no improvement in skill being obtained using three-month average gradients.

Table 23.LEPS skill scores for prediction of Manjimup May to October rainfall using Box 3 (centred on 106°E, 31°S) SST gradients. Data used is 1965 to 1998.

Gradient Month	LEPS Score	Gradient Months	LEPS Score
Jan	-1.21	11-1	3.54
Feb	4.01	12-2	4.95
Mar	1.28	1-3	4.30
Apr	5.43	2-4	8.11
May	3.19	3-5	6.23

Gradient Box 3 appears to provide the best predictions of May to October rainfall, particularly for Manjimup, with some moderate skill at Mingenew, Jarrahdale and Lake Grace in April and May. Forecasts using May gradient values however, are of little use as there is no lead-time.

Table 24.LEPS skill scores for the prediction of May to October rainfall using Box 3 (centred on 106°E, 31°S) SST gradients. Data used is 1982 to 1998.

Gradient Month	Mingenew	Jarrahdale	Manjimup	Merredin	Lake Grace	Kalgoorlie
Jan	-5.53	-5.92	-7.20	7.23	1.87	2.52
Feb	-6.40	-6.73	4.19	-4.89	-5.95	-7.99
Mar	2.16	-4.75	4.49	3.81	-2.73	-6.89
Apr	6.21	4.96	18.65	-1.07	2.14	-2.76
May	4.64	12.53	19.68	-6.56	15.42	-7.58

Table 25.LEPS skill scores for the prediction of May to October rainfall using Box 8 (centred on 114°E, 35°S) SST gradients. Data used is 1982 to 1998.

Gradient Month	Mingenew	Jarrahdale	Manjimup	Merredin	Lake Grace	Kalgoorlie
Jan	-5.00	-6.44	-6.64	-4.08	-3.85	-6.18
Feb	-7.18	-4.11	-2.85	-4.76	-6.84	-2.99
Mar	-7.28	-4.02	-4.08	8.72	16.23	-3.41
Apr	-0.69	-3.32	5.20	-5.72	-4.38	-3.62
May	-0.99	-1.63	6.28	-2.92	-7.39	-7.76

Temperature Tercile Prediction Using SST Gradients

As for rainfall the potential predictability of temperature variables using SST gradients was first tested using the full data set (1950 to 1998). Simultaneous correlations for two of the nine SST gradient boxes are given in Table 26. Gradient

Box 3 generally gave the highest correlation values with significant correlations for all six temperature stations. Gradient Box 9 (results not shown) had significant correlations with all six temperature stations, however the values were generally lower than those for Box 3. As an example, the relationship between SST gradient Box 3 and Lake Grace May to October mean temperature is graphically illustrated in Figure 8.

Table 26.Simultaneous correlation of SST gradient boxes with station May to October mean temperature (1950 – 1998). Box 3 is centred on 106°E, 31°S and Box 8 on 114°E, 35°S. The p-values for the correlation coefficients are given in brackets.

Station	Box 3	Box 8
Mingenew	0.385 (0.006)	0.266 (0.065)
Jarrahdale	0.487 (0.000)	0.371 (0.009)
Manjimup	0.375 (0.008)	0.197 (0.175)
Merredin	0.467 (0.001)	0.342 (0.016)
Lake Grace	0.467 (0.001)	0.281 (0.050)
Kalgoorlie	0.501 (0.000)	0.306 (0.032)

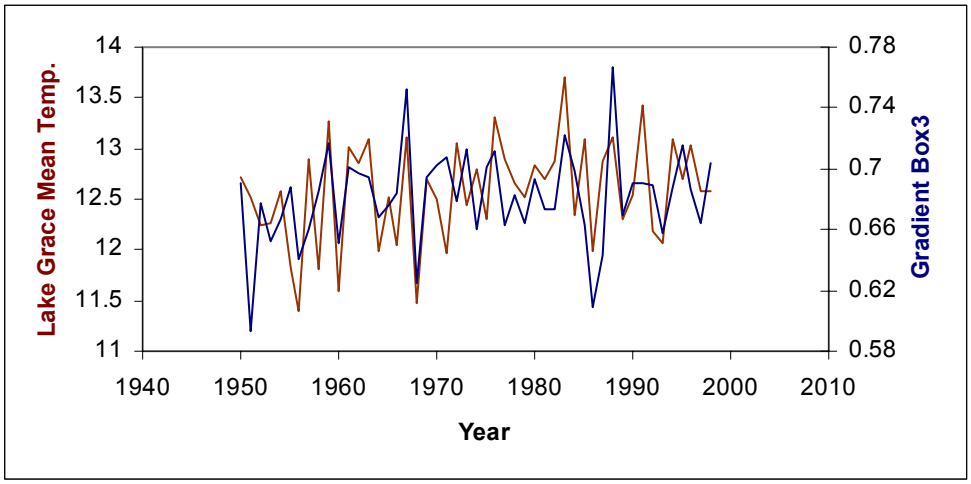

Figure 8. May to October Lake Grace mean temperature and May to October SST gradient Box 3.

Table 27.LEPS skill scores for the prediction of May to October mean temperature, using SST gradient Box 3. Data used is 1950 to 1998. Similar results were obtained when using three-month averaged SST gradients.

Gradient Month	Mingenew	Jarrahdale	Manjimup	Merredin	Lake Grace	Kalgoorlie
Jan	-2.00	-1.63	-2.17	-1.99	-1.99	0.31
Feb	-1.83	-2.00	-1.34	0.28	-1.21	-1.42
Mar	5.38	1.66	0.77	0.67	2.53	2.03
Apr	2.04	2.01	-0.98	4.55	0.95	1.27
May	4.62	0.90	-1.44	0.43	-1.88	3.70

Although generally high correlation values were found for simultaneous May to October mean temperature and SST gradient Box 3 the predictive ability of SST gradient Box 3 was not high (Table 27). Unlike the case with rainfall (see Figure 3) there were no obvious changes in the relationship between the SST gradients and mean temperature (see Figure 8). Therefore analyses were not carried out for shorter time periods.

Summary

Overall, the results of these tests of the use of SST gradients in winter prediction were somewhat disappointing. There was little evidence that the gradients could produce useful temperature forecasts. There was some evidence that winter rainfall predictions might be possible. However, this was only so using recent data – the earlier data showed no predictive relationship. This may suggest that earlier data were of poor quality. Retesting with future data will be required to confirm whether the recent predictability is real.

Wheat yield predictability

The most disappointing result from the above studies was the low skill apparently achievable for predicting winter rainfall, using either the SOI or SST patterns. Winter rainfall is clearly of importance for agricultural purposes, so it appears that the chances of forecasting crop yields are low. Nevertheless, a preliminary examination of the predictability of wheat yields was undertaken, for the shire of Yilgarn.

Data

A long term data set of shire-level wheat yields for the shire of Yilgarn (of which Southern Cross is a major town) was provided by D. Stephens of Agriculture Western Australia. These data were based on Australian Bureau of Statistics (ABS) census data from 1930 to 1996 and a sample survey (not a full census) for 1997. This data set had not been adjusted for advances in farming techniques so a simple linear regression against year was used to adjust the yields over the period 1950 to 1997. The raw and

adjusted yields are shown in Figure 9. The period 1950 to 1997 was chosen as it overlaps with the other data sets mentioned below.

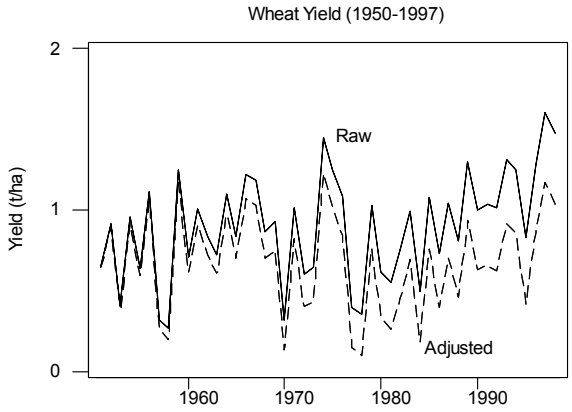

Figure 9. Raw and adjusted wheat yields for Yilgarn shire, 1950 to 1997.

High-quality monthly rainfall data were available from Kalgoorlie to the east of Southern Cross, and from Merredin to the west of Southern Cross. The period of rainfall records used in this study was 1949 to 1997. Monthly temperature data (mean minimum, mean maximum and diurnal temperature range or DTR) were also available at Merredin and Kalgoorlie.

Method

A statistical forecast scheme, similar to that used above for prediction of rainfall and temperature, was adopted for wheat yield prediction. Lagged values of the predictor variables time series (rainfall at Kalgoorlie, SST time score series, SOI) are used to forecast the probability of the wheat yield in pre-defined categories. In this study predictions were made for both wheat yield terciles (three equally probable categories) and medians (two equally probable categories).

Results

Table 28 lists the skill scores for tercile forecasts of wheat yield. Only months one to ten (January to October) are used to forecast the yield. It is evident from Table 1 that skilful prediction of wheat yield using SST1, SST2, SST1 and SST2 or the SOI is unlikely. A similar analysis using 3-month averaged SST and SOI values, with the average ending in month m, was also conducted but resulted in skill scores similar to those in Table 28.

Table 28.LEPS skill scores for wheat yields (terciles). The predictor month used to forecast the yield is given in brackets. For example, the first row of data is for January (m=1) and predictors using (m, m-2) use January and November (of the previous year).

Month	SST1(m)	SST2(m)	SST1&2(m)	SST1(m,m-2)	SST2(m,m-2)	SST1&2(m,m-2)	SOI(m)	SOI(m,m-2)
1	-2.05	-2.80	-5.02	-2.10	-3.81	-6.79	-2.51	-4.04
2	-1.23	-0.79	-2.19	-0.80	-2.36	-3.19	-2.45	-4.76
3	-0.16	1.45	1.01	-1.42	1.81	0.40	-1.52	-3.86
4	-0.98	-1.91	-2.92	-3.11	-2.79	-6.88	-1.16	-3.30
5	-1.40	-2.05	-3.25	-2.01	0.04	-2.24	-1.43	-2.64
6	-1.15	-1.97	-2.54	-3.50	-3.89	-7.10	-0.98	-3.38
7	0.26	-1.28	0.61	1.68	-2.71	-0.24	2.49	5.02
8	-0.82	1.68	1.88	-2.42	2.99	2.26	-1.43	-1.97
9	-2.00	-1.32	-2.64	0.88	-3.83	-0.09	0.25	0.78
10	-2.17	0.05	-1.66	2.69	-0.62	0.72	-1.62	-0.98

The skill scores for above and below median wheat yield forecasts are given in Table 29. When forecasting two categories of wheat yield there is more skill, in most months, than when forecasting for three categories. However the most skilful predictions are very late in the year (August and October) making their usefulness to wheat producers limited. Again, the analysis using three-month averaged SST and SOI values gave similar results, though no months had skill scores over 10. A subset of these results is illustrated graphically in Figure 10.

Table 29.LEPS skill scores for wheat yields (above/below median). The predictor month used to forecast the yield is given in brackets. For example, the first row of data is for January (m=1) and predictors using (m, m-2) use January and November (of the previous year).

Month	SST1(m)	SST2(m)	SST1&2(m)	SST1(m,m-2)	SST2(m,m-2)	SST1&2(m,m-2)	SOI(m)	SOI(m,m-2)
1	-1.61	-2.27	-3.95	0.62	-4.48	-3.66	-0.81	-3.05
2	-0.77	-1.70	-2.48	-2.40	-3.92	-6.77	-1.85	-3.51
3	-1.76	1.82	0.42	-3.86	3.82	2.04	-2.21	-2.46
4	-1.74	-1.63	-3.42	-2.55	-3.90	-5.95	-2.18	-4.03
5	-1.76	2.23	-3.25	0.10	0.43	2.40	-2.19	-4.49
6	-1.94	-0.32	-2.38	-0.24	-2.46	-1.41	-1.53	-3.48
7	-2.08	2.93	0.84	-1.58	0.84	-1.95	3.28	5.10
8	-2.18	11.07	8.87	-4.13	13.44	10.11	2.33	0.59
9	-1.73	5.89	3.96	0.06	3.78	5.34	5.05	3.09
10	0.13	2.45	2.05	5.45	9.66	10.47	-2.12	3.97

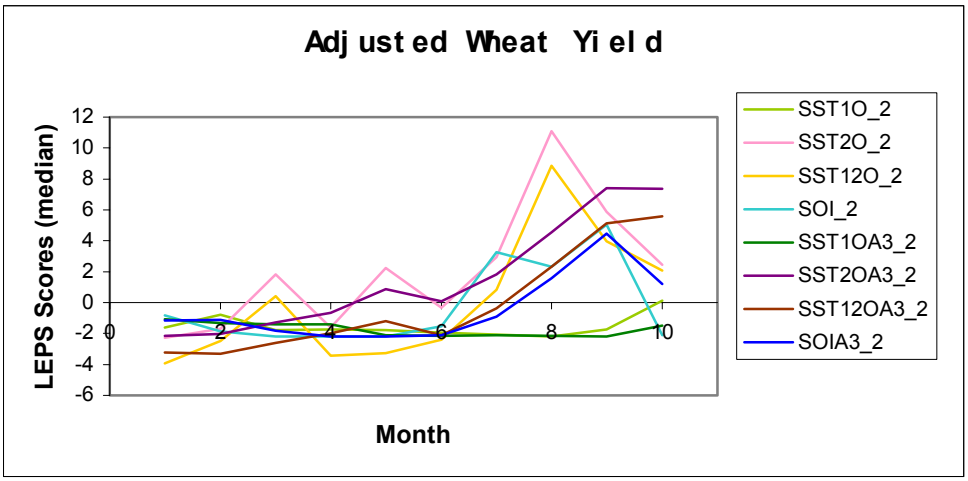

Figure 10. LEPS skill scores for forecasts of median wheat yield at Yilgarn by month. SST1O_2 uses SST1 in month m; SST2O_2 uses SST2 in month m; SST12O_2 uses SST1 and SST2 in month m; SOI_2 uses the SOI in month m; SST1OA3_2 uses three-month averaged SST1 values ending in month m; SST2OA3_2 uses three-month averaged SST2 values ending in month m; SST12OA3_2 used SST1 and SST2 three-month averaged values ending in month m; and SOIA3_2 uses three-month averaged SOI values ending in month m.

Table 30 lists the results for forecasts of tercile Yilgarn wheat yields using rainfall from Kalgoorlie and Merredin. The results for above/below median forecasts were similar. Forecasts using rainfall (either from Kalgoorlie or from Merredin) tend to have higher skill scores than those made using the SSTs or the SOI. In particular, when rainfall is used as a predictor skilful forecasts appear to be possible as early as April. The results from Table 30 are shown graphically in Figure 11.

Table 30.LEPS skill scores for Yilgarn wheat yields (terciles) using Kalgoorlie or Merredin rainfall. The predictor month used to forecast the yield is given in brackets. For example, the first row of data is for January (m=1) and predictors using (m, m-2) use January and November (of the previous year). Kal = Kalgoorlie, Mer = Merredin.

Month	Kal (m)	Mer (m)	Kal (m,m-2)	Mer (m,m-2)	Kal (3m)	Mer (3m)	Kal (3m,3m-1)	Mer (3m,3m-1)
1	-1.74	1.77	-3.72	3.20	-0.56	-1.15	-0.97	2.57
2	5.87	1.27	5.68	1.94	4.23	4.48	2.69	4.16
3	12.05	-1.27	10.58	0.73	10.92	2.30	12.69	0.45
4	30.29	12.73	31.21	12.21	22.21	8.97	23.66	8.95
5	-0.39	1.99	11.10	0.44	27.10	9.29	28.92	9.43
6	3.00	2.35	30.42	15.04	18.63	13.89	35.43	17.97
7	6.86	15.26	6.19	15.51	9.88	17.78	26.54	17.44
8	3.02	4.00	5.34	6.35	13.82	25.70	19.11	27.40
9	4.57	3.09	11.36	15.46	15.24	24.76	19.45	33.61
10	-1.21	-1.21	0.87	3.85	5.69	7.94	14.78	27.25

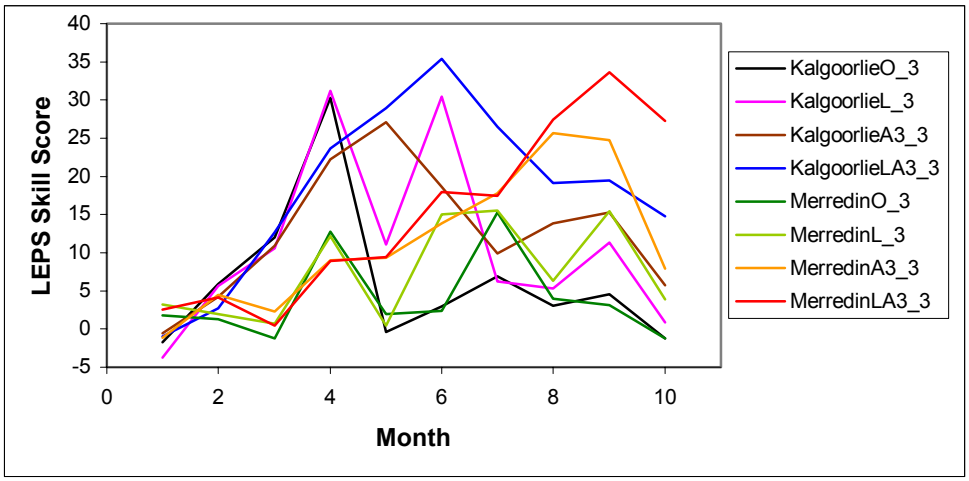

Figure 11. LEPS skill scores for forecasts of median wheat yield at Yilgarn by month using rainfall at Kalgoorlie or Merredin as predictors. The legend is as in Figure 6.

Table 31 lists the results for forecasts of tercile Yilgarn wheat yields using mean minimum monthly temperatures at Kalgoorlie and Merredin. Although not shown, the results for above/below median forecasts gave generally higher skill levels than for terciles, for example above/below median yield forecasts using Kalgoorlie (m,m-2) minimum temperatures had skill scores ranging from 4.47 to 14.85 when m was between 7 and 10. However, forecasts this late in the year are unlikely to provide useful information to farmers.

Table 31.LEPS skill scores for Yilgarn wheat yields (terciles) using Kalgoorlie or Merredin monthly mean minimum temperatures. The predictor month used to forecast the yield is given in brackets. For example, the first row of data is for January (m=1) and predictors using (m, m-2) use January and November (of the previous year). Kal = Kalgoorlie, Mer = Merredin.

Month	Kal (m)	Mer (m)	Kal (m,m-2)	Mer (m,m-2)	Kal (3m)	Mer (3m)	Kal (3m,3m-1)	Mer (3m,3m-1)
1	-0.38	-2.16	-2.18	-3.38	-2.22	-2.10	-0.20	-4.00
2	-2.15	-2.05	-4.77	-4.50	-2.56	-2.27	-2.98	-3.61
3	-2.34	-1.88	-2.23	-4.07	-2.36	-2.17	-4.73	-4.10
4	1.00	-0.02	-0.90	-2.60	-0.14	-0.71	-2.07	-3.33
5	0.00	-1.82	-2.02	-3.44	0.13	-1.41	-1.32	-3.44
6	-1.48	-2.09	-0.49	-2.16	1.41	-1.56	0.02	-2.76
7	3.91	1.31	3.36	-0.10	3.11	-1.24	1.22	-3.00
8	1.63	-0.56	0.04	-2.45	-1.85	-2.17	-0.31	-2.77
9	1.11	1.34	4.49	3.74	-1.77	-1.73	4.51	-0.99
10	-0.10	1.56	0.31	0.01	2.87	2.53	3.27	4.14

Table 32 lists the results for forecasts of tercile Yilgarn wheat yields using mean maximum monthly temperatures at Kalgoorlie and Merredin. Potentially useful skill levels were achieved when using three-month averages of maximum monthly temperatures for both Merredin and Kalgoorlie. The skill levels were generally greater in the latter months (after May). Mean monthly maximum temperatures at Kalgoorlie (three month average no lags) tended to provide more consistently high skill levels than the other combinations presented in Table 32.

Table 32.LEPS skill scores for Yilgarn wheat yields (terciles) using Kalgoorlie or Merredin monthly mean maximum temperatures. The predictor month used to forecast the yield is given in brackets. For example, the first row of data is for January (m=1) and predictors using (m, m-2) use January and November (of the previous year). Kal = Kalgoorlie, Mer = Merredin.

Month	Kal (m)	Mer (m)	Kal (m,m-2)	Mer (m,m-2)	Kal (3m)	Mer (3m)	Kal (3m,3m-1)	Mer (3m,3m-1)
1	5.14	-0.24	3.96	-1.82	1.89	-0.35	6.08	0.39
2	-2.63	-1.54	-4.63	-3.89	-0.35	-0.04	-0.99	-0.48
3	5.75	6.65	7.24	4.71	3.53	4.91	2.98	2.57
4	8.75	2.98	7.02	0.50	7.08	6.68	5.82	5.03
5	3.65	3.90	7.17	6.30	13.88	9.10	11.49	7.07
6	6.60	4.61	12.67	5.42	13.49	8.64	12.36	7.01
7	6.21	9.20	8.17	9.82	10.31	10.97	14.43	10.53
8	5.20	5.46	8.06	7.30	11.32	11.98	15.63	11.54
9	6.09	13.69	11.49	20.27	12.82	18.63	12.50	17.41
10	-1.96	0.68	3.07	4.86	5.90	11.70	10.28	14.21

Table 33 lists the results for forecasts of tercile Yilgarn wheat yields using the monthly diurnal temperature range at Kalgoorlie and Merredin. Higher overall skill was achieved when using the DTR over mean minimum, mean maximum temperatures, SSTs or the SOI, with useful skill levels appearing as early as March/April. The results from Table 33 are shown graphically in Figure 12. Similar skill levels were obtained when forecasting above/below median wheat yields.

Table 33.LEPS skill scores for Yilgarn wheat yields (terciles) using Kalgoorlie or Merredin monthly diurnal temperature range. The predictor month used to forecast the yield is given in brackets. For example, the first row of data is for January (m=1) and predictors using (m, m-2) use January and November (of the previous year). Kal = Kalgoorlie, Mer = Merredin. "-" indicates no LEPS score available.

Month	Kal (m)	Mer (m)	Kal (m,m-2)	Mer (m,m-2)	Kal (3m)	Mer (3m)	Kal (3m,3m-1)	Mer (3m,3m-1)
1	3.49	-0.91	-	-	2.37	0.86	3.11	1.64
2	-1.77	0.57	-	-	1.76	2.05	0.18	1.24
3	12.71	10.73	12.18	9.10	7.17	5.59	-	-
4	29.45	14.66	28.11	12.57	16.73	10.92	-	-
5	7.42	4.31	16.13	11.46	27.68	18.38	25.70	16.44
6	7.03	3.97	30.13	15.69	27.90	19.79	29.37	19.64
7	12.50	12.82	15.99	14.17	20.61	16.55	29.42	21.63
8	-0.85	-0.99	6.61	3.41	14.79	10.85	27.86	20.00
9	4.46	7.13	14.79	17.09	12.35	11.44	20.04	18.46
10	-2.28	-2.45	-3.30	-3.56	0.68	1.46	12.83	9.39

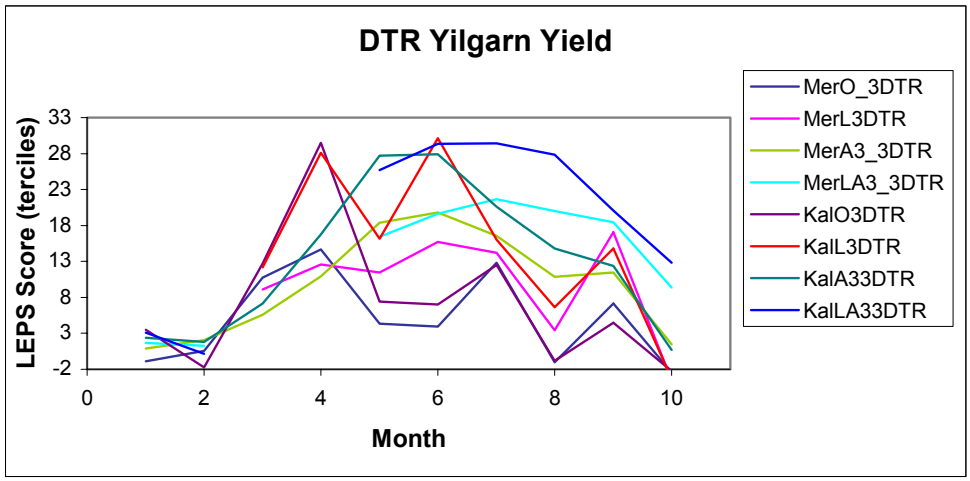

Figure 12. LEPS skill scores for forecasts of median wheat yield at Yilgarn by month using the DTR at Kalgoorlie or Merredin as predictors. The legend is as in Figure 10.

Discussion

Skilful prediction of wheat yield at Yilgarn appears possible using monthly rainfall values from Kalgoorlie or the diurnal temperature range at Merredin or Kalgoorlie, from as early as March. However, caution in interpreting these results is needed as high levels of skill around the time of planting may simply be a reflection of farming practices under prevailing rainfall and temperature regimes.

An illustration of the skill obtainable in this way is shown in Figure 13, where detrended yield is plotted against April Kalgoorlie rainfall. The separation of high yield and low yield years is quite clear.

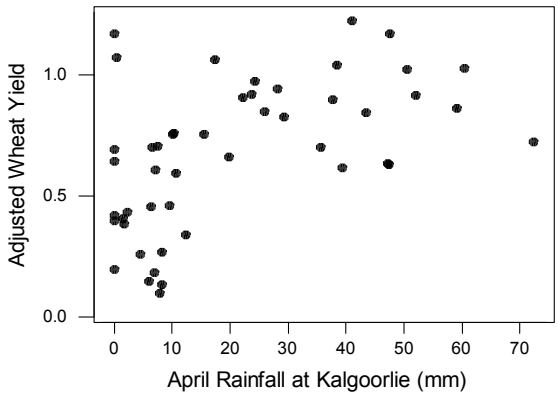

Figure 13: Wheat yield at Yilgarn (detrended) versus April rainfall at Kalgoorlie

Antarctic Circumpolar Wave (ACW)

Description.

The Antarctic Circumpolar Wave (ACW), first documented by White and Peterson (1996) is a large scale anomaly pattern in sea surface temperature (SST), sea level pressure (SLP) and associated wind fields. It is found in the Southern Ocean between approximately 40°S and the Antarctic coast, and consists of a wave number two pattern (i.e. two positive and two negative anomaly regions around a latitude circle). This pattern propagates eastward at about 45° longitude per year, resulting in a four year period at any point. The structure of the ACW is revealed in an EOF analysis of monthly SST anomalies over the Southern Ocean (25S to 65S), in Figure 14. The first two EOFs are in quadrature, ie they have the same basic spatial structure, but displaced by one half a wavelength, so that maxima or minima in one pattern coincide with nodal (zero) lines in the other. The principal components (EOF time series) are uncorrelated at zero lag, but strongly correlated at approximately 12 months lag, implying a 4-year periodicity in the evolution of the pattern.

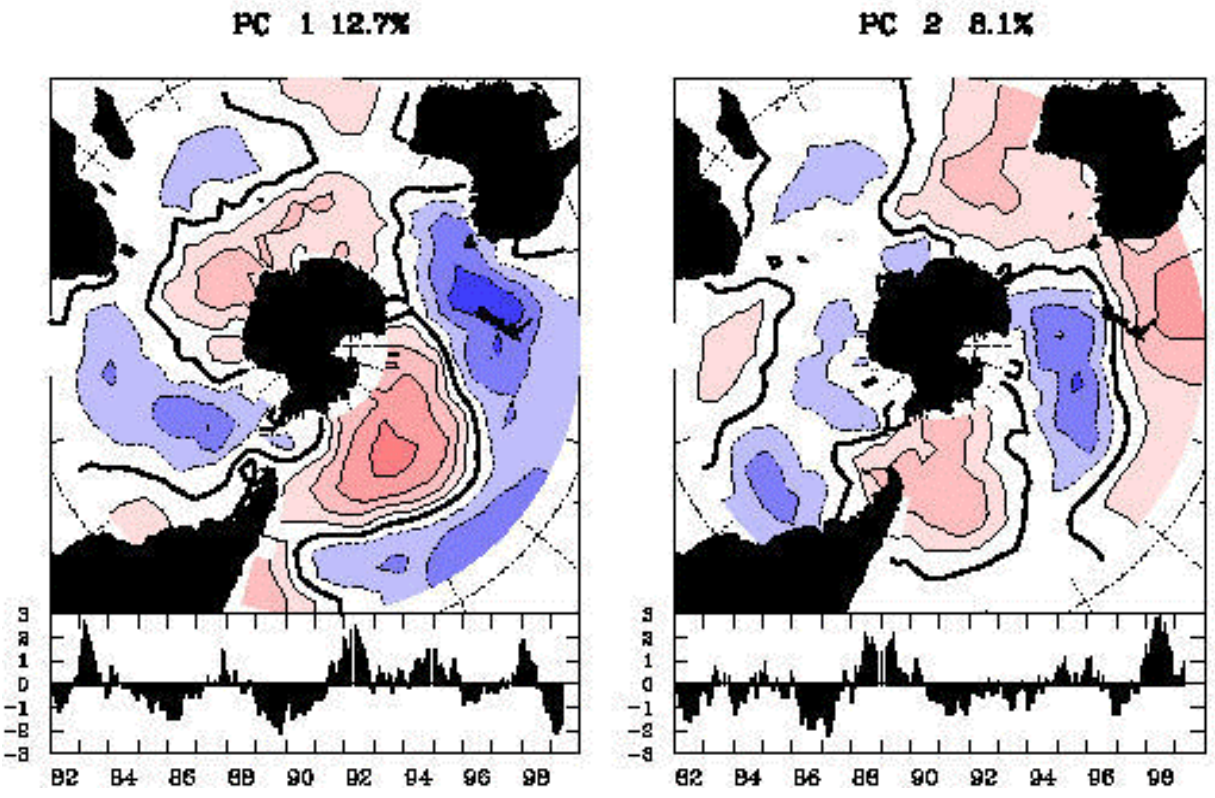

Figure 14. Spatial patterns and time series of first two EOFs of Southern Ocean (25S to 70S) monthly Sea Surface Temperature anomalies for period from January 1982 to April 1999. Contour interval 0.2, with zero contour heavy. Positive loadings shaded red, negative blue.

The propagating character of the ACW can also be seen in a Hovmoller (time - longitude) plot of SST and SLP anomalies along a latitude band (eg 50-60S, figure 15). Alternatively, the evolution of the EOF patterns can be tracked on a phase plot of

the two principal components (figure 16). As the wave propagates eastward, the observed SST anomaly pattern should project strongly onto a sequence
... +PC1 → +PC2 → -PC1 → -PC2 → +PC1…
Predictability of the ACW is largely based on the persistence of this approximately 4-year cycle.

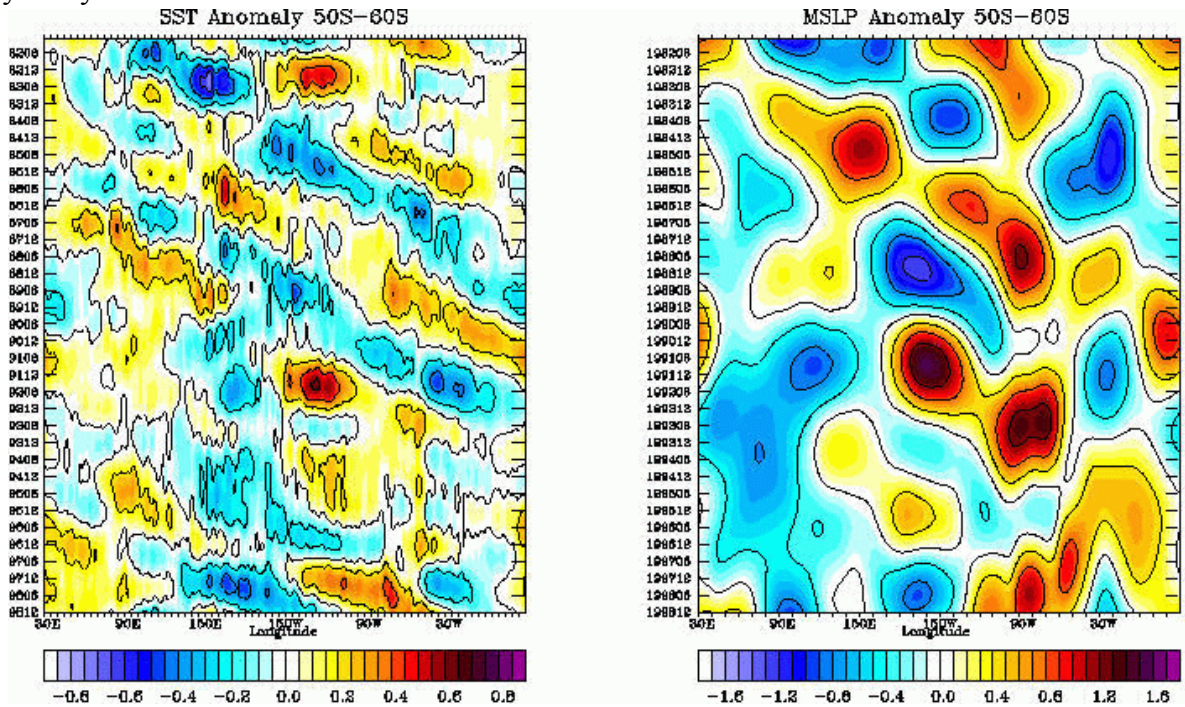

Figure 15. Hovmoller (time - longitude) plots of (a) SST anomalies and (b) MSLP anomalies for period Jan 1982 to Dec 1998, averaged over a 10 degree latitude band form 50S to 60S. Data is 2-7 year band pass filtered and has zonal mean removed.

Relations to the El Niño - Southern Oscillation and the Indian Ocean Dipole

Peterson and White (1998) suggest that ACW has a source region in the subtropical southwest Pacific, which in turn is driven by equatorial ENSO related anomalies. SST and SLP anomalies propagate from this region into the Southern Ocean. The extent of the ENSO / ACW connection is simply shown by the lagged cross-correlation between the SOI and the principal component time series (Figure 17) The two PCs are themselves uncorrelated at zero lag (as required by the EOF analysis), but are significantly correlated (-0.65) with PC1 lagging PC2 by approximately 12 months. The reverse correlation (PC1 leading PC2) is not as strong (+0.30), suggesting that the evolution of some parts of the nominal four year cycle are more reliable than others. This is also evident in the PC1 - PC2 phase plot (Figure 16) which suggests that the transition from +PC1 to +PC2 is not as robust as the rest of the cycle, which then "begins" with +PC2. This view is consistent with the hypothesis of Peterson and White (1998), since +PC2 has significant warm anomalies in the Tasman Sea region. These appear to propagate to the southeast, surrounding New Zealand in -PC1 and then to the southeast of New Zealand in -PC2. Both PCs have significant lagged correlations with the SOI, also only in one direction for each PC. PC1 lags the SOI by 3-6 months, while PC2 leads SOI by 6 months. The second EOF pattern has positive loadings in the Indian Ocean southwest of Western Australia, in a similar region to the maximum loadings on SST2 defined by Drosdowsky and Chambers (1998). The times

series of these components are also significantly positively correlated (+0.58) at a lag of two months. This suggests that subtropical (20S to 35S) Indian Ocean SST anomalies may also be linked to the ACW.

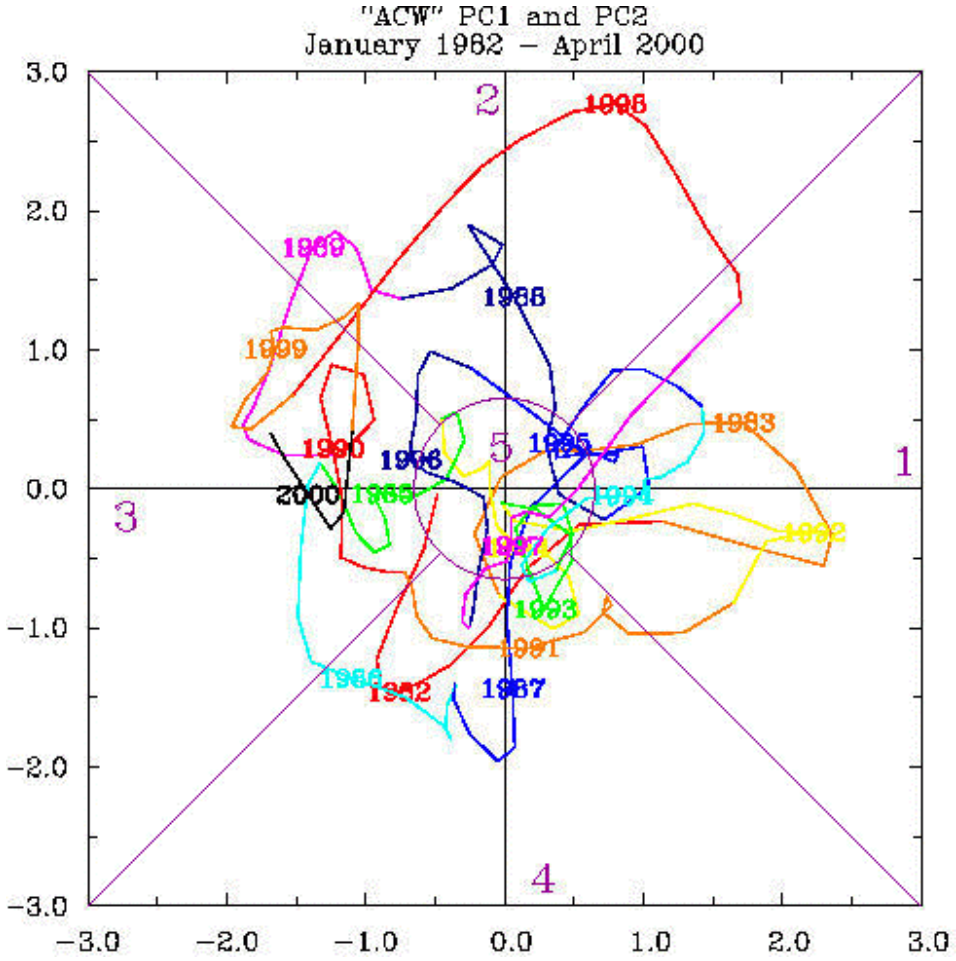

Figure 16. Phase plot of EOF amplitudes PC1 and PC2 for period Jan 1982 to May 2000. Each year is plotted at mid-year (June) point, and colour of trajectory changes each year. Light purple boundaries and numbers 1-5 refer to categories or phases used in Figure 5. Both time series are lightly smoothed with a 1-2-1 filter before plotting.

Effect of the ACW on Australian rainfall.

The ACW has persistent, large scale SST anomalies in the vicinity of Australia, and could therefore be expected to show some relationships with Australian rainfall. To examine this in a fairly simple manner, we adopt a compositing type approach. Each month is characterised as being in one of five phases, depending on which of the two EOF patterns is dominant. The boundaries defining each phase are shown in Figure 16. For each phase we then examine the rainfall distribution in the following season, presented in Figure 18 as the proportion of seasons in which the seasonal rainfall exceeds the median. The strongest signal appears with Phases 2 and 4, i.e., opposite signs in PC2. The positive phase of PC2 is associated with mainly wetter conditions over most of Australia, with drier conditions over the north and east in the negative phase. This is consistent with the relationship between PC2 and the SOI, i.e., PC2 and

the SOI are significantly positively related (at six months lag) so that positive PC2 is also associated with positive SOI. PC2 is also related to Indian Ocean SST anomalies, with positive PC2 implying positive SST anomalies in the Indian Ocean west of Australia. These in turn are associated with a dipole pattern in Australian rainfall, with wetter conditions over northern and eastern Australia, and drier conditions along the south coast.

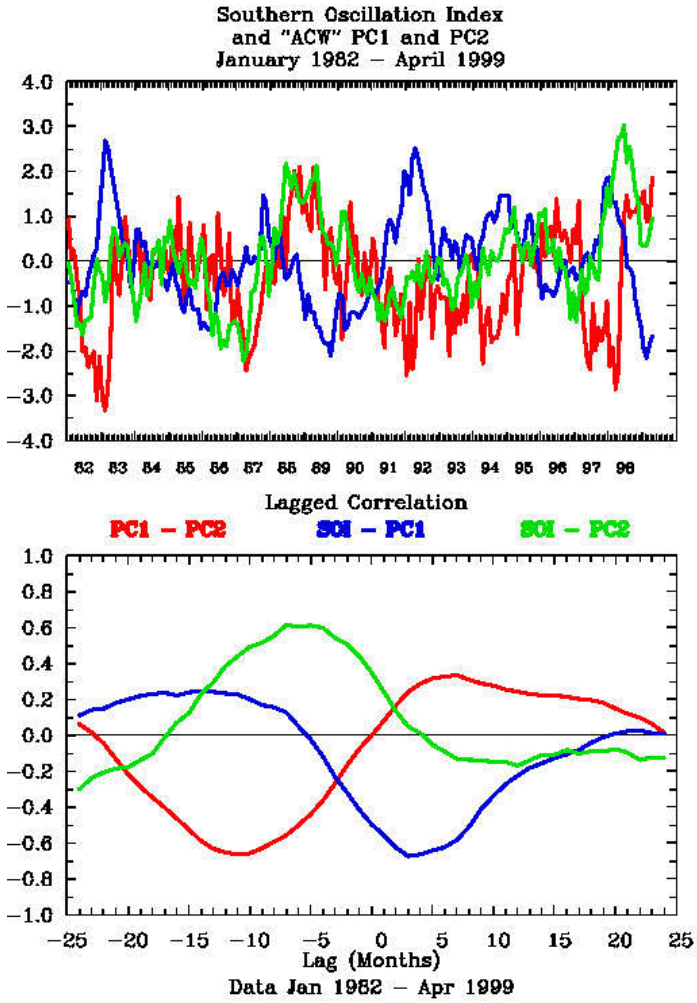

Figure 17(a) Times series of raw monthly values of PC1 (blue), PC2 (green) and the SOI (red) for period January 1982 to April 1999. (b) Lagged correlations between PC1 and PC2 (red), the SOI and PC1 (blue) and the SOI and PC2 (green) based on data in (a).

Summary

The independent skill of the ACW in forecasting Australian seasonal rainfall is therefore is difficult to quantify due to:
(i) The short period of reliable data - i.e., less than twenty years to describe a phenomenon with a nominal 4-year cycle.
(ii) The statistical, if not physical, connections with the El Niño - Southern Oscillation and the Indian Ocean SST anomalies which also have strong known associations with Australian rainfall.

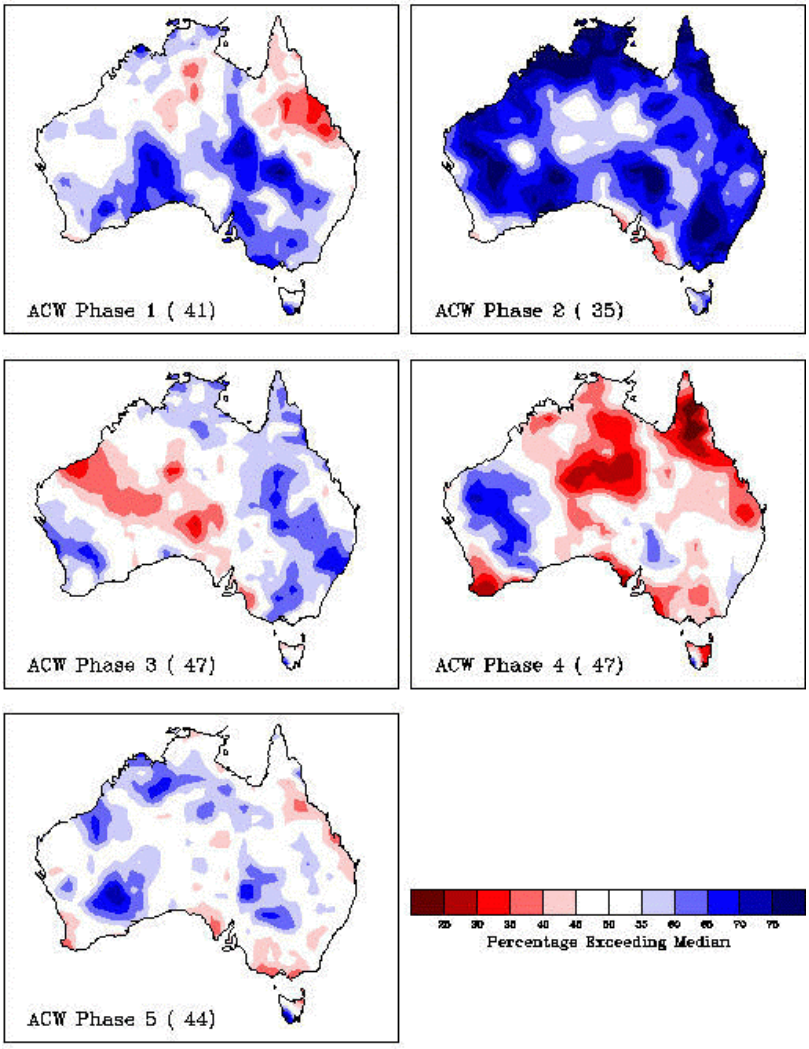

Figure 18. Percentage of seasons exceeding median rainfall following, one month later, months with ACW characterised by the five phases shown in Figure 16 (i.e., for January ACW phase, rainfall is in following March - May, etc).

Equatorial Indian Ocean SST Dipole

Saji et al (1999) and Webster et al (1999) independently proposed that an internal mode of variability in the equatorial Indian Ocean led to a dipole structure in SSTs which could affect the climate of the surrounding region. This dipole mode, it was suggested, was independent of the El Niño - Southern Oscillation. The strength of the dipole, measured by the equatorial SST gradient across the Indian Ocean, was only weakly, and non-significantly, correlated with the El Niño, according to both sets of authors. If this was so, then the strength of the dipole may have some influence on rainfall in Western Australia, separate to the influence of the El Niño - Southern Oscillation. It was thought worthwhile, therefore, to more carefully examine the independence, or otherwise, of the dipole mode. It should be noted that this dipole is somewhat distinct from the dipole-like correlation structure described by Nicholls (1989), that exhibited more latitudinal structure.

In fact the apparent "independence" of the equatorial dipole from the El Niño is an artifact of calculating correlations using all months on record, rather than first stratifying the data by season. For instance, if only the average September-November data are used then the correlation between NINO3 SST and the Indian Ocean dipole index defined by Webster et al. (1999) is 0.56 (data from 1958-97, p<.001). Time series of the two indices are shown in Figure 19. Apart from an occasional year (e.g., 1961) the strong relationship between the two is clear. Thus the equatorial Indian Ocean dipole is NOT independent of the El Niño - Southern Oscillation.

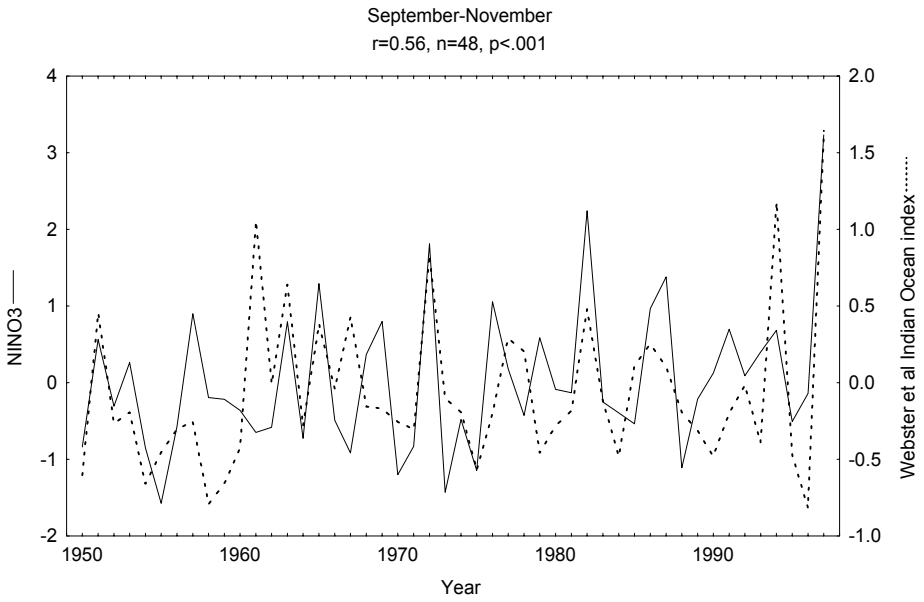

Figure 19. Time series of NINO3 SST anomalies and the Webster et al. (1999) index of the strength of the equatorial Indian Ocean SST dipole.

Closer examination reveals that the dipole of Saji et al. (1999) and Webster et al. (1999) is not even a dipole. If it was then there should be a consistent negative correlation between the western and eastern boxes that constitute the index of the

dipole strength. The correlation between the western and eastern boxes, again for September-November only, is actually only -.13 (n=40, non-significant). The time-series of the two boxes are shown in Figure 20. Interestingly, there are periods when there does appear to be some evidence of "dipole-like" behaviour (eg., the last few years of the time series). There are other periods however, when there is no evidence of such behaviour.

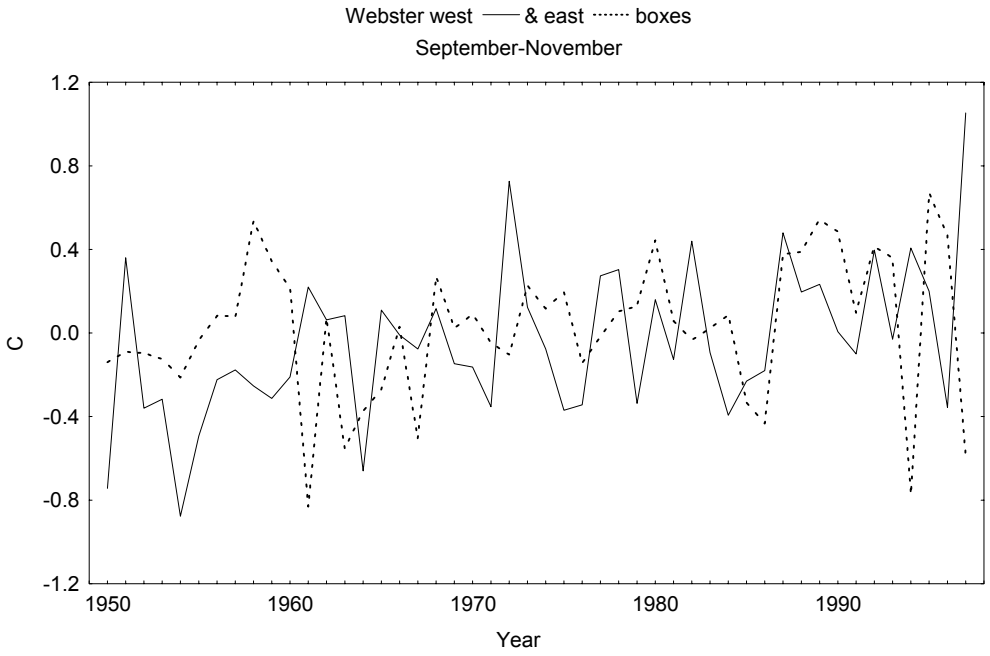

Figure 20. Time series of the eastern and western boxes of the Webster equatorial Indian Ocean SST dipole index.

Note that in Figure 20, there is clear evidence of an increase in SST over time, in both boxes. This warming would tend to offset any underlying negative correlation between the two boxes. That is, the coherent warming would confound the identification of a dipole-like structure. In order to determine the strength of this dipole-like behaviour we need to de-trend the SSTs in the two boxes. If this is done by linear regression against time, and the residuals from this de-trending are calculated, then the correlation between the two boxes is -.21. The larger magnitude of this correlation confirms that the warming trend is offsetting the tendency for a dipole-like structure.

So there is a weak dipole-like structure but, as we saw earlier, the strength of this dipole is closely related to the El Niño - Southern Oscillation. Is there any dipole-like behaviour other from that imparted by the El Niño - Southern Oscillation? To answer this we calculate the linear regressions of the SSTs in the two Indian Ocean boxes against NINO3 SSTs, then correlate the residuals. Note that this has been done after detrending of all SSTs to remove the coherent warming. The final residual SSTs in the two Indian Ocean boxes now have a correlation of –0.04 (n=40, not significant). That is, once the effect of coherent warming and the El Niño - Southern Oscillation are removed, there is essentially no dipole-like behaviour in the Indian Ocean. What dipole-like behaviour is found in the equatorial Indian Ocean simply reflects the differential effect of the El Niño - Southern Oscillation on the two edges of the ocean.

This reflects the overall situation. However, if the time series of the residual SSTs in the two Indian Ocean boxes are examined (Figure 21), a somewhat different pattern emerges. Now we find that there are periods when there does appear to be a strong dipole-like behaviour (1990 to date; 1958-1965), with another period (1970-1990) when the variations of the two boxes are in phase. That is, the lack of correlation between the two edges of the equatorial Indian Ocean does not reflect random variations but two possibilities of either the entire ocean acting as a dipole or both sides varying coherently.

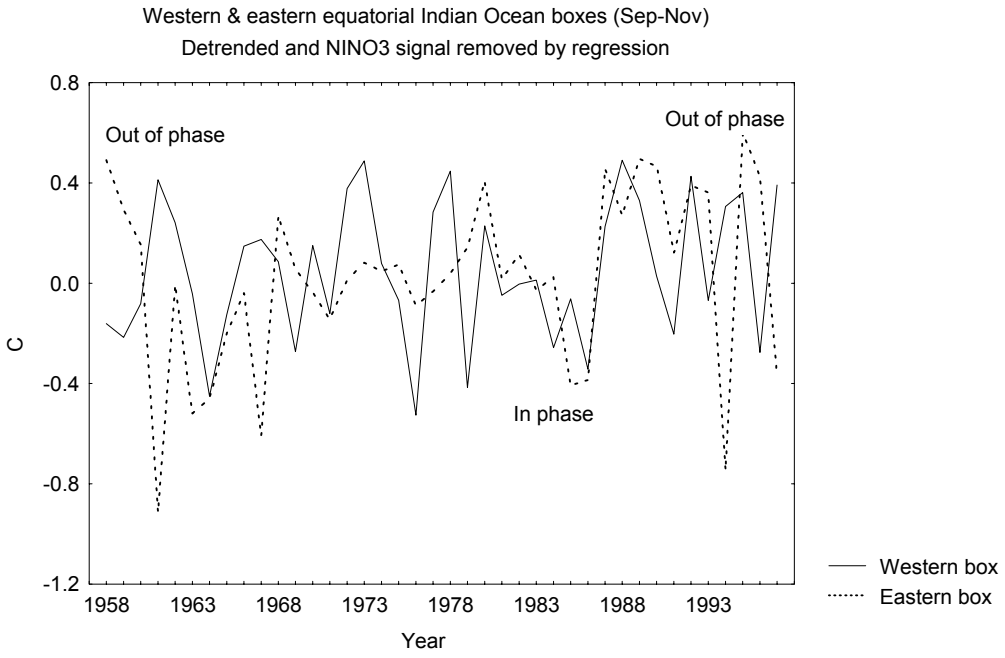

Figure 21. Time series of the western and eastern boxes comprising the Webster et al. (1999) dipole index, after detrending and removing the relationship with NINO3 SSTs.

Summary

There is no evidence of a consistent dipole-like behaviour in the equatorial Indian Ocean, apart from that imparted by the El Niño - Southern Oscillation. There are, however, periods when a dipole-like structure and behaviour appears. These are offset by other extended periods when both sides of the equatorial Indian Ocean vary in phase. This intriguing behaviour should be further investigated, to determine whether either form of Indian Ocean behaviour impacts on the countries surrounding the ocean.

Causes of decadal decline in rainfall in SWWA

There were three (initially two) aspects of this part of the study:

- *Examine long integrations of the BMRC climate model, forced with observed SSTs, to determine whether these reproduce the observed decline in rainfall*. The results from this were expected to provide guidance to the likely causes of the decline in rainfall. This part of the study has been delayed because of delays in obtaining the SSTs, and the extra work required for the first part of the Second Research Phase, and because of the addition of the third aspect of this part of the study (see below). However, some of the results obtained under the third aspect of this part of the study (see below) shed light on this question.
- *Use path analysis to examine relationships between possible predictor variables and rainfall.* Path analysis studies were reported in the Phase 1 report.
- *Investigate whether long-term variations in SWWA rainfall are related to distant factors (e.g., rainfall trends in other parts of the globe).* This aspect was added in May 2000, at the request of the IOCI Panel. The analysis has been done using the Climate Explorer web site of KNMI, using standard global data sets.

The first step was to determine other areas where precipitation had exhibited a similar (downward) trend to that of SWWA. Precipitation was correlated with year to determine trends; the result is shown in Figure 22. The area of SWWA exhibiting a decline in rainfall over the period 1958-1998 is quite small in this analysis (because the data set is on a relatively crude grid). The area with the most obvious decline is the Sahel. Areas with increases are found in eastern Europe and North America.

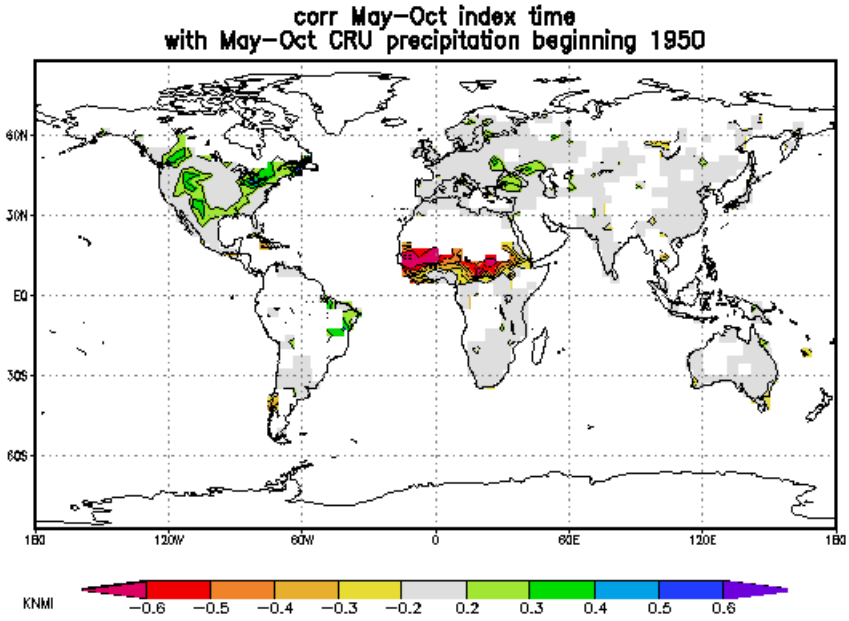

Figure 22. Correlation of year with precipitation from the CRU data set (?).

How are the trends in SWWA and the Sahel and elsewhere related? Figure 23 shows the correlation between observed rainfall at Manjimup and observed rainfall elsewhere in the world. There are strong positive relationships with rainfall across

southern Australia, and in the Sahel. There are negative correlations with North America rainfall.

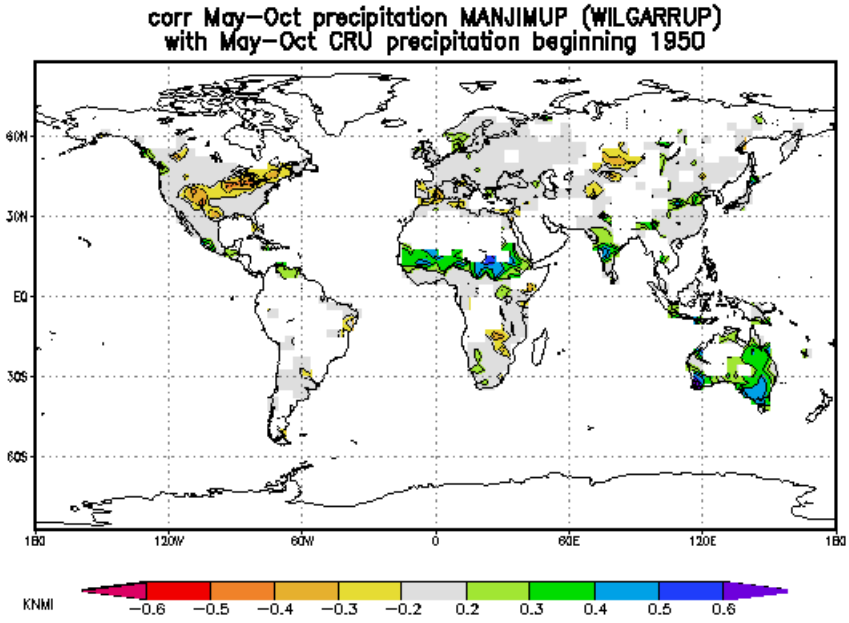

Figure 23. Correlation of Manjimup May-October rainfall with May-October precipitation elsewhere.

However, these correlations may simply reflect similar downward trends, rather than a more fundamental relationship which would also lead to strong correlations between interannual variations. This is clear from Figure 24 which shows the correlations of detrended rainfall across the globe, with detrended rainfall at Manjimup. The correlations with Sahel rainfall are weaker than with the original rainfall data, indicating that the correlation largely reflects the downward trends. Note that the detrended rainfalls in India are closely positively related to southern Australian rainfall. This reflects part of the global El Niño - Southern Oscillation pattern.

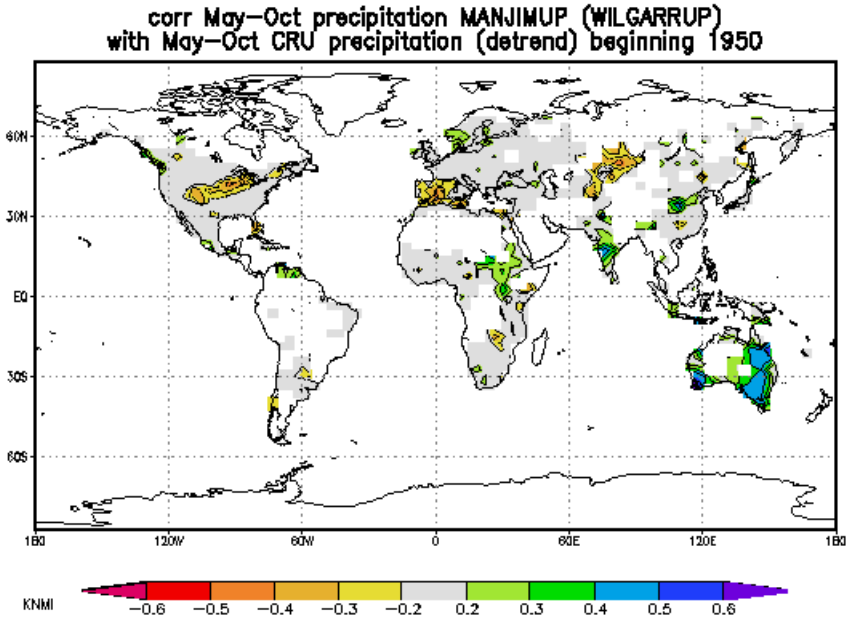

Figure 24. Correlation of Manjimup May-October rainfall with May-October precipitation elsewhere (all rainfalls detrended before correlations were calculated).

How are the precipitation trends shown in Figure 22 related to trends in temperatures, especially SSTs? Figure 25 shows the trend in sea surface and near-surface temperatures over land. Large increases are obvious in the Indian Ocean.

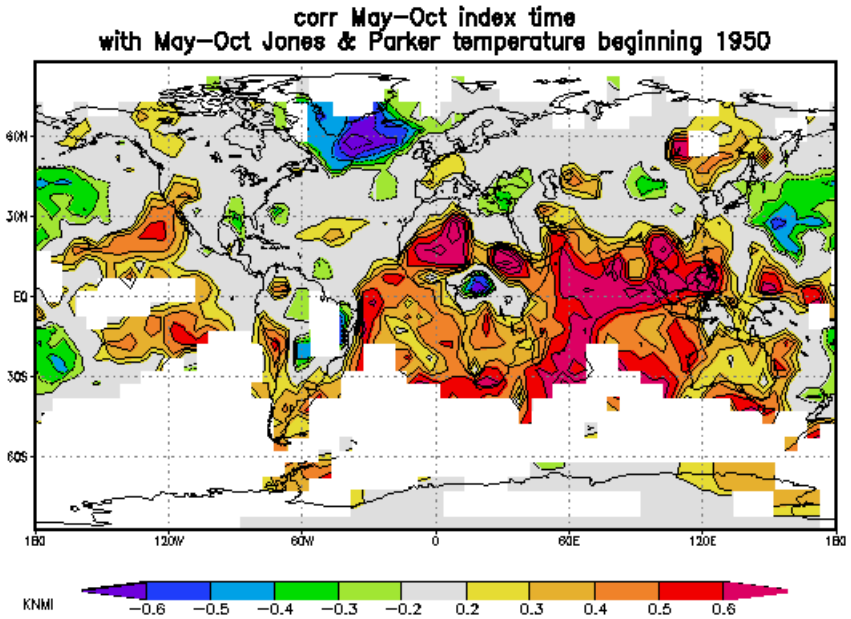

Figure 25. Correlation of near-surface temperature with time.

The trend in precipitation from the NCEP reanalyses is shown in Figure 26. These trends should be related to the trends in surface temperature, shown in Figure 25, if the SST trends are causing the precipitation trends. In fact the figure reproduces the strong downward trend in precipitation over the Sahel. However, the figure shows

increasing rainfall across Australia. This suggests that the decline in rainfall over SWWA is not related to, or forced by, trends in SSTs in the Indian Ocean (or that the model is unable to correctly reproduce interactions with SSTs leading to changes in SWWA rainfall).

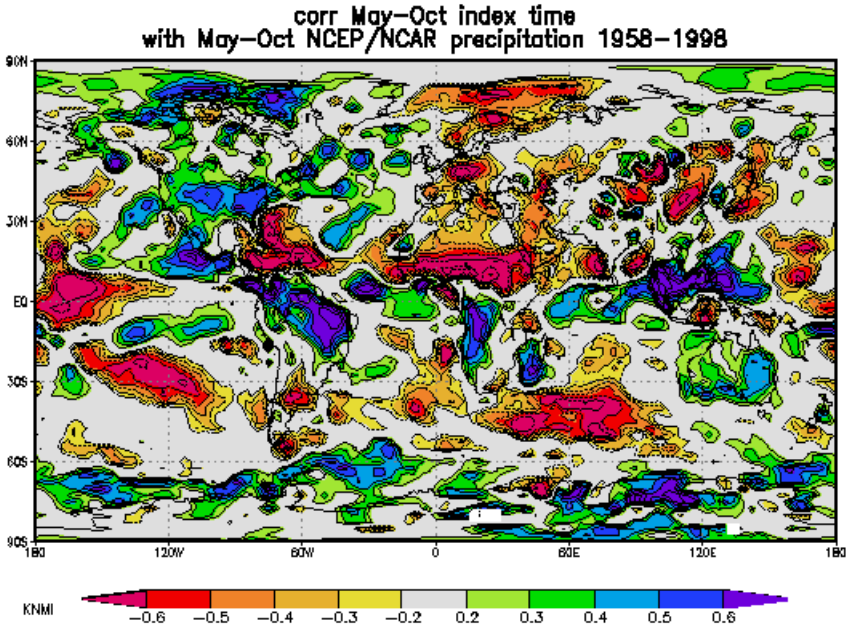

Figure 26. Correlation of NCEP "precipitation" with year.

Figure 27 shows the correlation with Manjimup precipitation and near-surface temperatures across the globe. Strong correlations are evident with Indian Ocean SSTs.

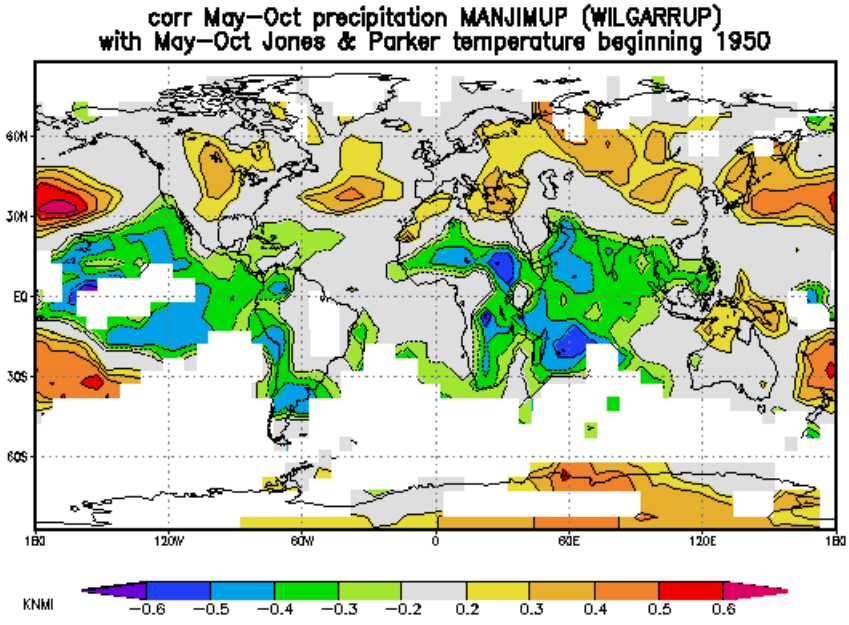

Figure 27. Correlation between May-October Manjimup rainfall and near-surface temperatures.

The correlations are substantially weaker if the data are detrended first (Figure 28). This tends to confirm the point made above, that the trend in precipitation at Manjimup (and elsewhere in the SWWA) is NOT directly related to the variations in Indian Ocean SSTs. Note that the pattern of correlations with SSTs in the Pacific Ocean is very much indicative of a relationship with the El Niño.

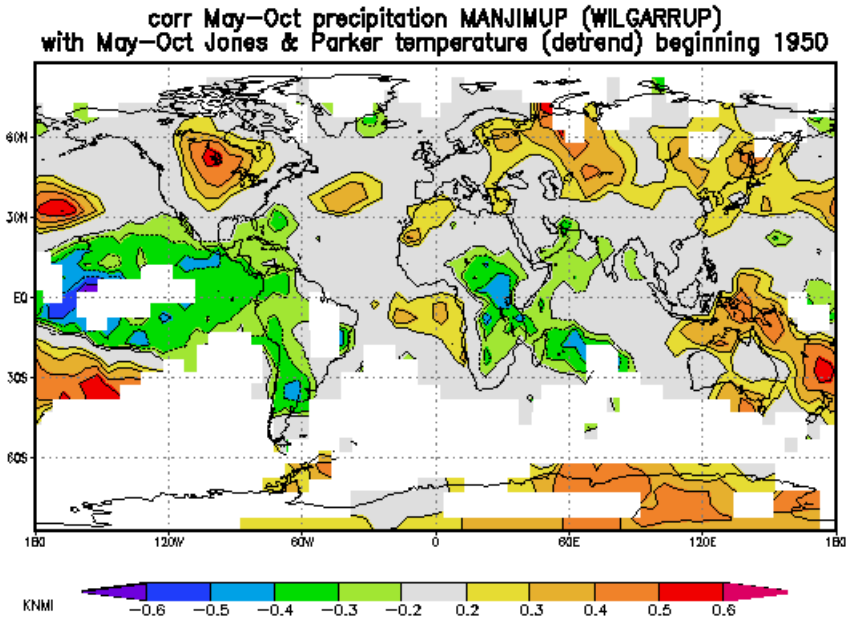

Figure 28. Correlation between May-October Manjimup rainfall and near-surface temperatures. Data detrended before calculation of correlations.

The correlation of Manjimup with (detrended) NCEP surface pressures (Figure 29) shows that an increase in pressure over and surrounding Australia, and stretching to the west, accompanies low rainfall in SWWA. Low pressures are usually found in the eastern Pacific. This pattern is somewhat similar to the pattern of pressure anomalies associated with an El Niño.

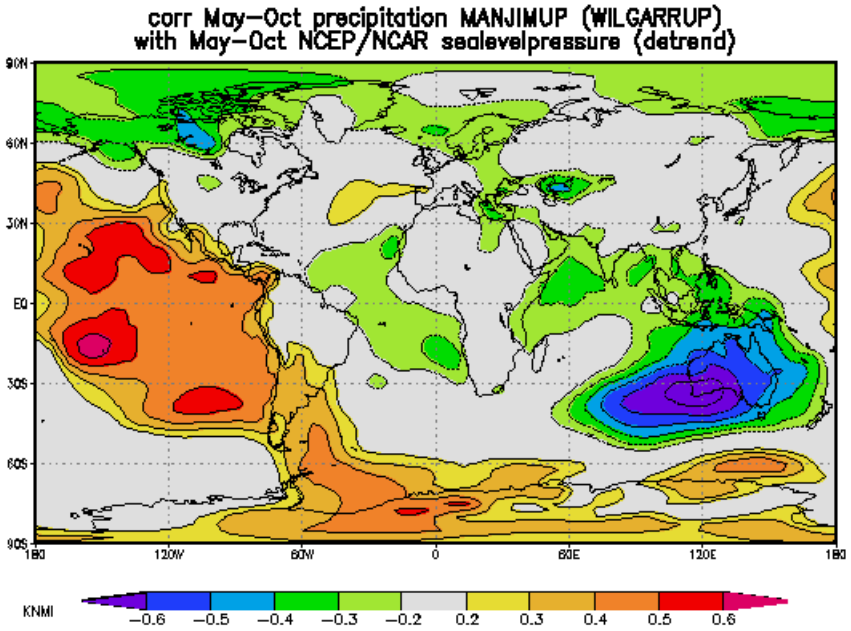

Figure 29. Correlation between May-October Manjimup rainfall and sea level pressure from NCEP reanalyses. Data detrended before calculation of correlations.

Figure 30 shows the trend in pressure from the NCEP reanalyses. Although the trends over the oceans, especially the southern oceans, are very suspect, trends over the continents should reflect reality. Over western Australia there has been a trend towards higher pressures. This would not be surprising, given the decline in rainfall in SWWA. However, why the NCEP reanalyses, despite this increase in pressure, also produces an increase in rainfall across the continent is not obvious.

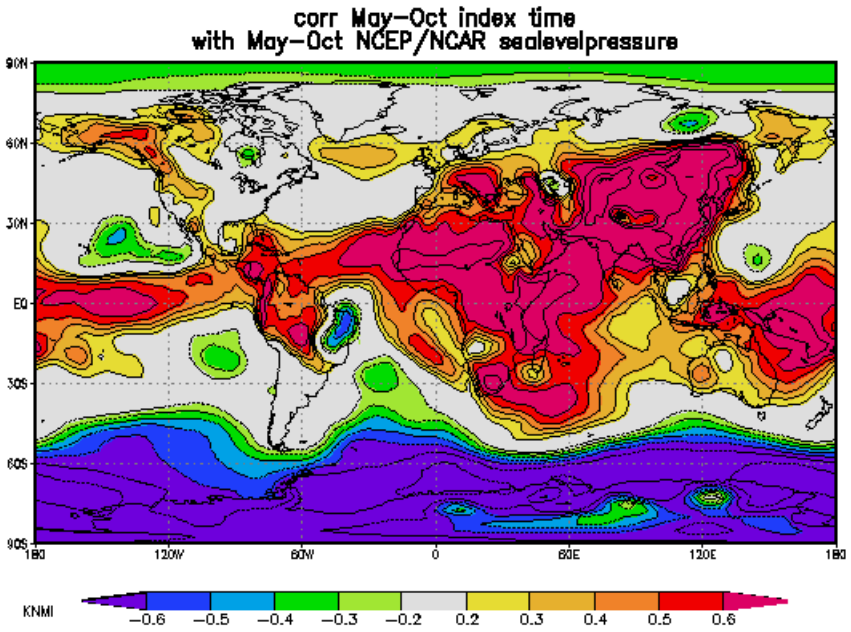

Figure 30. Correlation of year with sea level pressure. Note that the values over the southern oceans reflect changes in observing systems, rather than real trends.

Summary

This study does tend to confirm earlier work (reported in the BMRC report on Phase 1 work) suggesting that the decline in SWWA rainfall is not simply attributable to change sin Indian Ocean SSTs. However, there are problems with the use of NCEP reanalysis data to investigate this question, so the answer, at this stage, is not conclusive. If, however, further work does conclude that the decline is related to the changes in SSTs, we anticipate that the mechanism by which this is affected must be subtle (otherwise the analyses described here and in the BMRC report on Phase 1 work should have provided some support for this hypothesis).

CONCLUSIONS

This report describes the results of comprehensive BMRC studies of the predictability of interannual variations of SWWA Australia climate, and some study of the possible cause of the multi-decadal decline in SWWA winter rainfall. Not all of the work planned for the Second Research Phase has been carried out. In particular, studies using the BMRC climate model have not been completed (partly due to unexpected delays in obtaining new global SST fields). On the other hand extra work, in addition to that agreed to in the Second Research Phase plan, has been undertaken, at the request of Panel members. Specifically, spring predictability and wheat yield predictability has been investigated, along with the possible use of the equatorial Indian Ocean "dipole" in prediction of SWWA climate. As well, the possible use of SST gradients in prediction has been studied.

The major findings of the Second Research Phase BMRC work, are:
We found:

- Some skill in predicting
  - Spring and summer rainfall
  - Spring and summer temperature
  - Summer extreme temperatures
- More skill with SST1 or SST1 & 2 as predictors, than with SOI
- Little skill in predicting winter rainfall
- Considerable skill in predicting wheat yield (from observed climate)
- Little skill predicting for the SWWA from SST gradients in the southeast Indian Ocean
- "Differencing" of data (to avoid "breaks" in relationships) did not lead to improved forecasts
- The ACW seems related to Australian rainfall, but extra predictability provided by the ACW is difficult to quantify
- The equatorial Indian Ocean "dipole" is not really a dipole. But there is evidence that some behaviour in the Indian Ocean is independent of the El Niño - Southern Oscillation (and may therefore add to SWWA predictability studied thus far)
- Further evidence that the decline in SWWA winter rainfall is not simply due to changes in Indian Ocean SSTs.

ABBREVIATIONS & GLOSSARY

ACW: Antarctic Circumpolar Wave
DTR: Diurnal temperature range
EOF: Empirical orthogonal function
LEPS: Linear error in probability space
Loadings: Spatial pattern of EOF
MSLP: Mean sea level pressure
Scores: Time series of EOF values
SLP: Sea level pressure
SOI: Southern Oscillation Index
SST: Sea surface temperature
SST1: First EOF of Indian & Pacific Ocean SST
SST2: Second EOF of Indian & Pacific Ocean SST
SWWA: Southwestern Western Australia

REFERENCES

Drosdowsky, W., and L. Chambers. 1998. Near global sea surface temperature anomalies as predictors of Australian seasonal rainfall. *BMRC Research Report* No. 65, Bureau of Meteorology, Australia.

Jones, D.A. 1998. The prediction of Australian land surface temperatures using near global sea surface temperature patterns. *BMRC Research Report* No. 70, Bureau of Meteorology, Australia.

Nicholls, N., 1989. Sea surface temperatures and Australian winter rainfall. *J. Climate*, **9**, 965-973.

Nicholls, N., Chambers, L., Haylock, M., Frederiksen, C., Jones, D., and Drosdowsy, W., 1999: Climate variability and predictability for south-west Western Australia. In: *Towards understanding climate variability in south western Australia – Research reports on the First Phase of the Indian Ocean Climate Initiative*. IOCI, Perth, October 1999, 237 pp.

Peterson, R.G., and W.B. White, 1998: Slow oceanic teleconnections linking the Antarctic Circumpolar wave with tropical ENSO. J. Geophys. Res., 103, 24573-24583.

Saji, N. H., Goswami, B. N., Vinayachandran, P. N., and Yamagata, T., 1999. A dipole mode in the tropical Indian Ocean. *Nature*, **401**, 360-363.

Webster, P. J., Moore, A. M., Loschnigg, J. P., and Leben, R. R., 1999. Coupled ocean-atmosphere dynamics in the Indian Ocean during 1997-98. *Nature*, **401**, 356-360.

White, W.B., and R. Peterson, 1996: An Antarctic circumpolar wave in surface pressure, wind, temperature, and sea ice extent. Nature, 380,699-702.

Climate variability and predictability for southwest Western Australia

Ian Smith, Barrie Hunt,
Ian Watterson and Tracey Elliott

Second Research Phase Technical Report
for the
Indian Ocean Climate Initiative

CSIRO Atmospheric Research
PMB1, Aspendale, Victoria 3195
AUSTRALIA

TABLE OF CONTENTS

TABLE OF FIGURES

CAR RESEARCH PROPOSALS FOR IOCI SECOND RESEARCH PHASE (JULY 1999-DECEMBER 2000)

1. Multi-seasonal predictions using global climatic models

- Use the existing CSIRO Mark2 coupled prediction model to make hindcasts and predictions for 12 months ahead and evaluate their skill over SWWA.

- Develop the model initialisation scheme to try to include the Antarctic Circumpolar Wave, and evaluate its impact on predictions for SWWA.

- Commence development of the CSIRO Mark3 global coupled model for multi-seasonal predictions.

- Check the predictability of SWWA winter rainfall based on mean sea level pressure and sea surface temperatures southwest of WA for the preceding May using output from the 1000-year simulation.

- Evaluate the skill of simulating rainfall over SWWA with the Mark3 atmospheric general circulation model driven with observed sea surface temperatures. Determine whether the drying trend over SWWA is reproduced.

2. Millennial coupled simulations.

- Extend the earlier analysis of climatic trends, especially over SWWA based on the 1000-year simulation to include results from the 5000+year simulation now available.

- Use these data sets for a more detailed analysis of mechanisms involved in initiating and terminating climatic trends.

- Clarify the origins and controlling mechanisms of the north-west winds over Australia using the 1000-year simulation.

- Quantify the Antarctic Circumpolar Wave signal in the 1000-year simulation and determine its influence over SWWA.

3. Greenhouse simulations

- Use the output from new simulations with the Mark2 coupled model (involving realistic CO_2, O_3 and aerosol distributions starting in 1870) to evaluate any greenhouse contribution to the SWWA drying trend.

- Quantify the sensitivity of SWWA rainfall to varying greenhouse scenarios with the Mark2 model. (Four new scenarios are proposed).

- Conduct a preliminary evaluation of the SWWA greenhouse signal using the Mark3 coupled model.

4. Observational Studies

Use advanced signal detection techniques to analyse global historical oceanic and atmospheric data sets in order to:

- Clarify relationships and interactions between dominant modes of climatic variability, such as the El Niño Southern Oscillation (ENSO) phenomenon, the Antarctic Circumpolar Wave (ACW), the North Atlantic Oscillation (NAO) and the Arctic Oscillation (AO), and

- Examine the role that interactions between these climatic modes play in dictating rainfall relationships in SWWA.

Additions To CAR Work Plan

At the IOCIP Meeting (Number 7) on 15 October 1999, CSIRO climate model results were presented which referred to the timing and magnitude of changes to rainfall for SWWA due to the enhanced greenhouse effect (EGE). It was suggested then that, because the simulated changes occurred well into the 21st century, that it was unlikely that the EGE could have contributed significantly to the dry conditions over the past 30 years.

In December 1999, CAR released a (WA EPA-funded) report on simulated climate changes from a number of international models, including the CSIRO model. The consensus results again implied a strong possibility of dry conditions for winter late in the 21st century. However, an interpretation of the results was that the drying trend was not expected to become more severe. It became apparent in discussions that any such interpretations, and their implications for the future, required more careful explanation. Consequently, because of the importance to some industry sectors of long-term planning, it was decided that CAR should perform additional analyses of climate model results with the aim of clarifying rainfall expectations in the medium term (i.e. decades) compared to the long term (i.e. 100 years).

SUMMARY OF THE SECOND RESEARCH PHASE RESULTS

Multi-seasonal predictions

- When forced by observed sea surface temperatures (SSTs), the Mark3 climate model provides better simulations of rainfall over SWWA than the earlier Mark2 version. This improvement is seen in both the representation of the seasonal cycle, the amplitude of the seasonal cycle and the amplitude of interannual variations.

- There is no strong evidence for a protracted decline in simulated rainfall over the period when the observed decline took place.

- There is evidence of weak links between SWWA rainfall anomalies and SST anomalies in the Pacific Ocean but no evidence of any significant links to the Indian Ocean.

- A seasonal prediction model based on the Mark2 model has been developed and exhibits skill at predicting an index of El Niño/La Niña events.

Millennial coupled simulations

- Results from the 1000-year simulation with the coupled model indicate that links between Indian Ocean SSTs and rainfall over SWWA can be simulated as a consequence of changes in the atmospheric circulation driving pressure, winds, rainfall and SST changes rather than as a consequence of the SSTs driving the other variables. This tends to confirm the results of observational studies indicating that the Indian Ocean offers little in the way of predictability of SWWA winter rainfall.

- Similarly, an analysis of the relationship between an ACW-type phenomenon in the coupled model did not indicate that this provides a source of predictability for SWWA winter rainfall.

- Neither was it possible to identify any link between southern Indian Ocean SSTs and SWWA winter rainfall.

- Results from the 10,000-year simulation confirm earlier analyses, which indicate that annual rainfall totals over SWWA can exhibit variability on decadal, multi-decadal, and even millenial time scales due to internal processes.

- The results did not reveal any links between changes in rainfall at these time scales and changes in other variables such as SSTs.

Greenhouse simulations

- The latest CSIRO climate change simulations comprise ensembles and also take into account a range of CO_2 loadings and the effects of increased atmospheric sulphate content.

- The different experiments all yield a slight decrease in SWWA annual winter rainfall by the end of this century. Combined with increased temperatures (+3.0 ^{o}C) there is a slight decrease (-15%) in soil moisture.

- In addition, an equilibrium climate change simulation ($2xCO_2$ only) has been performed with the new Mark3 model. This is a simplified, but relatively inexpensive, greenhouse simulation.

- The Mark3 simulated global changes are somewhat less than the Mark2 results. Despite these differences, the results for SWWA are similar.

- None of the greenhouse simulations show evidence of any significant decrease in rainfall for the SWWA region over the period 1970-2000 (as has been observed)

- The internal (or "natural") variability in the various time series for rainfall tends to dominate any long-term trends over this century.

- The observed rainfall decline is likely to comprise, at most, a minor contribution from the enhanced greenhouse effect.

Observational analyses

- Results of analyses of historical mean sea level pressure data indicate that recent trends in an "Antarctic Oscillation" pattern are consistent with observed decreases in SWWA rainfall. However, the link does not explain the amount of decline observed over recent time.

Interpretation of greenhouse simulations from other models

- The results of climate change experiments from several different models (including the CSIRO model) have been stratified according the ability of each model to reproduce the seasonal cycle of rainfall for SWWA. As a result, only three models (the Hadley Centre model, the Geophysical Fluid Dynamics Laboratory (GFDL) model and the CSIRO model) were selected.

- Of these 3, the Hadley Centre model yields the largest percentage decrease in SWWA winter rainfall by the end of the century while the GFDL model yields the least.

- In each case there is little evidence that the observed decline can be attributed to the effects of the enhanced greenhouse effect.

- While there is evidence of rainfall declines similar to that observed, these are followed by periods of relative rainfall increases.

Conclusions

Sources of predictability

Results from the Mark2 coupled model simulations tend to confirm the results from observational studies which indicate that, at this stage, there are no obvious sources for significant predictability for SWWA winter rainfall. It is possible that SWWA winter rainfall may be affected by variations in SST at middle to high latitudes but observations are not (and have not been) sufficiently comprehensive. This may become apparent if the quality of observations improve over time (e.g. with improved satellite retrieval techniques). It is also possible that the Mark2 coupled model simulations of raw SWWA rainfall are not sufficiently accurate enough that reliable conclusions can be drawn from the experiments described here. However, the application of the existing coupled model to seasonal predictions as part of the last phase of research will also address these issues. In the first instance the model is initialized with the most recent observed SST anomalies which may be of better quality in the suspected key regions of interest. Secondly, the application of downscaling techniques has been shown to improve the rainfall product from these models and this is expected to improve the quality of the output. The improvements in going from the Mark2 to the Mark3 version also suggest that the potential exists for improved predictability.

Possible causes of the long-term dry conditions

Several factors have been cited as possible explanations for the drying trend. These include the enhanced greenhouse effect, land-use changes, air pollution or simply a natural fluctuation in the climate system which may, on the basis of millenial coupled simulations, be expected to reverse itself in the near future. In particular, previous analyses have indicated that, even without any external forcing, long-term dry periods are not uncommon within climate model simulations. Analyses strongly suggest natural climatic variability, although we cannot definitely rule out some minor contribution from other factors as indicated in the following figure.

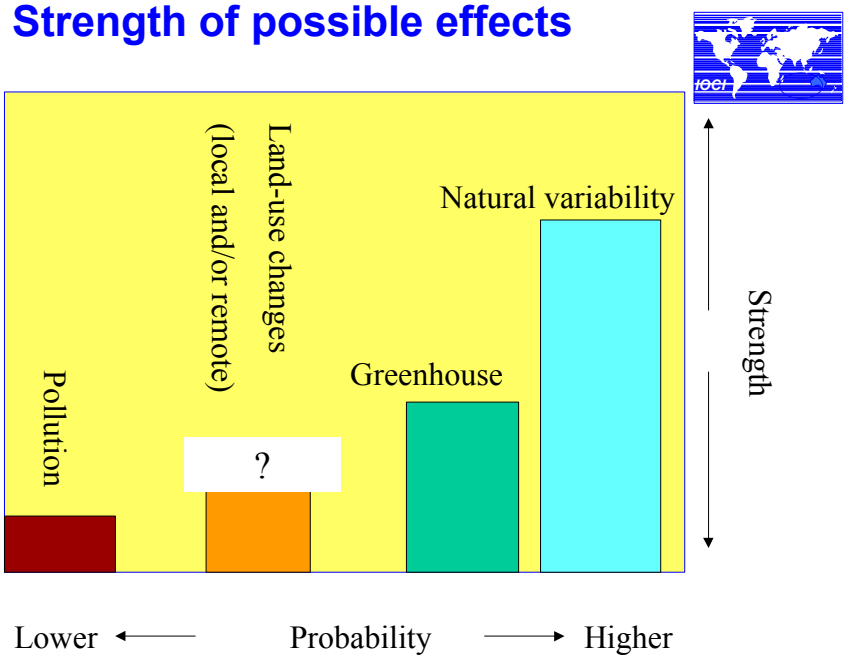

This figure is mainly qualitative and mainly represents an ordering of both the strength and probability of each possible factor. It represents a consensus view of the research partners based on all

the available evidence (both observational and model generated). In the case of land-use changes (for example) it is regarded as less likely to be a contributing factor than the enhanced greenhouse effect, more likely than air pollution, but its magnitude is very uncertain.

The important point to note is that natural variability implies that rainfall is as likely to be above average as it is below average over several decades. Therefore if the rainfall decline is part of the natural variability of climate in this region, then it is quite possible that above average rainfall will occur over the next decade or more. It is not possible to say when this will occur, other than to say that a wet winter this year or the next year would not be surprising.

RESULTS OF CAR IOCI SECOND RESEARCH PHASE STUDIES

1. Multi-seasonal predictions using global climatic models.

Introduction

A coupled prediction model, based on the CSIRO Mark2 version, has been developed that can be initialised with observations, run forward in time and used to simulate the evolution of global sea surface temperatures, pressure and rainfall. The aim of this development is to improve seasonal predictions for Australia at lead times of up to 12 months. Hindcasts have revealed useful skill at predicting Pacific SSTs at long lead times. In particular, there is evidence of skill at predicting SSTs in key regions with a lead time of 6 months.

The model, by design, is initialised with SST anomalies corresponding to observations. Cai et al. (1999) report that a version of this model, is capable of reproducing some of the features of the Antarctic Circumpolar Wave. In the version developed for seasonal predictions, SST anomalies associated with the Antarctic Circumpolar Wave are automatically incorporated. In theory, the model should be capable of simulating the impacts of this phenomenon if it contributes towards seasonal predictability. (It should be noted that, to date, there is little observational evidence that the ACW can contribute to the predictability of SWWA winter rainfall).

There are three methods for extracting seasonal predictions of rainfall from these types of models.

(a) Raw model rainfall output.

The Mark2 version of the global climate model was shown not to produce sufficiently accurate rainfall simulations for SWWA and therefore the raw model rainfall product is of limited use for this region. This version is being superceded by the Mark3 version and this section describes an assessment of the rainfall product from this new version.

(b) Statistical

In this method, simulations of key climatic indices are used to estimate rainfall according to the historical record. Given a prediction of a key SST index for July (say) from as early as January, it is possible to estimate the probabilities for rainfall being above or below average based on the historical record. This approach to seasonal predictions is most relevant to eastern and northern Australia where there are strong SST/rainfall relationships. This section also describes how this approach has been implemented.

(c) Downscaling

This method makes use of the simulated fields of temperature, humidity and pressure and yields a more credible estimate for local rainfall than the direct model product. This technique is under investigation as part of the next phase of research.

Mark3 rainfall simulations

As part of Atmospheric Research's own research activities, the atmospheric component of the CSIRO Mark3 model is being used to simulate the observed climate by forcing it with observed sea surface temperatures (SST). The first simulation covered only the timeframe 1979-1995 and was a contribution to the second international Atmospheric Model Intercomparison Programme (AMIP2). Currently five additional simulations are under way, for 1949-1998, using the Global Sea Ice and Sea Surface Temperature (GISST) datasets prepared by the U.K. Met. Office. To date three of the GISST runs have passed the 1990 year mark and were available for the present analysis.

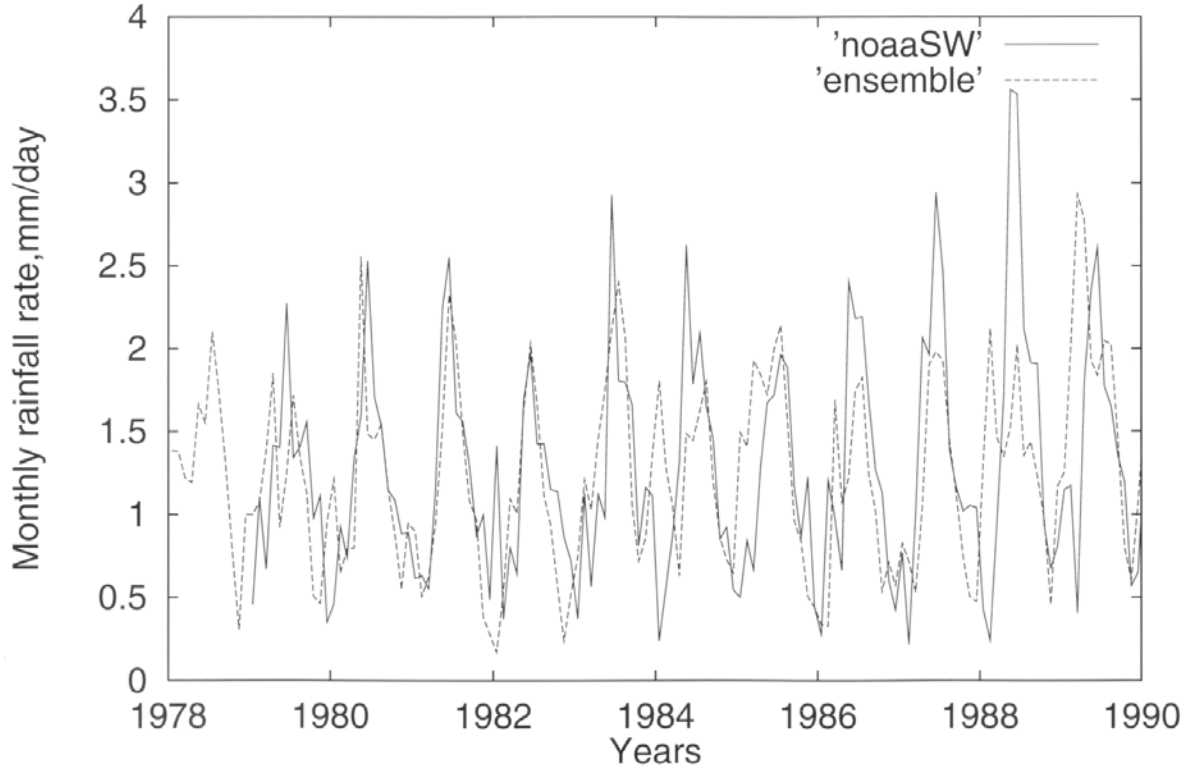

Figure 1. Comparison of observed rainfall (from the NOAA dataset) with the ensemble mean simulation results obtained by forcing the atmospheric component of the Mark3 CSIRO model with observed SST for the period 1978-1990.

The model outputs from these various simulations have been compared against observed rainfall for a region of SWWA (32°-35°S, 116°-120°E). The motivation behind this comparison is to determine how accurately it is possible to 'predict' rainfall in this region given a 'perfect' SST forcing field. This then permits an estimate to be made of the ultimate predictability of rainfall, compared with predictions involving a coupled global climatic model where the SSTs have to be predicted ab initio.

The first analysis was restricted to the AMIP2 period and used a global rainfall dataset made available by NOAA (Xie and Arkin, 1996). The observations (noaaSW) are compared with an ensemble of model outputs (ensemble) in Fig. 1. The ensemble comprises the mean of 3 GISST runs and the AMIP2 run. An ensemble is needed because the simulated rainfall is chaotic and averaging over a number of runs is required in order to improve the signal-to-noise ratio. The results in Fig. 1 reveal that it is possible to simulate both the seasonal cycle and much of the interannual variability of rainfall over the region with some accuracy over the period 1979-1986, but less so over the period 1987 to 1990. Enlarging the size of the ensemble may improve on this situation. Examination of the high frequency variability in this figure, suggests that for any given month only low confidence exists as regards predictability, even though the interannual and seasonal changes may be well-predicted. However, the improvements in the agreement in this figure for the Mark3 model, compared with a similar intercomparison for the Mark2 model in the previous IOCI report, indicates that future model improvements might at least partially rectify these current problems.

It is, however, necessary to evaluate model simulations/'predictions' in a broader purview than that provided by the time series in Fig. 1. For example, in Fig. 2 the global distributions of the observed (NOAA) and simulated rainfall (single GISST run) for August 1981 are compared. The overall patterns agree quite well with the marked exception of Australia. While the rainfalls for SWWA agree, the simulation produced much higher rainfall across most of Australia. This difference can be attributed to use of too high a temporal frequency (i.e. one month) comparison and the limitation to a

single simulation. The essential point which comes out of this analysis is that predictions for any selected region must be considered in the context of the global distribution to ensure that plausible outcomes are being obtained.

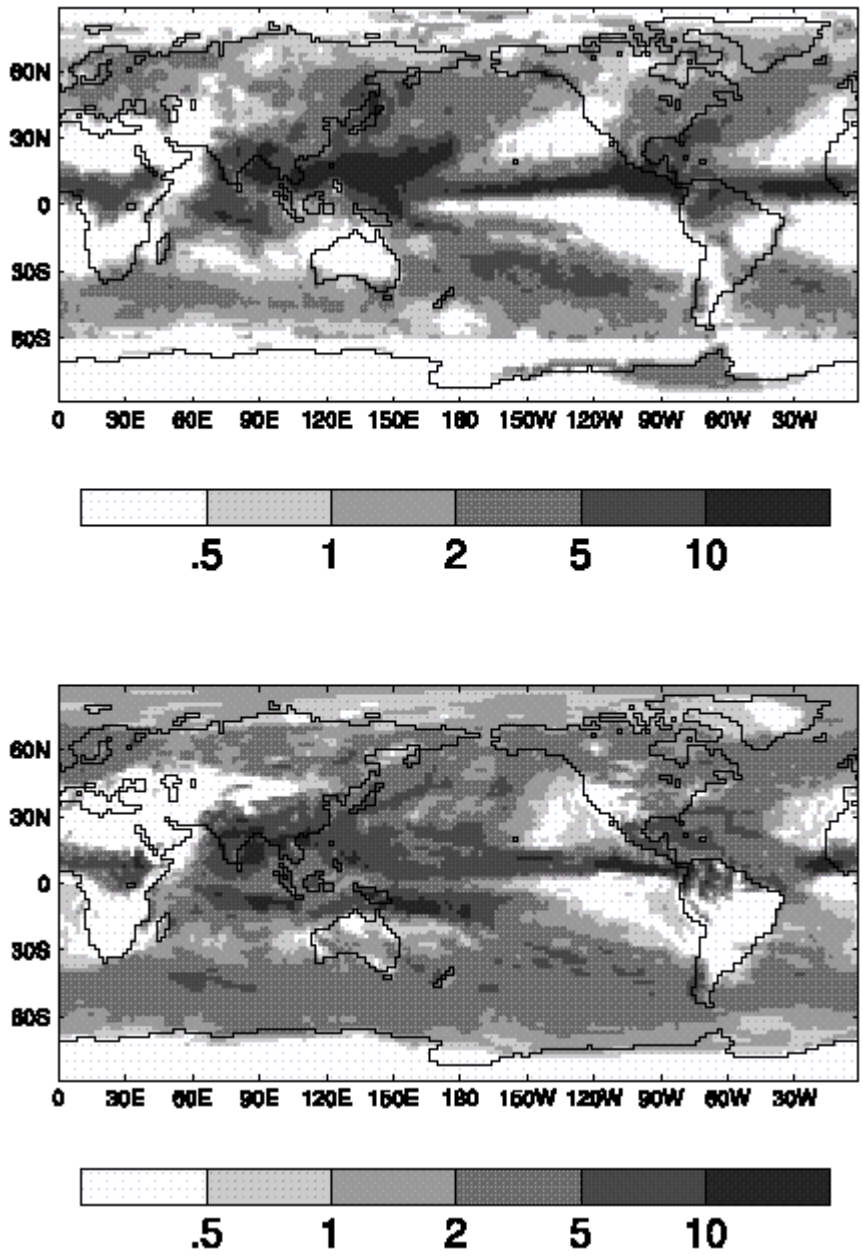

Figure 2. Observed (top) and simulated (bottom) rainfall distributions for August 1981. The simulated rainfall is based on a single run with the atmospheric component of the Mark3 CSIRO model. The shading corresponds to amounts in millimeters per day.

Comparisons with observed rainfall were also made with the GISST ensemble (3 runs) for the period 1949-1990. This highlighted a problem with the observational data. Two rainfall datasets were available for this period, the NCEP-NCAR global re-analysis and a high resolution analysis for Australia-only produced by the Queensland Department of Natural Resources (QDNR). A comparison of the rainfall for SWWA based on these two datasets is given in Fig 3. The overall lack of agreement is disturbing. The QDNR dataset, from the way it is derived, might be expected to resolve intense, local rainfall somewhat better than the NCEP-NCAR dataset, but such differences should prevail for the whole of the time period in the figure, not just the first 20 years. Even within the later period there

are marked disagreements, (e.g. 1975 and 1983). The utility of the QDNR dataset is also limited because of its restriction to Australia only.

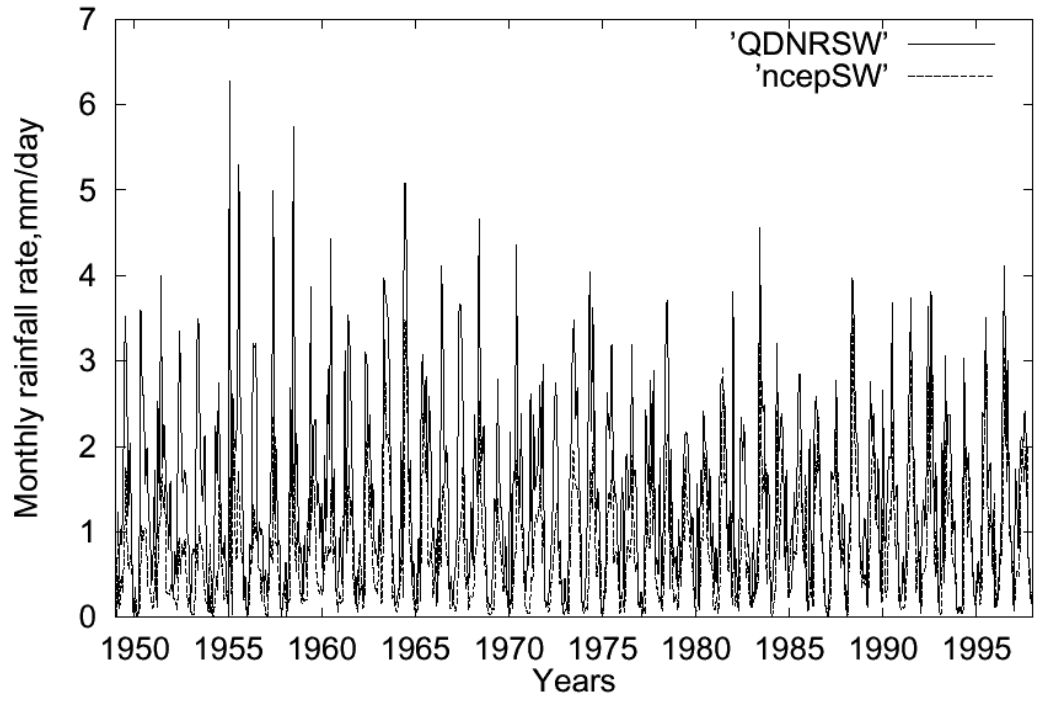

Figure 3. Observed rainfall values for SWWA as obtained from the NCEP-NOAA and QDNR analyses.

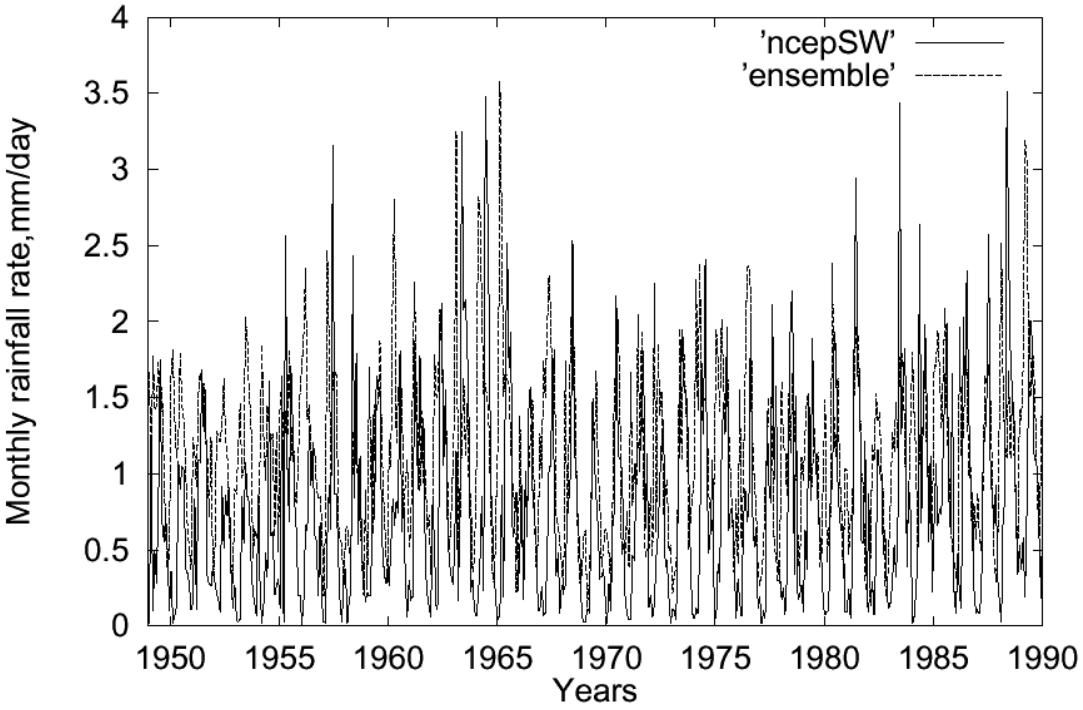

Figure 4. Comparison of observed rainfall (ncepSW) from the NCEP-NCAR dataset and simulated rainfall (based on a 3 member ensemble) for SWWA

The GISST ensemble (3 member) compares reasonably well with the NCEP-NCAR rainfall in Fig 4. Extreme peak values tend not to agree, but as these are normally attributable to a single month such agreement may not be achievable. Certainly enlarging the GISST ensemble to 10 members (which is planned) would be expected to improve overall agreement. Of particular interest is the fact that the GISST ensemble includes a rainfall reduction commencing after 1965 in Figure 4. What caused this decline, and whether it is related to SST changes, remains unclear. Certainly the decline shown in the figure is relatively sharp, which would argue against incremental CO_2 increases in the atmosphere through this period.

The comparison with the QDNR dataset is very different. The QDNR values better reflect the rainfall decline but Figure 5 also suggests that the model values underestimate the observed rainfall. The QDNR values (unlike the NCEP-NCAR values) are based purely on interpolated observations and represent small-scale rainfall features including topographic effects. These are generally not resolved by a coarse grid climate model and so the underestimates of rainfall totals is not unexpected.

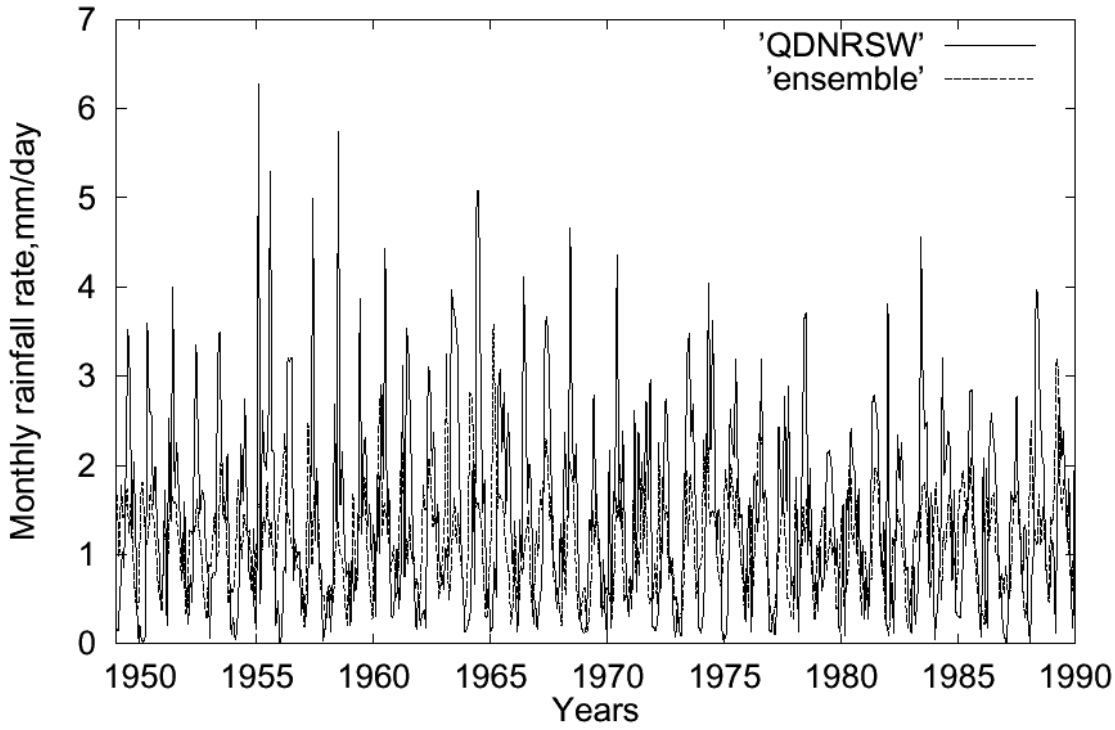

Figure 5. As for Fig. 4 but using the observed rainfall (QDNRSW) from the QDNR dataset.

A critical aspect is to demonstrate whether it is possible to predict SST distributions adequately for useful seasonal predictions of rainfall to be obtained. To this end it is important to know which regions of the ocean are most important as regards the influence of the SST distribution on SWWA rainfall. This was investigated by correlating the rainfall simulated for this region with the observed SSTs used to force the Mark3 model. The correlation coefficients, for the period 1949 to 1990, are shown in Fig. 6 for a single ensemble member of the GISST simulations. Results were remarkably similar for other ensemble members, indicating these correlations are a robust outcome. While the maximum correlations are somewhat below the 90% significance level, the results suggest that SST variability in the tropical Pacific is the major (albeit weak) influence on SWWA rainfall. Since the SST values in this oceanic region are the most predictable over the globe this, again, is encouraging as regards the ability of a coupled climatic model to predict the forcing field for the SWWA rainfall variations.

The improvement of the Mark3 CSIRO model compared with the Mark2 version indicates that future model development may offer even more encouraging prospects for seasonal predictions for SWWA. The agreement between the ensemble output and NCEP-NCAR and NOAA datasets reveals that considerable skill exists in 'predicting'/simulating rainfall for this region. This outcome will be quantified better when a larger simulated ensemble becomes available.

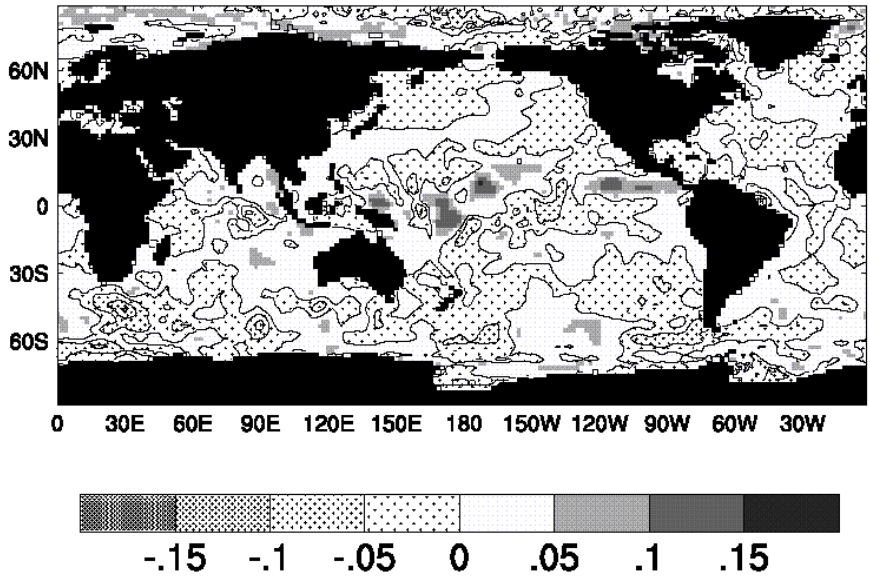

Figure 6. Correlation of observed sea surface temperatures with rainfall for SWWA as simulated with the Mark3 CSIRO atmospheric model.

Coupled/statistical model predictions

Figure 7 shows an example of predictions from the CSIRO model of the SST index referred to as NINO3.4, which provides a measure of El Niño or La Niña events. The observed values (circles) indicate that La Niña conditions have persisted from 2000 through to January 2001. The latest (at time of writing) predicted values (squares and diamonds), indicate that these conditions will slowly weaken during the remainder of the year. If relatively cool conditions persist through to April 2001, then Figure 8 provides an indication of the probabilities for autumn rainfall totals to exceed their median values. These probabilities are based on observations over the period 1950-1999. In this case the probabilities for exceeding the median are enhanced over northern and eastern Australia, reduced over much of Western Australia, but not altered significantly for SWWA. This is consistent with findings to date that El Niño and La Niña events do not have a large impact on autumn rainfall in this part of the continent. CSIRO Atmospheric Research now routinely makes this information available on the web site http://www.dar.csiro.au/res/cm/coca.htm .

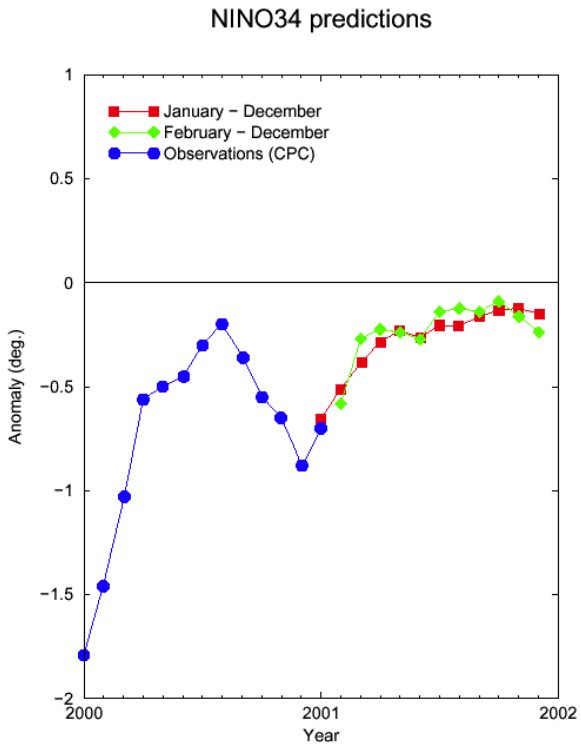

Figure 7. Predicted NINO3.4 index for 2001 from the CSIRO seasonal prediction model. Observed monthly values of the index January 2000 to January 2001 (circles), predicted values starting from January 2001 (squares) and February 2001 (diamonds).

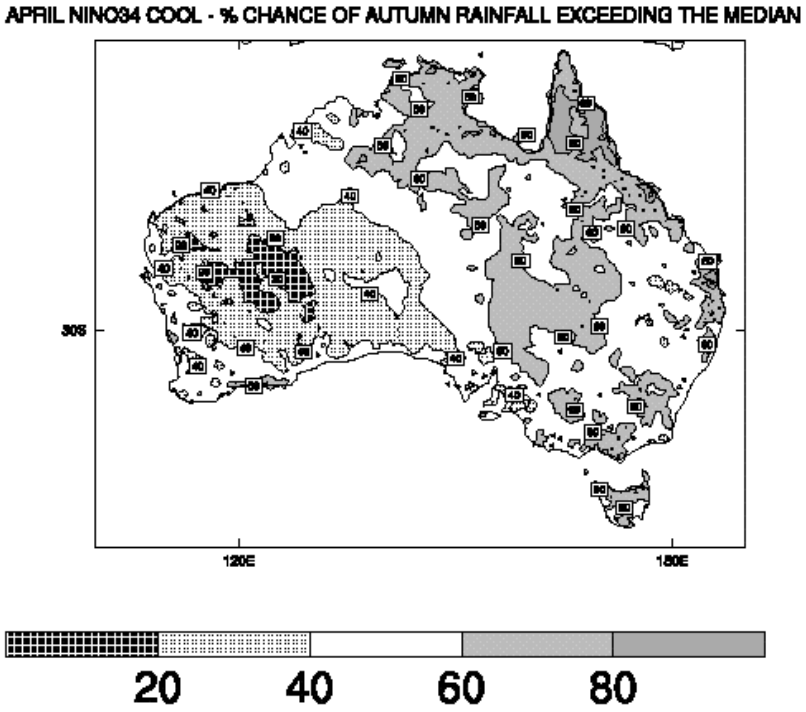

Figure 8. Probabilities for autumn rainfall totals exceeding their long-term median value when the NINO3.4 is in the cool category.

2. Millennial coupled simulations.

Introduction

Previous work (e.g. Smith et al., 2000) identified a link between SWWA winter rainfall and both sea surface temperatures and mean sea level patterns over the Indian Ocean. However, it appeared that these links offered little in the way of predictability and that they might arise as a consequence of the atmosphere directly forcing both the SSTs and the rainfall in this region. In the Phase 1 report, detailed results were presented from a 1000-year simulation with the Mark2 CSIRO coupled global climatic model. These results demonstrated that natural climatic variability could possibly account for the current drying trend in SWWA. A number of analyses were made highlighting the occurrence, frequency and amplitude of rainfall anomalies over the globe, which set the situation in SWWA in perspective. This section reports on the results of further analyses of the 1000-year simulation and an analysis of the 10,000-year simulation which address these issues.

Further analyses of the Mark2 coupled model 1000-year simulation

Eastern Indian Ocean SSTs

Observational studies (e.g. Smith et al., 2000) have found moderate (although barely significant given the limited length of the data) correlations between SSTs to the west of Australia and winter rainfall and surface temperatures in WA and appeared to indicate some potential predictability using May SSTs. The 1000-year coupled model simulation has been used to explore this relationship. While the GCM may have limitations due to its moderate resolution, it is expected to model the basic processes relating SSTs and rainfall, and the length of the run removes any uncertainty in the relationships, at least.

An SST pattern, based on the region implicated in the observational studies, was defined and an amplitude index for each month of the simulation was determined. The correlations between this index and winter (June-August) means in the same year over the 1000 years are shown in Figure 9.

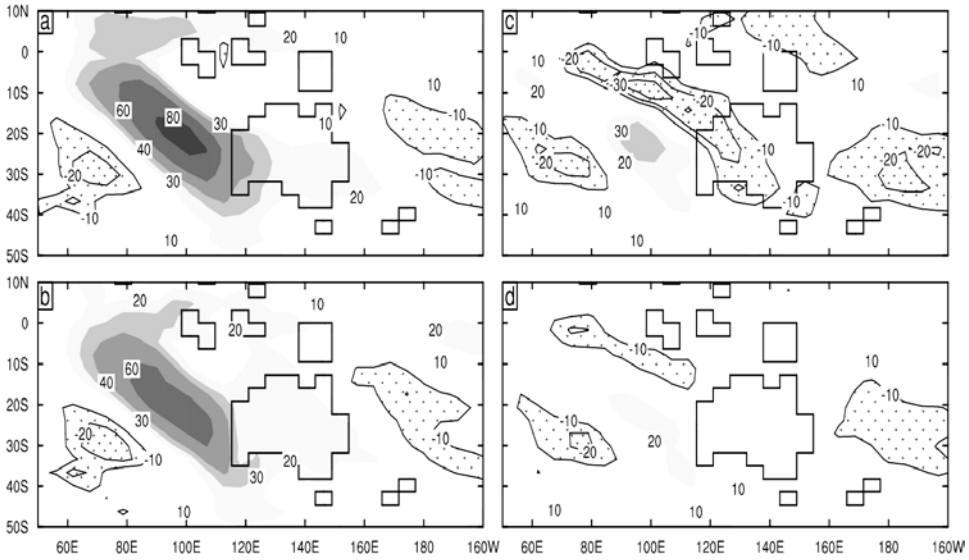

Figure 9. Correlations (x100) of SST index associated with SSTs to the west of Australia with mean surface temperature and rainfall during June-August in the 1000-year GCM simulation. Shown are the values for (a) SST index in July with surface temperature, (b) SST index in May with surface temperature, (c) SST index in July with rainfall, and (d) SST index in May with rainfall

The correlation pattern between the index and surface temperatures (Fig.9a) shows the SST pattern. It also shows that the SST anomalies are associated with land-surface temperature anomalies over much of the continent. Note that land temperatures vary more than SSTs, so the actual anomalies are more similar across the west coast than the correlations may suggest. The correlation pattern using the May index (Fig. 9b) indicates that both the SST and land-surface temperature anomalies tend to persist into winter. The correlation pattern between the July index and winter rainfall (Fig. 9c) shows that enhanced rainfall over the warmer ocean is associated with decreased rainfall in a band to the north and east, including central WA. This pattern resembles the association between Australian winter rainfall and Indian Ocean SSTs identified by Nicholls (1989). Smith (1994) demonstrated that this type of association is only simultaneous and offers little in the way of predictability. The model results confirm this since only the ocean rainfall is usefully predictable (Fig. 9d). From other results (not shown), it can also be shown that the SST anomalies in May are associated with low surface pressures that sometimes extend over land during winter but are very weak, and have little effect on WA rainfall. In contrast, the July index is large when the SST anomalies have been forced by surface heating during June and July due to northwesterly wind anomalies. The pressure over the land is higher than usual during those months, and rainfall lower - thereby indicating that the relationship is not one of the SSTs forcing the atmosphere, but rather the atmosphere forcing the ocean. Therefore, while there is little predictability associated with these Indian Ocean SST patterns, it should be noted that there is some evidence that they may be remotely forced by the Pacific Ocean as part of the ENSO "cycle" (see Baquero-Bernal and Latif, 2001).

The Antarctic Circumpolar Wave and its influence over SWWA

White (2000) has suggested that the Antarctic Circumpolar Wave may involve coupled atmospheric-ocean anomalies that include predictable rainfall anomalies over SWWA. Given the shortness of the data record, and the time-filtering performed in that and similar studies, this conjecture remains far from proven.

Cai et al. (1999) analysed 60 years from a CSIRO coupled model simulation and focussed on the results for Southern Ocean SSTs. While an ACW-type pattern was identified, it did not exhibit a clear propagating wavenumber-2 signal as in the observations. Given the completion of the 1000-year simulation with this model, a further assessment of the simulation of this high-latitude component is now possible. Firstly (and based on the observed ACW) an index with an amplitude of wave-2 structure was derived. For each phase position in May, the index was correlated with the following winter means of SST and rainfall. In each case the correlations with SST were relatively strong in the South Pacific (Fig.10a) but relatively weak in the Indian Ocean -again indicating that a propagating wave-2 structure is not prominent in the model. However, the correlations with equatorial Pacific SSTs supports the recent work of Cai and Baines (2001) which indicate that ENSO events play a major part in generating the high-latitude patterns. The correlation of the May index with winter rainfall (Fig. 10b) is very weak over WA, but less so over western Pacific rim where ENSO effects are apparent. Consequently, the results do not indicate that there is any significant predictability for WA based on ACW-like SSTs, at least within the current model.

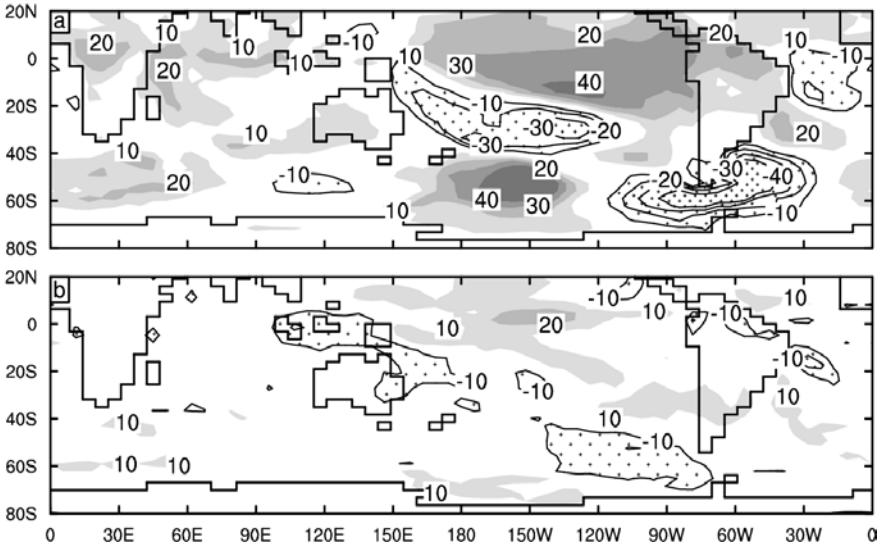

Figure 10. Correlations (x100) of an index associated with Southern Ocean wave-2 SSTs in May with (a) surface temperature and (b) rainfall during June-August in 1000-year GCM simulation.

Southern Indian Ocean SSTs

Focussing now on the Indian Ocean SSTs within the 1000-year simulation, an index has been derived that captures much of the variability to the southwest of Australia. Correlations between this index in July and winter SSTs identifies the region of interest (Fig.11a). A correlation was performed between the index in September and pressure anomalies during winter (Fig.11b) and between the index in May and the pressure anomalies in winter (Fig. 11c). The fact that the pressure anomalies in winter are associated more with the SSTs in September, rather than the SSTs in May with the pressures in winter confirm the previous findings that the atmosphere tends to drive the SST anomalies in this part of the world. In both these and other cases analysed, the precursor pressure anomalies are consistent with north-easterlies over the ocean surface, which leads to warming (see Watterson, 2000). Consequently, there is also no evidence of a significant predictability of winter rainfall from May SSTs (Fig.11d).

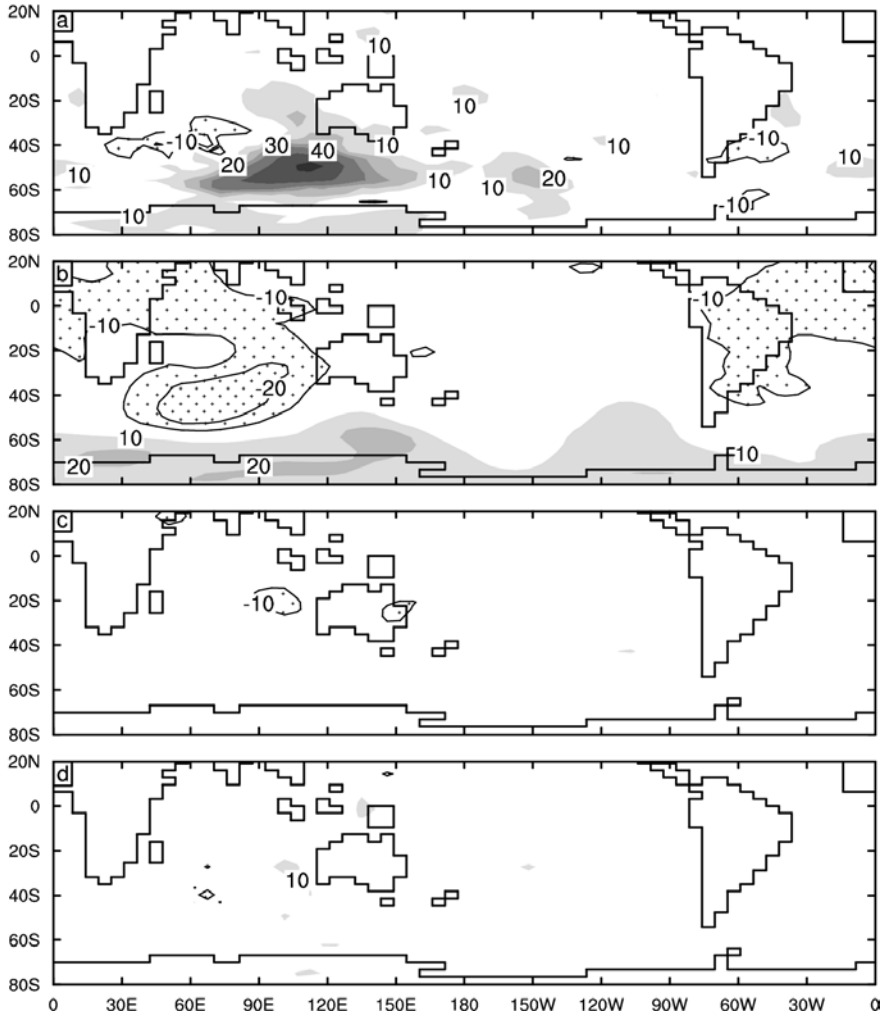

Figure 11. Correlations (x100) of SST index associated with SSTs to the southwest of Australia with mean surface temperature and rainfall during June-August in 1000-year GCM simulation. Shown are the values for (a) SST index in July with surface temperature, (b) SST index in September with surface pressure, (c) SST index in May with surface pressure, and (d) SST index in May with rainfall.

Analysis of the 10,000-year run

A new simulation with a slightly modified version of the Mark2 CSIRO model extending to 10,000 years has now been completed. The intention here is not to repeat the analysis made for the 1000-year run but to emphasize some aspects of millennial variability. However, it needs to be emphasized that decadal drying and wetting trends similar to those in the 1000 year run occurred in the 10,000-year run. Hence, there is a robust expectation that the SWWA drying trend is probably principally attributable to natural climatic variability as demonstrated via the model simulation.

An indication of annual mean rainfall variability over SWWA is given in Fig. 12 where all 10,000 years from the simulation are plotted. A rather stable situation existed with no major, long-term trends apparent in this time series. Negative rainfall anomalies rarely exceeded 0.4 mm day^{-1}, but positive anomalies ranging up to almost 1.00 mm day^{-1} occurred on a number of occasions.

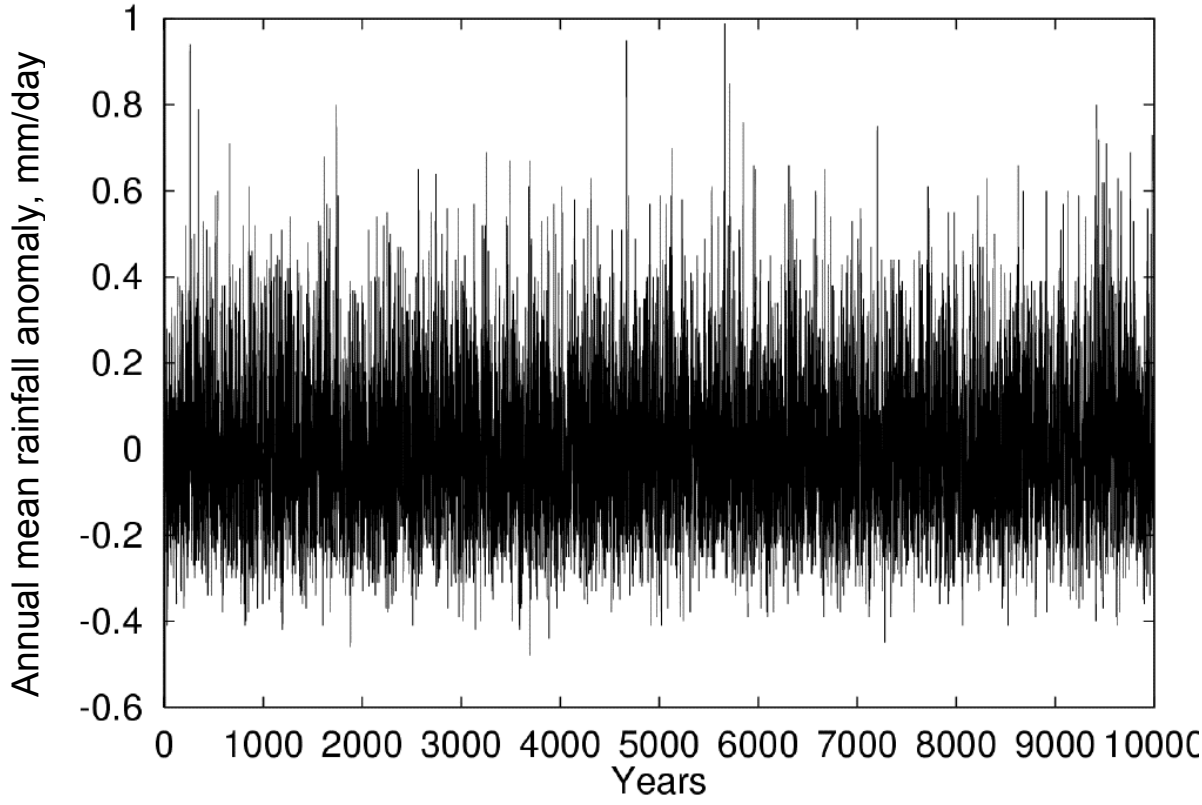

Figure 12. Time series of rainfall anomalies for SWWA from a 10,000-year simulation with the Mark2 CSIRO model.

Despite the apparent stability exhibited in this time series multi-millennial variability did occur. An example of such variability is shown in Fig. 13 and Fig. 14, where results for the first two millennia are compared. The raw, annual mean values in the right hand panels illustrate more clearly the temporal variability. Decade-long anomalies can be identified in these panels. In the left hand panels the rainfall anomalies are illustrated after having been smoothed with a 10-point running filter. These panels more clearly identify decadal-scale anomaly trends, and reveal that such smoothed trends can have durations of up to 50 to 60 years. These results confirm the conclusions made previously from the 1000-year simulation.

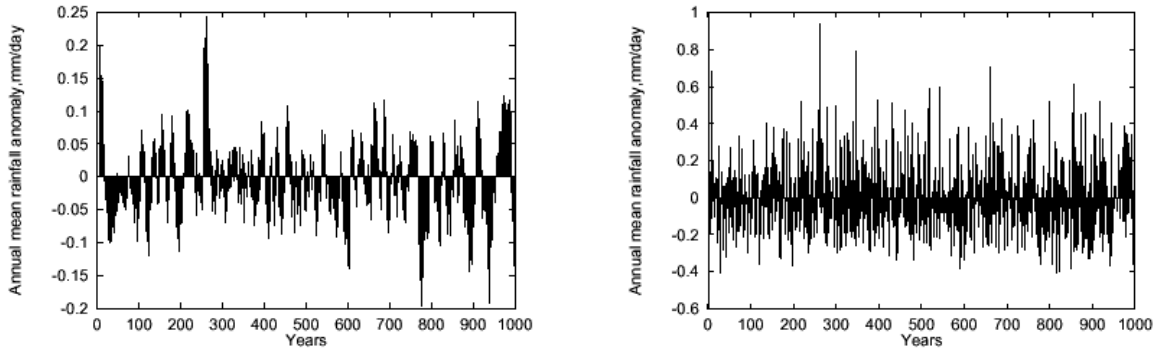

Figure 13. In the right hand panel annual mean rainfall anomalies are shown for the first one thousand years of the 10,000-year simulation. In the left hand panel the time-smoothed variations are given.

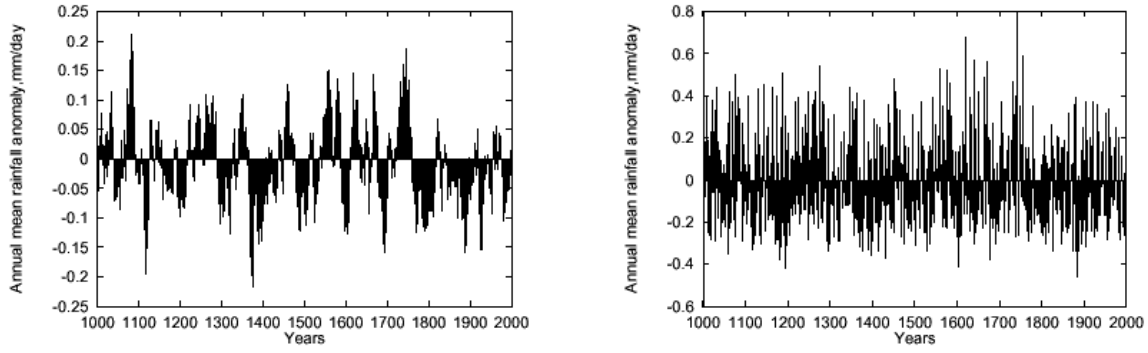

Figure 14. As for Fig. 13 but for the second one thousand years of the 10,000-year simulation.

There is, however, a more subtle aspect to these two figures. In Fig. 13 the periodicity in the left-hand panel can been seen to be predominantly decadal, whereas in Fig. 14 a longer term periodicity is apparent. To some extent this difference in periodicities is also discernible in the raw annual mean values in the right hand panels. Fourier analyzing these two millennia separately clarified this difference. The outcomes are very clearly displayed in Fig. 15 where the dominant periodicity for the second millennium is 100 years, while it is only 10 years for the first millennium.

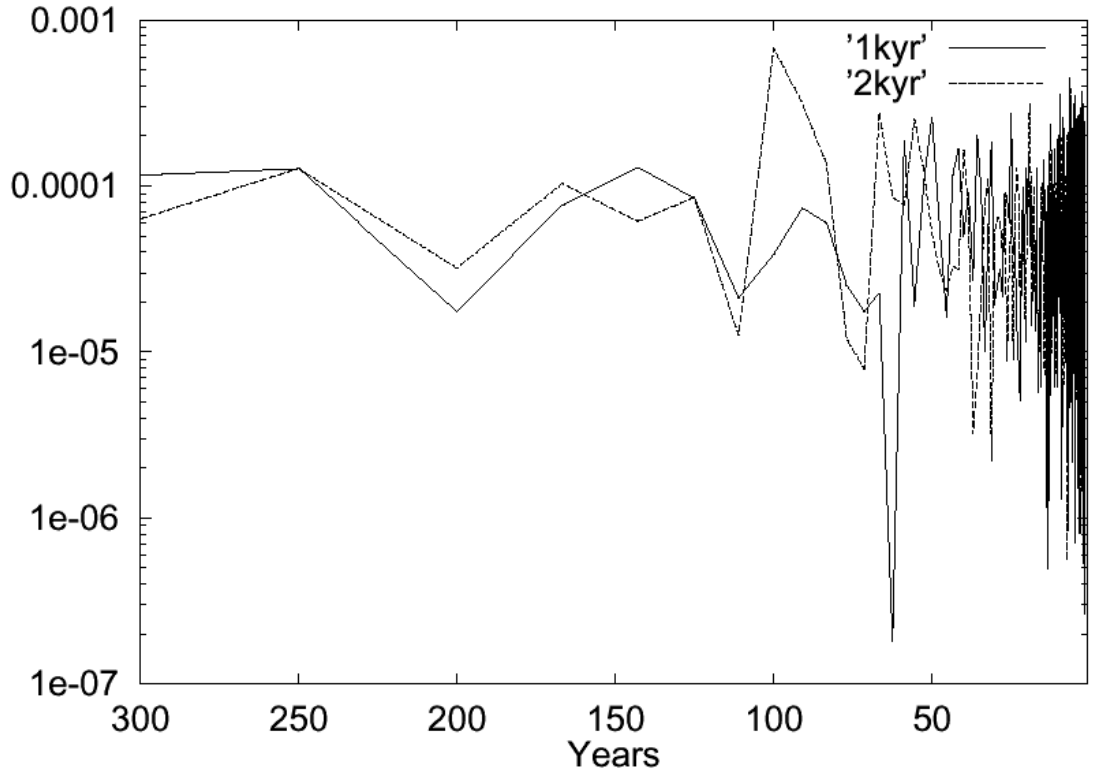

Figure 15. Spectral analysis of SWWA annual rainfall as simulated over two separate 1000-year periods.

The implication of this outcome is that while the 10,000 years of the simulation, as shown in Fig. 12, is basically stable, there are millennial variations within the simulation. Clearly, the resulting duration of rainfall anomalies have different characteristics. For example, from the viewpoint of stability of rainfall for agriculture or water supply the first millennium of the simulation would be preferable because of the shorter duration of the anomalies. Unfortunately, as regards SWWA, the observational record is too short to discriminate between these two situations. Nevertheless, from a planning perspective it is valuable to know that such differentiation between different rainfall periods may exist.

A considerable effort was made in attempting to clarify/identify possible mechanisms behind the decadal-plus length anomaly trends. Temperature anomalies, rather than rainfall anomalies, were considered in this analysis because temperature is a 'continuous' variable, unlike the intermittent nature of rainfall, and also experienced longer duration anomalies.

The analysis attempted to identify the physical processes associated with the commencement or termination of a persistent temperature anomaly with conditions for the Indian Ocean being particularly investigated. No consistency was found between different temperature anomalies as regards the dominant physical processes. Hence no clear mechanistic basis for initiation or termination of climatic trends was obtained.

An alternative approach was adopted which involved using an auto-regressive or Markov analysis. This analysis was used extensively on the 1,000-year simulation and revealed that rainfall trends could be represented by an order 1 Markov process. Using the Markov coefficients so-generated permitted rainfall anomaly time series to be regenerated that had the same characteristics as the originating time series. This outcome indicates that the rainfall anomalies simulated, and importantly the decadal trends, may be the result of random rather than systematic processes. This suggests that it may not possible to predict the occurrence of wet and dry trends, at least as simulated with the present

model. An order 1 Markov process also resulted from an analysis of the rainfall trends over SWWA using the 10,000-year simulation. Thus this outcome appears to be a robust result from the simulations.

However, when the Markov analysis was applied to temperature anomalies over the ocean an order 2 process was obtained. The regenerated time series using the corresponding Markov coefficients failed to reproduce the features of the original time series, both in amplitude and trend characteristics. This implies that solely random processes did not generate these oceanic temperature time series. As such some physical mechanisms were involved, presumably associated with the 'memory' attributable to the oceanic thermal inertia. In principal, these long-term temperature trends are predictable despite the failure, mentioned above, to identify the underlying mechanisms. How this conclusion can be exploited remains a matter to be determined by future research.

3. Greenhouse simulations

Introduction

This section reports on results from recent greenhouse climate simulations made with the Mark2 coupled model using four different scenarios (i.e. different amounts of carbon dioxide and aerosol distributions) and also preliminary results from the new Mark3 model using a simple mixed-layer ocean. The major aim of these studies is to identify any changes in rainfall that could be associated with the greenhouse effect and which could help explain the observed rainfall decline that occurred in SWWA around 1970, as well as investigating future possible rainfall changes.

Analyses of greenhouse scenarios using the Mark2 model

A new series of greenhouse simulations has been made or is being completed with the CSIRO Mark2 coupled global climatic model. This involves using the Special Report on Emission Scenarios (SRES) input data. The major difference compared with previous simulations made with the CSIRO model is that the SRES scenarios include sulphate emissions into the atmosphere, which induce a cooling effect. [This represents the so-called direct sulphate impact; the indirect impact which involves modification to cloud properties has not been included at this stage because of current uncertainties regarding the physical processes involved]. These simulations also include future changes in atmospheric ozone concentrations that are to be expected as chlorofluorocarbon concentrations decline in the stratosphere.

The SRES simulations cover the period 1990 to 2100 AD. However the simulations were effectively commenced in 1870, but have a common lead-in period 1870-1990, where *observed* values for CO_2 , ozone and sulphate were specified. Thus, this initial period of the simulation effectively is an attempt to replicate the observed climate for this period. The atmospheric CO_2 concentrations and sulphate aerosol burdens for the four SRES scenarios, known as A1, A2, B1 and B2, are shown in Fig. 16 and Fig. 17 respectively. The observed CO_2 and sulphate values for 1870 to 1990 are also included in these figures, which clearly show the divergence of the individual scenarios after 1990.

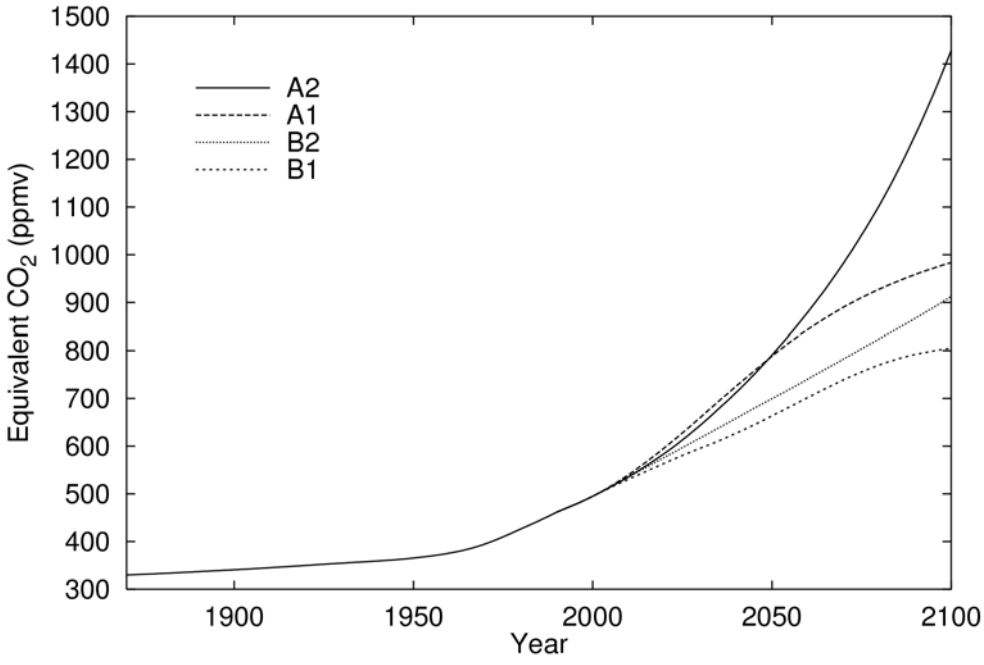

Figure 16. Equivalent atmospheric CO_2 concentrations for the four SRES scenarios

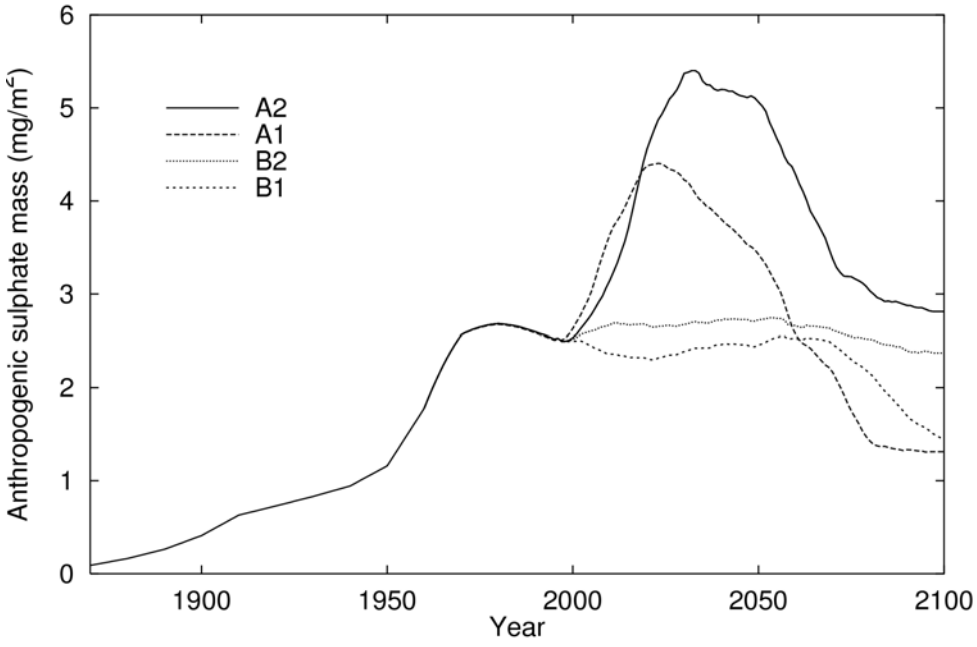

Figure 17. Annual mean sulphate aerosol burdens for the four SRES scenarios.

As can be seen from Fig. 16, these scenarios involve quite distinct CO_2 atmospheric concentrations by 2100 AD, ranging from 800 ppm for B1 to over 1400 ppm for A2. Such values should cover the actual CO_2 concentrations likely to exist in the atmosphere by 2100 AD. Separate sulphate burdens are associated with these scenarios, (Fig. 17) but the important aspect of all scenarios is the decline in these burdens by 2100 AD. This is based on the assumption that appropriate emission controls are widely implemented, and the relative proportion of natural gas usage to coal increases.

[Previous CSIRO greenhouse simulations (see Section 5) refer to the scenario known as IS92a, which assumes a 1% increase in effective greenhouse gas concentrations. In addition, previous results have attempted to take into account the effects of changes in aerosols, but in a relatively crude fashion. The SRES scenarios referred to here represent more realistic and representative scenarios since they involve different rates of CO_2 increases *and* different aerosol loadings. The effect of the aerosols is also parameterised in a more realistic fashion. As an approximation, the IS92a results probably represents results lying between those of the A2 and B2 scenarios.]

The CO_2 and sulphate variations between scenarios produce temporally varying climatic responses, so that for much of the time to 2100 AD these responses are not necessarily dominated by the maximum CO_2 concentrations associated with the A2 scenario. Since the SRES simulations commence in 1870 they can be used to investigate whether there is any greenhouse influence on the observed SWWA drying trend, which commenced in the late 1960s. Given the common lead-in period of 1870 to 1990 only one simulation was available, and because of chaos in the climatic system this need not be truly representative. In order to allow for chaotic influences an ensemble of simulations is currently being generated, for the B2 scenario, commencing in 1870 and running out to 2100 AD. An ensemble of five simulations is planned and four simulations have so far reached 1970, with individual simulations extending to later dates.

The rainfall time series for SWWA for these individual ensemble members, and the ensemble mean to 1970 are shown in Fig. 18.

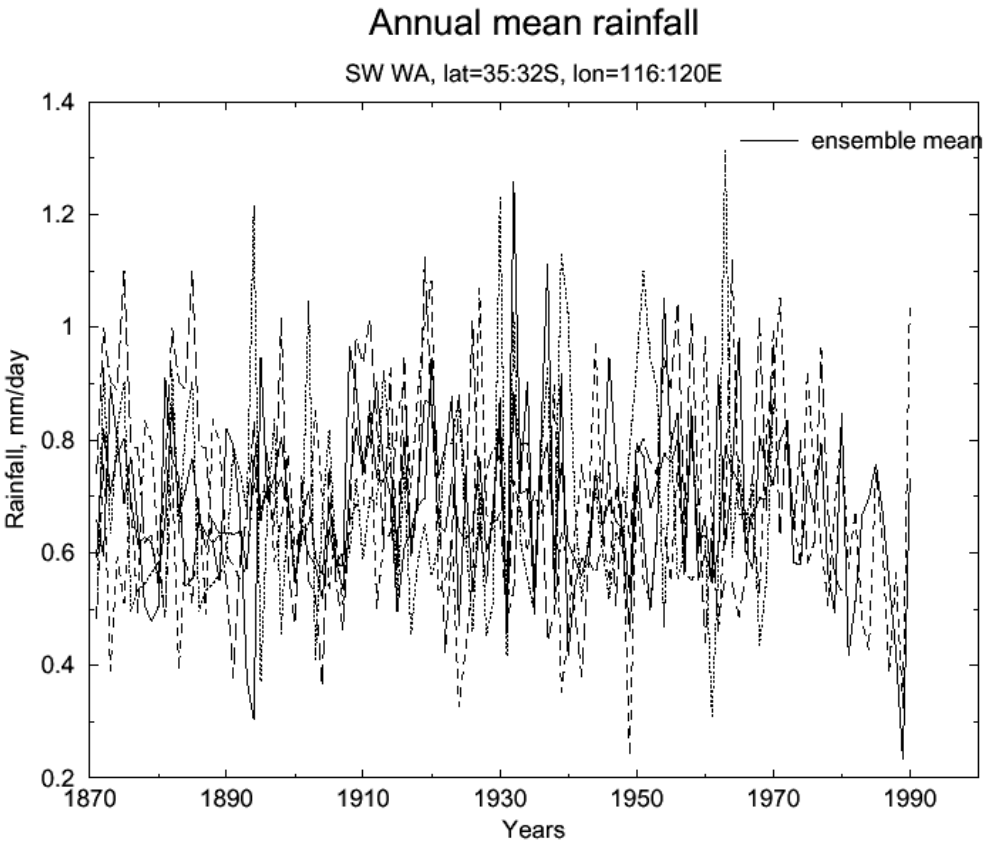

Figure 18. Time variation of rainfall for SWWA as produced in an ensemble of four simulations with the CSIRO Mark2 model based on the B2 scenario (At the time of writing, two go from 1870 to 1970 and two go from 1870 to 1990. It is planned that this ensemble will eventually comprise a total of 5 simulations, all going from 1870 to 2100). The four individual simulations are represented by the thin lines, the ensemble mean by the thick line.

The ensemble mean to 1970 indicates no sign of a drying trend for this region, although considerable interannual variability is present. Marked intra-ensemble variability occurred, which emphasises the need to generate ensemble means, particularly if short time periods are being considered. Although there is a suggestion of a drying trend for the two ensemble members which extend to 1990, there is also a recovery in 1990 itself. Until the complete ensemble is available, the presence or absence of a greenhouse-related drying trend cannot be excluded on the basis of Fig. 18. However, when the four scenario members are analysed for the period 1990 to 2100 AD, Fig. 19, there is only a slight indication of a drying trend over this period. While multi-member ensembles for each scenario would be desirable to clarify the impact of chaos, this is computationally impractical at this time. The indication from Fig. 19 is for only a slow drying trend to emerge in the SWWA under greenhouse conditions, which makes it unlikely that the *current* drying trend has any major greenhouse input. The downturn in the rainfall time series shown by the two ensemble members after 1980 in Fig. 18 would then appear to be associated with some chaotic affect rather than a greenhouse influence. When the ensemble of five runs is completed to 2100 AD this issue will be seen in perspective. Thus the observed drying trend in the SWWA can now be more confidently attributed to natural climatic variability, as indicated in the Phase 1 report and as discussed above. Of course, this statement is based on results from the CSIRO model only, other models might can indicate different outcomes (see Section 5).

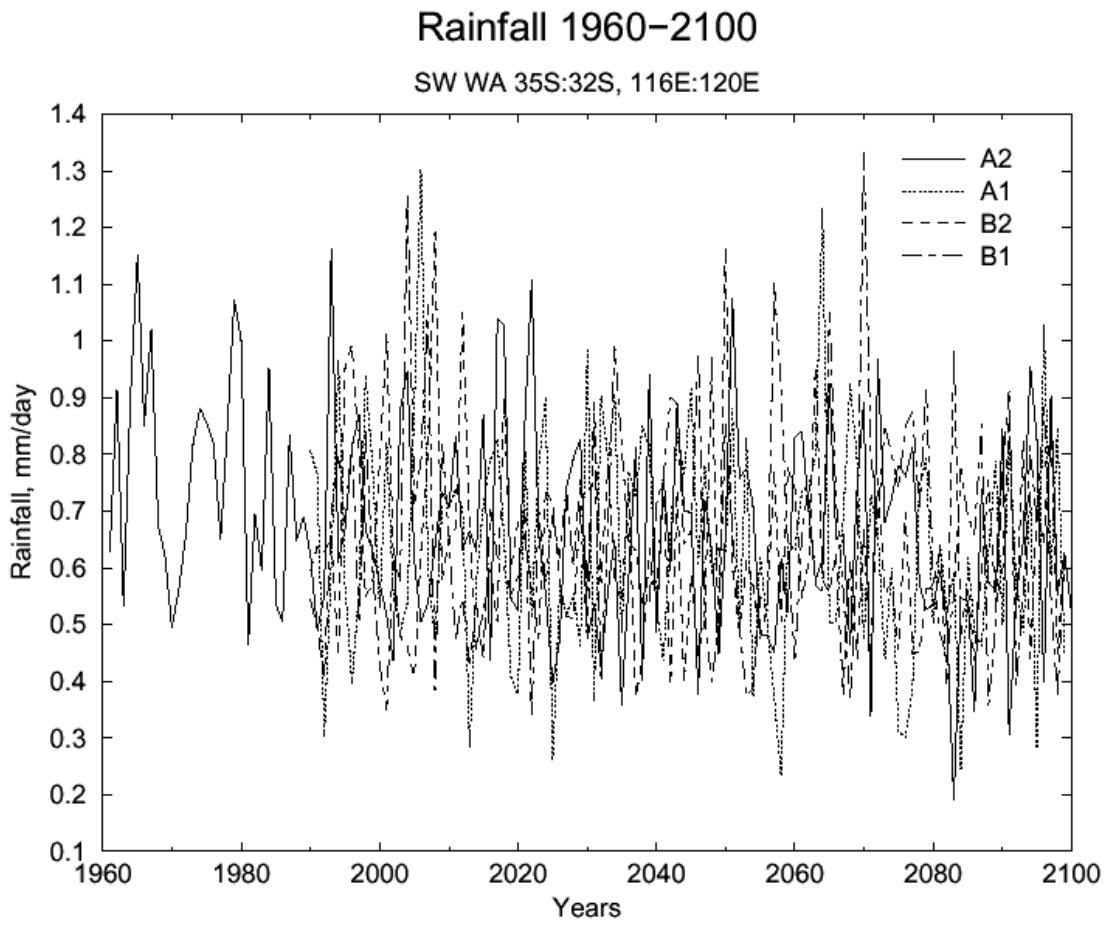

Figure 19. Time variation of rainfall for SWWA as produced with the CSIRO Mark2 model based on single simulations using the 4 SRES scenarios (A1, A2, B1 and B2).

A global perspective of potential rainfall changes under greenhouse conditions is presented in Fig. 20. This figure compared rainfall anomalies for the four SRES scenarios based on differences between the means of the last 30 years of the simulations and the first 30 years. Some systematic differences exist between the scenarios as regards the global distributions, which will not be discussed here, apart from noting that the B1 scenario produces the smallest rainfall anomalies. This is to be expected given the B1 CO_2 concentrations in Fig. 16.

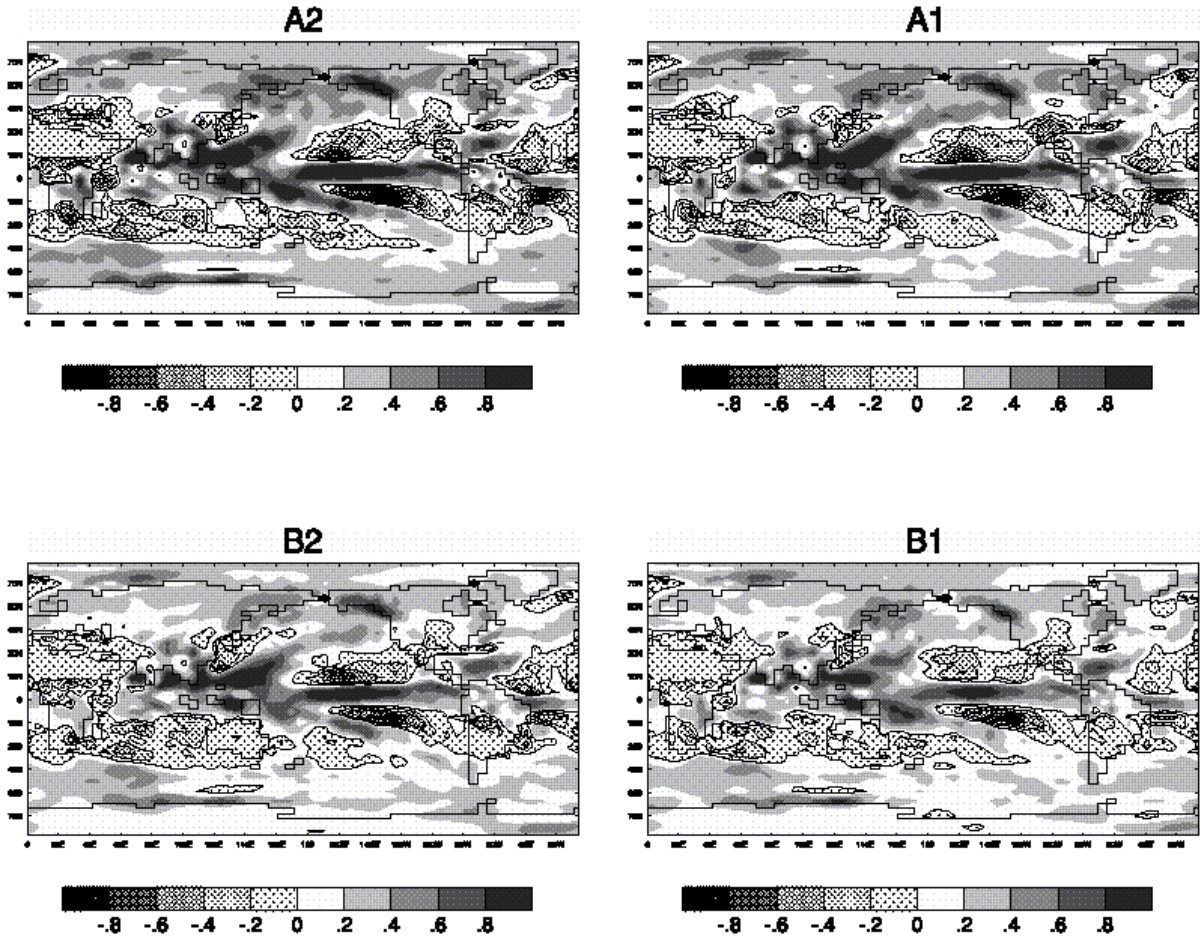

Figure 20. Rainfall anomalies for the four SRES scenarios defined as the difference between the mean of years 2070 to 2100 minus the mean of years 1960 to 1990 for annual mean conditions from the CSIRO Mark2 model. Colour bar coding is in mm day^{-1}.

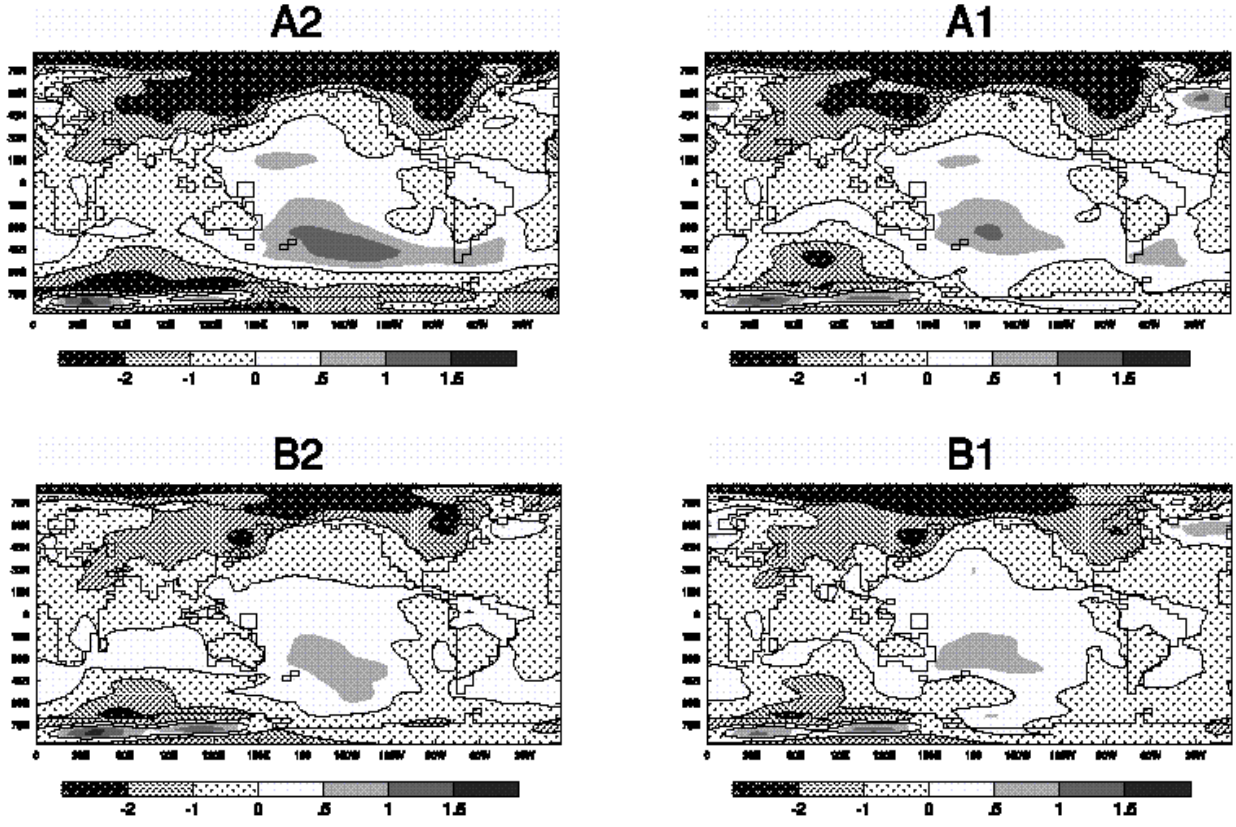

Figure 21. As for Fig. 20 but for surface pressure. The contour interval is hPa.

All the scenarios indicate reduced rainfall in SWWA, although different rainfall anomaly patterns exist over the rest of Australia. The important point to note is that reduced rainfall for these scenarios is not a unique outcome for the SWWA, but part of a general reduction in rainfall over much of the Earth's land surface under greenhouse conditions. The reduced rainfall over the SWWA is related generally to an increased surface pressure over this region, and into the southern Indian Ocean (see Fig. 21). Such a relationship is to be expected based on observed synoptic situations. Again the surface pressure anomalies vary with scenario. There is also an indication over the Pacific Ocean for more El Niño-type conditions to be expected under the greenhouse effect.

A more useful indicator of the greenhouse effect on agriculture and water supply is the change in soil moisture availability. This is shown in Fig. 22 and indicates reduced soil moisture content over most of the global land surface, as well as SWWA.

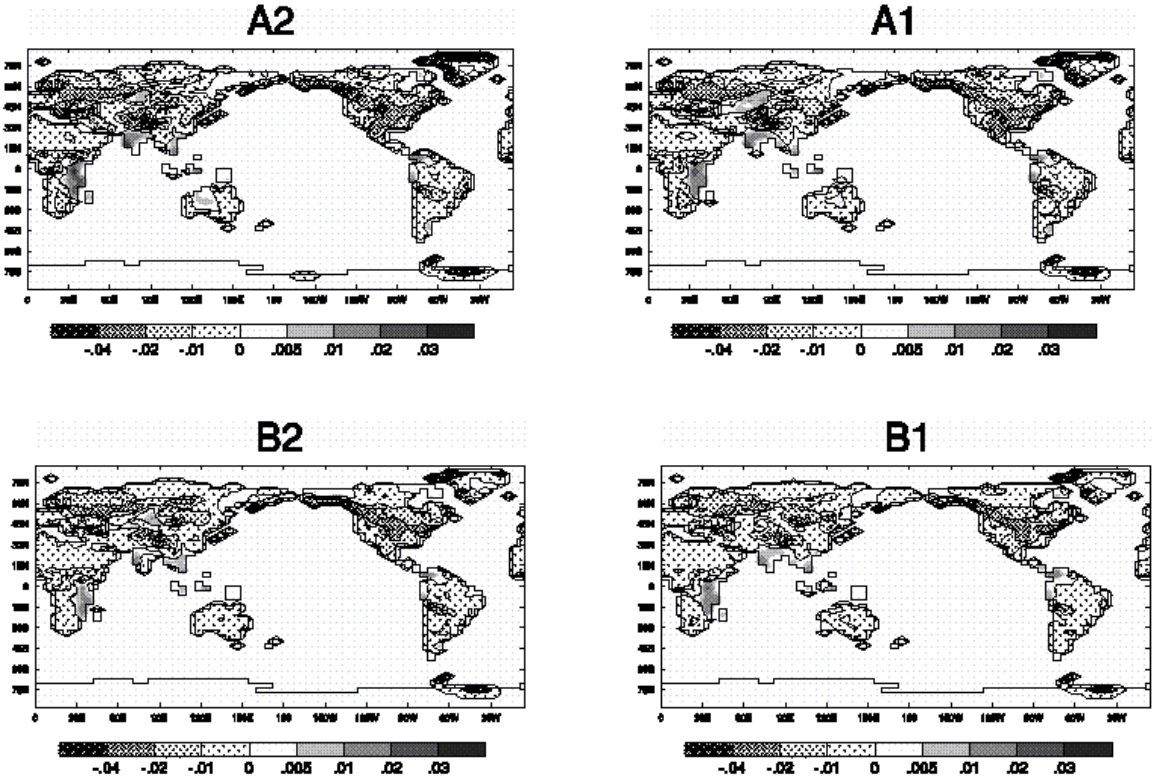

Figure 22. As for Fig. 20 but for soil moisture content.

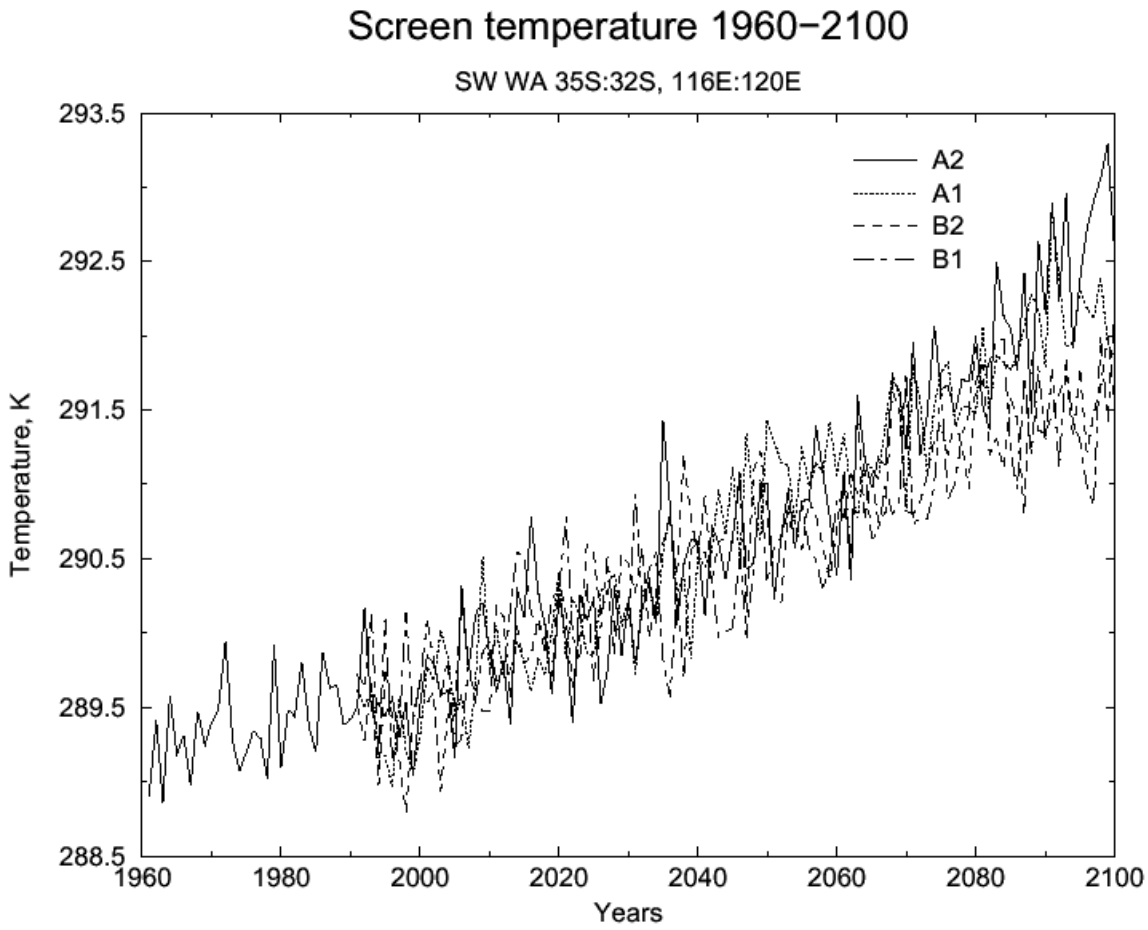

Figure 23. Time series of screen temperature for SWWA for the four SRES scenarios based on the CSIRO Mark2 model.

Even in regions where there is enhanced rainfall under greenhouse conditions it is possible to have reduced soil moisture. This results from evaporation increasing more rapidly than the rainfall increase due to the greenhouse-induced temperature rise. The screen temperature (i.e. 2-m height air temperature) changes over the course of the SRES scenarios are shown in Fig. 23 for SWWA.

Screen temperature increases of up to 4K are indicated in the figure. Although there is noticeable interannual variability a clear trend in temperature can be seen by about 2020 AD. After about 2080 AD the temperatures associated with the A2 scenario dominate, as would be expected from the CO_2 concentrations in Fig. 16. Prior to that time there is considerable intra-scenario variability.

The impact of the greenhouse effect on soil moisture content in the SWWA is illustrated in Fig. 24. There is an overall decline in soil moisture content for all four scenarios, as expected from Fig. 22, which amounts to about 15% by 2100 AD. However, there is very strong interannual variability for the individual scenarios, which could reduce the impact of this drying trend in any one year.

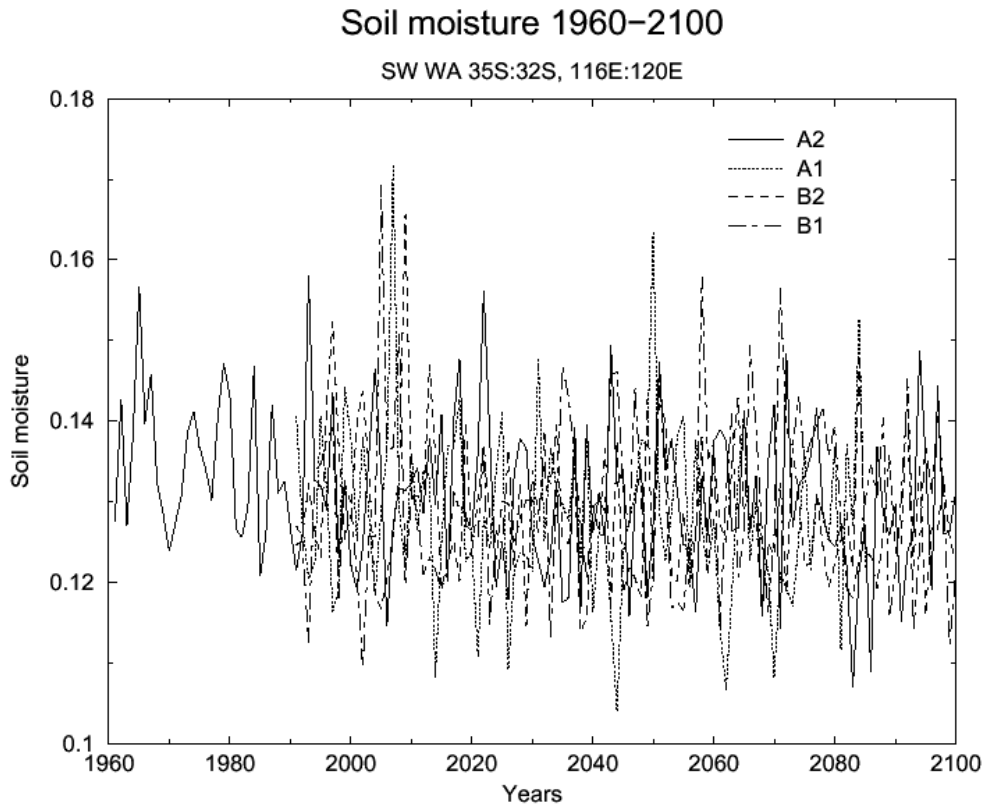

Figure 24. Time series of soil moisture amount for SWWA for the four SRES scenarios based on the CSIRO Mark2 model.

Summarising this section, it seems *unlikely* that the greenhouse effect has contributed to the present drying trend in SWWA. By 2100 AD an overall reduction in rainfall is indicated for this region (Fig. 19), which, combined with rising temperatures (Fig. 23) will result in reduced soil moisture content (Fig. 24). Very noticeable interannual variability is a feature of the time series for rainfall and soil moisture, but not temperature. Apart from the temperature trends, there is little distinction between the various SRES scenarios over the timeframe to 2100 AD for SWWA. Nevertheless, a continuation of the simulations past 2100 AD would probably highlight the different changes, particularly those due to the A2 scenario, which corresponds to the largest CO_2 concentrations. Beyond this time, the impact of the aerosol burdens (see Fig. 17) would become relatively smaller.

As a precautionary note, it needs to be appreciated that the SRES simulations to 2100 AD are based on single runs, whereas ensembles are desirable. Also results from a single global climatic model (CSIRO) have been used. Other models would undoubtedly produce some differences from the results presented here.

Preliminary analysis of greenhouse simulations with the Mark3 GCM

A simulation of climate changes due to a doubling of CO_2 has been performed using a version of the Mark3 GCM with a mixed-layer ocean. This version allows a rapid equilibration of the doubled CO_2 climate to be reached, and while it does not include the retarding effects of the deep ocean on the warming, in the case of the Mark2 model it has been found that the mixed-layer result is a good indication of long term changes simulated by the coupled model. A significantly smaller global mean warming of +2.6 ^{o}C was realized by the Mark3 model, compared with +4.3 ^{o}C for Mark2. The seasonal mean warming is typically +2 to +3 ^{o}C over Australia. These Mark3 results should be considered preliminary, due to both the non-transient nature of the simulation, the absence of any

aerosol forcing, and some minor changes made to the code in its subsequent conversion to a coupled GCM.

Seasonal rainfall rates for both the present or 1xCO_2 climate are shown in Figure 25, along with the doubled CO_2 changes. The seasonal contrast in the present climate is well simulated by the model, although the summer rainfall extends a little far south in WA. The relatively high resolution of the model (1.9 degrees), allows a clear depiction of the SWWA winter maximum. The results due to doubled CO_2 changes include small increases in annual rainfall over WA, although the winter SWWA decreases a little. These results need to be treated with caution since they differ from the more complete greenhouse simulations using fully coupled ocean models and only involve 20-year samples.

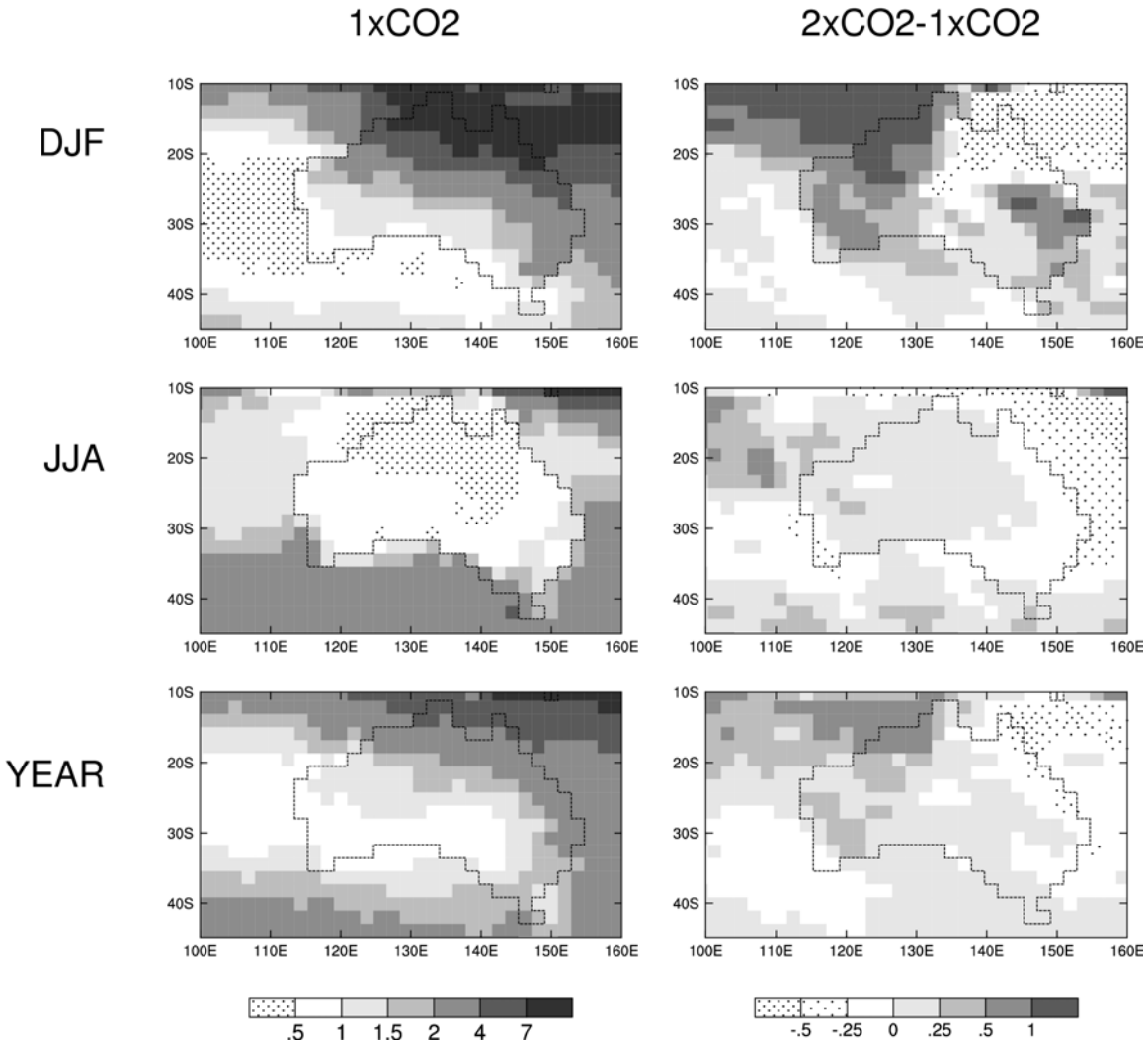

Figure 25. Rainfall rates (in mm per day) simulated by the Mark3 GCM, for (from top to bottom) December-February, June-August and the whole year. The left column shows the present climate rainfall, and the right the change after doubling CO_2, calculated from 20-year simulations of the 1xCO_2 and 2xCO_2 climates.

Figure 26 shows the simulated surface soil moisture fields, scaled so as to give similar magnitudes to those of rainfall. The seasonal variation partly follows the rainfall, although there is a relatively large amount of moisture in central Australia in winter. Changes in moisture mostly parallel those in rainfall. As was found in the results for the four SRES scenarios using the Mark2 model (see Fig. 24)

moisture for SWWA decreases both in winter and annually. Figure 27 shows the sub-surface soil moisture field, with similar scaling. Although the seasonal variation is, as expected, smaller than for the surface, the pattern of changes is similar.

Despite the limitations of this particular experiment, it is worth noting that the Mark3 model also simulates a decrease in rainfall and soil moisture for SWWA due to greenhouse effects. However, the simulated decreases appear to lie within the range of previous estimates.

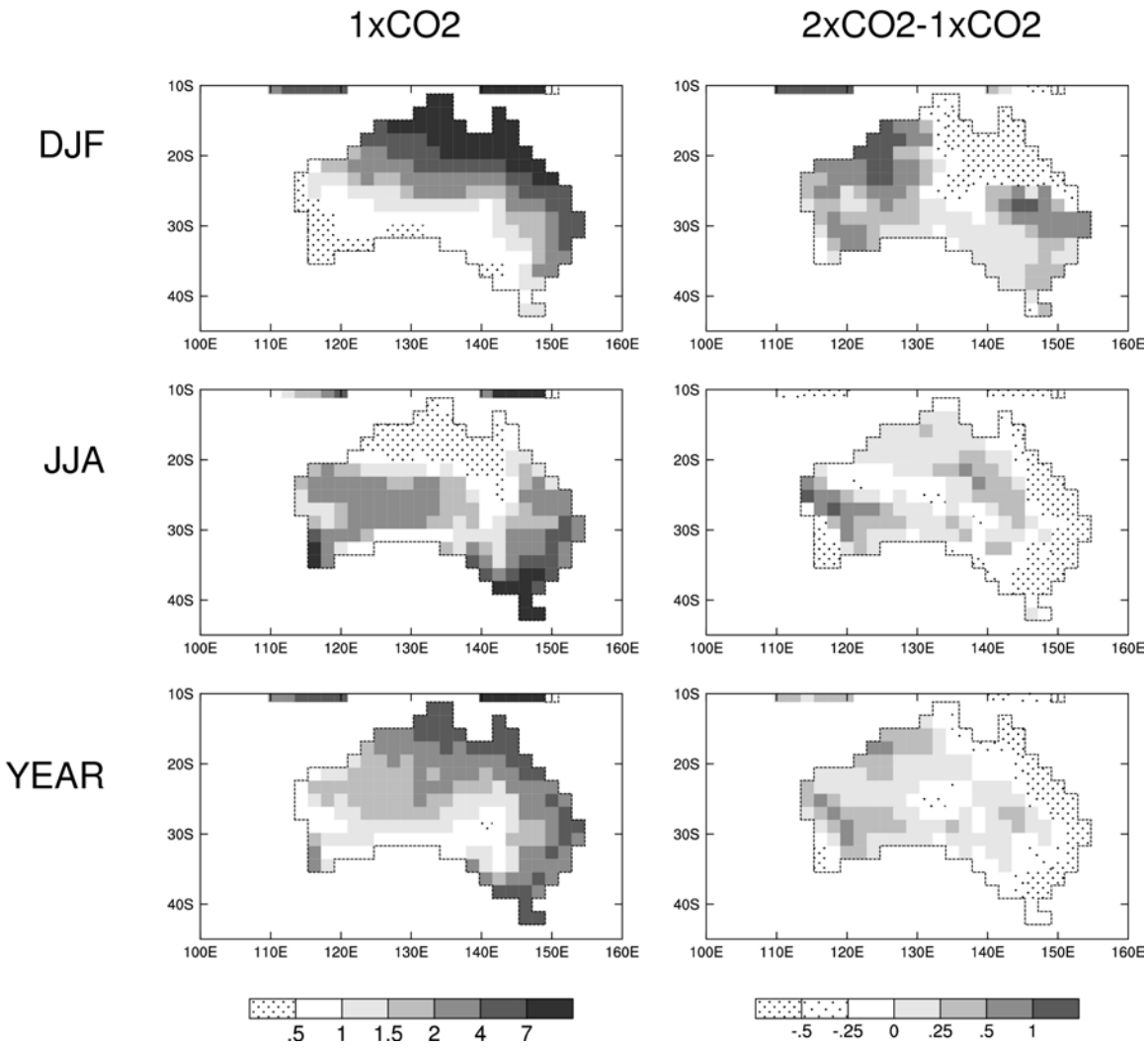

Figure 26. Surface soil moisture simulated by the Mark3 GCM, for (from top to bottom) December-February, June-August and the whole year. The left column shows the present climate values, and the right the change after doubling CO_2, calculated from 20-year simulations of the 1xCO_2 and 2xCO_2 climates.

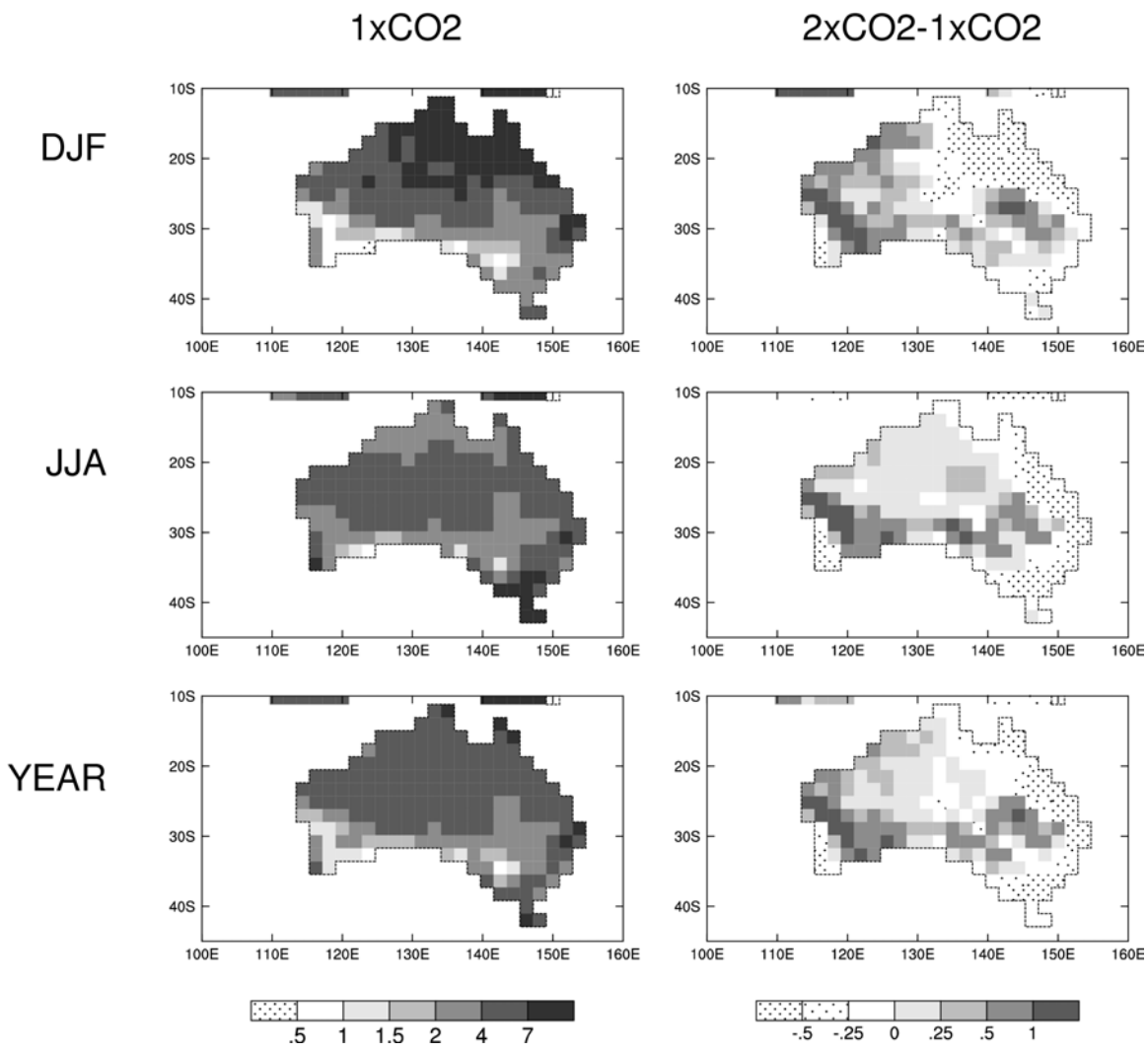

Figure 27. Sub-surface soil moisture simulated by the Mark3 GCM, for (from top to bottom) December-February, June-August and the whole year. The left column shows the present climate values and the right the change after doubling CO_2, calculated from 20-year simulations of the 1xCO_2 and 2xCO_2 climates.

4. Observational Studies

The role of southern hemisphere pressure patterns

An empirical orthogonal function (EOF) analysis of mean sea level pressure data for the Southern Hemisphere over recent time reveals a contrast between the mid and high latitudes which has been described as "an Antarctic Oscillation". This pattern (Fig. 28) is characterized by positive anomalies at high latitudes and negative anomalies at mid- to low- latitudes. The time series associated with this pattern (Fig. 29) indicates a weakening over recent time corresponding to increases in pressure over Australia. The correlation between this pattern and rainfall is shown in Fig. 30. The rainfall product is of limited value because it is mainly the result of a numerical weather prediction scheme and does not necessarily agree with observations. However, the correlation pattern is consistent with previous findings that have shown a link between increased mean sea level pressure (MSLP) and decreased rainfall over SWWA. The reason for trends in the MSLP pattern remain unclear at this stage but it is worth noting that similar trends are seen in climate change simulations. However, as already noted, the model simulations indicate that the contribution of any greenhouse-related changes in rainfall to the recent observed decline in SWWA rainfall is relatively small.

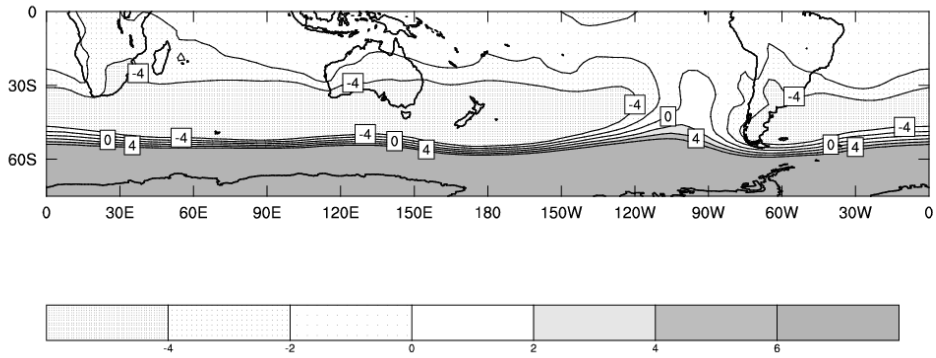

Figure 28. The first EOF pattern of Southern Hemisphere monthly MSLP data 1958-1998.

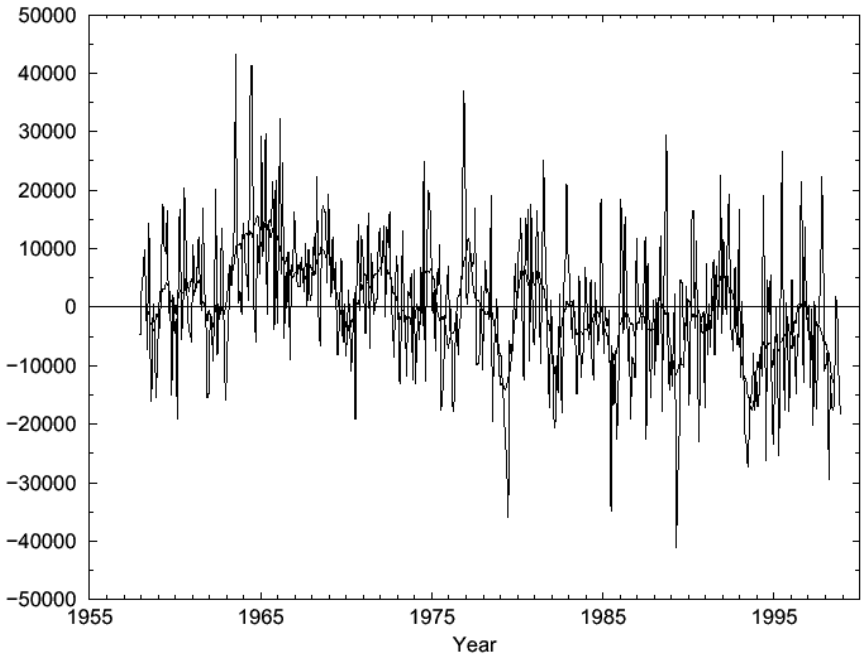

Figure 29. Time series of EOF1 1958-1998.

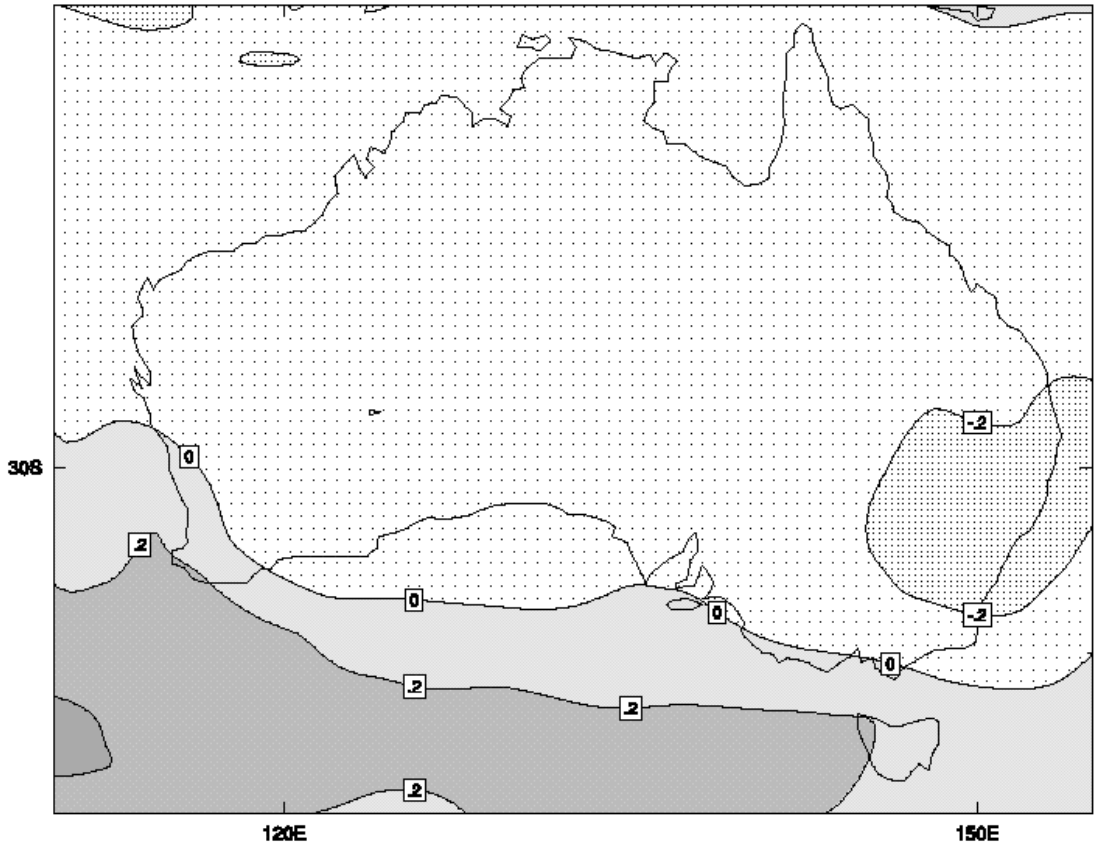

Figure 30. Correlations between MSLP EOF1 and NCEP monthly rainfall 1958-1998. The sign of the correlations is such that an increase in the amplitude of EOF1 corresponds to a decrease in rainfall over SWWA.

5. Interpretation of greenhouse simulations

Introduction

In December 1999, CAR released a Western Australia EPA funded report on simulated climate change based on the results of a number of international models, including the CSIRO model. The consensus results again implied a strong possibility of dry conditions for winter late in the 21st century. Because the models and the climate change experiments all tend to differ, the various simulations can be regarded as providing an ensemble encompassing the range of possible outcomes. In particular, there appeared to be a level of agreement amongst a number of models concerning a projected decrease in both winter and spring rainfall over SWWA.

This level of agreement could be interpreted as evidence of the existence of a robust signal in rainfall and therefore a reduced level of uncertainty for this part of the world. While this may be the case, it only represents one method of dealing with multiple climate change results. Rather than focus on the mean or the ensemble results, we have taken the further step of attempting to stratify the results according to some quality control criterion. In this case we have used the criterion that the simulated seasonal cycle of rainfall for the SWWA region must exhibit a winter maximum. This criterion is only satisfied by 3 of the 9 models, the Hadley Centre model, the GFDL model and the CSIRO Mark2 model. (This is also evident in the results from the Mark3 model shown in Fig. 25). We could invoke further criteria such as the mean and variance of simulated winter rainfall should agree with observations but this is regarded as too restrictive if we are attempting to focus on a relatively small region within a global domain. Therefore, we refer to the percentage changes in simulated rainfall and can summarise the results from the 3 selected models in Table 1.

Table 1. Projected percentage change in rainfall for SWWA, for various 30-year epochs, from the 3 models which exhibit a winter maximum in seasonal rainfall. For each model there are two sets of results corresponding to either aerosol ("a") or non-aerosol ("na") results. The inclusion of aerosols in the climate experiments tends to result in less greenhouse-induced warming and smaller rainfall changes.

MODELS	MAM	JJA	SON	DJF
HADCM2-na				
2010-2039	-27	-30	-8	0
2040-2069	-34	-31	-22	-22
2070-2099	-39	-36	-32	-48
HADCM2-a				
2010-2039	-9	-19	-15	-4
2040-2069	-5	-24	-30	-21
2070-2099	-32	-42	-31	-35
GFDL-na				
2010-2039	5	-8	-3	-3
2040-2069	12	0	-17	-4
GFDL-a				
2010-2039	7	-6	-11	-11
2040-2069	-4	-5	-17	0
CSIRO-na				
2010-2039	-1	-4	-2	1
2040-2069	-8	-10	-19	2
2070-2099	8	-13	-28	-23
CSIRO-a				
2010-2039	9	-8	-11	3
2040-2069	-12	-12	-16	17
2070-2099	-7	-1	-16	-10

The Hadley Centre model simulates the largest percentage reductions in winter rainfall - approximately 40% by the end of the century. The CSIRO model indicates a reduction of about 10% while the GFDL model indicates only minor reductions by the middle of the century. It is not our intention to try and interpret these results here but to look more closely at how these projected decreases manifest themselves over time - particularly during the latter stages of the twentieth century when the rainfall decline became apparent.

Figure 31 illustrates the time series of simulated winter rainfall for the SWWA region from each of the ("non-aerosol") experiments from the three models and from the "observed" rainfall time series (1907-1994) based on area-averaging the QDNR gridded rainfall data (e.g. see Smith et al.; 2000). In order to facilitate the comparison, each time series has been normalized about its long-term average and scaled by one standard deviation. Furthermore, each time series has been filtered using an 11-point running average. The top panel compares the Hadley Centre model results (which involve the largest projected decreases) with the observed time series. In this case both time series appear similar over the period 1907-1970 but diverge thereafter. There is evidence of a significant decline, similar to the observed decline occurring at about 2010. There is little evidence of continued decline thereafter. The important point to note is that in both cases, there exists considerable variability. In fact the filtered time series indicate the existence in the model results of relatively wet and dry periods lasting about 20 years or so.

The same comparison for the CSIRO model results is shown in the middle panel. In this case trend is much less evident but the decadal-scale fluctuations are still evident. In particular, it can be seen that the model simulates a relatively dry period around 1950 but relatively wet periods from about 2000 to 2030. Note that these results are not simulations of rainfall at any particular date, merely simulations of possible rainfall scenarios over time.

The final comparison (bottom panel) involves the GFDL model results. In this case there is no significant decrease in winter rainfall predicted. Even so, the time series reveals relatively dry periods that are comparable with the observed decline.

In summary, if the model projections are to be believed, then it can be argued that the variable of interest (rainfall in this case) must be simulated with some degree of credibility. We have stratified the results from various climate change models and have effectively reduced the number of believable results down to three. These three results indicate a range of decreases to SWWA winter rainfall by the year 2100 varying from zero to -40%.

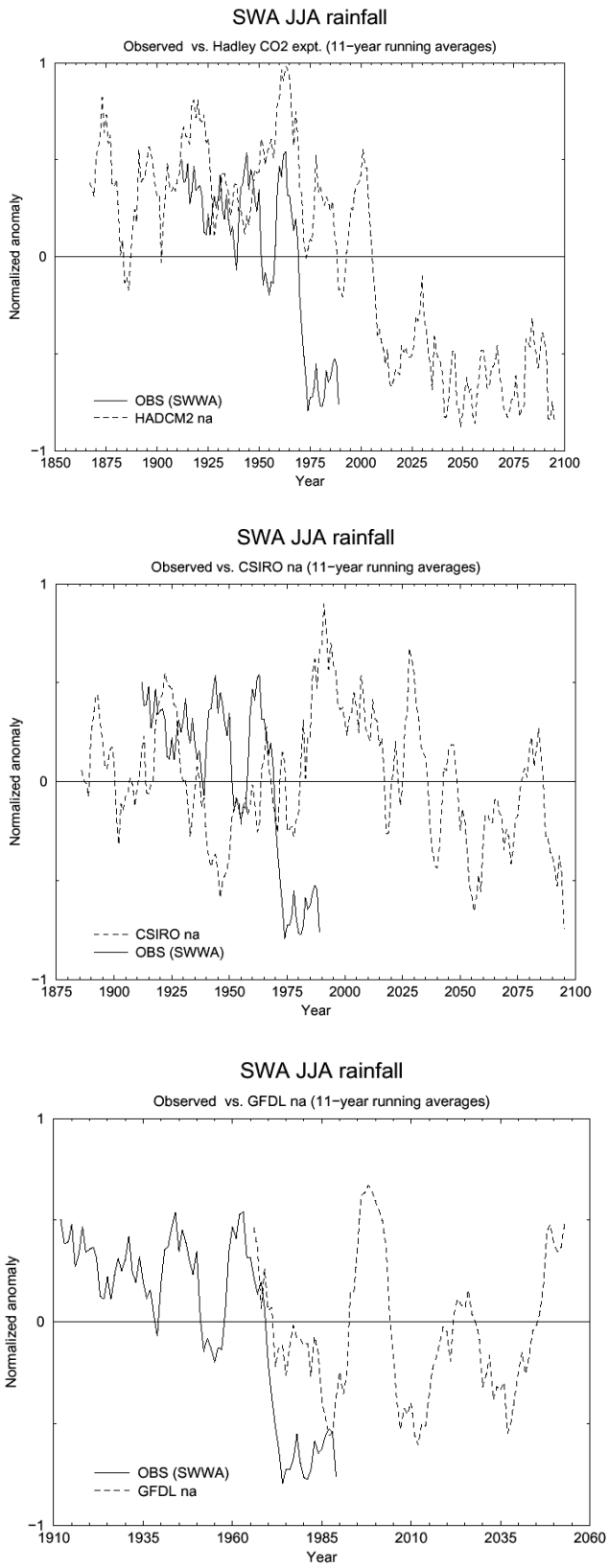

Figure 31. Winter rainfall anomalies from observations and as simulated in three greenhouse climate change experiments (no aerosol effects included): Hadley centre model (a), CSIRO model (b) and GFDL model (c). The anomalies are normalized with respect to their standard deviation over the complete period and have been smoothed with an 11-point running average.

Acknowledgment

The authors wish to thank Julie Penn for her help in formatting this report and manipulating graphics.

References

Banquer-Bernal, A. and M. Latif (2001) A dipole mode in the Indian Ocean? J. Climate, submitted.

Cai, W., P.G. Baines and H.B. Gordon (1999) Southern mid- to high-latitude variability, a zonal wavenumber 3 pattern, and the Antarctic circumpolar wave in the CSIRO coupled model. J.Climate, 12, 3087-3104.

Cai, W. and P.G. Baines (2001) Forcing of the Antarctic Circumpolar Wave by ENSO teleconnections, J. Geophys. Res., (in press).

Nicholls,N. (1989) Sea surface temperatures and Australian winter rainfall. J. Climate, 2, 965-973.

Smith, I.N. (1994) Indian Ocean sea-surface temperature patterns and Australian winter rainfall. Int. J. Climatol., 14, 287-305.

Smith I.N., P. McIntosh, T.J. Ansell, C.J.C. Reason and K.McInnes (2000) South-west Western Australian winter rainfall and its association with Indian Ocean climate variability, Int. J. Climatol., 20, 1913-1930.

Watterson, I.G. (2001) Wind-induced SST and rainfall anomalies in the Australian region. J. Climate, 14(9), 1901-1922.

White, B.W. (2000) Influence of the Antarctic Circumpolar Wave on Australia precipitation from 1958-1997. J. Climate, 13, 2125-2141.

Xie, P.D. and Arkin, P.A. (1996) Analyses of global monthly precipitation using gauge observations, satellite estimates and numerical model predictions. J. Climate, 9, 840-858.

STOCHASTIC DOWNSCALING EXPERIMENTS FOR SOUTHWEST WESTERN AUSTRALIA

Bryson C. Bates[1], *Stephen P. Charles*[1] *and Edward P. Campbell*[2]

[1]CSIRO Land and Water

[2]CSIRO Mathematical and Information Sciences

Second Research Phase Report

for the

Indian Ocean Climate Initiative

TABLE OF CONTENTS

LIST OF TABLES

LIST OF FIGURES

SUMMARY

During the first three years of the Indian Ocean Climate Initiative (IOCI), CSIRO Land and Water (CLW) has:

- Examined the utility of stochastic downscaling models and prospects for their use in a statistical-physical, interseasonal climate forecasting system for southwest Western Australia (SWA).

- Used stochastic downscaling as a means of unravelling the causes of the recent low precipitation sequence over much of the region.

Downscaling may be defined as the quantification of the relation of small-scale climate variables to larger scale atmospheric patterns. These patterns may be observed or simulated by general circulation models (GCMs).

Our studies for IOCI Second Research Phase (July 1999 – December 2000) have again focused on the application of an extended nonhomogeneous hidden Markov model (NHMM) to daily May to October precipitation across a network of 30 stations scattered throughout SWA. This model was selected on the basis of its documented performance and generality.

The original set of goals proposed by CLW for IOCI Second Research Phase were (IOCI, 1999):

- The development of a new NHMM framework that considers precipitation amounts and occurrences jointly.

- Investigation of the stationarity of NHMM parameters using global mean sea level pressure (MSLP) data sets.

- Driving the NHMM with global MSLP data sets to obtain insight into the long-term, temporal and spatial changes in historical synoptic patterns over SWA.

- Investigation of the relationship between the changes in synoptic patterns over time and the observed secular breaks in SWA precipitation.

- A new study of potential predictability using the new NHMM, the Mark 3 version of the CSIRO GCM and an updated historical sea surface temperature (SST) data set.

- For GCM grid cells around SWA, investigation of the interdecadal variability in a 1000-year, CSIRO9 Mark 2 GCM run with a view to detecting any secular changes in modelled atmospheric series and downscaled precipitation series and identifying their causes.

Five factors led to modification of the above goals. These factors were:

- The development and testing of the new NHMM framework described above by our collaborators at the National Center for Statistics and the Environment, University of Washington, Seattle. The new framework did not provide a noticeable improvement in model performance. Consequently, we continued our research efforts with the original model.

- The advent of the National Center for Atmospheric Research (NCAR) – National Centers for Climate Prediction (NCEP) Reanalysis dataset containing global atmospheric fields for the period 1958-1998. This dataset encompasses the timing of the low inflow sequence for the Perth water supply system and the period used for estimating the parameters of the NHMM (1978-1992). The Reanalysis dataset was derived by assimilating observed atmospheric data with a high resolution GCM.

- The postponement of the CSIRO Mark 3 GCM runs described above.

- An evaluation of the NHMM using the Reanalysis dataset that led to a revision of the set of atmospheric variables used by the model.

- A promising line of investigation regarding the cause of the low precipitation sequence over SWA.

Consequently the research goals pursued by CLW during IOCI Second Research Phase were:

- Evaluation of the NHMM using the Reanalysis dataset. This work would reveal any deficiencies in the NHMM and provide insight into the stationarity of its parameters.

- Following successful evaluation of the NHMM, investigation of the long-term temporal changes in historical synoptic patterns over SWA and thus identification of the cause of the observed secular breaks in SWA precipitation.

- Downscaling the 1000-year, CSIRO Mark 2 GCM run with a view to characterising the probability of the observed low precipitation sequence.

Our achievements and preliminary conclusions include:

- After revision of the set of atmospheric predictor variables used in the NHMM, it was found that NHMM parameter estimates derived from atmospheric and precipitation data for the period 1978 to 1992, inclusive, could be used to simulate monthly precipitation over SWA for the period 1958-1998. This suggests that the NHMM is robust against secular breaks in atmospheric circulation and precipitation, and that it may be a useful tool for downscaling an interseasonal climate forecast produced by a GCM.

- Analysis of the results obtained from the NHMM revealed an abrupt shift and a clearly defined trend in the frequency characteristics of synoptic patterns that influence precipitation occurrence over SWA. The timing and nature of these changes are consistent with the characteristics of the observed low precipitation sequence.
- The timing of the shift appears to coincide with the well-documented change in the behaviour of the El Niño – Southern Oscillation that occurred in the mid 1970s. The trend appears to be due to a different mechanism, and may be related to changes in the behaviour of the Antarctic Oscillation and an interaction between the Oscillation and El Niño.
- The changes in the frequency characteristics of the synoptic patterns and the resultant low precipitation sequence since the mid 1970s are due to changes in a combination of atmospheric variables reflecting the location and intensity of low and high pressure

systems, and the moisture content of the lower troposphere. The low precipitation sequence cannot be ascribed to change(s) in a single variable such as MSLP.

- Results from the downscaled 1000-year GCM run suggest the recent low precipitation sequence over SWA is uncommon but not extreme.

Future work will involve:

- Downscaling interseasonal climate forecasts from the coupled ocean-atmosphere CSIRO Mark 3 GCM for the winters of 2000 and 2001. This work will provide information about the reliability of forecasts and forecast lead-times.

- Exploring the Reanalysis dataset with a view to identifying the large-scale climatic forcing responsible for the low precipitation sequence since the mid 1970s. This work will involve a detailed investigation of the effects of El Niño and the Antarctic Oscillation on SWA precipitation.

Outcomes from this work will include:

- An assessment of the utility of downscaled, interseasonal climate forecasts from coupled ocean-atmosphere GCMs.

- Further insight into the large-scale climatic forcing that has caused the low precipitation sequence.

ACKNOWLEDGEMENTS

The work reported herein has received in-kind and financial support from several sources as well as the Indian Ocean Climate Initiative. The NCEP-NCAR reanalysis data were obtained from http://www.cdc.noaa.gov/, with the help of Wesley Ebisuzaki. Jack Katzfey and Mark Collier, CSIRO Atmospheric Research (CAR) provided advice on data extraction. We thank Barrie Hunt (CAR) and his staff for archiving the results of the 1000-year CSIRO Mk2 coupled GCM run at a daily time step; and Peter Whetton (CAR) for discussions about the Antarctic Oscillation and its possible relevance to southwest Western Australia, and the provision of Figure 4.3 in this report. We also thank the following people for their helpful discussions: Jim Hughes and Peter Guttorp, National Research Center for Statistics and the Environment (NRCSE), University of Washington, Seattle; John Cramb and Glen Cook, Bureau of Meteorology, Perth; and Brian Sadler, Chairman of the IOCI Panel. Partial funding was obtained from the Australian Government's National Greenhouse Research Program. Part of this work was carried out while Bates was a Visiting Scholar at the NRCSE from 1 to 27 May 2000.

1. INTRODUCTION

1.1 Downscaling Climate Model Simulations

Modelling the response of natural and agricultural systems to climate forecasts requires daily data at local and regional scales. The need for improved quantitative precipitation forecasts, and realistic assessments of the regional impacts of natural climate variability and possible climate change due to the enhanced greenhouse effect, has generated increased interest in regional climate simulation. Although existing general circulation models (GCMs) perform reasonably well in simulating climate with respect to annual or seasonal averages at sub-continental scales, it is widely acknowledged that they do not provide credible simulations of precipitation at the space and time scales relevant to local and regional impact analyses (Arnell *et al*., 1996; Gates *et al*., 1996).

The above problems have led to the development of statistical downscaling techniques to derive sub-grid scale weather from the coarse spatial resolution atmospheric data available from GCMs. Downscaling techniques include:

- Modelling the daily precipitation process through multivariate probability distributions conditional on explicitly derived, large-scale atmospheric circulation patterns (e.g., Bardossy and Plate, 1991, 1992; Bogardi *et al.*, 1993).

- Regressions on continuous atmospheric circulation indices, geographic location and topographical variables (Enke and Spekat*,* 1997; Huth, 1997; Wilby *et al.*, 1998).

- Artificial neural networks (e.g., Crane and Hewitson, 1998).

- Hidden Markov models (see below)

1.2 Nonhomogeneous Hidden Markov Model (NHMM)

The downscaling method used herein consists of a nonhomogeneous hidden Markov model (NHMM) to simulate precipitation occurrence and multiple linear regression to simulate precipitation amounts in southwest Western Australia (SWA) (Hughes *et al.*, 1999; Charles *et al*., 1999). Recall from IOCI (1999) that the NHMM relates synoptic-scale, atmospheric

circulation variables through a finite number of hidden (unobserved) weather states to multi-site, daily precipitation occurrence data. The NHMM determines the most distinct patterns in a daily multi-site precipitation occurrence record rather than patterns in atmospheric circulation. These patterns are then defined as conditionally dependent on a set of atmospheric predictor variables. The weather states are not defined *a priori*. A first-order Markov process defines the daily transitions from weather state to weather state. The process is described as nonhomogeneous as the transition probabilities are conditional on a set of atmospheric circulation predictors. The atmospheric predictors may include raw variables such as mean sea level pressure (MSLP) or derived variables such as north-south MSLP gradient. In this way, the NHMM captures much of the spatial and temporal variability of the precipitation occurrence process.

Model selection involves sequential fitting of several NHMMs with an increasing number of weather states and atmospheric predictors. The fit is evaluated in terms of the physical realism and distinctness of the identified weather states as well as a Bayesian information criterion (BIC). The objective is to select a NHMM that minimises the BIC, thus identifying a relatively parsimonious model that fits the data well. The most likely weather state sequence is obtained from the selected NHMM using the Viterbi algorithm. This permits the assignment of each day to its respective state (Hughes *et al.*, 1999). The ability to classify days into weather states that are distinct in terms of spatial precipitation occurrence pattern as well as synoptic situation means that the physical realism of the states can be assessed.

The joint distribution of daily precipitation amounts at multiple sites is evaluated through the specification of conditional distributions for each site and weather state (Charles *et al.*, 1999). The conditional distributions consist of regressions of transformed amounts at a given site on precipitation occurrence at neighbouring sites within a set radius. An automatic variable selection procedure is used to identify the neighbouring sites that provide useful information about at-site precipitation amounts. The neighbourhood radius is determined by steadily increasing its size until further increases result in marginal improvements in the proportion of total precipitation variability explained by the precipitation occurrences at neighbouring sites.

1.3 General Circulation Model

In this report we used a 1000-year run from the Mark 2 version of the spectral 9-level atmospheric GCM developed by the CSIRO Atmospheric Research (hereafter referred to as CSIRO9 GCM) at a horizontal resolution of R21 (roughly 700 km). Descriptions of the model can be found in McGregor *et al*. (1993) and IOCI (1999).

2. DESCRIPTION OF STUDY AREA AND DATA

We defined SWA as the region extending from about 30° to 35° south and 115° to 120° east (Figure 2.1). For the stations depicted in Figure 2.1, the percentage of annual precipitation that falls in the period from May to October varies from 66 to 86%: 25 stations have percentages greater than 71%. The majority of winter rains come from low pressure frontal systems. Thus we divided the year into the winter half-year (May-October) and summer half-year (November-April) seasons. A full set of results for the winter half-year is presented in this report.

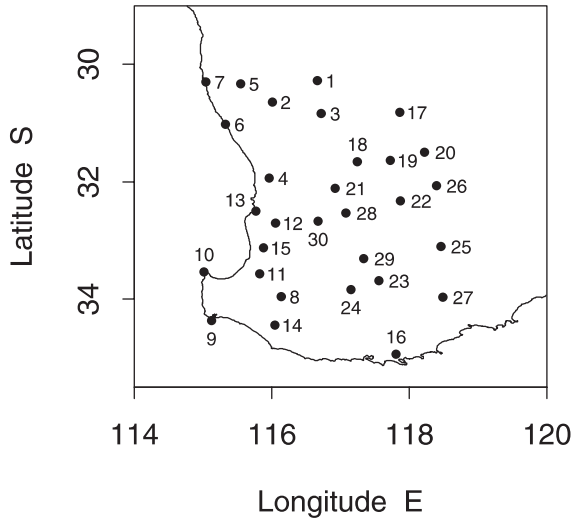

Figure 2.1 Location of daily precipitation stations in southwest Western Australia (for key to numerals see Table 2.1).

In our earlier work, the NHMM was fit to atmospheric and daily precipitation data for the period from 1978 to 1992. The data were obtained from the Bureau of Meteorology. Twenty-five atmospheric variables were derived from this data set, and the data interpolated to a rectangular 3.75° longitudinal by 2.25° latitudinal grid. An additional variable (850 hPa to 500 hPa thickness) was added to the list of candidate atmospheric predictors in 2000. The locations of the 30 precipitation stations considered are shown in Figure 2.1. A key to the numerals shown in Figure 2.1 is given in Table 2.1. These stations have no missing records over 1978-92. Further details are given in IOCI (1999).

Table 2.1 Details of Daily Precipitation Stations [Reproduced from IOCI (1999)].

No. (Fig. 2.1)	Station Name	Station No.	Elevation (m)	Annual Precipitation (mm)
1	Dalwallinu P.O.	008039	335.0	357
2	Moora (Moora Shire)	008091	203.0	461
3	Wongan Hills Res. Stn	008138	305.0	349
4	Perth Airport M.O.	009021	20.0	802
5	Dandaragan (Badgingarra Res. Stn)	009037	260.0	598
6	Lancelin	009114	4.0	627
7	Jurien	009131	2.0	560
8	Bridgetown P.O.	009510	150.0	843
9	Augusta (Cape Leeuwin A.W.S.)	009518	14.0	1000
10	Busselton (Cape Naturaliste L.H.)	009519	97.0	830
11	Donnybrook P.O.	009534	63.0	1002
12	Dwellingup (Forestry)	009538	267.0	1279
13	Mandurah (Park)	009572	15.0	888
14	Pemberton (Forestry)	009592	174.0	1213
15	Harvey (Wokalup Agric. Res. Stn)	009642	116.0	996
16	Albany A.M.O.	009741	68.0	805
17	Bencubbin (Bencubbin)	010007	353.0	320
18	Cunderdin P.O.	010035	236.0	368
19	Kellerberrin (composite)	010073	247.0	333
20	Merredin (Res. Stn)	010093	318.0	309
21	Beverley P.O.	010515	199.0	422
22	Corrigin P.O.	010536	295.0	378
23	Katanning P.O.	010579	310.0	485
24	Kojonup (composite)	010582	305.0	542
25	Lake Grace P.O.	010592	286.0	353
26	Narembeen P.O.	010612	276.0	332
27	Ongerup (Ongerup)	010622	286.0	383
28	Pingelly P.O.	010626	297.0	455
29	Wagin P.O.	010647	256.0	440
30	Wandering (Shire)	010648	280.0	626

Most of our analyses for IOCI Second Research Phase were based on the National Center for Atmospheric Research (NCAR) – National Centers for Climate Prediction (NCEP) Reanalysis dataset (Kalnay *et al*., 1996). The dataset contains a long record of global

analyses of atmospheric fields for the 41-year period from 1958 to 1998. Data are available at 0000, 0600, 1200, and 1800 GMT on a 2.5° latitude-longitude grid. The Reanalysis project involved the recovery of land surface, rawisonde, pibal, aircraft, satellite, and other data from different countries and organisations, data quality control, and the assimilation of the data with a frozen state-of-the-art analysis/forecast system. The use of a frozen system eliminates perceived climate jumps associated with changes in the data assimilation techniques. A 28-level spectral GCM with a horizontal resolution of T62 (roughly 210 km) is used in the assimilation system. Output variables are classified into four classes ("A" to "D") depending on the degree to which the variables are influenced by observations and/or the GCM. For example, MSLP is a class "A" variable since it is strongly influenced by observational data. Humidity is a class "B" variable in that the GCM has a strong influence on its value despite the existence of observational data that directly affect it. Reanalysis data for the atmospheric predictors in the NHMM were interpolated to the grid using for NHMM fitting.

Some studies have reported spurious temporal trends in Reanalysis fields (e.g., Hines and Bromwich, 1999; Marshall and Harangozo, 1999). We screened each atmospheric predictor series for changes in mean level that were large relative to the background variability in the Reanalysis data. We used the nonparametric jump-detection algorithm proposed by Qiu and Yandell (1998) to screen each of the atmospheric predictor series for spurious jumps in their means. Predictors that exhibited departures from normality were transformed prior to analysis. Given that the daily atmospheric predictor series for each winter half-year are serially correlated, we used a small window width to reduce the dependence as far as possible.

The data from the 1000-year GCM run were interpolated to the rectangular grid described above. The historical and modelled atmospheric data were centred using their respective means. This removes the effects of any bias in the modelled means on the downscaled simulations. There did not appear to be any bias in the modelled variances. Atmospheric variables derived from the modelled data were used as input to the NHMM: the NHMM was not fit to the GCM data.

3. EVALUATION AND MODIFICATION OF DOWNSCALING MODEL

3.1 Introduction

Recall from IOCI (1999) that a 6-state NHMM with three atmospheric predictors [the mean of MSLP across five grid points (hereafter referred to as mean MSLP), north-south MSLP gradient, and dew point temperature depression at 850 hPa (DT_d^{850})] could provide credible reproductions of at-site precipitation occurrence probabilities and their spatial association, and dry- and wet-spell length statistics at the seasonal (six-monthly) scale for the gauges listed in Table 2.1. DT_d^{850} is defined as the difference between the air and dew point temperatures at 850 hPa. Therefore, it is a measure of humidity in the lower troposphere. A dry spell is defined as a sequence of consecutive days during which daily precipitation remains below 0.3 mm. A wet spell is defined as a sequence of consecutive days during which daily precipitation equals or exceeds 0.3 mm. The precipitation occurrence patterns and the composite MSLP fields associated with the weather states are given in Figure 3.1.

In this section we use the NCEP-NCAR Reanalysis dataset to evaluate the NHMM. One thousand 41-year sequences of daily May to October precipitation were generated from the fitted NHMM, conditionally on the atmospheric predictors extracted from the Reanalysis dataset. For the first time the model's performance is subjected to scrutiny on a monthly rather than a seasonal time scale, and an out-of-sample-validation over a period that is wetter than but similar in length to the fitting period. Initial results indicated that the NHMM was inadequate. It was evident that the intraseasonal variation in the atmospheric circulation over SWA had not been fully captured by the model. Further investigation led to an augmented atmospheric predictor set for the NHMM. The modified NHMM is shown to resolve most of the performance deficiencies of the original model.

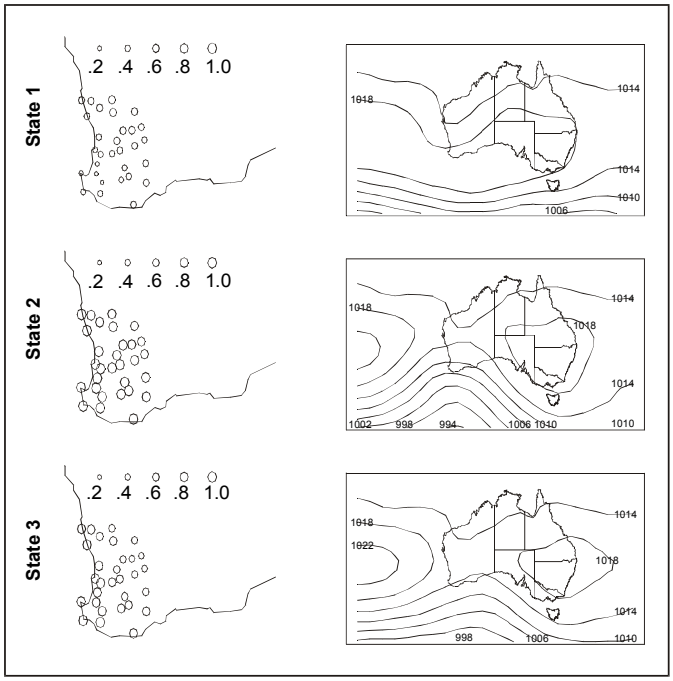

Figure 3.1(a) Precipitation occurrence patterns and MSLP averaged over all days classified under weather states 1 to 3. The diameters of the circles indicate daily precipitation occurrence probabilities at each site.

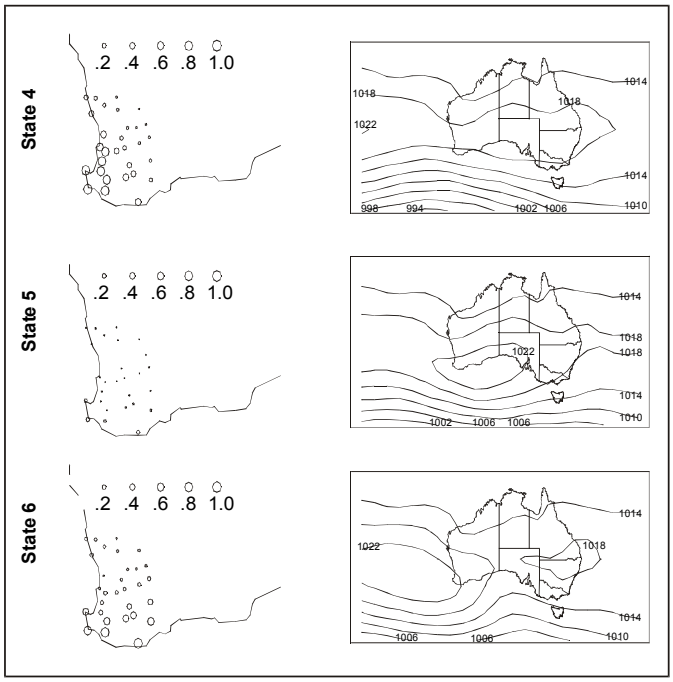

Figure 3.1(b) Precipitation occurrence patterns and MSLP averaged over all days classified under weather states 4 to 6. The diameters of the circles indicate daily precipitation occurrence probabilities at each site.

3.2 Evaluation of the NHMM

Figure 3.2 compares the simulated daily precipitation occurrence probabilities with historical values for the 30 sites for each month in the winter half-year over the fitting period (1978-1992). The NHMM underestimates precipitation occurrence during the wettest months (June and July) and overestimates occurrence in the driest months (September and October). Performance deficiencies are also apparent for May and August. Moreover, there is a cyclical variation in the sign and magnitude of the bias in the simulated probabilities across the winter half-year.

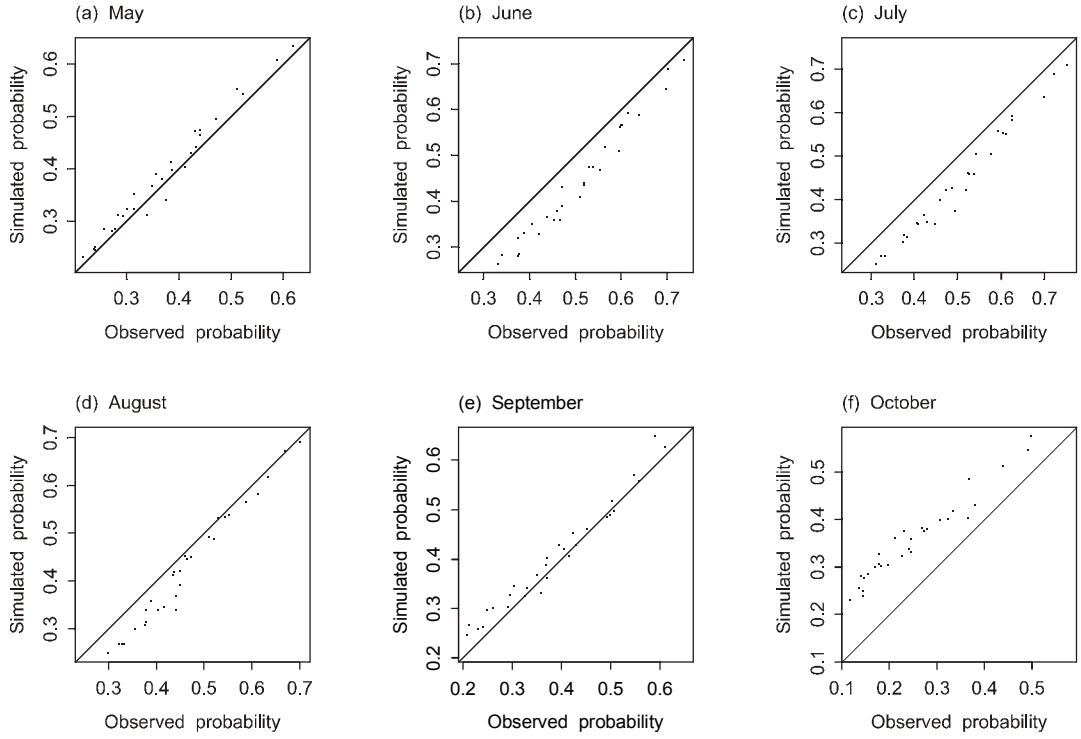

Figure 3.2 Comparison of simulated and historical daily precipitation probabilities for the period 1978–1992.

Similar problems were evident in the precipitation amount simulations. The seasonal distribution of the errors in the simulation of monthly precipitation amounts for Pingelly is given in Figure 3.3. The standardised residuals (e_i) shown are defined by

$$e_i = (r_i - m_i)/s_i, \qquad i = 1, \ldots, T \tag{1}$$

where r_i is the observed monthly precipitation amount for the i^{th} month, m_i and s_i are the mean and standard deviation of the 1000 simulated amounts for the i^{th} month, and

$T = 6*15 = 90$ for the 15-year fitting period. The standardised residuals exhibit a cyclical variation through the winter half-year. The simulated precipitation amounts for May and August are close to the observed, but the fit is poor to very poor for the remaining winter months. This suggests that at least one additional predictor is required for downscaling experiments at the monthly time scale.

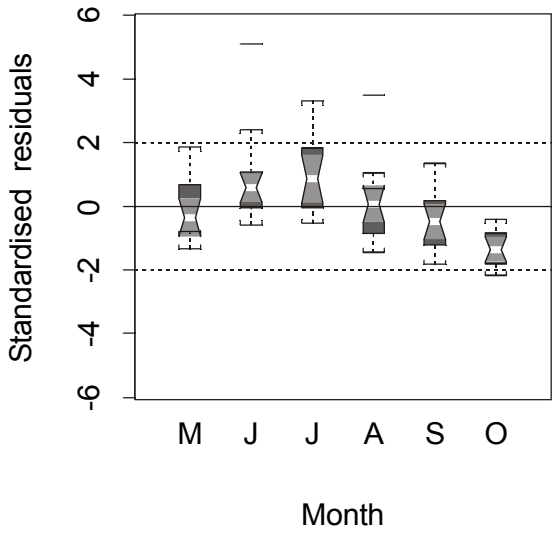

Figure 3.3 Box plots showing seasonal distribution of standardised residuals for Pingelly (Station 28) for the period 1978–1992.The edges of the boxes mark the upper and lower quartiles. The horizontal line within each box denotes the median, and the end points of the whiskers attached to each box denote the extremes. If the notches on two boxes do not overlap, this indicates a difference in location that is roughly significant at the 5% level.

An exhaustive but essentially fruitless search was undertaken to identify which of the remaining 23 atmospheric variables could account for the bias in the NHMM simulations. This suggested that the use of a combination of predictors might be required. We used canonical correlation analysis (CCA) to quantify the correlations between linear combinations of the precipitation occurrence residuals for the 30 sites and linear combinations of the atmospheric predictors for 1978-1992. In CCA, the pair of linear combinations having the highest correlation is determined first. The next pair to be considered has the highest correlation among all pairs that are uncorrelated with the first pair, and so on. The pairs of linear combinations are called canonical variables, and their correlations are called canonical correlations (Kshirsagar, 1972; Jobson, 1992).

Prior to the CCA, two atmospheric variables ("10" and "11") were removed from the predictor set since they are linear combinations of other predictors. Thus the number of canonical variables and correlations is min (30, 24) = 24. (Recall that there are 30 sites and

that there were 26 predictors before predictors "10" and "11" were dropped.) The atmospheric variables were standardised to zero mean and unit variance. The precipitation occurrence residuals are defined by

$$r_k^t = (R_k^t - p_k^t)/[p_k^t(1-p_k^t)] \tag{2}$$

where $R_k^t = 1$ if precipitation is greater than or equal to 0.3 mm at gauge k on day t and 0 otherwise, and

$$p_k^t = \sum_{j=1}^{6} P(R_k^t \mid S_j^t)\, P(S_j^t) \tag{3}$$

in which the probabilities $P(R_k^t \mid S_j^t)$ and $P(S_j^t)$ are determined from the fitted NHMM. We transformed the r_k^t to normality using an inverse probit transform. The estimates of the first three estimated canonical correlations were 0.568, 0.516 and 0.326.

A bar chart of the standardised coefficients for the first atmospheric canonical variable is given in Figure 3.4. This variable has a relatively large positive coefficient for variable "1" (mean MSLP), and relatively large negative coefficient for variable "2" (mean geopotential height at 500 hPa), and moderate positive coefficients for variables "7" (east-west MSLP gradient), "25" (850 hPa to 500 hPa thickness), and "26" (DT_d^{850}).

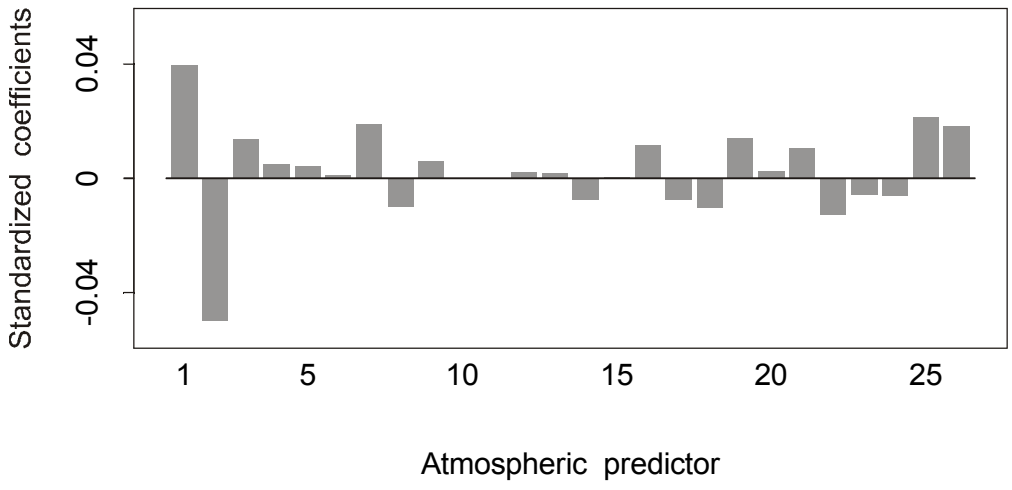

Figure 3.4 Bar chart of standardised coefficients for the first atmospheric canonical variable (for completeness, coefficients for variables "10" and "11" are shown as zero.)

A map of the standardised coefficients for the first precipitation occurrence residual canonical variable (hereafter called the first residual canonical variable) is given in Figure 3.5. Stations with large negative coefficients are concentrated along the south coast of SWA. Stations with large positive coefficients are located in the northeast corner of SWA and along the west coast. Thus the first residual canonical variable contrasts the error in the NHMM fit for stations along the south coast with that for the northeast corner and west coast. The moderate positive correlation between the first residual and atmospheric canonical variables suggests that this contrast is higher when centred mean MSLP, east-west MSLP gradient and DT_d^{850} are large relative to centred mean geopotential height at 850 and 500 hPa. Thus if rainfall occurs over SWA, it is more likely to occur in the north rather than the south due to the presence of a midlevel trough over the region or to the west. When centred mean MSLP, east-west MSLP gradient and DT_d^{850} are small relative to centred mean geopotential height at 850 and 500 hPa, rainfall will tend to occur in the south relative to the north due to a high pressure system situated to the west of SWA with a ridge forming along the south coast.

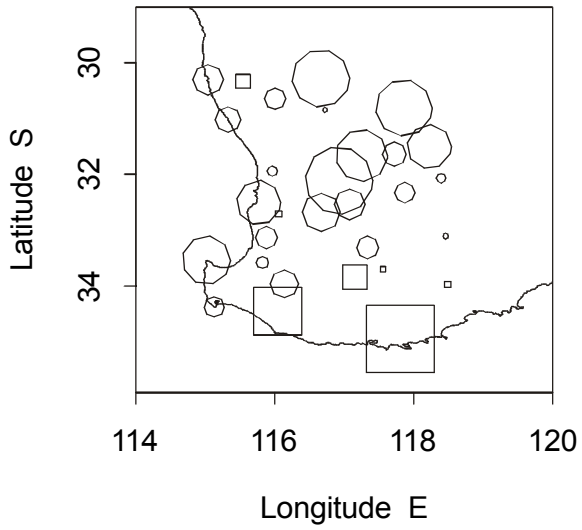

Figure 3.5 Map of standardised coefficients for the first precipitation occurrence residual canonical variable. Circles denote positive coefficients and squares negative coefficients. The diameter of the circles and the lengths of the sides of the squares are in direct proportion to the magnitude of the coefficients.

Figure 3.6 shows box plots of the first canonical variables for each month in the winter half-year. A seasonal cycle in both variables is apparent, and it is consistent with the size and sign of the bias evident in Figure 3.3. Pair-wise comparison of the notches on the boxes suggests that there is a noticeable difference between the medians from month to month.

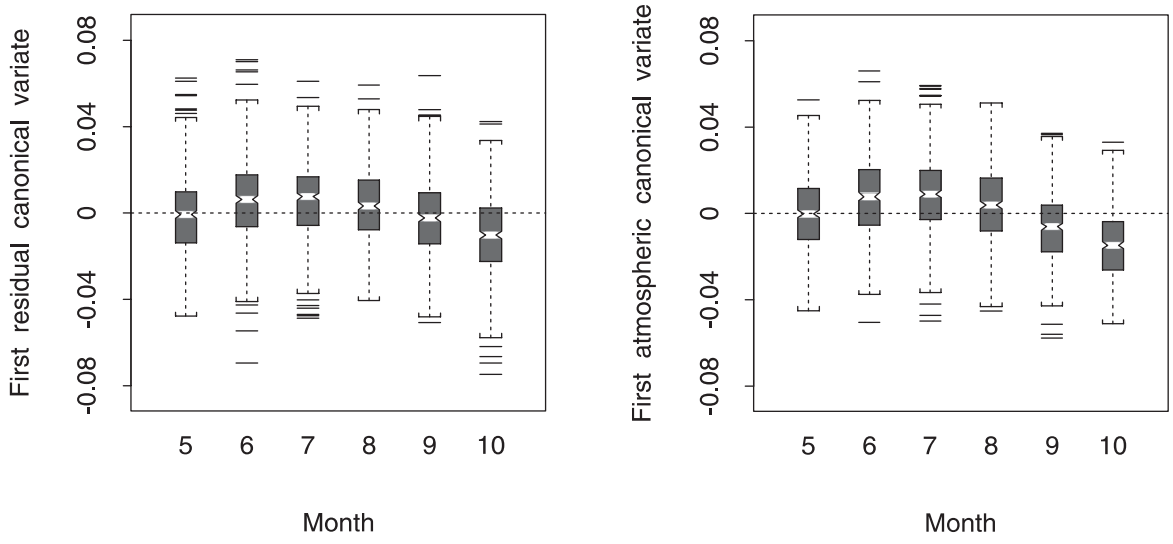

Figure 3.6 **Box plots of the first canonical variables grouped according to calendar month.**

Table 3.1 summarises the features of the scatter plots of the first atmospheric and residual canonical variables (y- and x-axes, respectively) for each weather state. For a given weather state, concentration of the values of these variables in a particular quadrant of the scatter plot indicates that the variables contain information about the occurrence of that state. Consider the columns of Table 3.1. Of the 362 data points in the 1st quadrant (upper left-hand side), 88% correspond to days assigned to States 3 to 6, and 61% to days assigned to States 4 and 5. These percentages are well above the percentage that would have been if all of the data points in the 1st quadrant had been distributed uniformly across the six weather states (i.e., 17% per state). Similarly, 88% of the 993 data points in the 2nd quadrant (upper right-hand side) correspond to days assigned to States 1, 2, 3, and 5 and 65% to days assigned to States 2 and 5. About 71% of the 401 data points in the 3rd quadrant (lower right-hand side) correspond to days assigned to States 2, 3 and 5. Also, 93% of the 1004 data points in the 4th quadrant (lower left-hand side) are correspond to days assigned to States 3 to 6, and 81% to days assigned to States 4, 5 and 6. Now consider the rows of Table 3.1. About 51% of the data points assigned to State 1 and 71% of the data points assigned to State 2 are located in the 2nd quadrant. About 53% of the data points assigned to State 4 and 70% of the data points assigned to State 6 are located in the 4th quadrant. These percentages are well above the percentage that would have been if all of the data points in a given weather state had been distributed uniformly across the quadrants (i.e., 25% per quadrant). Finally, consider positive values of the first atmospheric canonical variable alone. About 60%, 76%, 47%, 36%, 48%, and 25% of the data points for States 1 to 6, respectively, fall in the 1st and 2nd quadrants.

Thus the first atmospheric canonical variable captures information about the occurrences of States 2, 6 and, to a lesser extent, State 4.

Table 3.1 Numbers of Data Points in Quadrants of the Scatter Plots of the First Canonical Variables for Each Weather State in the Modified NHMM.

Weather State	Quadrant				Subtotal
	1st	2nd	3rd	4th	
1	16	90	38	34	178
2	29	385	94	38	546
3	46	137	86	121	390
4	113	90	59	297	559
5	106	264	106	290	766
6	52	27	18	224	321
Total	362	993	401	1004	2760*

* (1992-1978+1) (31+30+31+31+30+31) = 2760.

3.3 Modification of the NHMM

The results described in section 3.2 suggest the incorporation of the first atmospheric canonical variable into the predictor set for the NHMM. A stepwise regression analysis and an analysis of all-subset regressions based on leaps and bounds were undertaken to see whether a small subset of the 24 atmospheric variables could capture most of the information in the first precipitation canonical variable. This did not prove to be the case. Consequently, a NHMM with four atmospheric predictors (the fourth being the first atmospheric canonical variable) was fit to the observed atmospheric and precipitation data for 1978-92. The precipitation occurrence patterns and the composite MSLP fields associated with the weather states for the modified NHMM are almost identical to those given in Figure 3.1 and will not be given here for the sake of brevity.

Figure 3.7 compares the daily precipitation occurrence probabilities simulated by the modified NHMM with historical values for each month in the winter half-year over the period 1978-1992. Comparison of Figures 3.2 and 3.7 reveals a noticeable improvement in model fit, particularly for the months of June and July (the wettest months of the year) and October (the driest month of the winter half-year).

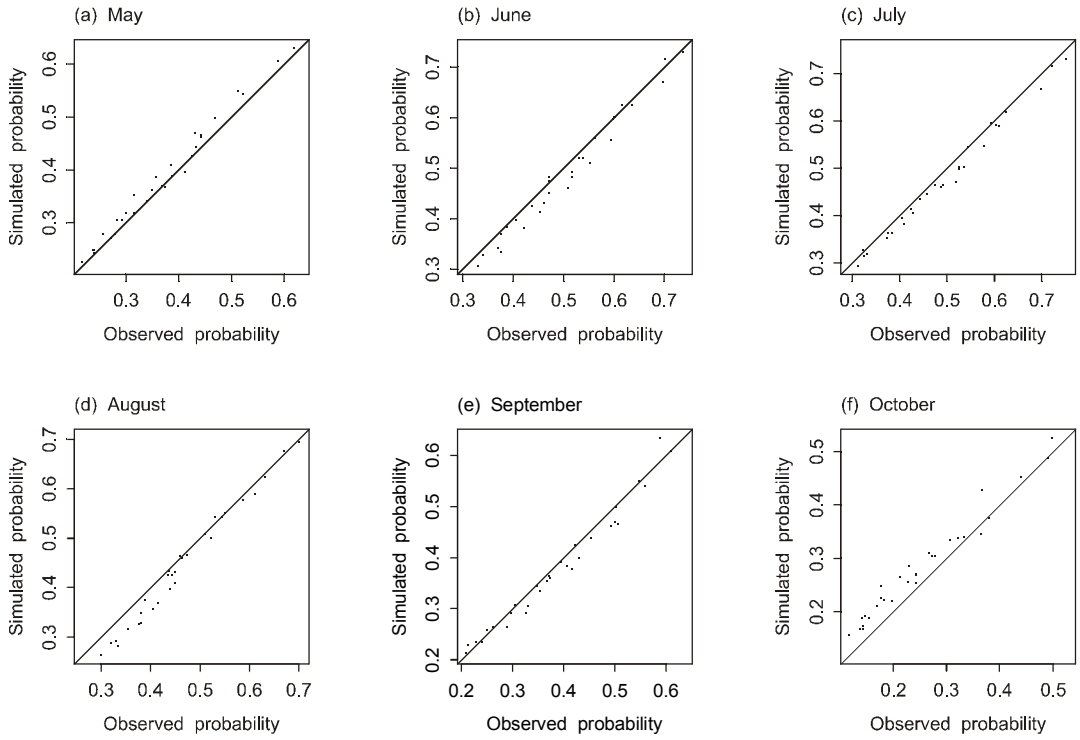

Figure 3.7 **Comparison of simulated and historical daily precipitation probabilities for the period 1978–1992 (modified NHMM).**

The seasonal distribution of the errors in the simulation of monthly precipitation amounts for Pingelly is given in Figure 3.8. Comparison of Figures 3.3 and 3.8 reveals a noticeable improvement in fit for the months of June, July, October, and perhaps September.

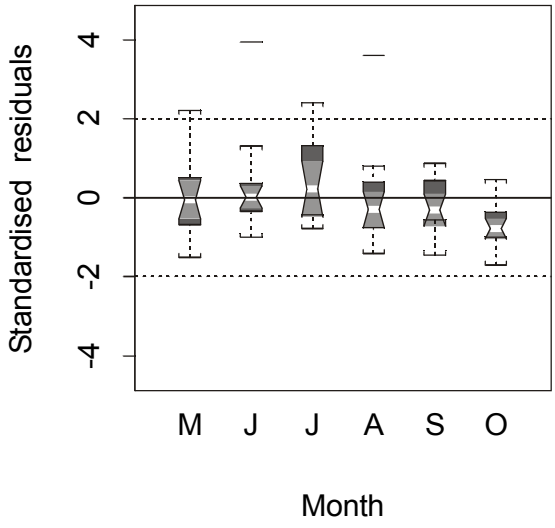

Figure 3.8 **Box plots showing seasonal distribution of standardised residuals for Pingelly (Station 28) for the period 1978–1992 (modified NHMM).**

The seasonal distribution of the monthly standardised residuals for Pingelly for the test period 1958 to 1977 is given in Figure 3.9. (Recall from section 3.2 that data for this period were not used to fit the NHMM.) The residuals exhibit a cyclical variation through the winter half-year. However the line $e = 0$ lies between the upper and lower quartiles in each case. With the exceptions of July and August, the distributions of the residuals are not symmetrical about the median in their middle regions (25^{th} to 75^{th} percentiles), and other diagnostics such as quantile-quantile plots (not shown) indicate departures from normality. The distribution for July contains an apparent outlier $(e = 4.02)$. Little evidence of serial correlation was found in the residuals. Consequently, we used the Wilcoxon signed-rank statistic to test the null hypothesis that the mean of the standardised residuals for a given month is zero against the alternative hypothesis that the mean is not zero. The test statistics for the months May to October were found to be significant at the 0.189, 0.011, 0.185, 1.00, 0.575, and 0.105 levels. Thus there is little evidence against the null hypothesis for all months other than June for which there is some evidence against the null hypothesis.

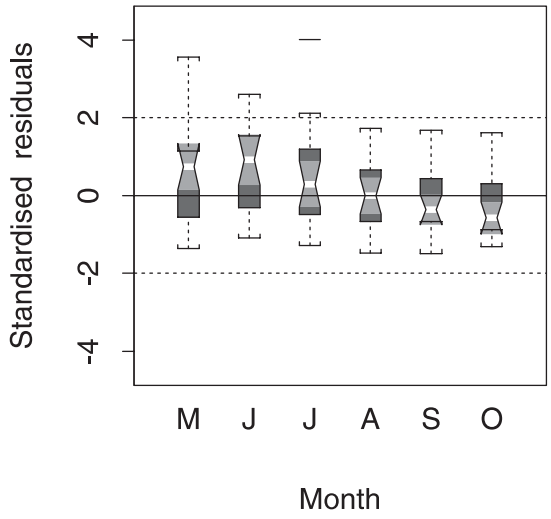

Figure 3.9 Box plots showing seasonal distribution of standardised residuals for Pingelly (Station 28) for the period 1958–1977 (modified NHMM).

A time series plot of monthly standardised residuals for Pingelly for the period 1958 to 1998 is given in Figure 3.10. Overall, the residuals form a horizontal band of uniform height centred about the line $e = 0,$ and 3% of the standardised residuals lie outside of the interval $-2 \le e \le 2$. Similar plots have been obtained for the remaining 29 stations. All stations have monthly standardised residuals greater than 3, but these residuals comprise only 1.3% of the 30*6*41=14760 station-months and do not exhibit any temporal trends. This suggests

that the atmospheric predictors in the modified NHMM have accounted for any long-term time effects (such as changes in the atmospheric circulation over SWA) that are inherent in the Reanalysis data. Given that the period 1958 to 1977 was wet relative to 1979 to 1992, this suggests that the modified NHMM is robust against the effects of climate shifts and trends on precipitation over SWA.

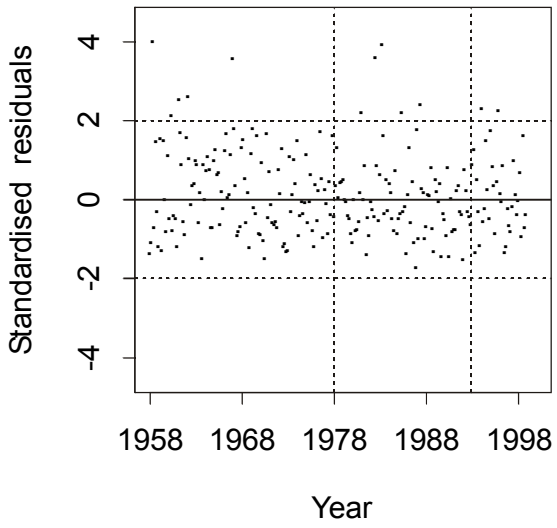

Figure 3.10 Monthly standardized residual series for Pingelly (Station 28) for the period 1958–1998 (modified NHMM). Broken vertical lines denote the fitting period for the NHMM (1978 to 1992).

4. EXPLANATION FOR THE MULTIDECADAL, WINTER PRECIPITATION DECLINE OVER SOUTHWEST AUSTRALIA

4.1 Introduction

The overall decline in annual precipitation over SWA since around the middle of the 20th century has been the subject of much interest [see citations in IOCI (1999) and Tapp and Cramb (2000)]. Most of the decrease is evident in the winter half-year (May-October) when about 80 percent of the annual precipitation occurs. The number of rain days in the winter half-year has decreased over much of the region, and the average intensity and frequency of rare high-precipitation events during that season have decreased.

The winter precipitation decline has had a marked effect on the surface water resources of the Perth region over the last 25 years. Figure 4.1 shows a bar chart of the total annual inflow for the major reservoirs in the Perth water supply system. The water year is defined by the period from May to April. Since the 1975 water year, dam inflows have been consistently smaller than those in the past and, with only one exception (1996), smaller than the long term mean annual inflow. Only once has an annual total precipitation at Perth exceeded the 70th percentile since 1967 (Tapp and Cramb, 2000).

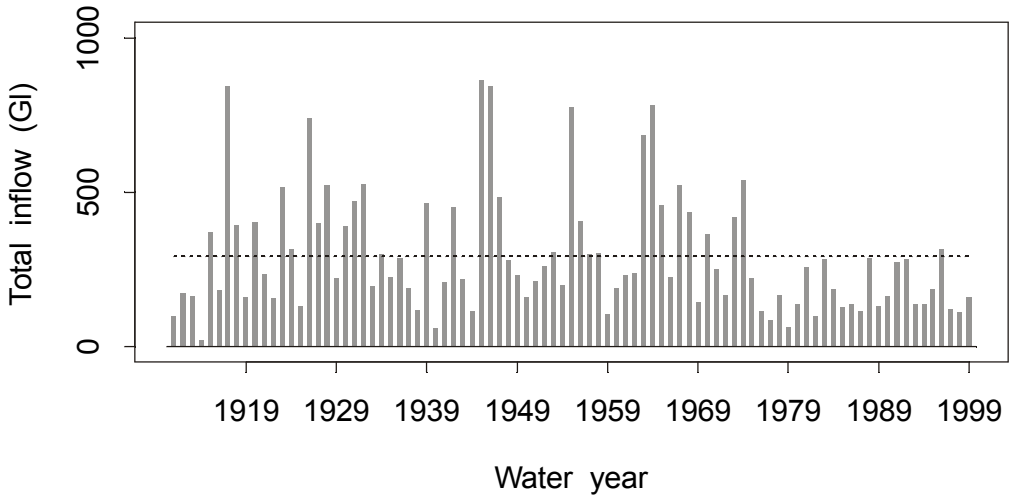

Figure 4.1 Annual inflow series for major surface water sources, Perth Water Supply System. Dashed line shows mean annual inflow for complete record. (Series supplied by Water Corporation of Western Australia.)

The timing of the abrupt shift in the inflow series roughly coincides with changes to the frequency characteristics of El Niño and a marked warming in the Indian Ocean after 1976 (see citations in Clark *et al.,* 2000). Since 1975, El Niños are twice as frequent as La Niñas. This suggests that an investigation of the atmospheric circulation over SWA for the period covered by the Reanalysis dataset (1958-1998) could be revealing.

4.2 Approach

The linkage between the winter precipitation decline and regional changes in atmospheric circulation are investigated using the NCEP-NCAR Reanalysis dataset, observed daily precipitation series for the 30 sites shown in Figure 2.1, and the modified nonhomogeneous hidden Markov model (NHMM) described in section 3. Recall that the transition from a given weather state to another in the NHMM is conditioned on a relatively small number of atmospheric variables (predictors) derived from the Reanalysis dataset. Thus any changes in the evolution of the weather states may be linked to temporal changes in the atmospheric predictors.

We hypothesized that the recent precipitation decline in SWA was caused by a change in the atmospheric circulation that occurred around 1976; and that this change would manifest itself in both the atmospheric predictor series used to condition the weather state transition probabilities in the NHMM and the weather state sequence derived from the fitted NHMM.

We split the atmospheric predictor series and the weather state sequence into two parts with the breakpoint occurring at October 31st in either 1974, 1975, 1976, 1977, or 1978. These breakpoints encompass the large-scale climate shift that occurred around 1976. The periods from 1958 to the breakpoint year, and the year following the breakpoint to 1998, are hereafter called Epoch 1 and Epoch 2.

Our analysis consisted of three parts:

(1) Comparison of the NHMM weather state sequence for 1958 to the mid–70s with that for the mid–70s to 1998. The comparison was made on a winter and a calendar month basis. Plots of weather state probability series were used to discern any changes in synoptic patterns that may have occurred prior to the mid-70s.

(2) An exploratory data analysis comparing the atmospheric predictor series for Epoch 2 with that of Epoch 1.

(3) A sensitivity analysis to investigate whether the precipitation decline since the mid–70s can be attributed to changes in the behaviour of a single predictor in the NHMM.

4.3 Methods

4.3.1 Analysis of Weather State Sequence

a. Changes in steady-state probabilities of weather states

We used a two-sample *t*-test to assess the statistical significance of differences between the means of the winter weather state probability series for Epochs 1 and 2. Exploratory analyses indicated that the data did not exhibit significant autocorrelation or departures from normality. Rather than set an essentially arbitrary significance level, we used the probability value (*P*-value) to measure the strength of the evidence against the null hypothesis that the means are equal. The *P*-value is the probability that a test statistic at least as extreme as that observed could have arisen by chance.

b. Changes in weather state counts for each calendar month in winter

When the sampling interval is reduced from six months to one month, the number of occurrences of any given weather state is relatively low. Therefore, it is more appropriate to consider weather state counts (a discrete random variable) rather than weather state probability (a continuous random variable). Given that weather state counts series are discrete, we used lag plots to check for serial correlation in the counts series for each period: little evidence of serial correlation was found. An exploratory analysis of the counts data indicated that the underlying probability distributions were multimodal. This precluded inferences based on commonly used discrete probability distributions. Consequently, we used randomization to test the hypothesis that average weather state counts for Epoch 2 are the same as those for Epoch 1. That is, to test whether the observed counts series for the weather states are likely or unlikely to have arisen by chance.

Randomization testing is a procedure that is less dependent on distributional assumptions than conventional statistical methods. It involves the determination of the *P*-value of a test statistic computed for an observed dataset by comparing the statistic's value with the

distribution of values obtained by calculating the test statistics for a large number of re-orderings of the data (Manly, 1991). Here the *P*-value is the proportion of values that are as extreme or more extreme than the test statistic's value in the randomization distribution.

Box plots of the weather state counts data indicated the presence of extreme sample values and long-tailed probability distributions in several instances. Thus the sample mean would be a poor estimator of location. For each calendar month *m* and weather state *s* we test for a difference between the median weather state counts for Epochs 1 and 2. The test statistic is defined by

$$\widetilde{c}_{ms} = \widetilde{c}_{1ms} - \widetilde{c}_{2ms} \tag{4}$$

where $\widetilde{c}_{1ms}$ and $\widetilde{c}_{2ms}$ are the median counts for weather state *s* in Epochs 1 and 2, respectively. We used two-sided tests throughout since marked increases or decreases in weather states counts across the two epochs are of interest. Thus large positive and large negative values of $\widetilde{c}_{ms}$ are regarded as evidence against the null hypothesis that the medians are equal. We used 5000 randomizations for each *m* and *s* pair in (4) since complete enumeration of all possibilities would require an impractical $41!/20!(41-20)! \approx 10^{12}$ re-orderings of the observed dataset.

c. Changes in weather state transition probabilities

The application of 6×6=36 univariate two-sample *t*-tests to the components of weather state transition probability matrices could lead to the possibility of obtaining a significant result by chance alone. Therefore, we used the Hotelling two-sample T^2-test. Let *N* denote the number of weather states and $\mathbf{X}^i$, $(i = 1, \cdots, N)$, denote a transition probability matrix with elements:

$$x_{ij}^{i} = \overline{P(S_j \mid S_i)}_{\tau}; \quad j = 1, \cdots, N-1, \quad \tau = 1, \cdots, n \tag{5}$$

where $\overline{P(S_j \mid S_i)}_{\tau}$ denotes the estimated one-step transition probability of going from weather state *i* on one day to weather state *j* on the next day during year τ. The probability $\overline{P(S_N \mid S_i)}_{\tau}$ is ignored since

$$\overline{P(S_N \mid S_i)_\tau} = 1 - \sum_{j=1}^{N-1} x_{ij}^i \tag{6}$$

We used the Hotelling two-sample T^2-statistic to test the null hypothesis that the population mean vectors of the transition probability matrices for both Epochs are identical against the alternative hypothesis of different means (Chatfield and Collins, 1980). Let $\mathbf{X}_1^i$ and $\mathbf{X}_2^i$ denote the matrices defined by (5) for the pre-1978 and post-1978 periods, respectively. The T^2-statistic is defined by

$$T^2 = \frac{n_1 n_2}{n_1 + n_2} (\bar{\mathbf{x}}_1^i - \bar{\mathbf{x}}_2^i)^T \mathbf{S}^{-1} (\bar{\mathbf{x}}_1^i - \bar{\mathbf{x}}_2^i) \tag{7}$$

where $\bar{\mathbf{x}}_1^i$ and $\bar{\mathbf{x}}_2^i$ denote the column means of $\mathbf{X}_1^i$ and $\mathbf{X}_2^i$, the superscript T denotes the transpose of a vector or matrix, and $\mathbf{S}$ denotes the pooled estimate of the common covariance matrix:

$$\mathbf{S} = \frac{(n_1 - 1)\mathbf{S}_1 + (n_2 - 1)\mathbf{S}_2}{n_1 + n_2 - 2} \tag{8}$$

in which $\mathbf{S}_1$ and $\mathbf{S}_2$ denote the sample covariance matrices of $\mathbf{X}_1^i$ and $\mathbf{X}_2^i$. The statistic

$$F = \frac{n_1 + n_2 - p - 1}{(n_1 + n_2 - 2)p} T^2 \tag{9}$$

has the variance ratio F distribution with degrees of freedom p and $n_1 + n_2 - p - 1$.

The T^2-distribution is a multivariate generalization of the Student t-distribution. Thus the T^2-test assumes that the transition probability matrices have a multivariate normal distribution with the same, though unknown, covariance matrix. Although the T^2-statistic is not sensitive to the assumption of equal covariance matrices when the sample sizes are approximately equal, severe departures from normality may be cause for concern. Consequently, we used randomization tests with 5000 randomizations each to check the P-values of the T^2-statistics computed from the observed transition probability matrices.

4.3.2 Exploratory Analysis of Atmospheric Predictor Series

The exploratory analysis focused on comparisons of the probability distributions of the predictors for Epochs 1 with those for Epoch 2. The analysis consisted of two plots for each predictor: a Tukey mean-difference (m-d) plot (Cleveland, 1993); and a plot of the smoothed density estimates (Venables and Ripley, 1994) for each Epoch. Let E_{1p} and E_{2p} denote the p^{th} quantile for a given predictor for Epochs 1 and 2, respectively. (The p^{th} quantile is the value of the predictor below which 100p of the values fall.) The m-d plot graphs the differences $E_{1p} - E_{2p}$ against the means $(E_{1p} + E_{2p})/2$. Thus the differences will be zero if the empirical distributions for Epochs 1 and 2 are the same, while systematic deviations from the zero difference line indicate the nature and size of differences between the distributions. Density estimates can give valuable indications of features such as skewness and multimodality in data. The oldest density estimator for univariate data is the histogram. However, the interpretation of the features in a histogram is sensitive to the choice of the number of class intervals and starting point of the class intervals. We used *kernel density* smoothers instead.

4.3.3 Sensitivity Analysis

The atmospheric predictors enter the NHMM in a nonlinear fashion. Therefore, it is difficult to discern whether the low precipitation sequence is due to changes in one atmospheric predictor alone or a combination of predictors. We assessed the impact of a change in the distribution of any one of the three key predictors (mean MSLP, north-south MSLP gradient and DT_d^{850}) by transforming its pre-1978 distribution to its post-1978 distribution. For a given key predictor x, the transformation is described by $x_2 = F_{X_2}^{-1}(F_{X_1}(x_1))$ where x_1 and x_2 denote Epochs 1 and 2, and $F_{X_i}(), \; i = 1, 2,$ denotes the cumulative distribution function for the i^{th} Epoch. The transformed values of the fourth predictor (i.e., first atmospheric canonical variable) were determined using the x_2 values and the pre-1978 values for the remaining 23 predictors. One-thousand, 20-year sequences of daily winter precipitation were generated from the fitted NHMM, conditionally on the 20-year sequence for each transformed atmospheric predictor with the pre-1978 distributions for the remaining key predictors left unchanged. The statistics of the simulated weather state and precipitation sequences obtained were then compared with those obtained from simulations driven by the post-1978 data.

4.4 Results

4.4.1 Analysis of Weather State Sequence

Table 4.1 reports the results of the two-sample, two-sided *t*-tests for the steady-state probability series for States 3 and 5. There is very strong evidence against the null hypothesis for State 3, and the strength of the evidence is insensitive to breakpoint selection. Some sensitivity to breakpoint selection is evident for State 5. Nevertheless, the strength of the evidence against the null hypothesis is strong to very strong. For States 1, 2, 4, and 6, the *P*-values lie in the interval $0.087 \leq P\text{-value} \leq 0.798$. Thus there is little evidence against the null hypothesis for these states.

Table 4.1 Comparison of mean probabilities of States 3 and 5 for Epochs 1 and 2.

	State 3		State 5	
Breakpoint	***t*-statistic**	***P*-value**	***t*-statistic**	***P*-value**
1974	5.313	4.64×10^{-6}	-4.182	1.58×10^{-4}
1975	5.240	5.86×10^{-6}	-3.621	8.35×10^{-4}
1976	5.024	1.16×10^{-6}	-3.654	7.58×10^{-4}
1977	4.488	6.21×10^{-5}	-3.296	0.002
1978	4.158	1.70×10^{-4}	-2.905	0.006

Table 4.2 reports the results of the randomization tests for monthly weather state counts for States 3 and 5. Some sensitivity to breakpoint selection is evident. However, for July and August there is strong evidence against the null hypothesis that mean State 3 counts for Epoch 2 are the same as those for Epoch 1. October is the only month for which the evidence against this null hypothesis is weak. For May to August, there is some to very strong evidence against the null hypothesis that mean State 5 counts for Epoch 2 are the same as those for Epoch 1.

Table 4.3 reports the results of the Hotelling two-sample T^2-tests for the weather state transition probability matrices for States 2, 3 and 5. (For States 1, 4 and 6 there is little evidence against the null hypothesis that the population mean vectors of the transition probability matrices for both Epochs are identical.) The *P*-values obtained using the distributional assumption about the transition probability matrices and randomization are in essential agreement, and are fairly insensitive to breakpoint selection. For transitions *from* State 2 there is very strong evidence against the null hypothesis that the population mean

vectors for both Epochs are identical. Inspection of time series plots of $\overline{P(S_3 \mid S_2)}$ and $\overline{P(S_4 \mid S_2)}$ for 1958-1998 revealed underlying decreasing and increasing trends, respectively. Thus the corresponding means for Epochs 1 and 2 are quite different. In contrast, there is little evidence that the transition probabilities from any state *to* State 2 have changed. For transitions *from* State 3 there is strong to very strong evidence against the null hypothesis. The mean $\overline{P(S_3 \mid S_3)}$ for Epoch 2 is lower than that for Epoch 1, while the mean $\overline{P(S_5 \mid S_3)}$ for Epoch 2 is noticeably higher than that for Epoch 1. These findings provide further insight into the change in frequency of State 3 in that the day-to-day persistence of State 3 has decreased and the frequency of the transition from State 3 to dry conditions region-wide (State 5) have increased during 1958-1998. The *P*-values for transitions *to* State 3 are sensitive to breakpoint selection, and the level of evidence against the null hypothesis ranges from little to strong. There is little evidence against the null hypothesis that the probabilities of transitions *from* State 5 *to* any other state or the same state have not changed. However, for transitions *to* State 5 there is strong evidence against the null hypothesis: for Epoch 2 the $\overline{P(S_5 \mid S_j)},\ j = 1, \ldots, 6,$ are higher than those for Epoch 1.

Table 4.2 ***P*-values from randomization tests on monthly weather state counts for States 3 and 5.**

Break-point	Winter Month					
	May	**June**	**July**	**August**	**September**	**October**
State 3						
1974	0.016	0.002	0.002	0.002	0.013	0.109
1975	0.012	3×10^{-4}	0.003	0.002	0.003	0.024
1976	0.015	0.013	0.002	0.002	0.003	0.054
1977	0.015	0.008	0.006	0.004	0.012	0.073
1978	0.011	0.010	0.004	0.007	0.003	0.050
State 5						
1974	0.002	1×10^{-4}	1×10^{-4}	0.011	1×10^{-4}	0.007
1975	0.006	0.002	1×10^{-4}	0.014	0.033	0.018
1976	0.016	0.004	1×10^{-4}	0.014	0.055	0.016
1977	0.014	0.011	0.014	0.016	0.122	0.036
1978	0.007	0.046	0.024	0.012	0.209	0.209

Table 4.3 Results of Hotelling two-sample T^2-tests comparing the mean weather state transition probabilities for Epochs 1 and 2.

Weather	Transition From State *S*		Transition to State *S*	
State, *S*	*F* statistic	*P*-value*	*F* statistic	*P*-value*
1974				
2	7.754	0.0001	1.834	0.124
3	5.363	0.0009	3.838	0.0054
5	0.632	0.677	4.123	0.0035
1975				
2	6.828	0.0002	1.691	0.155
3	4.199	0.0043	4.016	0.0041
5	0.471	0.795	3.892	0.0050
1976				
2	6.081	0.0004	2.058	0.0864
3	5.294	0.0010	3.096	0.0166
5	0.888	0.500	4.570	0.0019
1977				
2	8.246	< 0.0001	1.403	0.244
3	4.000	0.0056	2.822	0.0256
5	0.590	0.708	3.736	0.0063
1978				
2	8.823	< 0.0001	1.226	0.319
3	3.536	0.011	2.263	0.0622
5	0.503	0.772	4.311	0.0027

* *P*-values based on the assumption that transition probability matrices have a multivariate normal distribution.

Although the above results *may* seem to be inconsistent with those reported in Table 4.1, the relationship between the steady state and transition probabilities is described by the following system of equations:

$$\begin{aligned} P(S_i) &= \sum_{k=1}^{N} P(S_k)\, P(S_i \mid S_k), \quad i = 1, \cdots, N \\ \sum_{i=1}^{N} P(S_i) &= 1 \end{aligned} \tag{10}$$

Hence $P(S_i)$ is a nonlinear function of the components of the i^{th} column of the transition probability matrix, and the effects of changes in these transition probabilities on the steady state probability will not take a simple form.

Plots of the winter weather state probability series for states 3 and 5 are given in Figure 4.2. Although interannual variability is evident in both plots across the 1958-98 period, it is apparent that the frequency of State 3 declined from 1958 to the mid–70s and has remained stationary since that time (Figure 4.2a). In contrast, the frequency of State 5 increased abruptly around the early to mid–70s (Figure 4.2b) and has remained stationary since the apparent break. Consider the precipitation occurrence patterns and corresponding composited MSLP fields for States 3 and 5 given in Figure 3.1. If kinks in the isobars of low pressure systems in MSLP charts can be interpreted as indicative of the presence of cold fronts (Sturman and Tapper, 1996, p. 171), a reduction in the frequency of State 3 indicates a reduction in the occurrence of post-frontal rainfall. An increase in the frequency of State 5 indicates a decrease in the number of rain days across SWA. This is due to an increase in the frequency of dry easterly or northeast winds around high pressure systems centred to the east of the region.

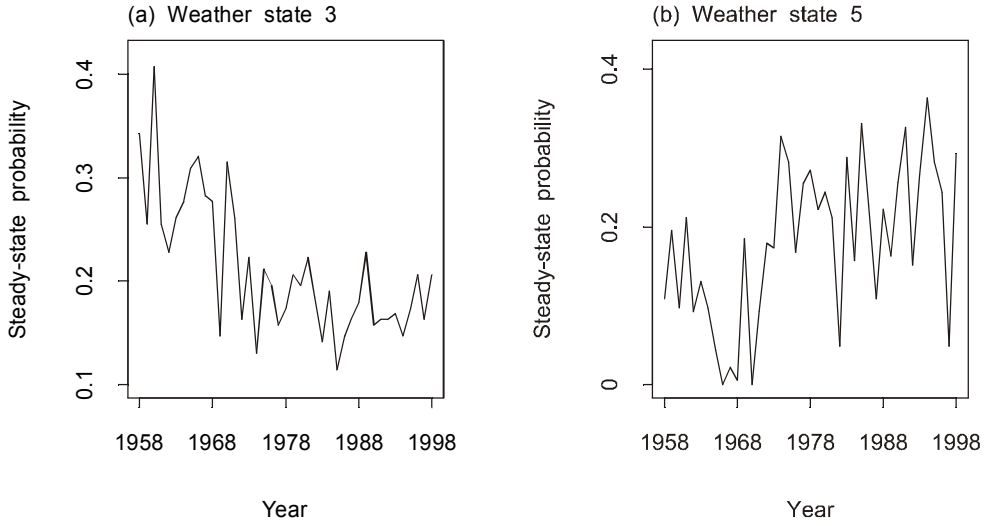

Figure 4.2 Interannual variability of steady-state probabilities for weather states 3 and 5.

The underlying shift and trend evident in Figure 4.2 suggest that the observed low precipitation sequence is due to climate forcing by at least two large-scale and possibly interacting mechanisms. The mid-70s break in the probability series for States 3 and 5 roughly coincides with the timing of the observed change in the behaviour of El Niño (see section 4.1). The presence of high pressure systems in the Australian region is more pronounced during El Niño episodes, and the change in the frequency of State 5 is consistent with the decline in the number of La Niña episodes relative to El Niños. The decline in the

frequency of State 3 may be linked to a change in the behaviour of the Antarctic Oscillation. One index of the Oscillation is the first empirical orthogonal function (EOF) of sea level pressure (SLP) for the latitudinal band between 20 and 60º S. Figure 4.3(a) depicts the SLP anomaly when the index is positive; a region of lower than usual SLP surrounds the Antarctic continent while regions of higher than usual SLP occur at middle latitudes. Under these conditions, westerly airflow in the mid latitudes is suppressed. Figure 4.3(b) shows the index time series derived from the Reanalysis record by CAR. The index is negative in sign prior to the mid-70s, and positive thereafter. Also, the index increases from high negative values in the early 1960s to positive values in the late 1970s.

Inspection of Figure 3.1 suggests that States 2 and 4 also involve southwest to westerly airflow. As noted above, the mean transition probabilities *from* State 2 for Epoch 2 are different to those for Epoch 1. Comparison of the composite MSLP plots for States 2 and 3 suggests that both conform to the typical pattern of a trough between two anticyclones that is conducive to the development of cold fronts. Fronts separate two air masses of contrasting wind, temperature and density, and in the Australian region are largely due to the interaction of subtropical and polar air. These features are not as apparent in the composite MSLP plot for State 4. State 4 appears to be indicative of weak frontal systems, or frontal systems that are centred too far south to penetrate the hinterland. Recall that no significant change in the steady-state or transition probabilities for State 4 was detected. Overall, these results suggest that the hypothesised linkages between the low precipitation sequence and changes in the behaviour of El Niño and the Antarctic Oscillation need to be subjected to a detailed meteorological analysis.

4.4.2 Exploratory Analysis of Atmospheric Predictor Series

Figure 4.4 shows mean-difference and smoothed density plots for the key atmospheric predictors when Epochs 1 and 2 are defined as the periods 1958–76 and 1977–98, respectively. The post-1976 changes in the probability distributions of the predictors differ from each other. The MSLPs for Epoch 2 are roughly equal to MSLPs for Epoch 1 plus a constant of 0.6 hPa. The spread of N-S MSLP gradient for Epoch 2 is marginally larger than that for Epoch 1. The distribution of DT_d^{850} values for Epoch 2 has a longer upper tail than that for Epoch 1. This suggests that when the lower troposphere is dry, it is much drier in Epoch 2 than in Epoch 1.

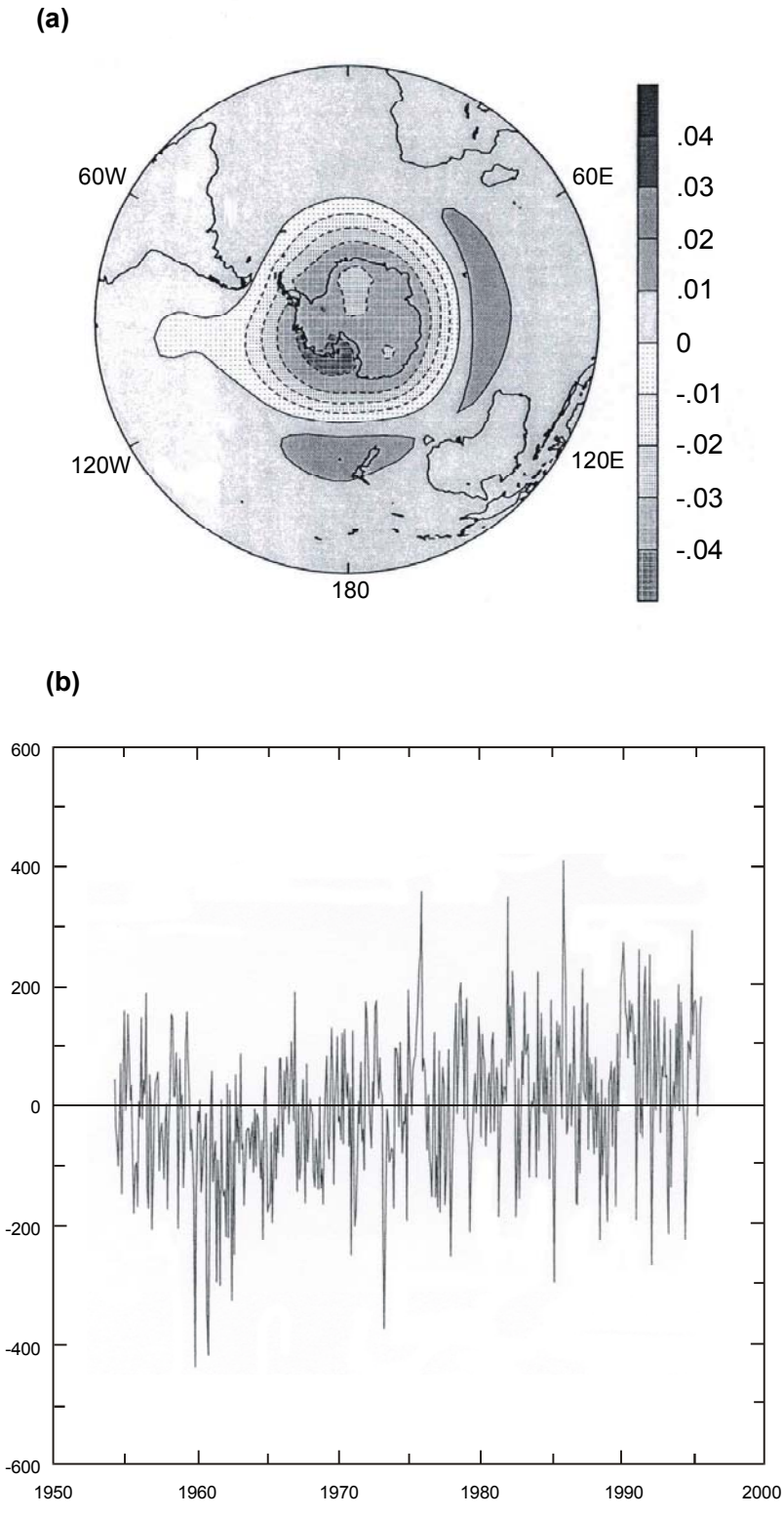

Figure 4.3 Antarctic Oscillation: (a) pressure anomaly when the first EOF of sea level pressure is positive, (b) time series of the first EOF. (Source: Peter Whetton, CSIRO Atmospheric Research.)

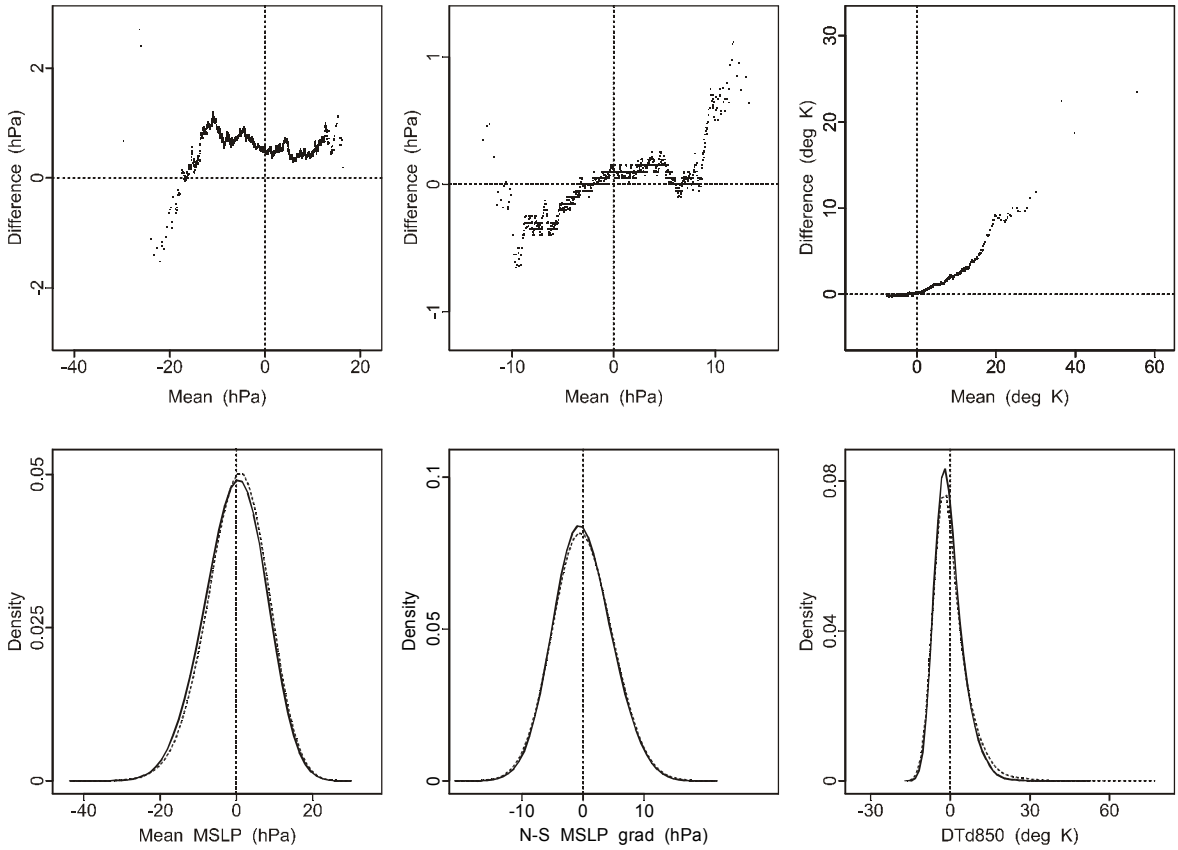

Figure 4.4 Mean-difference plots and smoothed density estimates of centred, NHMM atmospheric predictor series for the periods 1958–76 (Epoch 1) versus 1977–98 (Epoch 2). In each density plot the density estimates for 1977-1998 are shown as dotted curves.

4.4.3 Sensitivity Analysis

Results from the sensitivity analysis are given in Figure 4.5. The probability residuals for a particular weather state are defined herein as the difference between the 'observed' steady state probabilities for each year in the 1979-1998 period and the mean of the 1000 simulated probabilities for each year. The raindays residuals are defined as the difference between the observed mean values of the number of raindays at each site for 1979-1998 and their simulated means. The rainfall residuals are defined as the difference between the observed mean values of rainfall amounts at each site for 1979-1998 and their simulated means.

Perusal of Figure 4.5 indicates that post-1978 changes in any one of the three predictors alone cannot explain the decline in the frequency of State 3 nor the number of rain days over SWA (Figures 4.5a and 4.5c). In contrast, the increase in the frequency of State 5 can be explained by changes in any one of the three predictors (Figure 4.5b). The results for mean winter

precipitation (Figure 4.5d) are not informative given that the NHMM simulations based on the 1979-98 Reanalysis data are slightly biased. Nevertheless, it is apparent that the changes in weather state frequency and precipitation across SWA are due to changes in a combination of atmospheric predictors rather than a single predictor.

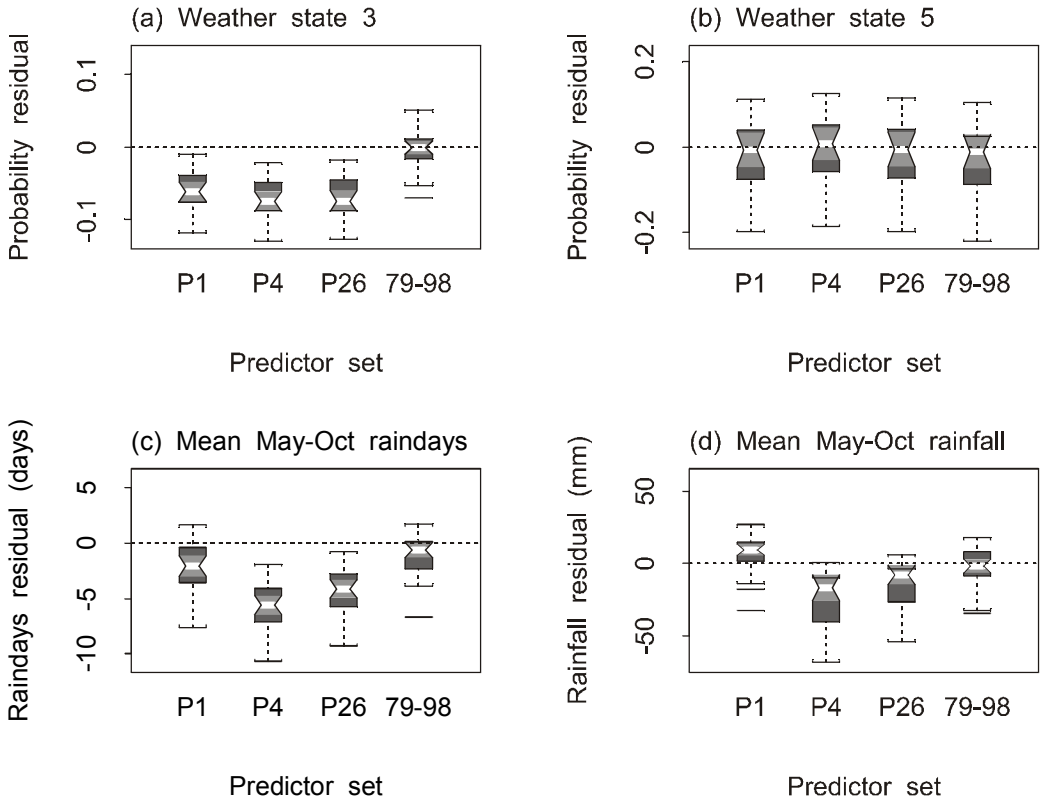

Figure 4.5 Box plots of results from sensitivity analysis: (a) and (b) show differences between observed and mean simulated weather state probabilities, (c) shows differences between mean observed rain days and mean simulated rain days for all 30 sites, and (d) shows the relative percentage error in mean simulated precipitation across the 30 sites. P1, P4 and P26 denote results for transformed mean MSLP, north-south MSLP gradient and DT_d^{850}, respectively, and 79-98 denotes results when the post-1978 data for all predictors are used to drive the modified NHMM.

4.5 Discussion

Other workers have investigated the causes of the low precipitation sequence over SWA. Allan and Haylock (1993) found that wet and dry periods over most of the region are associated with enhanced and weaker mean westerly airflow, respectively. Smith *et al*. (1999) noted an increase in winter MSLPs over SWA since the late 1960s and a decrease in cyclonic activity immediately south of WA over the same period. Our results are consistent with these earlier findings in that comparing the last twenty years (Epoch 2) with the previous twenty years (Epoch 1):

- Winter MSLP for Epoch 2 is equal to that for Epoch 1 plus an additive shift of 0.6 hPa (Figure 4.4).

- There has been a significant reduction in the number of days when precipitation is generated by westerly airflow (Figures 3.1a and 4.2).

- There has been a significant increase in anticyclone activity (Figures 3.1b and 4.2).

Tapp and Cramb (2000) have speculated that changes in atmospheric circulation that are not well reflected by changes in MSLP may also affect regional precipitation. We have found that when the lower troposphere has been dry in Epoch 2, there is a tendency for it to have been drier than in Epoch 1 (Figure 4.4). We have also demonstrated that the low precipitation sequence is due to a combination of changes in sea level pressure and low-level humidity variables rather than a single pressure variable alone (Figure 4.5).

4.6 Conclusions

Our results indicate that:

- There is strong to very strong evidence of changes in the synoptic patterns over SWA during the last 40 years.

- There are marked reductions in the incidence of precipitation generated by moist westerly and south-west winds, and the number of rain days due to an increase in the frequency of high pressure systems centred to the east of SWA.

- The changes in weather state frequency, and hence precipitation occurrence and amount, are due to a combination of changes in several atmospheric variables (mean MSLP, north-south MSLP gradient and DT_d^{850}) rather than any one predictor.

We have *speculated* that the large-scale mechanisms responsible for the low precipitation sequence may be changes in, and a possible interaction between, the behaviour of El Niño and the Antarctic Oscillation over the period covered by the Reanalysis dataset. This hypothesis should be subjected to detailed meteorological analysis.

5. LOW FREQUENCY CLIMATE VARIABILITY

5.1 Introduction

Previous work by CSIRO Atmospheric Research (IOCI, 1999) has indicated that the observed low precipitation sequence for SWA is unusual in a historical and global context. In this section, we attempt to place the observed sequence in a regional context by applying the NHMM to the daily atmospheric fields produced by the 1000-year, CSIRO Mk 2 coupled GCM run. This approach produces a daily precipitation sequence of length 1000 years for each of the 30 sites in SWA (Figure 2.1 and Table 2.1).

Consider the 40-year period from 1958 to 1997. One way of characterising the recent precipitation decline over SWA is to compute the difference between the mean precipitation across all 30 sites for the period 1958 to 1977 and the mean precipitation across all 30 sites for 1978 to 1997. This difference will hereafter be referred to as the observed mean difference. We estimate the probability of a mean difference that is at least as severe as the observed as follows:

- For each of the 961 periods of length 40 years in the 1000-year GCM run, compute a simulated mean difference by subtracting the mean precipitation for the last 20 years across all 30 sites from the mean precipitation for the first twenty years.

- Collate and sort the 961 simulated mean differences.

- Compare the observed mean difference to the empirical quantiles of the distribution of the simulated mean differences.

5.2 Results and Discussion

Figure 5.1 compares the distribution of simulated mean differences with the observed mean difference (27.2 mm). About 9.5% of the simulated mean differences are greater than the observed mean difference, indicating that the observed low precipitation sequence is uncommon but not extreme.

However, the above finding is subject to three caveats:

- It assumes that the 1000-year GCM run produces a credible simulation of low-frequency changes in atmospheric circulation over SWA.

- It assumes that the parameters of the NHMM are stationary over the length of the GCM simulation.

- The GCM simulation is not a reconstruction of climate variability over the last 1000 years, as temporal variations in solar forcing, volcanism and the atmospheric concentration of carbon dioxide over that period have not been accounted for. That is, the simulation is a scenario derived for present day conditions only.

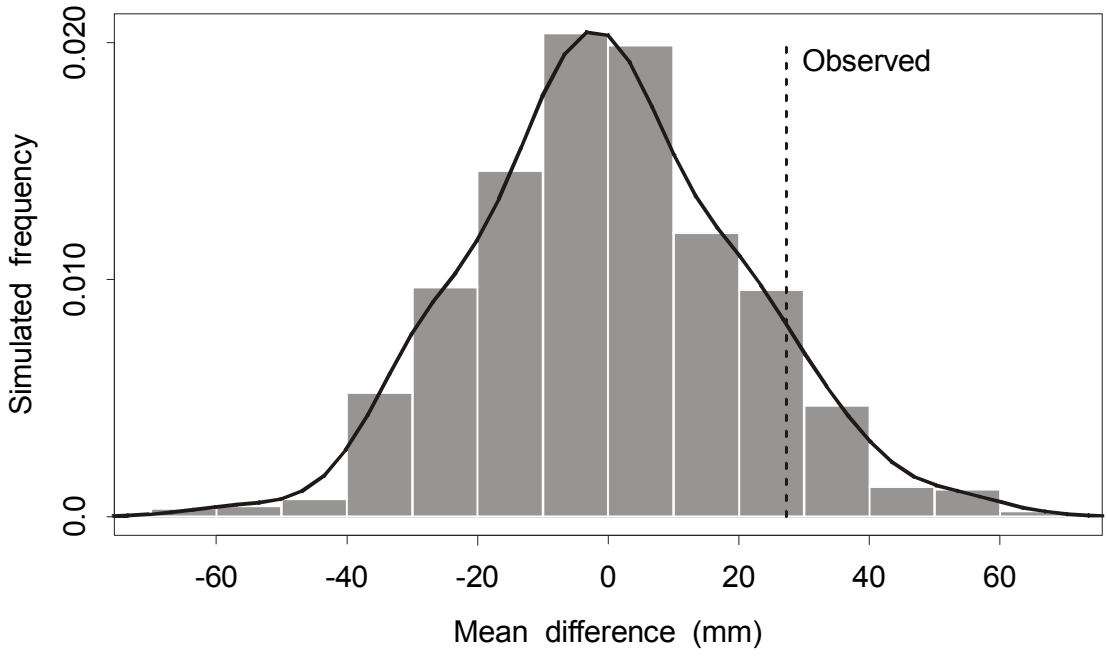

Figure 5.1 Comparison of the observed mean difference and simulated mean differences.

6. CONCLUSIONS

6.1 Summary of the Investigation

Our investigations for Second Research Phase of the Indian Ocean Climate Initiative (IOCI) have focused on:

- Split-sample testing of an extended nonhomogeneous hidden Markov model (NHMM) for daily winter (May to October) precipitation across a network of 30 stations scattered throughout southwest Western Australia (SWA).

- Using the NHMM and observed atmospheric fields to discern the causes of the low precipitation sequence in SWA at the synoptic scale.

- Deriving an estimate of the probability of the observed low precipitation sequence over the last two decades.

Our main findings are as follows:

- Initial testing revealed that the NHMM did not capture the dynamic behaviour of the atmosphere at intra-seasonal time scales. A modified version of the NHMM incorporating an augmented atmospheric predictor set was shown to resolve most of the performance deficiencies of the original model. This suggests that provided coupled ocean-atmosphere GCMs could provide reasonable interseasonal forecasts of the large-scale atmospheric circulation over SWA, reasonably reliable forecasts of monthly precipitation at sites across the region can be obtained.
- A sudden change in spatial precipitation occurrence patterns occurred in the mid 70s. Changes in the location and strength of depressions and anticyclones, and the moisture content of the lower troposphere, are evident.
- The low precipitation sequence over the last 20 years is due to changes in a combination of several atmospheric variables rather than a change in any one variable.
- Within the winter half-year, the number of days when the entire southwest is essentially dry is larger than in the past due to the increase in the number of days when anticyclones

are centred to the east of the region. This *may* be due to the change in the behaviour of El Niño that occurred around 1976.

- There has been a reduction in the frequency of precipitation in coastal regions due to a reduction in westerly airflow. There is a declining trend in the frequency of this precipitation pattern from 1958 to the mid-70s, with some evidence of oscillations about the trend. The trend has been absent for the period from the mid-70s to present. This *may* be due changes in the Antarctic Oscillation and an interaction between the Oscillation and El Niño.
- In a regional context, the low precipitation sequence over the last 20 years is uncommon but not extreme.

6.2 Future Research

Our proposed research plan for Phase 5 of IOCI is as follows:

- Downscaling of a sequence of staged, interseasonal climate forecasts using CAR's coupled ocean-atmosphere GCM, and comparison of downscaled precipitation with observations. This work will reveal the lead time for reliable forecasts (if any), and any so-called 'predictability barriers' during the winter half-year.

- Further investigation of the effects of El Niño and the Antarctic Oscillation on winter precipitation over SWA.

- Development of an air temperature module for the NHMM. This module will simulate minimum daily temperature and temperature range (maximum minus minimum daily temperature).

Our proposed research linkages for Phase 5 are:

- *CSIRO Atmospheric Research* – deriving interseasonal forecasts of monthly precipitation over SWA by downscaling a staged sequence of coupled CSIRO Mark 3 GCM simulations, and obtaining further insight into the relationships between key atmospheric predictors and large-scale forcing mechanisms.

- *Bureau of Meteorology (Research Centre and Perth Regional Office)* – collaboration on the final synthesis report for policy makers.
- *University of Washington, Seattle* – consultation on strategic issues related to further development of the NHMM.
- *CSIRO Mathematical and Information Sciences* – advice on advanced statistical issues and obtaining further insight into the relationships between key atmospheric predictors and large-scale forcing mechanisms.

7. REFERENCES

Allan, R.J. and Haylock, M.R. (1993). Circulation factors associated with the winter rainfall decrease in southwestern Australia. *J. Climate, 6,* 1356-1367.

Arnell, N., Bates, B.C., Lang, H., Magnuson, J.J. and Mulholland, P. (1996). Hydrology and freshwater ecology. In: *Climate Change 1995: Impacts, Adaptations and Mitigation of Climate Change: Scientific-Technical Analyses.* Contribution of Working Group II to the Second Assessment Report of the Intergovernmental Panel on Climate Change. R.T. Watson, M.C. Zinyowera, and R.H. Moss (ed.), Cambridge Univ. Press, Cambridge, 325-363.

Bardossy, A. and Plate, E.J. (1991). Modelling daily precipitation using a semi-Markov representation of circulation pattern occurrence. *J. Hydrol*., 122, 33-47.

Bardossy, A. and Plate, E.J. (1992). Space-time model for daily precipitation using atmospheric circulation patterns. *Water Resour. Res., 28*(5), 1247-1259.

Bogardi, I., Matyasovszky, I., Bardossy, A. and Duckstein, L. (1993). Application of a space-time stochastic model for daily precipitation using atmospheric circulation patterns. *J. Geophys. Res.*, *98*(D9), 16653-16667.

Charles, S.P., Bates, B.C. and Hughes, J.P. (1999). A spatio-temporal model for downscaling precipitation occurrence and amounts. *J. Geophys. Res.,* 104(D24), 31657-31669.

Chatfield, C., and A. J. Collins, 1980. *Introduction to Multivariate Analysis.* Chapman and Hall, London, 246 pp.

Clark, C.O., Cole, J.E. and Webster, P.J. (2000). Indian Ocean SST and Indian summer precipitation: Predictive relationships and their decadal variability, *J. Climate, 13,* 2503-2519.

Cleveland, W.S. (1993). *Visualizing Data*. AT&T Bell Laboratories, New Jersey, 360 pp.

Crane, R.G. and Hewitson, B.C. (1998). Doubled CO_2 precipitation changes for the Susquehanna basin: down-scaling from the GENESIS general circulation model. *Int J Climatol., 18*, 65-76.

Enke, W. and Spekat, A. (1997). Downscaling climate model outputs into local and regional weather elements by classification and regression. *Clim. Res.*, *8*, 195-207.

Gates, W.L., Henderson-Sellers, A., Boer, G.J., Folland, C.K., Kitoh, A., McAvaney, B.J., Semazzi, F., Smith, N., Weaver, A.J. and Zeng, Q.-C. (1996). Climate models - evaluation. In: *Climate Change 1995: The Science of Climate Change*. Contribution of Working Group I to the Second Assessment Report of the Intergovernmental Panel on Climate Change, J.T. Houghton, L.G. Meira Filho, B.A. Callander, N. Harris, A. Kattenberg, and K. Maskell (ed.), Cambridge Univ. Press, Cambridge, 229-284.

Hines, K.M. and D.H. Bromwich (1999). Artificial surface pressure trends in the NCEP/NCAR Reanalysis over the Southern Ocean. Proc. of the Second WCRP International Conference on Reanalyses, Wokefield Park, UK, 23-27 August 1999. WCRP-109; WMO/TD-985, pp. 50-53.

Hughes, J.P., Guttorp, P. and Charles, S.P. (1999). A non-homogeneous hidden Markov model for precipitation occurrence. *Appl. Statist.*, *48* (1), 15-30.

Huth, R. (1997). Potential of continental-scale circulation for the determination of local daily surface variables. *Theor. Appl. Climatol., 56*, 165-186.

IOCI, (1999). *Towards Understanding Climate Variability in South Western Australia – Research Reports of the First Phase of the Indian Ocean Climate Initiative.* Indian Ocean Climate Initiative (IOCI), Perth, 237 p.

Jobson, J.D., 1992. A*pplied Multivariate Analysis.* Springer-Verlag, New York, 731 pp.

Kalnay, E. and Co-authors (1996). The NCEP/NCAR 40-year reanalysis project. *Bull. Amer. Meteor. Soc., 77*, 437-471.

Kshirsagar, A.M., 1972. *Multivariate Analysis.* Marcel Dekker, New York, 534 pp.

Manly, B.F.J., 1991. *Randomization and Monte Carlo Methods in Biology*. Chapman and Hall, London, 281 pp.

Marshall, G.J. and S.A. Harangozo (1999). A preliminary validation and analysis of NCEP/NCAR Reanalysis monthly MSLP data over the South Pacific/Southern Ocean region. Proc. of the Second WCRP International Conference on Reanalyses, Wokefield Park, UK, 23-27 August 1999. WCRP-109; WMO/TD-985, pp. 77-80.

McGregor, J.L., Gordon, H.B., Watterson, I.G., Dix, M.R. and Rotstayn, L.D. (1993). The CSIRO 9-level atmospheric general circulation model. *CSIRO Div. Atmos. Res. Tech. Paper No. 26*, 89 pp.

Qiu, P. and B. Yandell, 1998. A local polynomial jump-detection algorithm in nonparametric regression. *Technometrics*, **40**, 141-152.

Smith, I.N., McIntosh, P., Ansell, T.J., Reason, C.J.C. and McInnes, K. (2000). South-west Western Australian winter rainfall and its association with Indian Ocean climate variability. *Int. J. Climatol., 20,* 1913-1930.

Sturman, A. and Tapper, N. (1996). *The Weather and Climate of Australia and New Zealand*. Oxford University Press, Melbourne, 476 pp.

Tapp, R. and Cramb, J. (2000). *Some Aspects of Variability and Recent Trends in Rainfall in South-West Western Australia.* Bureau of Meteorology, Tech. Rept 72, May 2000, 28 p.

Venables, W.N. and Ripley, B.D. (1994). *Modern Applied Statistics with S-Plus.* Springer-Verlag, New York, 462 p.

Wilby, R.L., Hassan, H. and Hanaki, K. (1998). Statistical downscaling of hydrometeorological variables using general circulation model output. *J. Hydrol.*, *205*, 1-19.

APPENDIX A - GLOSSARY

General circulation	The global-scale wind system that largely determines the broad climate patterns on Earth.
Dew point temperature	Temperature to which air needs to be cooled for condensation to occur at a given atmospheric pressure and mixing ratio.
Downscaling	Quantification of the relation of local- and regional-scale climate variables to larger scale atmospheric patterns. These patterns may be observed or simulated by dynamical climate models.
Dry spell	A sequence of consecutive days during which daily precipitation remains below 0.3 mm.
Front	The transition zone or interface between two air masses of contrasting wind, temperature and density.
Geopotential height	The work that must be done against gravity to raise a mass of 1 kg from sea-level to the level of interest in the atmosphere.
Markov process	A stochastic process in which the 'future' is determined by the 'present' and is independent of the 'past'.
Mean Sea Level Pressure	Total atmospheric pressure at the average height of the sea for all tidal stages over a 19-year period.
Mixing ratio	Ratio of the mass of water vapour to the mass of dry air in a given volume of air.
Precipitation	Any and all forms of water that falls from clouds and reaches the earth's surface.
Quantile	The value of a variable below which a certain proportion of the variable values will fall.
Wet spell	A sequence of consecutive days during which daily precipitation equals or exceeds 0.3 mm.

APPENDIX B - LIST OF ACRONYMS

BIC	Bayesian information criterion.
CAR	CSIRO Atmospheric Research
CCA	Canonical correlation analysis
CLW	CSIRO Land and Water.
EOF	Empirical orthogonal function
GCM	General circulation model.
GMT	Greenwich Mean Time: the 24-hour time scale used throughout the scientific and military communities. Other names for this time measurement are Universal Time Coordinate (UTC) and Zulu (Z).
CSIRO9	Spectral 9-level general circulation model developed by CSIRO Atmospheric Research.
IOCI	Indian Ocean Climate Initiative.
MSLP	Mean sea level pressure.
NCAR	National Center for Atmospheric Research.
NCEP	National Centers for Climate Prediction.
NHMM	Nonhomogeneous hidden Markov model
SLP	Sea level pressure
SST	Sea surface temperature.
SWA	Southwest Western Australia.

Nonlinear Statistical Methods for Climate Forecasting

Edward P. Campbell

CSIRO Mathematical and Information Sciences

Bryson C. Bates and Stephen P. Charles

CSIRO Land and Water

Report of Second Research Phase

for the

Indian Ocean Climate Initiative

CONTENTS

***** - Contains material of a technical statistical nature- please see *Suggested Reading* at the end of the summary.

LIST OF TABLES

LIST OF FIGURES

Summary

We summarise in this report the Indian Ocean Climate Initiative's (IOCI) work to date to develop a statistical procedure for modelling nonlinear climate phenomena. This procedure is motivated by the physical idea of a switching mechanism that causes different climate states to prevail for some period of time. There is a range of evidence to support these ideas, much of which was discussed in the Phase I report, and will be further discussed here. A simple example is the well-known phenomenon in the tropics where enhanced convection can occur when sea surface temperatures are greater than about 29°C, so different rainfall regimes apply either side of this threshold temperature.

A key feature of the procedure that we have developed is that it is not based on the typically strong statistical assumptions needed to perform a text book analysis. The statistical assumptions required are instead implied by the physical paradigm. We call this procedure a Bayesian threshold model, for reasons that will become clear below.

At the conclusion of this phase of IOCI we have developed and tested the Bayesian threshold model using monthly rainfall data at Rottnest Island and Manjimup. This represents the diversity of Southwest WA to some extent; Rottnest Island has been included in particular because there seems to be little scope for land-use change to have impacted rainfall patterns at this location. This has required some statistical research to underpin the Bayesian threshold model, and the detailed development is contained in a manuscript that has been submitted for publication. The manuscript is attached in Appendix C to this report. The method is relatively easy to use and can identify important predictors and the key lags at which they act to influence a climate variable, such as rainfall. It is possible to examine the impact of different switching variables and identify the likely number of thresholds in the switching variable, although this is the subject of ongoing work as it is currently somewhat ad hoc.

Whilst the main purpose of the case studies to date has been to support the development of the Bayesian threshold model, some interesting physical links have been observed. We cite them as evidence at this stage that the model is behaving as we would expect, rather than providing great insights. Searching for leading rainfall indicators is necessarily collaborative in nature, not simply a statistical modelling exercise, but can now incorporate a new nonlinear statistical tool.

Clear indications of switching behaviour have been found in the rainfall time series. For Rottnest Island no connection with monthly rainfall and the El Niño-Southern Oscillation (ENSO), as measured by the Southern Oscillation Index (SOI), has been found. A seemingly strong link has been found at Manjimup however. We have also examined the use of sea surface temperature gradient in the mid-Indian Ocean as a switching variable. There is evidence that it plays a role in switching rainfall regime at both sites considered, but the relationship appears to be especially strong at Rottnest Island, providing a leading indicator of winter rainfall.

If we conceive of a 'true' switching mechanism, it seems unlikely that this will be a very simple process. Physical intuition suggests that a *combination* of patterns in the Indian, Southern and Pacific Oceans is more likely to cause a switch in rainfall regime. This is because the climate system is driven by interaction between oceans as well as the oceans

and the atmosphere. Preliminary work suggests that the Bayesian switching model can readily be adapted to a more general framework that will facilitate the search for such climate interactions. We intend to pursue this as time permits.

Our key priority for the last phase of IOCI is to apply the Bayesian switching model, and our statistical expertise more generally, to a range of case studies developed in collaboration with the contributing partners.

Key Points:

- We have developed a physically motivated statistical model ('Bayesian switching model') for modelling nonlinear climate processes.
    - Changes between climate regimes are triggered by a switching variable, and alternative switching variables can be compared.
- The Bayesian switching model can identify good predictors and the lags at which they influence climate variables, such as rainfall.
- We have reached the point where a nonlinear time series approach can be applied to practical problems.
- There is some evidence that SOI and mid-Indian Ocean SST gradients play a role in switching between rainfall regimes. This is cited at this stage as evidence that the new nonlinear approach is producing sensible results, rather than new insights *per se*.
- Interactions between climate processes are likely to influence rainfall in Southwest WA. Some reasonably straightforward extensions to the Bayesian switching model will facilitate the search for subtler climate teleconnections arising from such interactions.
- The focus of future work will be the development of case studies with IOCI's contributing partners.

Suggested Reading

The work summarised in this report represents an overview of an statistical research effort. For most readers there is more technical detail than is necessary to understand the methods used and the progress made. The technical details are important for completeness however. We suggest two paths through this report:

For readers interested in the statistical research issues: Read in the order presented, but a first reading of Appendix C is appropriate after §2.

For readers not interested in the statistical research issues: §2.5 contains an overview of the technical material and so is optional but is of general interest; §3 is optional as it

contain some substantial technical material; §4.2 and Appendix C should be skipped completely.

1 Introduction

Many advances in climate forecasting have been brought about by the statistical analysis of available data. These advances occur when the analysis of climate data poses questions that encourage us to new physical understanding; when we can achieve this then there is a solid foundation on which to build better climate forecasting systems. Given the complex, inter-related nature of the climate system this can be a very difficult process in practice.

The bulk of statistical climatology work reported in the literature (see: *Campbell et al., IOCI Phase I Report*) uses conventional statistical methods to explore for physical relationships. Such techniques often make strong assumptions about the nature of the physical systems being studied. For example, it is typically assumed that linear relationships exist between variables of interest and that the physical processes do not change their behaviour with time. The gap between what the statistical methods can deliver and the true nature of the physical systems being studied must be bridged by a good deal of intuition. This is unfortunate because it is very likely that many important physical questions are never posed because the statistical "searchlight" is inadequate.

IOCI is quite unique in that a statistical research capability is woven into the initiative. The objective of our work is to examine the nature of climate processes and to develop statistical methods appropriate for the analysis of data arising from such processes. Based on our work in Phase I it became clear that there is a need to develop methods that can model nonlinear climate phenomena.

We have undertaken to develop a statistical methodology that will also provide uncertainty measures for forecasts. That is, rather than just giving a rainfall estimate we will provide a probability distribution for a rainfall forecast. We have been using monthly rainfall to develop our methods because it is such a difficult quantity to model, but do not limit our scope to rainfall. It is our intention to identify relevant applications of the methods developed in partnership with IOCI's contributing partners.

In this report we document the work to date in the statistical method development. In section 2 we describe the physical rationale for the methods being developed; section 3 describes case studies of monthly rainfall at Rottnest Island and Manjimup that have been used to test the methods as they're developed. A discussion of our results to date is given in section 4 with some conclusions in section 5.

2 Year 3 Development Path

2.1. Probability Distributions for Forecasts

There are two key features of a climate forecast that a decision-maker in climate-impacted sector must balance in reaching their decision. First, the climate pattern forecasted and, second, the uncertainty associated with the forecast. Different decisions are required for different levels of uncertainty. For example, if a forecast is known to be

highly accurate and very clearly forecasts boom conditions for wheat farmers say, then a sensible decision might be to expand wheat production. In a situation of greater uncertainty, with the same forecast climate pattern, to manage risk in a sensible fashion it is advisable to maintain a more balanced crop portfolio.

To provide a complete statement of uncertainty we need to integrate (assimilate) information from a variety of sources. These encompass uncertainties in available climate data, the forecast system used and the availability of expert knowledge. Such expert knowledge would typically include both a meteorological and a decision-maker's perspective. A final integrated statement of uncertainty would be a probability distribution for a climate output- such as next year's wheat production, to continue the above example.

The Bayesian statistical framework is ideal for integrating uncertainty information, so we have chosen to develop our methods within the Bayesian framework. The Bayesian approach begins with a statement of knowledge prior to the collection of data ("prior knowledge"). This information is expressed as a probability distribution, allowing us to specify quantities such as "most likely value," "average value" etc. Our uncertainty can then be expressed via the spread of prior knowledge. The prior knowledge is then combined with the data via a mathematical rule known as Bayes' Theorem to form an integrated expression of uncertainty posterior to data collection ("posterior knowledge"). This is illustrated heuristically in Figure 1. We see that the data have greatly reduced uncertainty, as the posterior is much more concentrated on a particular value than the prior.

In addition to providing a powerful scientific framework for drawing inferences from data there are also a number of technical advantages. In particular, in climate prediction we are most concerned with finding good predictors and the time lags at which these predictors influence climate. In comparison with more conventional statistical methods the Bayesian framework offers much more flexibility in identifying good predictors with fewer technical mathematical concerns.

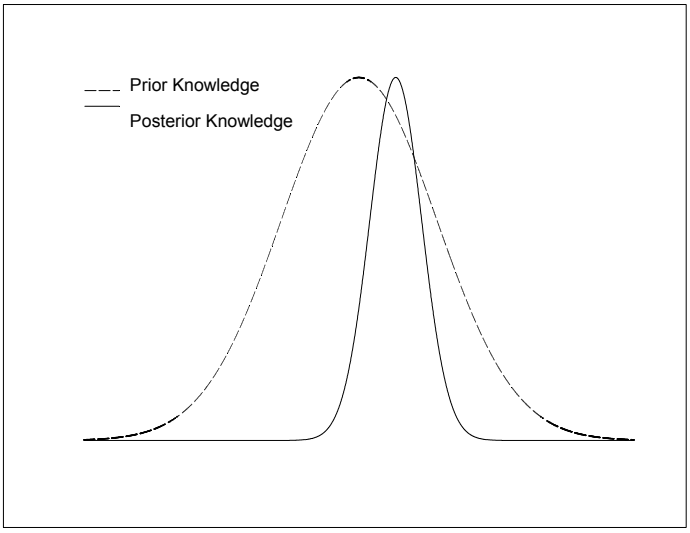

Figure 1 The Bayesian process of integrating data and expert opinion.

2.2. Climate Switching Models

Much of the statistical analysis undertaken in climate research uses so-called linear statistical techniques to identify climate processes. There is however significant evidence that the climate system can behave in strikingly nonlinear ways. For example, *Graham and Barnett* [1987] show that in the tropics enhanced convection occurs at Sea-Surface Temperatures (SSTs) greater than about 29ºC. This implies that different rainfall forecasting systems apply depending on whether SST is above or below the threshold temperature of 29ºC. In general there may well be a delay between the threshold SST being reached and the resulting switch in rainfall regime. In each rainfall regime we assume that different linear climate processes apply. This is depicted in Figure 2 with a linear approximation superimposed for reference.

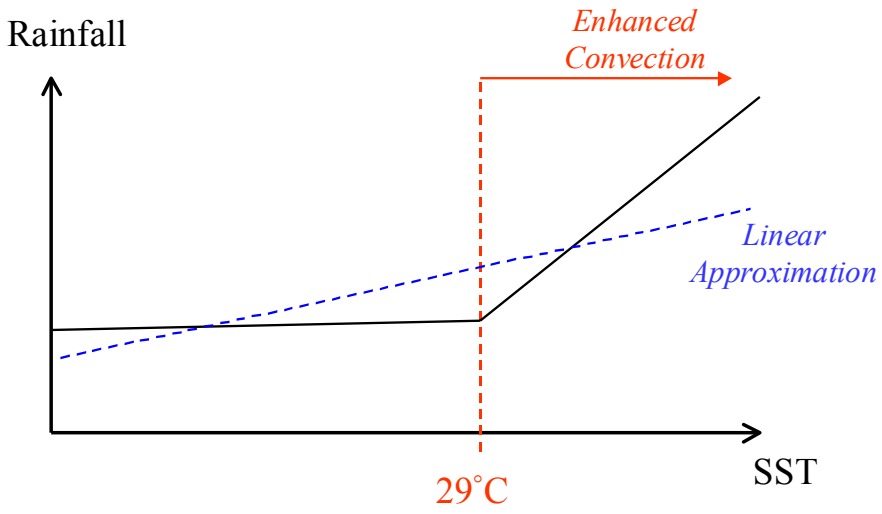

Figure 2 Nonlinear relationship between Rainfall and SST.

A similar result was found by *Hsieh et al.* [1999] in the context of predicting Canadian prairie wheat yield from Pacific Ocean SSTs. If a linear system applies then SST anomalies in low and high yield years should be of similar magnitude, but with opposite signs. Instead they found major asymmetries in SST anomalies and that only low yields are predictable from SST anomalies. If this information is ignored then a potentially misleading forecast system will result; at best it will have little skill.

Palmer [1999] examined climate prediction from a nonlinear perspective, providing theoretical justification for a climate system that resides in equilibrium states for periods of time, subject to occasional rapid switching between states. Palmer found some evidence in available data to support this view. The threshold SST idea described above is consistent with this view, with SST providing the switch between states.

There is therefore a strong argument for developing statistical models incorporating the concept of threshold behaviour. Such models will allow a more physically motivated analysis of available data than has hitherto been the case. The key research activity of the CSIRO Mathematical & Information Sciences (CMIS) group has been to develop a statistical method for identifying good predictors in a Bayesian nonlinear framework. The results of the work to date are described in section 3 where the monthly rainfall case studies are described. The theoretical work underpinning the case studies is described in the manuscript appended to this report.

2.3. Incorporating Ocean-Atmosphere Interactions

Rainfall arises from an interaction between the oceans and the atmosphere. This means that information on the atmosphere or oceans alone my not be sufficient to forecast climate; it may be necessary to have knowledge of both. In particular there may be combinations of conditions in the oceans and atmosphere that provide a leading indicator of enhanced rainfall or drought. It may also be the case that *combinations* of past ocean conditions are more important than individual SST values.

The interaction concept is a very powerful one. An example of a statistically significant interaction effect is shown in Figure 3. In this case we require SST to be high both 3 and 6 months prior to winter to experience high winter rainfall. Whilst SST 6 months ago is a leading indicator of rainfall it must be sustained until 3 months before winter to produce high winter rainfall.

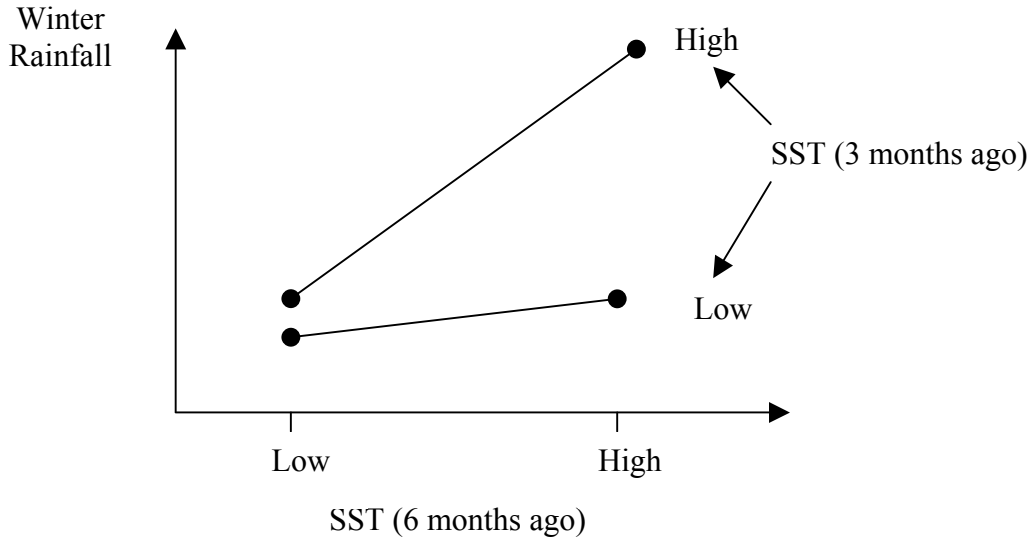

Figure 3 Example of an interaction effect in SST influencing rainfall.

Interaction effects of this type can be very difficult to detect in climate data. An approach to doing this is to include a product term "SST (-6 months) × SST (-3 months)" in the models we fit to the data. An approach to this problem is currently under development for application in the final stage of IOCI.

In the context of IOCI's work, Indian, Pacific and Southern ocean conditions as well as atmospheric conditions are of great relevance. Australia's island continent status is uniquely complex in this regard, so interactions between 3 oceans and the atmosphere are clearly relevant to climate prediction.

2.4. Modelling Approach

It is common practice to model deviations ("anomalies") from long term climate trends in preference to modelling the raw data. The main purpose for this is so that predictors beyond simple climatological averages can be sought. From a nonlinear perspective the calculation of anomalies carries the risk that important information might be lost. For example, it could well be that different climate regimes have different seasonal patterns. It is also the case that the method used to remove long term trends can introduce features of its own.

We have chosen not to model anomalies. Instead we seek to capture the seasonal pattern of, e.g. rainfall, by incorporating rainfall as the leading term in the model. Subsequent

terms in the model, such as SST, will therefore only be included if they explain rainfall variation additional to the rainfall history itself. The modelling approach may be summarised as:

$$\text{Rain}(\text{today}) = \text{Rain}(\text{history}) + \text{SST}(\text{additional to rain history}).$$

This applies to each regime identified, so different terms can be selected in each regime.

2.5. Development of Methodology

Within a nonlinear, climate-switching framework we have identified a need to provide probability distributions for forecasts and to identify the time lags at which important predictors influence climate. These requirements present a challenging statistical problem. An approach developed by CSIRO Mathematical and Information Sciences is described in detail in the manuscript in Appendix C. This manuscript is still in peer review at the time of writing.

For the interested reader, the approach uses an extended Markov chain Monte Carlo (MCMC) approach known as Reversible Jump MCMC (RJMCMC). In MCMC we set-up a carefully defined random walk over the parameter space of a particular model in order to summarise the posterior distribution of the model's parameters. RJMCMC extends the random walk to range over a collection of models. In this way we can conduct model selection and parameter estimation simultaneously.

3 Case Studies

3.1. Description of Data

Monthly rainfall data (mm) for Rottnest Island and Manjimup were selected from Bureau of Meteorology's high quality data set. Manjimup has been selected as representative of an inland site in the Southwest, whilst Rottnest Island has been selected since it is free of any concerns regarding land-use change. For Manjimup we used monthly rainfall data from 1950 to 1993 for model fitting. In the case of Rottnest Island, rainfall data were only available until 1992 at the time of this study. Data from 1950 were used so that credible use of sea surface temperature could be made.

Some pre-processing of the rainfall data has been undertaken. First, rainfall data are typically highly skewed which can cause large rainfall events to have undue influence of the model-fitting procedure. In particular, linear time series models will tend to have an artificially high order in such circumstances. This could bias the comparison of linear with nonlinear models. To avoid this we have first transformed the rainfall data to be more nearly symmetric (using a Box-Cox transformation). As an aid to numerical stability all of the time series used were scaled to have mean 0 and standard deviation 1.

One of the switching variables we have used is the SST gradient at Point 27, 3 (Bureau of Meteorology naming convention) in the mid-Indian Ocean. This measures the north-south difference in SST at this point. This has been found by to have substantial

correlation with Manjimup rainfall [Lynda Chambers, *pers. comm.*]. The Bureau of Meteorology supplied the SST gradient data used in our case study, as were the SOI data.

3.2. Manjimup Monthly Rainfall

3.2.1 Predicting Rainfall From The Rainfall History Only

As a first step we fit a threshold model to the monthly rainfall data alone, so we assume that a threshold exists in the rainfall time series rather than in SST. This is a reasonable starting point for investigating the performance of the threshold approach by seeking evidence of nonlinearity in the rainfall time series.

To fit a threshold model we must determine the number of thresholds that are present. In Figure 4 we present a diagnostic[1] for choosing the appropriate number of thresholds. On the vertical axis we plot a measure of the support[2] in the data for a threshold parameter taking a value on the horizontal axis. We expect to see a cloud of points with a noisy spike at a value where there is support for a threshold. In this case there is a distinct spike at a value of about –1.1. This suggests that there is evidence for a low rainfall regime and a normal to high rainfall regime. In the analysis to follow we assume the presence of 1 threshold.

[1] In practice a number of these plots are produced at different scales. The final figure is focused on the region in which the threshold appears to be located.

[2] The likelihood of the time series plotted as a function of the threshold parameter.

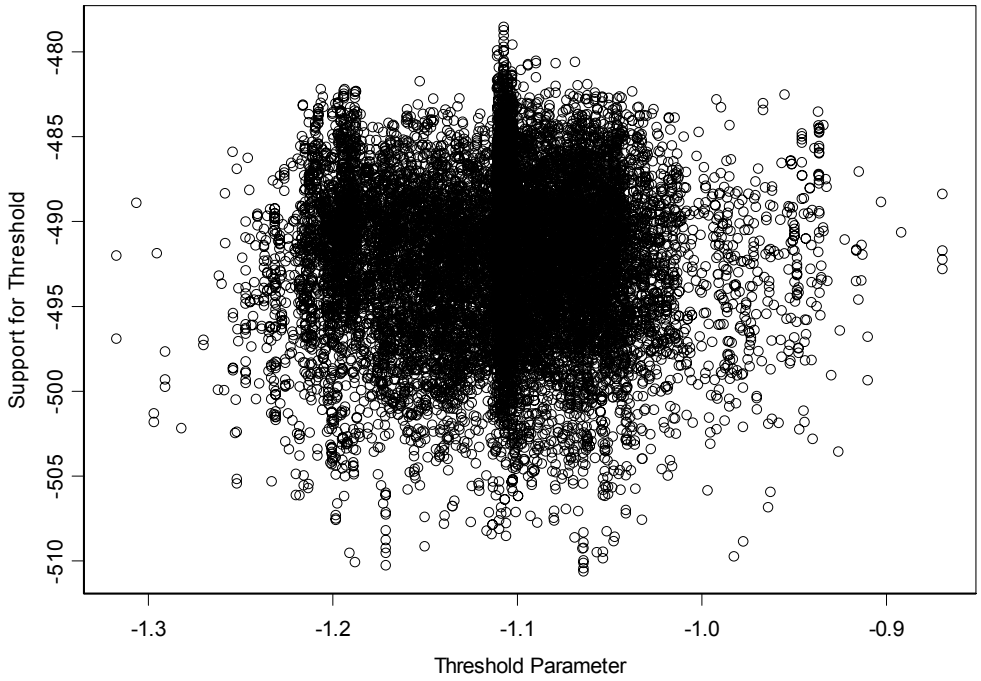

Figure 4 Diagnostic plot for choosing the number of thresholds and their approximate locations.

We can calculate some simple summaries of the resulting model fit. To get some insight into how well the procedure is performing we can use the resulting parameter estimates to calculate 1-month-ahead predictions for each observed monthly rainfall amount,[3] and the result is shown in Figure 5. We see that the correlation between the predicted and observed values is 0.782. This is a reasonable performance given that we have only used the rainfall history. In general the approach under-predicts the largest observed events. This is not unexpected, and it is likely that a predictor such as sea surface temperature will be required to predict such events.

[3] We must exclude a number of values at the beginning of the time series because the model uses past values of rainfall to forecast the future. This means that we cannot predict the first few values of the time series.

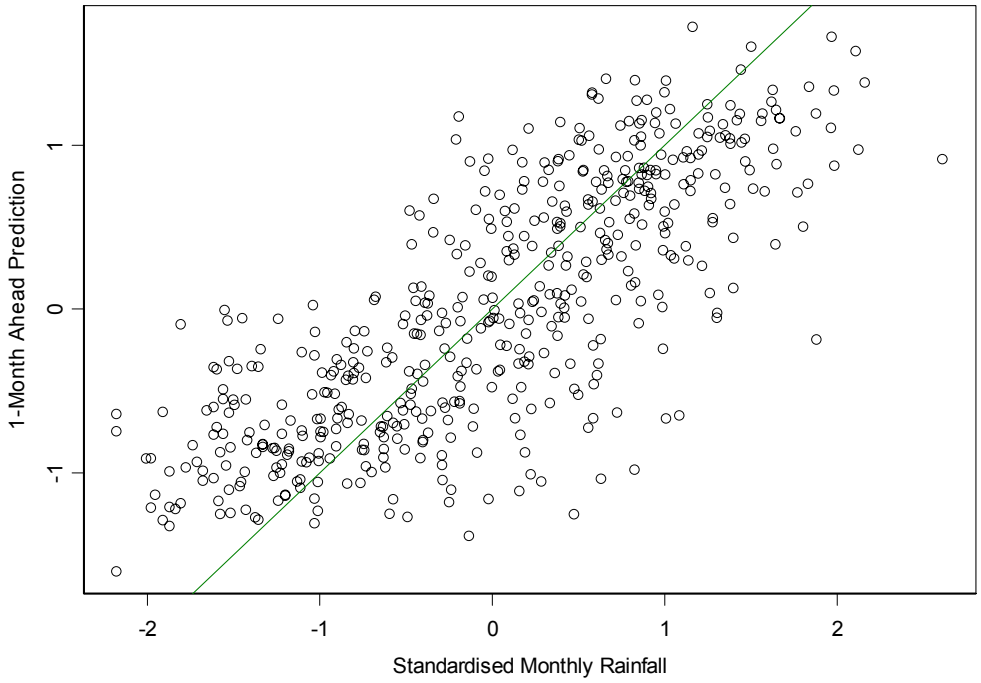

Figure 5 1-month-ahead predictions of monthly rainfall at Manjimup. The correlation between predicted and observed rainfall is 0.782.

An important feature of the method we are developing is that it identifies the important time lags essentially automatically. The parameter estimates are shown in Table 1. At this stage the method retains all lags up to the longest, so we present the statistically significant terms only; the estimated model orders correspond to the model having the highest probability. The credibility intervals quoted for individual parameters incorporate model uncertainty[4] by including competing models in the calculation, not just the model having highest probability. Notice first that the high and low rainfall regimes are quite different, having time lags of 6 and 16 months respectively. The high rainfall regime also has a relatively complicated structure. This is an important point: a linear fit may be able to produce a similar global fit, but is likely to perform poorly within a particular rainfall regime. The variance parameter is more clearly defined in regime 2 because there are more observations than in regime 1, which is quite typical of threshold models.

[4] Since we don't know the correct predictors to use we need to account for this important source of uncertainty.

	Parameter	Estimate	95% Credibility Interval
	Threshold	-1.11	-1.21, -1.01
Regime 1: 'Low' Rainfall	Order	6	4, 7
	Intercept	-0.261	-1.13, 0.639
	Lag-4	-0.332	-0.649, -0.0332
	Lag-6	-0.186	-0.510, 0.000
	Variance	0.54228	0.38445, 0.74765
Regime 2: 'Normal/High' Rainfall	Order	16	14, 17
	Intercept	-0.0188	-0.0843, 0.051
	Lag-1	0.232	0.126, 0.348
	Lag-4	-0.139	-0.231, -0.0457
	Lag-5	-0.0924	-0.180, -0.00445
	Lag-7	-0.105	-0.198, -0.00515
	Lag-11	0.179	0.0797, 0.273
	Lag-13	0.242	0.143, 0.340
	Lag-14	-0.0902	-0.190, 0.000
	Lag-16	-0.0756	-0.192, 0.000
	Variance	0.38454	0.33614, 0.44096

Table 1 Model-averaged parameter estimates with 95% credibility intervals. Only statistically significant parameters are shown, correct to 3sf except for variance parameters which are shown correct to 5sf.

For comparison with the threshold model we have also fitted a conventional linear time series model. The 1-month-ahead predictions are shown in Figure 6, with a correlation between predicted and observed values of 0.785 with an order 20 model. Notice that this does not include an intercept term, which we always include in the nonlinear model because such parameters can help to model highly volatile time series. Overall the number of parameters in this case is essentially the same, with the same global performance. Interestingly the order of the linear model is higher than for either of the rainfall regimes identified by the threshold model. This is in keeping with the concepts illustrated in Figure 2: in order to achieve the same overall quality of fit a higher order model is required. In reality there seems to be evidence for different rainfall regimes having different physical characteristics.

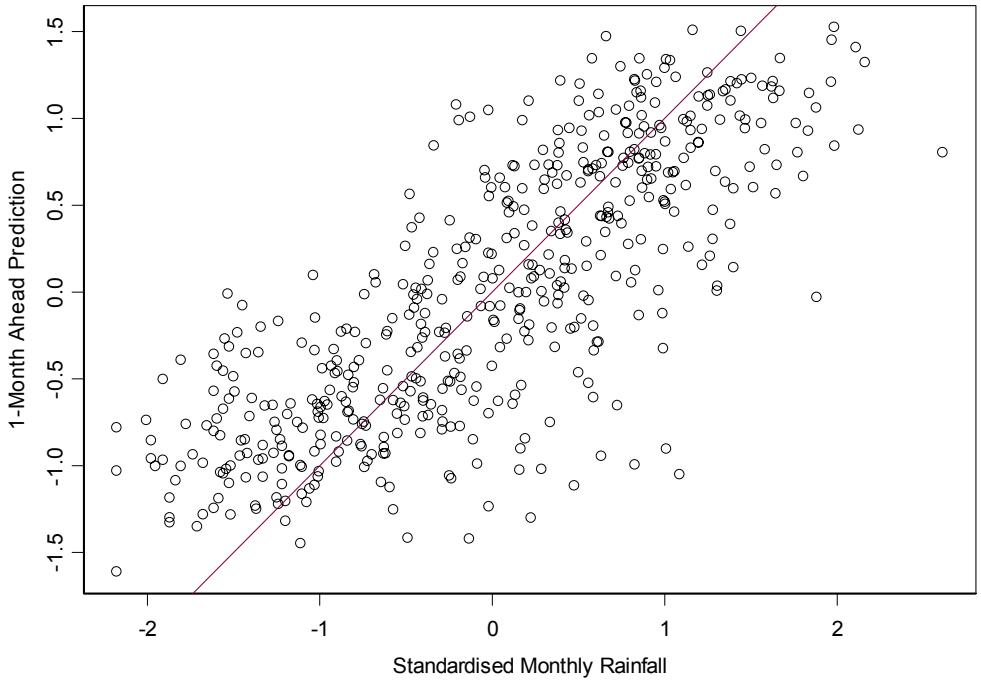

Figure 6 Results from fitting a conventional linear autoregressive model (order 20); the correlation between 1-month-ahead predictions and standardised monthly rainfall is 0.785.

3.2.2 Predicting Rainfall Using The Southern Oscillation Index (SOI) As A Switch

Nonlinear modelling of the rainfall time series in isolation has provided evidence for climate switching. However, it seems unlikely that rainfall itself is the cause of the switching behaviour. One possibility is the El Niño-Southern Oscillation (ENSO), as measured by the Southern Oscillation Index (SOI). However, it is likely that the impact of SOI on southwest WA rainfall will be delayed. We have used a delay of 1 month in the first instance to examine this issue.

A stable threshold seemed to be present at around +1.5, so we examined the threshold diagnostic plot in this vicinity (Figure 7). There is clear support for a threshold at approximately +1.7, with a rapid drop in support below +1.6 and above +1.8.

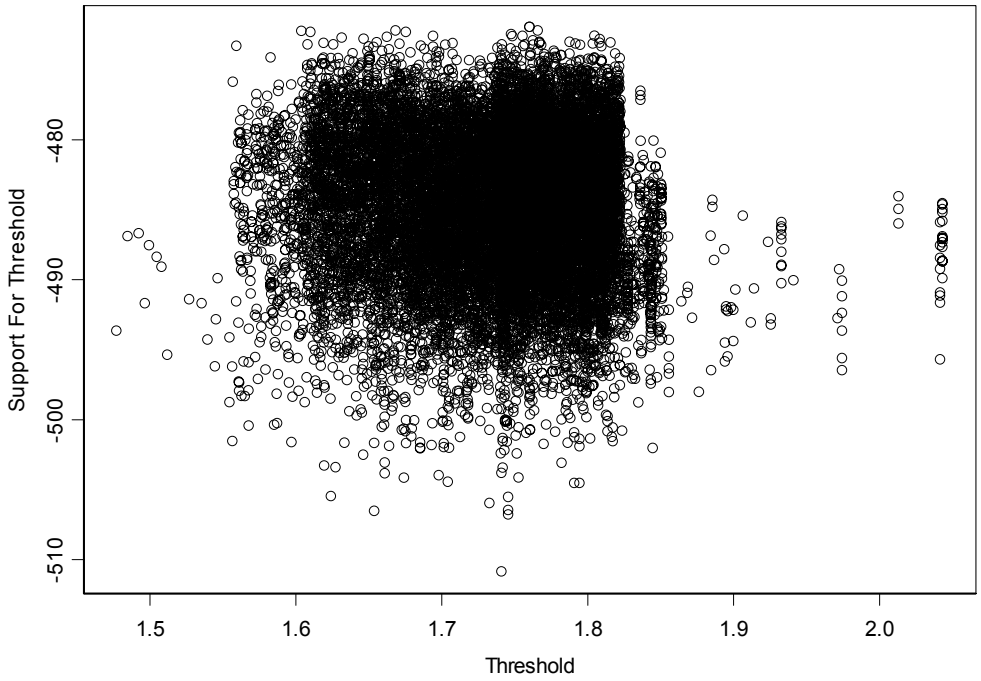

Figure 7 Diagnostic plot for choosing the number of thresholds and their approximate locations for Manjimup rainfall using SOI as the switching variable.

The 1-month ahead predictions obtained are shown in Figure 8; we see that there is a correlation of 0.788 between the observed and predicted values. The corresponding parameter values are shown in Table 2. The structure of the fitted model is remarkably similar to the rainfall-only model fitted above, particularly the 'Normal/High' rainfall regime. It is therefore very tempting to suggest that SOI plays a physical role in rainfall at Manjimup.

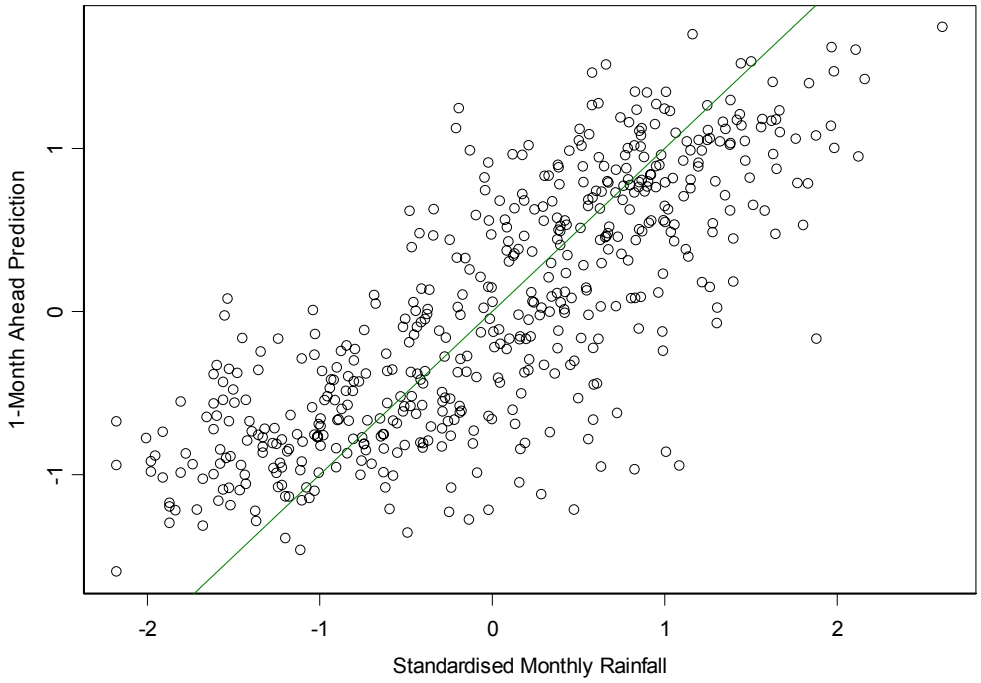

Figure 8 1-month-ahead predictions of monthly rainfall at Manjimup, using SOI as the switching variable. The correlation between predicted and observed rainfall is 0.788.

	Parameter	Estimate	95% Credibility Interval
	Threshold	1.74	1.61, 1.82
Regime 1: 'Low' SOI	Order	16	14, 17
	Intercept	-0.00965	-0.0639, 0.0454
	Lag-1	0.203	0.114, 0.295
	Lag-4	-0.163	-0.254, -0.0731
	Lag-7	-0.0918	-0.183, -0.00469
	Lag-11	0.150	0.0566, 0.240
	Lag-13	0.234	0.146, 0.326
	Lag-14	-0.0943	-0.181, -0.000874
	Lag-16	-0.114	-0.210, 0.000
	Variance	0.39108	0.34085, 0.44835
Regime 2: 'High' SOI	Order	5	1, 7
	Intercept	0.158	-0.360, 0.587
	Lag-4	0.505	0.000, 1.24
	Lag-5	-0.364	-1.00, 0.000
	Variance	0.65143	0.25265, 1.5537

Table 2 Model-averaged parameter estimates with 95% credibility intervals for Manjimup rainfall using SOI as the switching variable. Only statistically significant parameters are shown, correct to 3sf except for variance parameters which are shown correct to 5sf.

In this case it seems that low rainfall in Manjimup is associated with large positive values of SOI, which is an indicator of El Niño events (Figure 9), although there is a clear exception to this rule. The influence of ENSO on Northern and Eastern Australia is well known, but is a less recognised influence on the climate of Western Australia. On the evidence of this analysis it seems that quite extreme El Niño events can influence rainfall in Manjimup- the threshold for SOI being at +1.74 standard deviations to cause a low rainfall regime to be initiated. This does mean however that relatively few observations are available to characterise this regime.

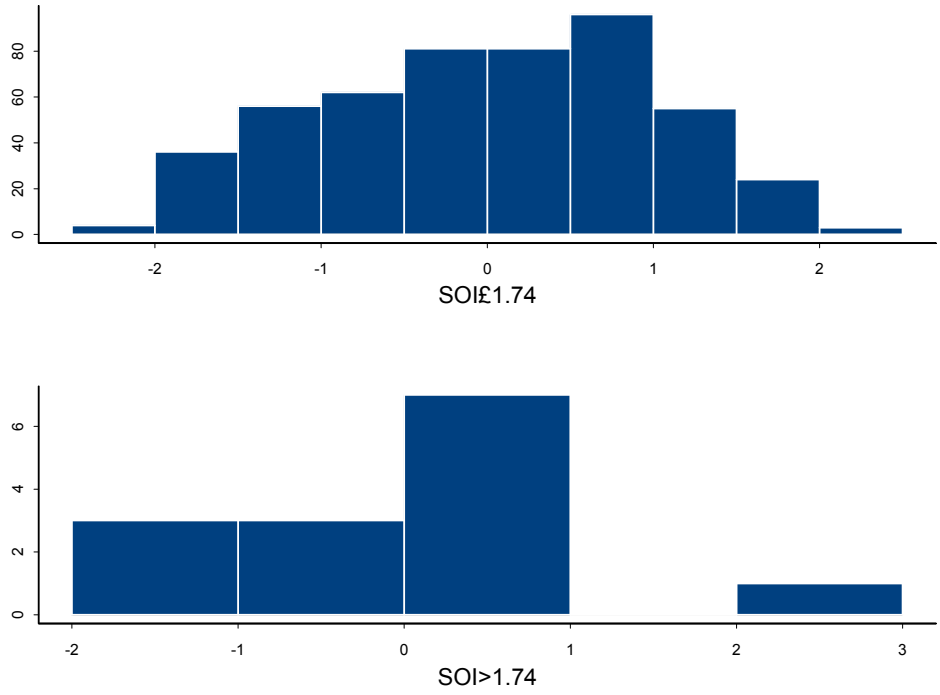

Figure 9 Distribution of Manjimup rainfall for the two SOI regimes.

The dates and rainfall amounts corresponding to the 'High SOI' regime are shown in Table 3, with runs of consecutive months highlighted. The exceptionally high rainfall event in the high SOI regime corresponds to August 1955. There is a run of high SOI values in April-May 1971 and August-October 1975. In general the events are scattered through the calendar year with all seasons represented; the months not present are March, June, July and November. It is interesting to note that the core winter rainfall months of June and July are not present, although there are of course relatively few observations in the 'High SOI' regime.

In the analysis so far a delay of 1 month in the influence of the switching variable has been assumed. With a large scale effect such as ENSO it is worth looking for a longer delay. Analysis of a delay of 3 months gave very similar results to those presented above, although the SOI threshold was found to be somewhat lower at +1.57. The threshold framework is not ideally suited to searching for delayed threshold effects. However, the extension noted in section 2.3 for incorporating interactions is much more suited to such a search. This issue will be explored further.

In experiments using SOI as a predictor in the model it was found that parameter estimates were less stable than when SOI was used only as a switching variable. Whilst there was some evidence that SOI helps to explain the historical data, it does not seem to provide any additional predictive capability, except as a switching variable.

Year	Month	Standardised Rainfall
1955	August	2.61340
1970	December	-1.90830
1971	**April**	**-0.50198**
1971	**May**	**0.85507**
1973	December	-1.57610
1974	February	-0.57156
1974	April	0.34738
1975	**August**	**0.39667**
1975	**September**	**0.54747**
1975	**October**	**-0.28775**
1976	January	0.22630
1988	October	0.15450
1988	December	-1.26000
1989	May	0.38692

Table 3 Dates and rainfall amounts corresponding to the 'High SOI' regime.

3.2.3 Predicting Rainfall Using SST Gradient As A Switch

The threshold diagnostic plot is shown in Figure 10. There is a clear clustering around –1.5, although there seems to be some uncertainty in the location of this threshold given the smear of points towards and beyond –2.0. This suggests that the threshold is not completely stable. Indeed there were signs of some instability during the course of the subsequent analysis, which requires further investigation.

1-month ahead predictions are shown in Figure 11 below. The correlation between observed and predicted rainfall is 0.789, which is comparable to the other models fitted to Manjimup rainfall. Note that the low-SST gradient regime is of zero order; that is, rainfall in this regime is just a random scatter with no correlation through time. The predicted rainfall therefore does not vary in time and is the estimated intercept in regime 1 (-0.809). The full set of parameter estimates used to produce Figure 11 are shown in Table 4.

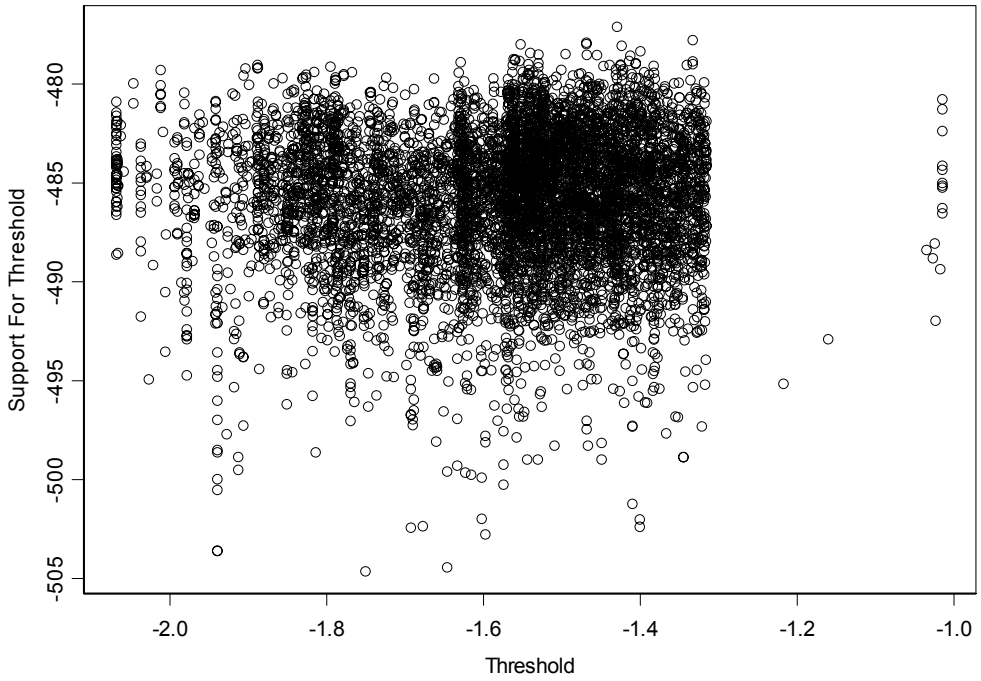

Figure 10 Diagnostic plot for choosing the number of thresholds and their approximate locations for Manjimup rainfall, using SST gradient as the threshold.

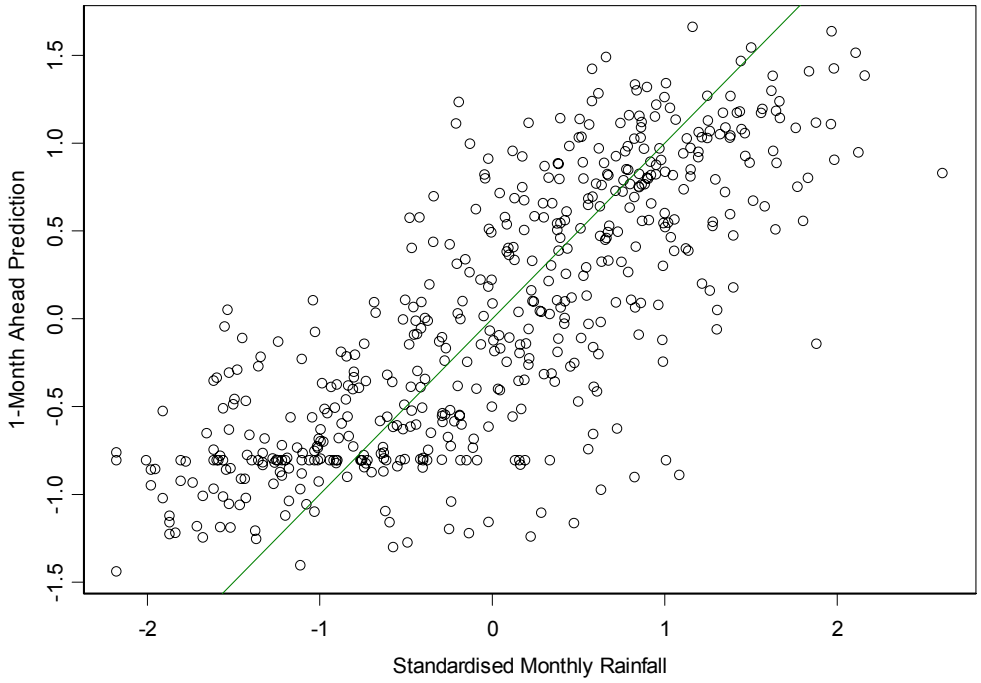

Figure 11 1-month-ahead predictions of monthly rainfall at Manjimup using SST gradient as the switching variable. The correlation between predicted and observed rainfall is 0.789.

	Parameter	Estimate	95% Credibility Interval
	Threshold	-1.59	-2.02, -1.15
Regime 1: Low SST gradient	Order	0	0, 1
	Intercept	-0.809	-1.09, -0.286
	Variance	0.57279	0.35474, 1.0464
Regime 2: High SST gradient	Order	16	13, 18
	Intercept	0.00941	-0.0522, 0.0708
	Lag-1	0.200	0.105, 0.295
	Lag-4	-0.153	-0.241, -0.0578
	Lag-5	-0.0998	-0.192, -0.00922
	Lag-7	-0.103	-0.190, -0.013
	Lag-13	0.226	0.135, 0.313
	Lag-16	-0.0916	-0.193, 0.000
	Variance	0.38890	0.33503, 0.44810

Table 4 Model-averaged parameter estimates with 95% credibility intervals. Only statistically significant parameters are shown, correct to 3sf except for variance parameters which are shown correct to 5sf.

The rainfall distributions in each of the SST gradient regimes are shown in Figure 12. The low SST gradient regime is clearly associated with low rainfall. Considering the parameter estimates in Table 4 once again, there are clear similarities with the previous fitted models in the structure of the normal to high rainfall regime in particular. This would suggest that there exists a reasonable basis for considering SST gradient as a switching mechanism.

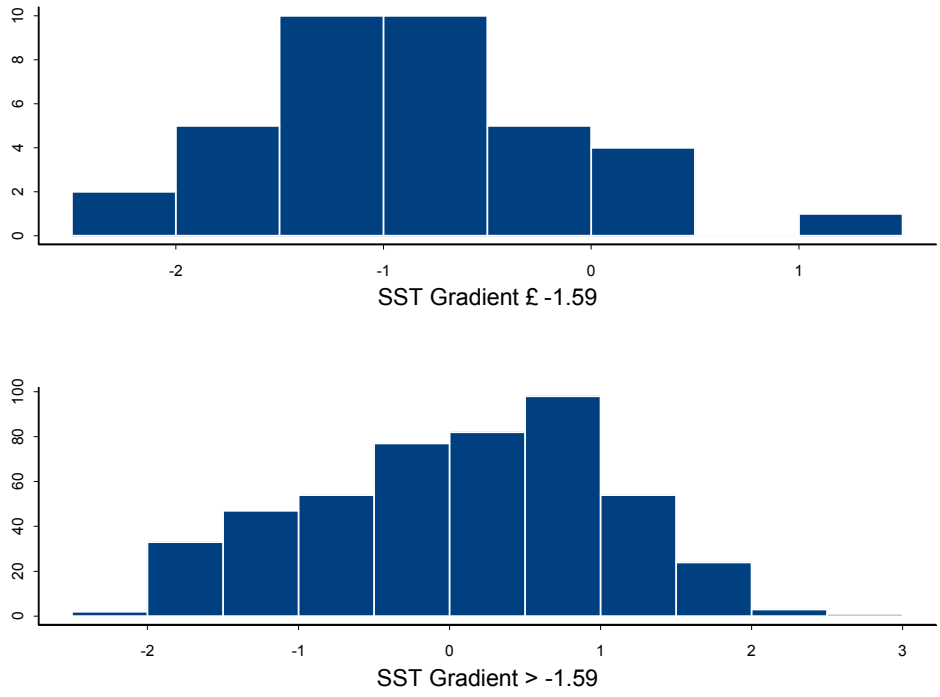

Figure 12 Monthly rainfall distributions at Manjimup for each SST gradient regime. (Note: different plotting scales for each regime)

The distribution of the two regimes is shown in **Table 5**. It is clear from this that the low SST gradient regime is a summer rainfall feature and does not provide an indicator of winter rainfall. A more detailed search of the high rainfall regime may detect a further threshold.

Month	Number of Rainfall Months In Regime:	
	SST Gradient ≤ -1.59	SST Gradient > -1.59
January	2	40
February	16	26
March	18	24
April	1	41
May	0	43
June	0	43
July	0	43
August	0	43
September	0	43
October	0	43
November	0	43
December	0	43
	37	475

Table 5 Number and distribution of months across SST gradient regimes for Manjimup monthly rainfall.

3.3. Rottnest Island Monthly Rainfall

3.3.1 Predicting Rainfall From The Rainfall History Only

The threshold diagnostic plot is shown in Figure 13. Once again there appears to be evidence for a threshold in the vicinity of –1.1, although on this occasion there appears to be a discontinuity present. This suggests that there is evidence for complicated behaviour in this region.

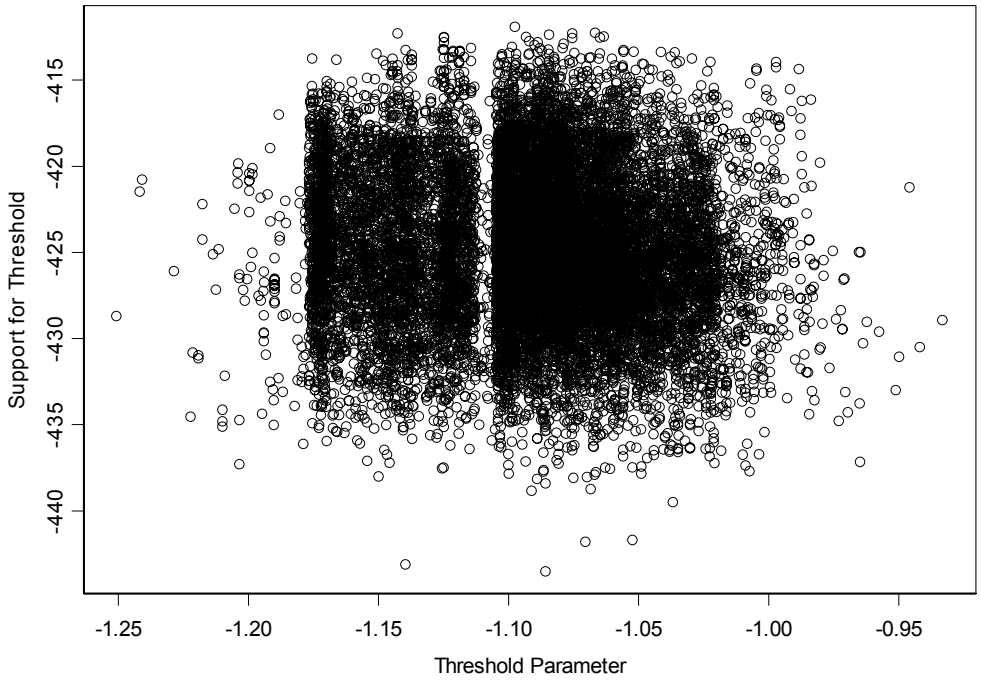

Figure 13 Diagnostic plot for choosing the number of thresholds and their approximate locations for Rottnest Island rainfall.

The 1-month ahead predictions are plotted against their observed values in Figure 14; the correlation of 0.821 is somewhat higher than for Manjimup. The vertically aligned points in the bottom left of the plot correspond to dry months in the observed record. The time series model at present does not explicitly account for dry periods. We see again that the largest observed events are consistently under-predicted.

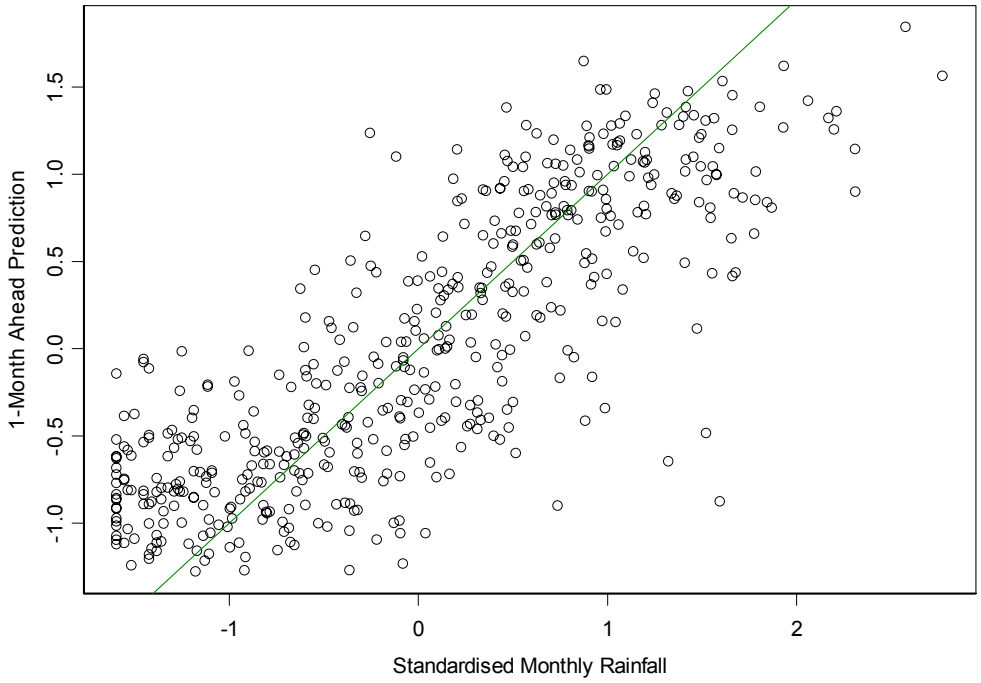

Figure 14 1-month-ahead predictions of monthly rainfall at Rottnest Island. The correlation between predicted and observed rainfall is 0.821.

The parameter estimates used to derive the predictions are shown in Table 6. The 1-month-ahead predictions for the corresponding linear model are shown in Figure 15, which is an order 19 model. The threshold model suggests that there are two rainfall regimes distinguished by a threshold at about –1.1. There is a 'Low' regime of order 4, which is essentially a contrast between rainfall 2 and 4 months previously. The 'Normal/High' regime has a much longer time dependency of 13 months, with more structure than for the 'Low' regime.

	Parameter	Estimate	95% Credibility Interval
	Threshold	-1.09	-1.17, -1.02
Regime 1: 'Low' Rainfall	Order	4	4, 6
	Intercept	-0.427	-1.19, 0.335
	Lag-2	0.321	0.0776, 0.571
	Lag-4	-0.433	-0.629, -0.208
	Variance	0.55373	0.41108, 0.74165
Regime 2: 'Normal/High' Rainfall	Order	13	13, 18
	Intercept	-0.00376	-0.0648, 0.0568
	Lag-1	0.144	0.0465, 0.250
	Lag-7	-0.101	-0.188, -0.0140
	Lag-11	0.262	0.172, 0.355
	Lag-12	0.126	0.0175, 0.230
	Lag-13	0.277	0.189, 0.366
	Variance	0.28853	0.24976, 0.33405

Table 6 Model-averaged parameter estimates with 95% credibility intervals. Only statistically significant parameters are shown, correct to 3sf except for variance parameters which are shown correct to 5sf.

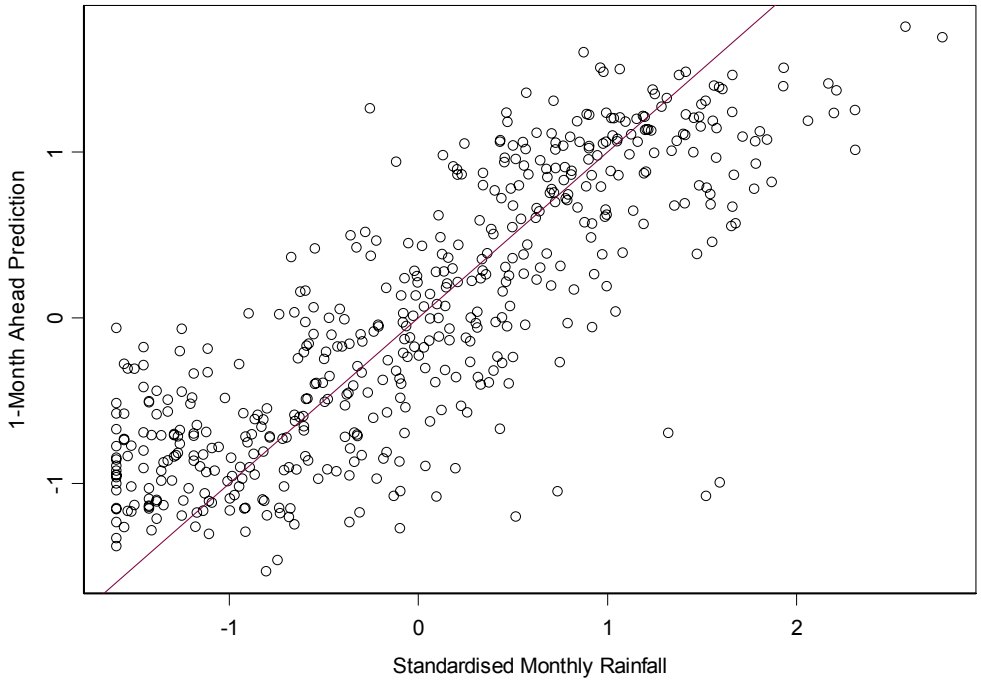

Figure 15 Results from fitting a conventional linear autoregressive model (order 19); the correlation between 1-month-ahead predictions and standardised monthly rainfall is 0.825.

3.3.2 Predicting Rainfall Using The Southern Oscillation Index (SOI) As A Switch

No evidence was found that SOI provides any additional contribution to the rainfall history. When SOI was included as a predictor, using rainfall as the switching variable, the estimates obtained were unstable. When SOI was used as the switching variable, but not as a predictor, no stable threshold was found.

This is quite a stark comparison with Manjimup where SOI did seem to influence monthly rainfall. The case for an SOI influence on Rottnest Island monthly rainfall seems to be weak on the basis of this analysis.

3.3.3 Predicting Rainfall Using SST Gradient As A Switch

We first investigate using SST gradient as the switching variable, but without including SST gradient as a predictor in the model. The threshold diagnostic plot is shown in Figure 16, and there is clear evidence for a threshold at approximately –0.85. The 1-month ahead predictions for rainfall are shown in Figure 17, and we see that the correlation between predicted and observed rainfall is 0.829. The parameter estimates used to generate these predictions are shown in Table 1. There are some strong similarities in the structure of the SST gradient regimes here with the rainfall regimes found in section 3.3.1. They are not as closely matched as the SOI results for Manjimup however.

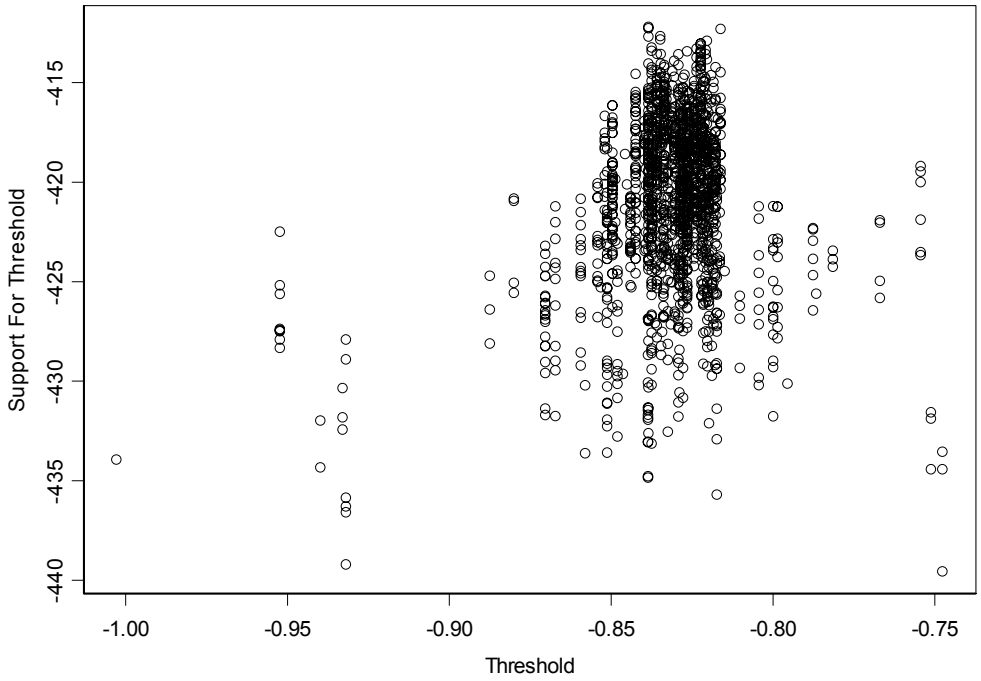

Figure 16 Diagnostic plot for choosing the number of thresholds and their approximate locations for Rottnest Island rainfall, using SST gradient as the threshold.

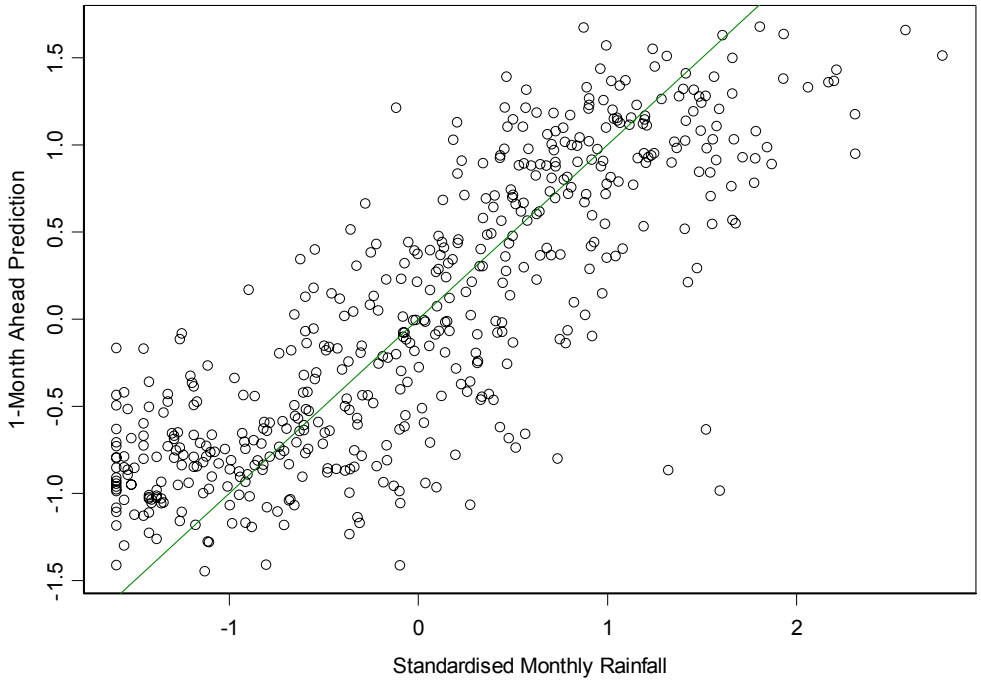

Figure 17 1-month-ahead predictions of monthly rainfall at Rottnest Island using SST gradient as the switching variable. The correlation between predicted and observed rainfall is 0.829.

	Parameter	Estimate	95% Credibility Interval
	Threshold	-0.831	-0.851, -0.805
Regime 1: Low SST gradient	Order	5	5, 5
	Intercept	-0.510	-0.804, -0.248
	Lag-2	0.295	0.0878, 0.478
	Lag-4	-0.378	-0.664, -0.141
	Lag-5	-0.313	-0.572, -0.0569
	Variance	0.51144	0.38359, 0.67864
Regime 2: High SST gradient	Order	13	13, 13
	Intercept	0.0555	-0.00467, 0.113
	Lag-1	0.215	0.119, 0.307
	Lag-4	-0.0874	-0.167, -0.00691
	Lag-7	-0.0950	-0.181, -0.0112
	Lag-11	0.265	0.172, 0.359
	Lag-13	0.242	0.150, 0.329
	Variance	0.27942	0.23820, 0.32471

Table 7 Model-averaged parameter estimates with 95% credibility intervals. Only statistically significant parameters are shown, correct to 3sf except for variance parameters which are shown correct to 5sf.

It is of some interest to compare the rainfall patterns defined by the two SST gradient regimes identified, and these are shown in Figure 18. We see that the low SST gradient regime is associated predominantly with below average rainfall. The rainfall months associated with the regimes are shown in Table 8, and it seems clear that the high SST gradient is associated with winter rainfall in particular. There is therefore some potential here to develop a predictive model for monthly rainfall.

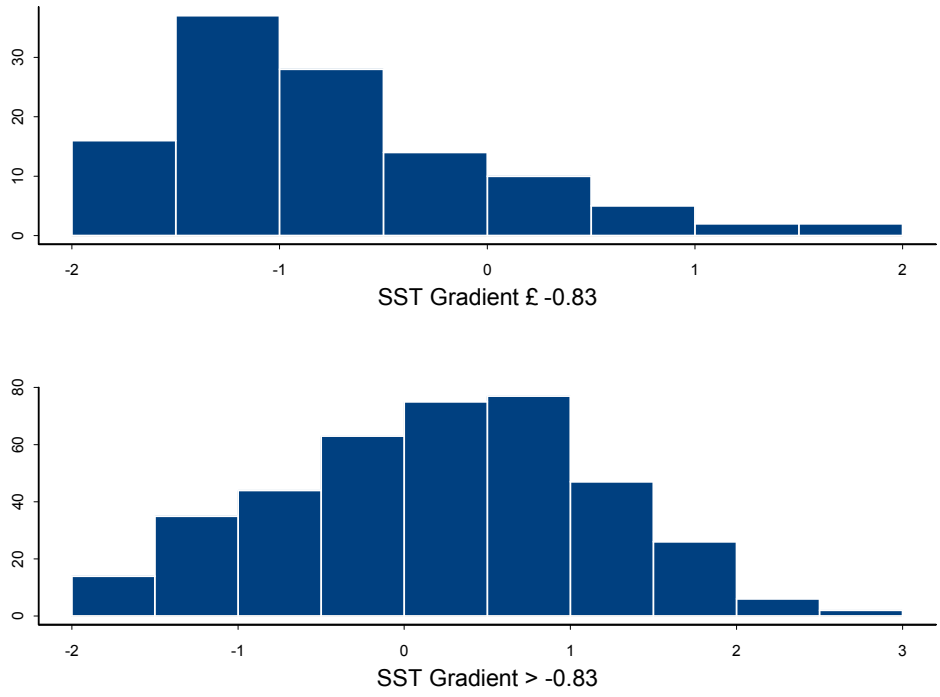

Figure 18 Monthly rainfall distributions at Rottnest Island for each SST gradient regime. (Note: Different plotting scales for each regime)

Month	Number of Rainfall Months In Regime:	
	SST Gradient ≤ -0.83	SST Gradient > -0.83
January	21	20
February	37	5
March	38	4
April	14	28
May	1	41
June	1	41
July	1	41
August	1	41
September	0	42
October	0	42
November	0	42
December	0	42
	114	389

Table 8 Number and distribution of months across SST gradient regimes for Rottnest Island monthly rainfall.

4 Discussion

4.1. Physical Interpretations

The case studies presented in this report were primarily used to develop and test the nonlinear statistical methodology. For the purposes of discussion we set this aside for the moment. We note that the new method has produced sensible results, which is the outcome we were seeking at this stage of its development.

Some interesting differences have emerged between the two study sites of Rottnest Island and Manjimup. In the case of monthly rainfall at Rottnest Island we have found no significant link to the Southern Oscillation. There does however appear to be a link in the case of Manjimup. This is supported by a comparison of the results where SOI and rainfall are used as the switching variable. The regimes found using rainfall as the switching variable were almost identical to those found when using SOI as the switching variable. This suggests that SOI can be used to explain the switching behaviour of the monthly rainfall series at Manjimup.

Whilst a rainfall teleconnection with the Southern Oscillation is not widely recognised, there is some existing evidence. For example, *Crowder* [1995] pp240-41 notes severe rainfall deficits in April 1982 through February 1983 in the far Southwest. This was a very severe El Niño event. This period was not detected in our Manjimup case study, but this may be because the high-SOI regime was not particularly well defined.

It was found that SOI did not work well as a predictor in the statistical modelling, only as a switching variable. Thus SOI can in principle be used to forecast switches in rainfall regime, but not as a simple predictor of future rainfall values.

There is some evidence that SST gradient in the Indian Ocean influences rainfall at both Rottnest Island and Manjimup. This is physically reasonable since SST gradient is measuring a capacity for winds to be generated in the mid-Indian Ocean. It is not difficult to see how a change in circulation patterns beyond a critical value could cause a switch in rainfall regime.

The nature of circulation patterns is that they act on very large scales. It may therefore be more realistic to develop a switching variable that is a *combination* of broad scale circulation patterns. It would be of particular relevance to incorporate data from the Southern (if feasible) and Pacific Oceans if this were to be done.

Key Points:

- Different physical mechanisms appear to influence rainfall at Rottnest Island and Manjimup.
- There is some evidence that the Southern Oscillation plays a role in causing switches between rainfall regimes.
- Sea surface temperature gradient in the mid-Indian Ocean seems to influence switching of rainfall regime at Rottnest Island. It seems to be a leading indicator of winter rainfall, and there seems to be the basis for a winter rainfall prediction scheme. It also seems to play a role at Manjimup, but is less well defined than for Rottnest Island.
- There is a case for developing switching variables that are combinations of variables representing circulation patterns in the Indian, Southern (if feasible) and Pacific Oceans. The extension to the Bayesian threshold method discussed below will be of some use.

4.2. Statistical Issues

The statistical methodology has been found to work well on a practical level. It is reasonably straightforward to simultaneously identify important lags and estimate the corresponding parameters. The identification of the number of thresholds and the delay is somewhat ad hoc however. In standard practice penalised likelihood methods would be used, although not particularly satisfactorily. However, a more promising approach is to use spline methods to estimate the generating mechanism of the time series. In this richer setting the thresholds become knot points, and the choice of knot points is a somewhat easier problem to solve. The delay is expressed through the lags associated with the knot points, and is essentially automatic. The methodology developed so far seems to be reasonably straightforward to adapt to this more general approach.

During the final phase of IOCI we will produce probability distributions for forecasts, which will incorporate a complete statement of uncertainty. These probability distributions can also be used to validate the nonlinear modelling.

An issue that has yet to be resolved in an entirely satisfactory way is the choice of prior distributions for the model orders in each regime. The results reported here use Poisson distributions, but some of our results suggest that better mixing could be obtained by placing a hyper-prior on the Poisson mean- a gamma distribution would result in a negative binomial prior overall. We will investigate this point in the on-going work.

Key Points:

- The statistical methodology we have developed is working well.
- Some physically interesting results have already been obtained.
- Probability forecasts will be produced in the next phase.
- The choice of prior distributions for model orders has not been fully resolved. An approach using hyper-priors on model order will be considered.
- A collaborative effort with the new nonlinear tool is required to extract maximum value from it.

5 Conclusions

The primary task for CSIRO Mathematical & Information Sciences (CMIS) during this phase of IOCI has been to develop the statistical methodology to the point where it can usefully be applied. We have reached this point, although there are still some potentially useful extensions that can be pursued, particularly in relation to modelling climate interactions. However, the focus of CMIS' work for the remainder of IOCI will be on the detailed development and analysis of case studies identified by the contributing partners.

The case studies described here have been presented in the spirit of testing whether sensible results are obtained using the methodology developed, rather than seriously seeking rainfall predictors. The task of seeking rainfall predictors is a collaborative exercise, which now has an additional nonlinear tool to make use of. In our case studies we have found some evidence that predictors such as the Southern Oscillation (SOI) and sea surface temperature (SST) gradient have some potential to provide a climate switching mechanism in the threshold model framework described by Figure 2. In the case of SOI we found a stark difference in that there appeared to be an influence on Manjimup rainfall but not on Rottnest Island rainfall. For Manjimup it seems that the Southern Oscillation has some impact in extreme cases, but by no means supplies a complete picture.

There is some evidence that SST gradient in the mid-Indian Ocean causes switching of rainfall regime at Rottnest Island in particular, and clearly seems to be linked to winter rainfall. There is a basis here for exploring predictive models for winter rainfall. There does also seem to be some influence on Manjimup rainfall. It could well be that an underlying climate switch should be formed from a *combination* of processes, rather than Indian and Pacific Ocean influences on their own. The methodology developed by CMIS could be adapted to aid a search for such combinations.

Key Points:

- We have developed a physically motivated statistical model ('Bayesian switching model') for modelling nonlinear climate processes.
    - Changes between climate regimes are triggered by a switching variable, and alternative switching variables can be compared.
- The Bayesian switching model can identify good predictors and the lags at which they influence climate variables, such as rainfall.
- We have reached the point where a nonlinear time series approach can be applied to practical problems.
- There is some evidence that SOI and mid-Indian Ocean SST gradients play a role in switching between rainfall regimes. This is cited at this stage as evidence that the new nonlinear approach is producing sensible results, rather than new insights *per se*.
- Interactions between climate processes are likely to influence rainfall in Southwest WA. Some reasonably straightforward extensions to the Bayesian switching model will facilitate the search for subtler climate teleconnections arising from such interactions.
- The focus of future work will be the development of case studies with IOCI's contributing partners.

References

Crowder, B., *The Wonders of the Weather,* Australian Government Publishing Service, Canberra, 1995.

Graham, N. E. and Barnett, T. P., Sea surface temperature, surface wind divergence, and convection over tropical oceans, *Science,* **238,** 657-659, 1987.

Hsieh, W. W., Tang, B. and Garnett, E. R., Teleconnections between Pacific sea surface temperatures and Canadian prairie wheat yield, *Agric. For. Meteor.,* **96,** 209-217, 1999.

Palmer, T. N., A nonlinear dynamical perspective on climate prediction, *J. Clim.,* **12,** 575-591, 1999.

Appendix A- Glossary

Cross-referenced terms and acronyms are shown in italics.

Anomaly	It is usual to express climate data as deviations from the long term average, and this deviation is known as an anomaly.
Bayesian	A statistical framework that expresses uncertainty using probability distributions. Bayesian statisticians explicitly combine data with subjective knowledge to learn about physical processes. This is accomplished using *Bayes' theorem*.
Bayes' Theorem	As implemented in scientific practice, this theorem essentially states that uncertainty conditional on available data and expert knowledge is proportional to the product of the uncertainty in the data and the uncertainty in expert knowledge.
Delay	In physical systems there may well be a time delay between cause and effect, and this is captured by a so-called delay parameter.
Interaction	In physical systems the effect of one variable may depend on the value of another. For example, a low pressure system will not bring rainfall when sea surface temperature is low. In this case sea surface temperature is said to interact with air pressure.

Knot Point	When using *splines* we divide up the domain of a function so that it can be approximated by a set of simple functions. The points at which the domain is divided are known as knot points.
Linear	A general term to describe relationships that can be represented as straight lines between two variables, or hyperplanes for many variables.
Markov chain Monte Carlo	A computationally intensive technique that uses simulation techniques to implement *Bayesian* statistical methods. This term is universally known by the acronym *MCMC*.
Nonlinear	A general term to describe relationships that cannot be described as straight lines or hyperplanes, as is the case for *linear* relationships.
Posterior Distribution	A probability distribution that integrates expert knowledge and available data, and is typically calculated using *Bayes' theorem.*
Reversible Jump MCMC	A methodology for choosing optimal statistical models in a *Bayesian* statistical framework, motivated by *MCMC* ideas.
Spline	A technique for approximating functions, typically accomplished by breaking the domain of the function into segments within each of which some simple function is

	fitted to the data. The boundaries between domains are known as *knot points*.
Switching Variable	In *threshold models* of a physical system a key variable causes the system to switch behaviour. This key variable is known as a switching variable.
Time Series	A set of data recorded sequentially in time.

Appendix B- List of Acronyms

CLW	CSIRO Land and Water.
CMIS	CSIRO Mathematical and Information Sciences.
CMR	CSIRO Marine Research.
ENSO	El Niño-Southern Oscillation
IOCI	Indian Ocean Climate Initiative.
MCMC	Markov chain Monte Carlo.
SOI	Southern Oscillation Index
SST	Sea Surface Temperature.
SWA	Southwest Western Australia.

Appendix C- Submitted manuscript describing the statistical methods developed by IOCI for the case studies.

At the time of writing the manuscript is under peer review for possible publication in the *Journal of Time Series Analysis*. A copy of the current version is available from the author:

e-mail: eddy.campbell@csiro.au

Tel: (08) 9333 6203